COMBUSTION TURBINE OPERATION AND OPTIMIZATION MODEL

by

JEET SENGUPTA

B.E., University of Pune, 1995

M.S., Kansas State University, 2003

AN ABSTRACT OF A DISSERTATION

submitted in partial fulfillment of the requirements for the degree

DOCTOR OF PHILOSOPHY

Department of Mechanical and Nuclear Engineering
College of Engineering

KANSAS STATE UNIVERSITY
Manhattan, Kansas

2012

Abstract

Combustion turbine performance deterioration, quantified by loss of system power, is an artifact of increased inlet air temperature and continuous degradation of the machine. Furthermore, the combustion turbine operator has to meet ever changing stricter emission levels. Different technologies exist to mitigate the impact of performance loss and meeting the emission standard. However an upgrade using one or more of the available technologies has associated capital and operating costs. Thus, there is a need for a tool that can evaluate power boosting and emission control technologies in concert with the machine maintenance strategy.

This dissertation provides the turbine operator with a new and novel tool to examine each of the upgrades and determine its suitability both from the cost and technical stand point. The main contribution of this dissertation is a tool-kit called the Combustion Turbine Operation and Optimization Model (CTOOM) that can evaluate both power-boosting and emission control technologies. It also includes a machine maintenance model to account for degradation recovery. The tool-kit is made up a system level thermodynamic optimization solver (CTOOM-OPTIMIZE) and two one-dimensional, mean-line, aero-thermodynamic component level solvers for the compressor (CTOOMCOMP1DPERF) and the turbine (CTOOMTURB1DPERF) sections.

In this work, the cogeneration system as given by the classical CGAM problem was used for system level optimization. The cost function was modified to include the cost of emissions while the maintenance cost of the combustion turbine was separated from the capital cost to include a degradation recovery model. Steam injection was evaluated for NO_x abatement, power boosting was examined by both the use of inlet air cooling and steam injection, and online washing was used for degradation recovery. Based on the cost coefficients used, it was seen that including the cost of emissions impact resulted in a significant increase in the operational cost.

The outcomes of the component level solvers were compressor and turbine performance maps. It was demonstrated that these maps could be used to integrate the components with the system level information.

COMBUSTION TURBINE OPERATION AND OPTIMIZATION MODEL

by

JEET SENGUPTA

B.E., University of Pune, 1995

M.S., Kansas State University, 2003

A DISSERTATION

submitted in partial fulfillment of the requirements for the degree

DOCTOR OF PHILOSOPHY

Department of Mechanical and Nuclear Engineering
College of Engineering

KANSAS STATE UNIVERSITY
Manhattan, Kansas

2012

Approved by:

Major Professor
Dr. Donald Fenton

Copyright

Abstract

Combustion turbine performance deterioration, quantified by loss of system power, is an artifact of increased inlet air temperature and continuous degradation of the machine. Furthermore, the combustion turbine operator has to meet ever changing stricter emission levels. Different technologies exist to mitigate the impact of performance loss and meeting the emission standard. However an upgrade using one or more of the available technologies has associated capital and operating costs. Thus, there is a need for a tool that can evaluate power boosting and emission control technologies in concert with the machine maintenance strategy.

This dissertation provides the turbine operator with a new and novel tool to examine each of the upgrades and determine its suitability both from the cost and technical stand point. The main contribution of this dissertation is a tool-kit called the Combustion Turbine Operation and Optimization Model (CTOOM) that can evaluate both power-boosting and emission control technologies. It also includes a machine maintenance model to account for degradation recovery. The tool-kit is made up a system level thermodynamic optimization solver (CTOOM-OPTIMIZE) and two one-dimensional, mean-line, aero-thermodynamic component level solvers for the compressor (CTOOMCOMP1DPERF) and the turbine (CTOOMTURB1DPERF) sections.

In this work, the cogeneration system as given by the classical CGAM problem was used for system level optimization. The cost function was modified to include the cost of emissions while the maintenance cost of the combustion turbine was separated from the capital cost to include a degradation recovery model. Steam injection was evaluated for NO_x abatement, power boosting was examined by both the use of inlet air cooling and steam injection, and online washing was used for degradation recovery. Based on the cost coefficients used, it was seen that including the cost of emissions impact resulted in a significant increase in the operational cost.

The outcomes of the component level solvers were compressor and turbine performance maps. It was demonstrated that these maps could be used to integrate the components with the system level information.

Table of Contents

Nomenclature

A	Area of annulus	m^2
AFR	Air –to-fuel ratio	Dimensionless
C	Capital cost	$
$\dot{C}$	Cost rate	$/s
C_m	Velocity - Gas (Axial)	m/s
CRF	Cost recovery factor	Dimensionless
DAR	Ratio of Actual AFR to Stoichiometric AFR	Dimensionless
$HbyCRatio$	Ratio of hydrogen atoms to carbon atoms in a fuel	Dimensionless
I	Rothalpy	kJ/kg
LHV	Lower heating value	kJ/kg
$LMTD$	Log Mean Temperature Difference	K
M	Mach Number	Dimensionless
MW	Molecular Weight	kg/kmol
N	Speed - Rotational	rpm
N_{hrs}	No of operating hours	hours
P	Pressure	Pa
$Power_{IAC}$	Power for inlet air cooling	kW
$\dot{Q}$	Heat transferred	kW
T	Temperature	K
U	Velocity - Blade	m/s
V	Velocity - Gas (Absolute)	m/s
W	Velocity - Gas (Relative)	m/s
W	Power	kW
a	Velocity of sound	m/s
a	Location of maximum camber	m
c	Chord length	m

c_f	Cost of fuel per energy unit	\$/MJ
$c_{emission}$	Cost of emissions per unit flow rate	\$/kg/s
c_{NO_x}	Cost of NO_x per unit flow rate	\$/kg/s
$f_{onlinewash}$	Frequency of online wash	hrs
h	Enthalpy	kJ/kg
$l_{totalreco}$	Total degradation recovery	%
$l_{onlinereco}$	Total degradation recovery due to online washing	%
$l_{offlinereco}$	Total degradation recovery due to offline washing	%
$\dot{m}$	Mass flow rate	kg/s
mf	Mass fraction	Dimensionless
o	Throat dimension	m
p	Partial pressure	Pa
r_m	Radius at mean-line	m
r_{eval}	Radius of evaluation – user specified	m
s	Entropy	kJ/kg-K
s	Pitch	m
t_m	Blade thickness - Maximum	m
t_e	Blade thickness- Trailing Edge	m
y	Mole fractions	Dimensionless
z	Axial distance	m

Greek letters

α	Flow angle (Absolute)	°
β	Flow angle (Relative)	°
γ	Ratio of specific heats ($\frac{c_p}{c_v}$)	Dimensionless
$\imath$	Angle of incidence	°
δ	Angle of deviation	°

ρ	Density	kg/m^3
κ	Blade metal angles	°
η	Efficiency	Dimensionless
θ	Stagger angle	°
ϕ_{RH}	Relative Humidity	Dimensionless
ϕ_m	Maintenance factor	Dimensionless
Δp	Pressure drop	%
$\Delta T_{appraoch}$	Approach temperature	K
ΔT_{pinch}	Pinch temperature	K

Subscripts

APH	Air preheater
AC	Air cooler
C	Compressor
CC	Combustion chamber
G & PT	Gas and power turbine
HRSG	Heat recovery steam generator
IAC	Inlet Air Cooling
P	Pinch point
a	Absolute
a	Air
c	Capital
c & m	Capital and maintenance
da	Dry air
eco	Economizer
env	Environment
eva	Evaporator
f	Fuel
g	Combustion products
m	Maintenance

r	Relative
s	Steam
$steaminject$	Steam injected
v	Vapor
w	Water
$wash$	Washing
θ	Tangential component of velocity

List of Figures

List of Tables

Acknowledgements

At the outset, I express my sincerest gratitude to Dr. Donald Fenton for consenting to supervise my dissertation. I extend my deep appreciation to all my committee members Dr. Swenson, Dr. Glasgow, Dr. Beck and Dr. Betz for agreeing to be on my committee on a very short notice and also for juggling around their schedules to accommodate the examination. I also extend it to the graduate school appointed chair Dr. Ben-Itzhak for the same reason. I was fortunate enough to interact with some of my committee members Drs. Fenton, Beck, and Glasgow during classes I have taken with them. I did not have the pleasure to take any class with Dr. Swenson but I did make up for it by downloading the tool DIGXY from his webpage which I have used extensively in this dissertation. Same is the case with Dr. Betz who joined the faculty much later after I left Manhattan, KS. However, the excitement she exhibited when I requested her to serve on my committee inspired me to get back to Florida and get started with my work again. I want to thank Dean Dr. Carol Shanklin for her timely assistance and inputs on overcoming some of the critical challenges in the academic process. This work started out with some funding form BP America and I thank their rotating equipment group and specifically Mr. John Platt for the same.

I am especially thankful to Dr. Kirby Chapman for providing me with the unique opportunity to attend graduate school in the US, for supervising my master's thesis and for initiating me towards my doctoral degree. The seven years at the National Gas Machinery Laboratory were the formative years of my rather long academic life and would undoubtedly remain the most cherished ever. I would remain forever grateful to Mrs. Sandra Chapman who ensured that not only the important things (pay-check, enrolment, editorial reviews on manuscripts) were taken care of but also the most trivial things (how to fix your Volvo when it dies!!!). I have known the late Dr. Prakash Krishnaswami as a mentor both academically and personally and his loss has been particularly painful which has taught me to appreciate life better.

I acknowledge Ms. Sarah Buchanan's effort for facilitating the completion of all the paperwork required. Without her help it would be hard to imagine the innumerable trips I would have to make from Ft. Lauderdale, FL to Manhattan, KS.

I thank Dr. Tim Bremner, my current supervisor at Hoerbiger Corporation of America, for providing me the support necessary to complete this dissertation. It is quite unthinkable that I

could have accomplished this without his support. I thank Mr. Matthias Huschenbett for giving the internship opportunity with Hoerbiger and Mr. Rainer Ponzel for providing me my first full time position with Hoerbiger in the US. I thank Drs. Rudolf Scheffrahn and Robin Giblin-Davis for graciously providing me with office space for the last four months at the University of Florida's Ft. Lauderdale Research and Extension Center. I also thank Mr. Mikhail Ryabin for setting up a network connection at the UF's office space to help me get access to the UF library system.

This dissertation is an outcome of reading exhaustively the work other people have done. It is quite impossible to thank all the authors but one author Dr. Carl Knopf made this work a lot simpler than it looked when I started out with. I also thank Mr. Satish Motipalli for spending time to help me compile some C++ DLL's which form a significant feature of this dissertation.

I can never thank Mr. Sunil Gogate, my supervisor at Kirloskar Ebara, enough for inspiring me to pursue higher academic degrees. At the same breath, I would also thank Mr. Umeno, my colleague at Ebara, for generating some mesmerizing eighth order pump curves that baffled my mind then but it set forth the quest to learn those techniques to accomplish something similar. This dissertation is filled with many such curves.

In any journey that spans over a few years there always are people who leave deep influences. I can never forget the warmth and sense of belongingness that the Hahn's (Richard and the late Joann) provided me with when I stepped into Manhattan. They not only introduced me to various aspects of the American culture and ways of life but also extended their curiosity to learn about my culture and country. Bob (Robert) Deteau, my first and only American room-mate, not only provided me with tips on how to succeed in graduate school but also on how heat transfer was an integral part of cooking. Thanks to Bob, for the first time in my life, I also spent some quality time with a pet, his golden retriever. I would forever remain indebted to Chandana Ghosh, Ashik Srinivasan, the Chakrabarti's (Leena and Amit) for their support and help when I needed it the most. Sujatha Prakash was my orthopedic consultant in Manhattan. I thank for her that interesting role and for the many wonderful meals she fixed as we chatted over discussing the best orthopedic in town. It was inspiring to see someone who dealt with her own set of injuries and personal tragedies and yet move forward in life. During the last four years of my stay in Manhattan Shilpa, Satish, and Sunitha were a constant fixture in my life. It was a pleasure

to have them around, especially Shilpa who would somehow always know when I needed her help the most.

One of the highlights of my program at K-State was my involvement with the music society SABHA. I thank Priya Voothuluru for persuading me to take up the challenge. At times when things went wrong I cursed her the most, but when it culminated as the fine year for SABHA I was glad for what she did. It was then I met Disha with whom the friendship has transcended both time and place. She is perhaps the only friend with whom I am still in contact.

For most people the journey usually ends in the town you go to school in. For me as I started with full time employment in between the program, the last four years have been in Florida where I have come across people who have made a difference to my life. They have influenced my personal life which is as much important as someone's influence on my academic or professional life. Garima and Vivek taught me to appreciate life to its fullest and with zest. It's a pleasure to have them in my life which has changed for better with their stepping in.

It is impossible to thank my father so I will not even attempt doing that. He has inspired me in many ways but most importantly taught me to be a self-less person.

Dedication

To Mithai and Ma, the two women in my life

Chapter 1 - Introduction

Goal

Combustion turbine, more commonly known as gas turbine, is widely used either as a power generating device or as a mechanical driver. The goal of this research was to develop a performance modeling tool, for the combustion turbine, which can evaluate performance advantages to system upgrades.

The need for upgrade - Characterizing the combustion turbine performance its deterioration and means to offset the deterioration

Combustion turbine performance is essentially characterized by the power developed at a single operating point, usually called as the rated power. However, there are other quantities of interest such as the fuel flow rate and the highest temperature attained in the thermodynamic cycle (firing temperature) which can provide additional insight into the turbine performance and is thus routinely used to quantify performance. A commonly used industry metric to quantify combustion turbine performance is the heat rate. Heat rate is the ratio of fuel energy input to the output power and thus heat rate has an inverse relation to the output power. Therefore, increased heat rate which would alternately mean drop in power developed would signify deterioration of performance. Additionally, increase in emissions would be the other characteristic of performance deterioration. The following paragraphs identify the parameters that cause performance deterioration and commercially available technologies to offset the same.

Inlet air condition

The combustion turbine performance is influenced by anything that affects the density and/or mass flow rate of air at the inlet. Since ambient air is drawn in at the inlet the ambient air condition i.e. the air temperature, pressure (i.e. the site elevation) and humidity will affect the inlet air density which in turn influences the performance. Thus, to establish a baseline all combustion turbines are always rated for the inlet ambient condition of 15°C, 1.013 bar and 60% RH established as a reference by ISO standard. Any increase or decrease in the inlet ambient air quality described below is with reference to this ISO condition.

Increase in inlet air temperature reduces the power output i.e. increases the heat rate. Every combustion turbine would have its own temperature effect data usually provided as correction curves by the manufacturer. For a single shaft GE MS7001 turbine a 5°C increase in temperature would translate into a 3% drop in power or a 1% increase in heat rate (Brooks. 2000). On heavier frame turbines, the power output could drop by as much as 20% with a corresponding heat rate increase of about 5% when ambient temperature reaches 40°C (Al-Amiri, et al. 2006). Thus, for a combustion turbine unit even when brand new there is performance deterioration from nighttime to daytime. Similarly, identical turbine units located in the Saharan desert would perform worse than one located in Canada. The impact of increase in inlet air temperature can be mitigated by inlet air cooling.

Inlet air pressure is a function of the site elevation. Similar units installed at different elevation would perform differently since the air density reduces as the site elevation increases. Decrease in air density would result in a proportional reduction in mass flow rate and power developed. However, the heat rate remains unaffected (Brooks. 2000). An increase in 2400 m in elevation from the ISO condition could result in a 30% drop in power (Brooks. 2000). Standard altitude correction curves are provided for power correction. However, once installed at a particular location there will be very little day-to-day variation in the ambient pressure and thus negligible performance deterioration.

The other inlet air characteristic that influences the performance is the humidity. Humid air is less dense than dry air and thus higher the humidity lower is the density which in turn lowers the mass flow rate at the inlet. This results in a drop of power or increased heat rate. Manufacturers provide first order humidity correction charts to account for the same. The direct impact of increase in humidity from the ISO specific humidity on the performance deterioration is not terribly severe. An increase from 60% RH to 130% RH has correction factors less than 0.4% for power reduction or 0.8% for heat rate increase (Brooks. 2000). However, more than the direct impact, humidity has an indirect impact on the performance through the control system algorithm used in the combustion turbine. Depending on the governing mechanism the power could reduce or increase. This work does not delve into modeling the governing mechanisms and thus the effect of humidity on performance will be limited to examining its impact on air temperature alone.

It is evident from above that the increase in air temperature is the primary cause of performance deterioration as far as the influence of the ambient air is concerned. Clearly, the technique to mitigate the impact of increase in air temperature would be to cool the inlet air. Inlet air cooling (IAC) is thus identified as a possible system upgrade to boost power and reduce heat rate. Inlet air cooling has been commercially successfully achieved by evaporative cooling, chillers, LNG vaporization or a combination of these referred to as hybrid (Phillips and Levine. 2004). Bianchi, et al. (2010) present a detailed review and comparison of the different power augmentation technologies using IAC. Evaporative cooling includes the use of wetted media (Mehraban, et al. 2012), fogging (Al-Amiri, et al. 2006, Bhargava, et al. 2005, Mee. 1999) or wet compression (Bracco, et al. 2007, Khan. 2009, Sanaye and Tahani. 2010). Chillers could be either of the mechanical type (Ameri, et al. 2005, Farzaneh-Gord and Deymi-Dashtebayaz. 2011) or of the absorption type (Mohanty and Paloso Jr. 1995, Popli, et al. 2011). An alternative to inlet air cooling for power boosting is the use of water or steam injection into the combustor (Bultzo. 1969, Coutant. 1959, Ediss. 1966, Ediss. 1970, Heard. 1976, Stephens and Boho. 1965)

Exhaust emissions

Nitrogen oxides (NO_x), carbon monoxide (CO), unburned hydrocarbons, sulfur oxides and particulate matter are the combustion turbine exhaust emissions. Emission regulations have become more stringent over the years. Thus, older combustion turbine units that met the environmental regulations may not be able to meet the ever changing standards. Emission levels are a function of the fuel used (natural gas or distillate oil), type of engine (single shaft or two shaft), the thermodynamic cycle used (simple or combined) and the operating characteristics. Similar to the output power, emissions are also reported at ISO base conditions.

NO_x is usually reported in parts per million by volume dry (ppmvd) with 15% oxygen in the exhaust or on lb/hr basis. NO_x is a direct function of the combustion temperature. It is also a function of the air-to-fuel ratio where the maximum NO_x occurs at slightly lean air/fuel mixtures. Water injection has been successfully used for NO_x control within 25 ppmvd (Fitts, et al. 1990). Steam injection is the other alternative means used to reduce NO_x and can reduce NO_x by 70% from unabated NO_x (Anonymous, 2006). Both water and steam injections are done into the flame area which reduces the flame temperature and thereby the thermal NO_x. Inlet fogging is the other technique to reduce NO_x and can provide about 18% reduction from unabated NO_x (Mee. 1999,

Sexton, et al. 1998). As seen in the previous section, inlet fogging can also provide power augmentation and thus is a very useful upgrade. Exhaust treatment using selective catalytic reduction (SCR) is an alternative technique to reduce NO_x. The SCR technology reduces NO_x by injecting ammonia into the flue gas. The ammonia reacts with NO_x in the presence of catalyst to form water and nitrogen. SCR technology is often used in conjunction with steam injection and the combination reduced NO_x from 148 ppmv (uncontrolled) to 9 ppmv for the MS6001 gas turbine (Anonymous, 1993). Another NO_x reduction strategy is the use of Dry Low No_x or $SoLoNO_x$ combustors where the combustion process is staged over two stages. The first stage has a richer fuel-air mixture which lowers the combustion temperature while the second stage runs lean. It can provide about $1/10^{th}$ reduction of NO_x from standard combustors. These combustors also reduce CO and unburned hydrocarbons (Cowell. 2003). CO reduction can also be achieved by using exhaust treatment i.e. the use of catalyst.

Degradation

Degradation of the engine components over its operational life is the other cause of performance deterioration. The mechanisms of combustion turbine degradation are fouling, erosion, corrosion, damage by foreign objects and abrasion. A detailed description of each of these mechanisms is available in Kurz and Brun (2001), Kurz and Brun (2007), Kurz and Brun (2009), Kurz, et al. (2009). One of the earliest characterizations of fouling problem in turbomachines was presented by Upton (1974). The paper also covered briefly the erosion and corrosion mechanisms. According to the author, since ingestion of air-borne particles was the fundamental cause of fouling, the effect of fouling was most severe in the compressor section of the combustion turbine. Thus, investigations have been done on the effects of fouling in the compressor section of the combustion turbine (Vigueras Zuniga. 2007) or in an axial compressor alone (Baker. 2002). The consequences of fouling are increased tip clearances; changes in airfoil geometry and/or increased surface roughness, all of which will lead to lower compressor discharge pressure and eventually loss of turbine power developed. Diakunchak (1991) estimated an annual cost of approximately $522,500 on a 46 MW machine due to degradation on account of fouling on a simple cycle turbine with no injection. Thus, for a three year operating period the cost of degradation would be about 1.5 million dollars. Since fouling is caused by buildup of particles on the airfoil or at the tip clearances some of the degradation due to fouling can be

recovered by washing while some may not be recovered (Diakunchak. 1991) at all. Washing can be done either online i.e. the turbine is in operation or offline when the turbine is brought to a halt. Washing is thus part of the overall machine and plant operational and maintenance strategy. Since off-line washing requires shut-down of the machine most turbine operators perform this activity as a part of their time based plant shut-down maintenance program. However, if fouling causes severe performance deterioration then such a time bound maintenance plan would result in continuous loss of turbine power or increased fuel consumption and consequently impact the plant output. Therefore, good filtration system and regular online washing can mitigate some of the deterioration due to fouling. However, there is a cost associated with online washing and thus the frequency of the same needs to be made based on economic considerations. Asplund (1997) provides a comprehensive cleaning strategy for a wide variety of combustion turbines. There is a significant amount of literature on compressor fouling, its recovery and its modeling (Lakshminarasimha and Saravanamuttoo. 1986, Lakshminarasimha, et al. 1994, Meher-Homji, et al. 2009, Millsaps, et al. 2004, Saravanamuttoo and Lakshminarasimha. 1985, Seddigh and Saravanamuttoo. 1990, Tarabrin, et al. 1996, Tarabrin, et al. 1998). On the turbine side, fouling can effectively block the cooling passages in turbine blades thus resulting in higher turbine temperatures and loss of turbine efficiency.

Fouling alone is not the only mechanism which leads to changes in airfoil geometry and increased surface roughness. Erosion to some extent is also responsible for the same. The effect of erosion as a degradation mechanism has been studied in detail by Ghenaiet (2001). Some earlier work on the same was reported by Singh, et al. (1996), Tabakoff and Balan (1983), Tabakoff (1987). Clearly, fouling as the degradation mechanism has attracted more attention partly because some of the performance deterioration can be recovered whereas for erosion the only way for performance recovery would be part replacement. Part replacement upgrades could involve flange-to-flange replacement or replacement of individual blade rows, blade repairs, tip seal replacement etc. depending on the extent of erosion. Such replacement or machine overhauls also are part of the comprehensive operation and maintenance plans to minimize production losses due to repair based shut downs.

The other degradation mechanisms i.e. damage due to foreign object and corrosion also warrant part replacements. An example of such a part replacement would be of hot gas path components such as the turbine blades or combustion liners due to hot corrosion. It can be thus

concluded that recovery of performance deterioration due to component degradation can be done only by an effective maintenance plan.

The need for this work

The brief review above has shown that a system upgrade would encompass techniques to boost power (alternately reduce heat rate) and reduce emissions in concert with a comprehensive operation and maintenance (O&M) strategy and multiple alternatives exist to meet that objective. Upgrade solutions are usually provided by vendors specializing in combustion turbine upgrades. However, these vendors usually have expertise only in specific upgrade solutions and tend to promote those among the combustion turbine operators. With a plethora of vendors and their upgrade solutions it becomes challenging for the operator to make judicious choices. It is therefore necessary to develop an optimization model that includes power boosting, emissions, and machine maintenance strategies. To the best of the author's knowledge such an optimization model that includes machine maintenance strategies as an optimization variable is not available.

Contributions of this dissertation and its outline

The contributions of this dissertation are:

1. A thermo-economic model for a cogeneration combustion turbine system with power boosting, emission control and degradation models is presented in Chapter 2. The thermo-economic model was developed in MS Excel.
2. Chapters 3 and 4 extend the system level thermodynamic models to component level models for the compressor and the turbine. This allows for a more detailed investigation into component level changes. The component level models are aero-thermodynamic models based on the mean-line analysis technique for the turbomachinery components (compressor and turbine sections). Appropriate loss models as available in open literature to characterize design point and off-design losses were incorporated. The component level models were developed in FORTRAN 90.
3. Chapter 5 presents the overview of the computer program both the MS Excel model and the FORTRAN code.

4. Chapter 6 describes the case studies and validation examples for the optimization problem and for the compressor and turbine component models.
5. Chapter 7 summarizes the work done and outlines the conclusions and future work.

Chapter 2 - Thermo-economic system optimization

The combustion turbine (CT) system

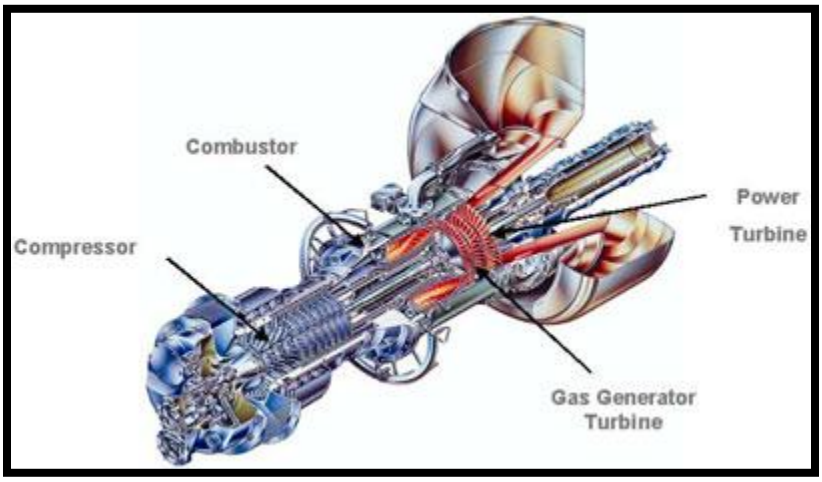

Figure 2-1 Cut-away of a combustion turbine system (www.eetd.lbl.gov)

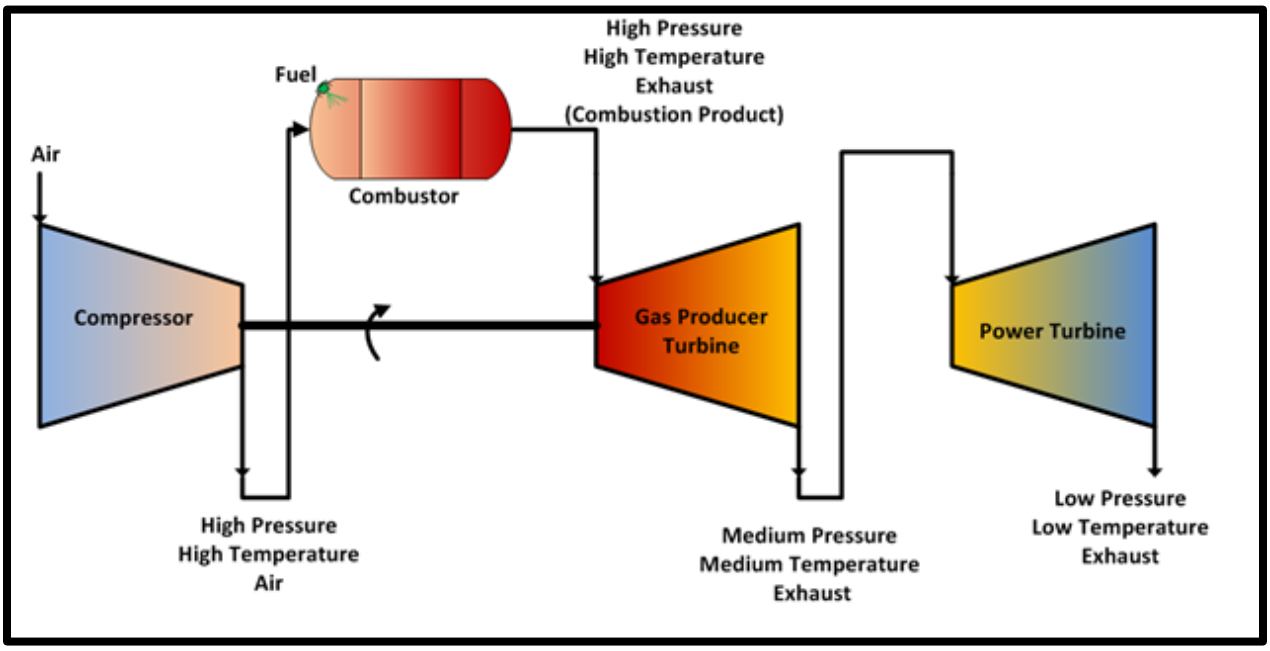

Figure 2-2 Simple cycle system

Figure 2-1 shows the cut-away of a commercially available combustion turbine (CT) system. Any combustion turbine system will have four primary components i.e., the compressor, the combustor, the gas generator (gas producer) turbine and the power turbine. Figure 2-2 shows

the schematic of the CT system and also illustrates the basic operations of the components. Ambient air is drawn into the compressor where it is compressed consequently raising both the pressure and the temperature. This high pressure high temperature air is fed to the combustor. In the combustor it mixes with the injected fuel and this air-fuel mixture is ignited. The combustion process results in very high pressure high temperature exhaust gas. The exhaust gas is then expanded in the gas generator or gas producer section of the CT system which reduces both the pressure and the temperature of the exhaust gas referred to as medium pressure medium temperature exhaust in the Figure 2-2. The primary role of the gas producer turbine is to supply enough power to the compressor to operate and is only a driver for the compressor. Thus, the three components i.e., the compressor, the combustor and the gas producer turbine are really a system that feed and drive each other and don't seem to be doing any useful work. However, the exhaust gas leaving the gas producer turbine has enough energy left which when further expanded in the power turbine can be used to drive external devices. So, it's really the power turbine that is the power generator but can do so only in conjunction with the other three components. The power turbine can be on the same shaft or on a different shaft (as in the Figure 2-2). Though the fundamental processes for any CT system remain as described above there are many other additional processes that often take place. These are, and not limited to, bleed air from compressor stages for cooling the combustor and/or cooling the turbine blades, changing the stator vane angle setting in the compressor to change its operational characteristics, using dual fuel system in the combustor or steam/water injection to reduce NO_x etc. Furthermore, some CT systems employ a twin shaft design where a high pressure compressor is driven by a high pressure turbine and a low pressure compressor driven by a low pressure turbine. A detailed review of the different gas turbine configurations is provided in Bathie (1996), Boyce (2012) and Soares (2008). Simple cycle CT systems are most commonly used as mechanical equipment drivers. The driven equipment can be in a wide variety of applications such as gas transmission pipelines, exploration and production both onshore and offshore, or even downstream refinery operations. For a system level evaluation, characterization of the downstream equipment and its operating envelope is paramount. Therefore, for the purpose of developing the model, it was assumed that the CT is used for power generation. Usually, a power generation CT would not operate on a simple cycle but on a modification of the simple cycle.

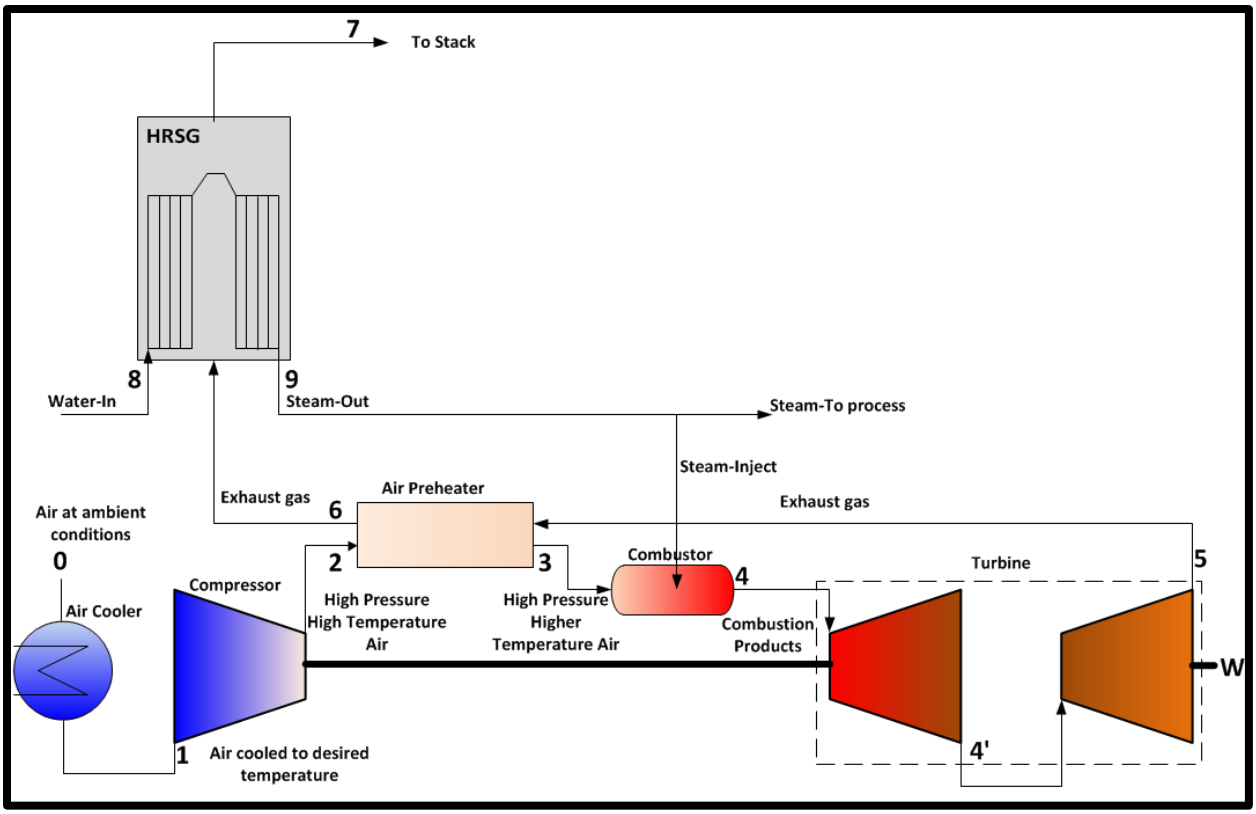

Figure 2-3 Cogeneration system

The primary modifications are the use of an air-preheater in between the compressor and the combustor. It should be noted that the air preheating is accomplished by the exhaust gas leaving the power turbine. The exhaust gas leaving the air preheater then further continues into the Heat Recovery Steam Generator (HRSG) resulting in steam being produced. Thus, the system not only delivers power at the shaft end of the power turbine but also delivers steam. Such a system is known as the cogeneration system. The focus of this dissertation was to develop a comprehensive model that included power boosting, emission control and degradation. Thus, two power boosting technologies were incorporated into the system i.e. steam injection and inlet cooling. Steam injection was also a NO_x abatement strategy. Furthermore, a machine maintenance strategy was included in the system model.

Combustion turbine system optimization

Optimization of any system necessitates identifying the objective function which is then either maximized or minimized. The objective function is expressed in terms of the decision variables and the solution to the optimization problem seeks to determine the most optimal

combination of the decision variables that can result in either a maximum or minimum value of the objective function. The minimization optimization problem is given by equation (2.1) (Vanderplaats. 2005):

$$\min f(x) \tag{2.1}$$

subject to,

$$g_j(x) = 0, \text{ for } j = 1, ..., m_e \tag{2.2}$$

$$g_j(x) \geq 0, \text{ for } j = m_e + 1, ..., m \tag{2.3}$$

$$x_l \leq x \leq x_u \tag{2.4}$$

Equation (2.2) and (2.3) are the equality and inequality constraints. As seen there are a total of m constraints. Of these there are m_e number of equality constraints while the rest are inequality constraints. Equation (2.1) is a minimization problem. A maximization problem would simply mean a minimization of the negative of the objective function. Equation (2.4) refers to bound constraints where the decision variables are controlled between lower and upper bounds. Bounds are an artifact of either numerical or physical constraints. Problems where there is more than one objective are known as multi-objective optimization problems. A minimization of a multi-objective function also called as vector minimization problem is mathematically expressed as (Rao. 2010):

$$Find\ \mathrm{X} = \begin{Bmatrix} x_1 \\ x_2 \\ \vdots \\ \vdots \\ x_n \end{Bmatrix} \tag{2.5}$$

Which minimizes, $$f_1(\mathrm{X}), f_2(\mathrm{X}) \ldots, f_k(\mathrm{X}) \tag{2.6}$$

Subject to $$g_j(\mathrm{X}) = 0, \quad j = 1, 2, \ldots, m_e \tag{2.7}$$

$$g_j(\mathrm{X}) \leq 0, \quad j = m_e + 1, m_e + 2, \ldots, m \tag{2.8}$$

The subscript k in equation (2.6) denotes the number of objective functions to be minimized. No solution vector X exists that can minimize all the k objective functions simultaneously. Therefore, the concept called the Pareto optimal solution is used in multi-objective functions. A feasible solution X is called Pareto optimal if no other feasible solution Y

exists such that $f_i(\mathrm{Y}) \leq f_i(\mathrm{X})$ for $i = 1, 2, \ldots, k$ with $f_j(\mathrm{Y}) < f_i(\mathrm{X})$ for at least one j. In other words, a feasible vector X is called Pareto optimal if no other feasible solution X would reduce some objective function without causing a simultaneous increase in at least one other objective function.

There are many methods to solve a multi-objective optimization problem i.e., the ε constraint method, weighting method (Rangaiah. 2009), utility function method, global criterion method, bounded objective function method, lexicographic method and the goal programming method (Rao. 2010). In the ε constraint method the multi-objective optimization problem is transformed into a single objective function problem by retaining only one of the objectives and converting all other objectives into inequality constraints. This method was used in this work.

The three fundamental objectives were to minimize the system operating cost, minimize the NO_x but maximize the degradation recovery. Of these three objectives, the objective that was retained was minimizing the system operating cost. The remaining two objectives i.e. minimizing the NO_x and maximizing the degradation recovery were converted into constraints. This was done because the level of NO_x is always mandated by emission regulations so achieving a minimum is not necessarily a principal objective. Similarly, complete degradation recovery is never a possible option. Thus, rather than trying to achieve a maximum recovery by retaining it in the objective function, it seemed more plausible to apply a reasonable constraint on the amount of degradation recovery required. Therefore, the system then comprised of only one objective function with two additional constraints. Changing the constraint values on these two constraints would then provide a Pareto optimal if desired.

Thus, the objective function was the system operating cost which was a combination of the fuel consumption cost, equipment capital cost, and the maintenance cost of the system. For i components in a system, the objective function was (Bejan, et al. 1996)

$$\dot{C}_t = \dot{C}_f + \sum_i \dot{C}_{c,i} + \sum_i \dot{C}_{m,i} \tag{2.9}$$

The terms in equation (2.9) are cost rates in \$/s. However, equation (2.9) does not account for the cost of environmental impact. Thus, equation (2.9) was modified to include the additive term (Frangopoulos. 1992):

$$\dot{C}_t = \dot{C}_f + \sum_i \dot{C}_{c,i} + \sum_i \dot{C}_{m,i} + \dot{C}_{env} \tag{2.10}$$

Valero et al. (1994) suggested combining the cost rates for capital cost and maintenance cost by the use of a maintenance factor ($\phi_{m,i}$). Thus, instead of two separate terms $\sum_i \dot{C}_{c,i}$ and $\sum_i \dot{C}_{m,i}$, these can be combined into $\sum_i \dot{C}_{c\&m,i}$. In such a case, the objective function in equation (2.10) can be modified to:

$$\dot{C}_t = \dot{C}_f + \sum_i \dot{C}_{c\&m,i} + \dot{C}_{env} \tag{2.11}$$

However, this approach did not allow any characterization of maintenance procedures and their incorporation into the optimization process as a decision variable. Therefore, in this work an independent model for the maintenance cost rate was proposed. The focus of this work was on the CT system alone and thus a maintenance cost rate model was proposed only for the maintenance of the CT. For the other components such as the HRSG, the air preheater, and the air cooler the maintenance factor model were retained. The objective function can be recast as:

$$\dot{C}_t = \dot{C}_f + \dot{C}_{c\&m,APH} + \dot{C}_{c\&m,HRSG} + \dot{C}_{c\&m,AC} + \dot{C}_{c,C} + \dot{C}_{c,CC} + \dot{C}_{c,G\&PT} + \dot{C}_{m,C,CC,G\&PT} + \dot{C}_{env} \tag{2.12}$$

For the ith component Valero et al. (1994) suggested the following capital and maintenance cost rate model:

$$\dot{C}_{c\&m,i} = \frac{C_i (CRF_i)\phi_{m,i}}{3600 N_{hrs}} \tag{2.13}$$

It is a function of the capital cost (purchase cost) of each equipment (C_i), it's capital cost recovery factor (CRF_i) which is the annualized return on investment, the number of operating hours (N_{hrs}) and the maintenance factor ($\phi_{m,i}$). Thus, the capital and maintenance cost rate models for the air preheater ($\dot{C}_{c\&m,APH}$), heat recovery steam generator ($\dot{C}_{c\&m,HRSG}$), and the air cooler ($\dot{C}_{c\&m,AC}$) were obtained from equation (2.13):

$$\dot{C}_{c\&m,APH} = \frac{C_{APH} (CRF_{APH})\phi_{m,APH}}{3600 N_{hrs}} \tag{2.14}$$

$$\dot{C}_{c\&m,HRSG} = \frac{C_{HRSG} (CRF_{HRSG})\phi_{m,HRSG}}{3600 N_{hrs}} \tag{2.15}$$

$$\dot{C}_{c\&m,AC} = \frac{C_{AC} (CRF_{AC})\phi_{m,AC}}{3600 N_{hrs}} \tag{2.16}$$

However, as described earlier the cost rate models for the compressor, the combustion chamber, and the turbine (gas generator and power) were distributed into two parts, i.e. the capital cost rate model and the maintenance cost rate model. The capital cost rate models for the compressor ($\dot{C}_{c,C}$), the combustion chamber ($\dot{C}_{c,CC}$), and the turbine (gas generator and power) ($\dot{C}_{c,G\&PT}$) were obtained from equation (2.13) by excluding the maintenance factor:

$$\dot{C}_{c,C} = \frac{C_C(CRF_C)}{3600N_{hrs}} \tag{2.17}$$

$$\dot{C}_{c,CC} = \frac{C_{CC}(CRF_{CC})}{3600N_{hrs}} \tag{2.18}$$

$$\dot{C}_{c,G\&PT} = \frac{C_{G\&PT}(CRF_{G\&PT})}{3600N_{hrs}} \tag{2.19}$$

The maintenance cost rate was an artifact of the machine maintenance procedure and schedule. From the CT standpoint it is intrinsically related to the degradation of the same. All CT's will exhibit performance deterioration over time and will never run at the desired design point as time progresses. This deterioration is due to fouling, erosion, and/or corrosion. Irrespective of the deterioration mechanism the fundamental effect of the deterioration is the loss of system efficiency, which in this case would translate into a loss of plant power output and/or steam generated. Some of the loss in system efficiency can be recovered by online and offline washing. Online washing is usually carried out on a continuously running machine at about 80% load. The online washing system comprises of a set of spray nozzles that inject heated distilled water and/or detergent into the machine. The washing continues for about 10 to 15 minutes. This recovers most of the deterioration that had accumulated since the last wash. Online washing can be done daily, once in two days, etc. The frequency of online washing will be a cost contributor to the maintenance cost of the CT. The online washing is supplemented by an off-line washing which depends on the maintenance strategy and can vary from two weeks to six months. The cost rate model for the deterioration recovery due to washing can then be expressed as a function of the cost of washing ($C_{wash,C,CC,G\&PT}$) as:

$$\dot{C}_{m,C,CC,G\&PT} = \frac{C_{wash,C,CC,G\&PT}}{3600N_{hrs}} \tag{2.20}$$

The cost rate of fuel $\dot{C}_f$ was expressed in terms of the fuel flow rate ($\dot{m}_f$), the lower heating value of the fuel (LHV) and the fuel cost per energy unit (c_f) as:

$$\dot{C}_f = c_f \dot{m}_f LHV \tag{2.21}$$

The cost rate of environmental impact $\dot{C}_{env}$ was expressed in terms of the emission flow rate ($\dot{m}_{emission}$) and the emission cost per unit flow rate ($c_{emission}$) as:

$$\dot{C}_{env} = c_{emission} \dot{m}_{emissions} \tag{2.22}$$

In this work the only component of emissions that were evaluated was the NO_x. Thus, equation (2.22) can be recast as:

$$\dot{C}_{env} = c_{NO_x} \dot{m}_{NO_x EI} \tag{2.23}$$

In equation (2.23), the cost per unit flow rate of NO_x (c_{NO_x}) is expressed in \$/kg of NO_x.

The capital cost of any equipment and the cost of washing are really empirical information obtained either from the manufacturer's pricelist or collected over time at the operational site as would be in the case for cost of washing. However, from an optimization standpoint these costs need to be expressed in terms of decision variables. These can be either obtained from open literature such as those provided in Valero et. al (1994) or developed independently. The capital cost models for compressor (C_C), combustor (C_{CC}), gas generator and power turbine ($C_{G\&PT}$), heat recovery steam generator (C_{HRSG}), and air preheater (C_{APH}) are similar to those provided by Valero et. al (1994) with modifications to include the injected steam. The cost models for the inlet air cooling (C_{IAC}) and for the degradation recovery i.e. washing (C_{wash}) were developed independently based on empirical information available in open literature and relevant assumptions:

$$C_C = \left(\frac{C_{11} \dot{m}_a}{C_{12} - \eta_C} \right) PR_C \left(\ln PR_C \right) \tag{2.24}$$

$$C_{CC} = \left(\frac{C_{21} \dot{m}_a}{C_{23} - PR_{CC}} \right) \left(1 + \exp(C_{23} T_4 - C_{24}) \right) \tag{2.25}$$

$$C_{G\&PT} = \left(\frac{C_{31} (\dot{m}_a + \dot{m}_f + \dot{m}_{steaminject})}{C_{32} - \eta_{G\&PT}} \right) \ln(PR_{G\&PT}) \left(1 + \exp(C_{33} T_4 - C_{34}) \right) \tag{2.26}$$

$$C_{APH} = C_{41}\left(\frac{(\dot{m}_a + \dot{m}_f + \dot{m}_{steaminject})(h_5 - h_6)}{U_{APH} LMTD_{APH}}\right)^{0.6} \quad (2.27)$$

$$C_{HRSG} = C_{51}\left[\left(\frac{Q_{eco}}{LMTD_{eco}}\right)^{0.8} + \left(\frac{Q_{eva}}{LMTD_{eva}}\right)^{0.8}\right] + C_{52}\dot{m}_{steam} + C_{53}\left(\dot{m}_a + \dot{m}_f + \dot{m}_{steaminject}\right) \quad (2.28)$$

$$C_{IAC} = C_{61} * P_c \quad (2.29)$$

$$C_{IAC} = C_{71} * \frac{P_c}{m_{steaminject}} \quad (2.30)$$

$$C_{wash} = C_{81} * f_{onlinewash} + C_{82} + C_{83} \quad (2.31)$$

The formulation of the objective function was completed after making appropriate choice of decision variables and associated constraints. Seven different variables were chosen as the decision variables i.e., PR_C, η_C, $\dot{m}_f$, $\dot{m}_{steaminject}$, $\eta_{G\&PT}$, T_3 and $f_{onlinewash}$. The process constraints were the power to be delivered by the system ($PowerGenerated$) and the steam to be generated ($SteamGenerated$), the NO_x level to be attained (NO_xLevel), and the degradation recovery ($Degradationreco$) to be achieved. All these constraints were inequality constraints:

$$W_{system} \geq PowerGenerated \quad (2.32)$$

$$\dot{m}_{steam} \geq SteamGenerated \quad (2.33)$$

$$\dot{m}_{NO_x} \leq NO_xlevel \quad (2.34)$$

$$\eta_{reco} \geq Degradationreco \quad (2.35)$$

The equality constraints were a result of the thermodynamic performance model of the system that needs to be satisfied.

Thermodynamic performance model of cooler

Inlet air cooling can be accomplished by evaporative cooler, inlet fogging, or use of a refrigeration system either of the mechanical or absorption type. Each system has different physics and thus different cooling models. In the present work it was assumed that the air was cooled using chilled water. Such a system would be representative of using a refrigeration system. Since, the goal was to only determine the amount of cooling load required to cool the inlet air from conditions at state 0 to the conditions at state 1, the refrigeration system was not modeled. The energy required by the cooler is comprised of the energy needed to cool the dry air

from T_0 to T_1, to cool the vapor from T_0 to T_1, and if the cooling is accompanied by condensation of water vapor then the energy needed for the same.

$$\dot{Q}_{dryair} = \dot{m}_{1dryair}\left(h_{1dryair} - h_{0dryair}\right) \tag{2.36}$$

$$\dot{Q}_{vapor} = \dot{m}_{1vapor}\left(h_{1vapor} - h_{0vapor}\right) \tag{2.37}$$

$$\dot{Q}_{condensation} = \dot{m}_{condensate}\left(h_{g1vapor} - h_{l1vapor}\right) \tag{2.38}$$

$$\dot{Q}_{cooling} = \dot{Q}_{dryair} + \dot{Q}_{vapor} + \dot{Q}_{condensate} \tag{2.39}$$

The refrigeration load in tons was then calculated using:

$$Load_{refrig} = \frac{\dot{Q}_{cooling} * 1000}{1200 * 3.4121} \tag{2.40}$$

$$Power_{cooling} = \frac{Load_{refrig}}{\eta_{chiller}} \tag{2.41}$$

Equations (2.36), (2.37), and (2.38) require the following information; the amount of dry air, the amount of moisture present in the air, the amount of condensate, and the relevant enthalpies. These were determined by a detailed humidity model. Furthermore, the mass flow rate of the condensate was computed from:

$$\dot{m}_{condensate} = \dot{m}_{vapor1} - \dot{m}_{vapor0} \tag{2.42}$$

Humidity model

The humidity model was developed assuming that the moist air is a mixture of the dry air and the water vapor. The humidity model was required both at the inlet and the exit of the cooler i.e. at state 0 and 1. In the equation set developed below, subscript j denotes either 0 or 1 to determine the conditions at the state of interest. The saturated pressure of water vapor at the inlet temperature was calculated from the model provided by Flatau et. al (1992). It is a polynomial function of the temperature alone. In this work the symbol $\langle\ \rangle$ is the notation used for expressing properties evaluated as a function of other properties.

$$P_{vsat_j} = f\left\langle T_j \right\rangle \tag{2.43}$$

The partial pressure exerted by the vapor on the mixture was then obtained from the known relative humidity (ϕ_{RH_j}).

$$p_{v_j} = \phi_{RH_j} P_{vsat_j} \tag{2.44}$$

The partial pressure exerted by the dry air on the mixture was calculated by applying Dalton's law of partial pressure.

$$p_{da_j} = P_j - p_{v_j} \tag{2.45}$$

The mole fractions of the water vapor and dry air in the mixture were:

$$y_{v_j} = \frac{p_{v_j}}{P_j} \tag{2.46}$$

$$y_{da_j} = 1 - y_{v_j} \tag{2.47}$$

The molar mass of the water vapor and dry air in terms of kg/kmol of the mixture were then obtained from:

$$m_{mv_j} = y_{v_j} MW_{water} \tag{2.48}$$

$$m_{mda_j} = y_{da_j} MW_{air} \tag{2.49}$$

And the mass fractions were:

$$mf_{da_j} = \frac{m_{mda_j}}{m_{mda_j} + m_{mv_j}} \tag{2.50}$$

$$mf_{v_j} = \frac{m_{mv_j}}{m_{mda_j} + m_{mv_j}} \tag{2.51}$$

The mass of dry air and the mass of water vapor in the moisture were obtained from:

$$\dot{m}_{da_j} = \dot{m}_a * mf_{da_j} \tag{2.52}$$

$$\dot{m}_{v_j} = \dot{m}_a * mf_{v_j} \tag{2.53}$$

And, the humidity ratio was calculated from:

$$\omega_j = \frac{\dot{m}_{v_j}}{\dot{m}_{da_j}} \tag{2.54}$$

The entropy of the humid air was then obtained from:

$$s_j = \left(mf_{a_j}\right) s\left\langle p_{da_j}, T_j \right\rangle + \left(mf_{v_j}\right) s\left\langle p_{v_j}, T_j \right\rangle \tag{2.55}$$

In equation (2.55) the entropy of the dry air at the relevant partial pressure and temperature $s\left\langle p_{da_j}, T_j \right\rangle$ was obtained from a C++ property routine "Thermodynamic Properties

in SI" (TPSI) provided by Knopf (2011). The routine is based on the work done by Reynolds (1979). Similarly, the properties of water vapor were also obtained from the TPSI package.

Finally, the enthalpy of the humid air was calculated from:

$$h_{dd_j} = \left(mf_{da_j}\right) h\left\langle p_{da_j}, T_j \right\rangle \tag{2.56}$$

$$h_{v_j} = \left(mf_{v_j}\right) h\left\langle p_{vj}, T_j \right\rangle \tag{2.57}$$

$$h_j = h_{da_j} + h_{v_j} \tag{2.58}$$

Thermodynamic performance model of the compressor

The entropy at the compressor inlet s_1 was obtained from equation (2.55). For an isentropic compression, the isentropic entropy at state 2 was same as that at 1.

$$s_{2,isen} = s_1 \tag{2.59}$$

The pressure at state 2 was calculated using the decision variable (PR_{AC}).

$$P_2 = P_1 * PR_{AC} \tag{2.60}$$

The isentropic temperature and enthalpy were determined using the TPSI routines.

$$T_{2,isen} = f\left\langle P_2, s_{2,isen} \right\rangle \tag{2.61}$$

$$h_{2,isen} = f\left\langle P_2, s_{2,isen} \right\rangle \tag{2.62}$$

The enthalpy at state 2 was then determined using the known enthalpies at state 1, isentropic enthalpy at state 2, and the compressor isentropic efficiency.

$$h_2 = h_1 + \frac{h_{2,isen} - h_1}{\eta_{AC}} \tag{2.63}$$

Subsequently, the temperature at state 2 was obtained from the TPSI package.

$$T_2 = f\left\langle P_2, s_2 \right\rangle \tag{2.64}$$

Thermodynamic performance model of the air preheater – air side

The pressure downstream of the preheater on the air side was obtained using a known pressure drop. It should be recalled that the temperature at state 3 was a decision variable and thus a user specified value would commence the calculations.

$$P_3 = P_2\left(1 - \Delta p_{APH,a}\right) \tag{2.65}$$

The enthalpy at state 3 was obtained from the TPSI property routine.

$$h_3 = f\left\langle P_3, T_3 \right\rangle \tag{2.66}$$

Thermodynamic performance model of the combustor

The pressure at state 4, i.e., downstream of the combustion chamber was calculated similar to the state 3 except for the use of a known pressure drop across the combustor.

$$P_4 = P_3\left(1-\Delta p_{CC}\right) \tag{2.67}$$

The mass and energy conservation across the combustion chamber resulted in the following equations:

$$\dot{m}_a + \dot{m}_f + \dot{m}_{steaminject} = \dot{m}_g \tag{2.68}$$

$$\dot{m}_a\left(h_3 - h_{a,ref}\right) + \dot{m}_f LHV = \dot{m}_g\left(h_4 - h_{g,ref}\right) + \dot{Q}_{CC} \tag{2.69}$$

Where,
$$\dot{Q}_{CC} = \dot{m}_f LHV\left(1-\eta_{CC}\right) \tag{2.70}$$

Equation (2.69) can be recast as:

$$\dot{m}_a\left(h_3 - h_{a,ref}\right) + \dot{m}_f LHV = \dot{m}_g\left(h_4 - h_{g,ref}\right) + \dot{m}_f LHV\left(1-\eta_{CC}\right) \tag{2.71}$$

$$\dot{m}_a\left(h_3 - h_{a,ref}\right) + \dot{m}_f LHV\eta_{CC} = \dot{m}_g\left(h_4 - h_{g,ref}\right) \tag{2.72}$$

$$\dot{m}_a\left(h_3 - h_{a,ref}\right) + \dot{m}_f LHV\eta_{CC} = \left(\dot{m}_a + \dot{m}_f + \dot{m}_{steaminject}\right)\left(h_4 - h_{g,ref}\right) \tag{2.73}$$

$$\left(h_4 - h_{g,ref}\right) = \frac{\dot{m}_a\left(h_3 - h_{a,ref}\right) + \dot{m}_f LHV\eta_{CC}}{\left(\dot{m}_a + \dot{m}_f + \dot{m}_{steaminject}\right)} \tag{2.74}$$

In equation (2.74) fuel flow rate ($\dot{m}_f$) and the steam injected ($\dot{m}_{steaminject}$) were both decision variables. The enthalpies at the reference condition were determined from:

$$h_{a,ref} = f\left\langle P_{a,ref}, T_{a,ref} \right\rangle \tag{2.75}$$

$$h_{g,ref} = f\left\langle P_{g,ref}, T_{g,ref} \right\rangle \tag{2.76}$$

The formulation of equation (2.74) is left at $h_4 - h_{g,ref}$ because the combustion library implemented here uses that as an input for the calculations or returns that as an output. The calculations of the product side properties involve combustion reaction calculations and thus the same are explained next.

Combustion reaction calculations

The combustion reaction of a moles of a hydrocarbon fuel with b moles of dry air (DA) along with steam injection is expressed as:

$$a\left(C_xH_y\right)+b\left(DA\right)+c\left(H_2O\right)\rightarrow d\left(CO_2\right)+e\left(H_2O\right)+f\left(DA\right)-g\left(O_2\right) \tag{2.77}$$

A chemical balance of the above gives the molar constituents of the products as:

$$d=ax \tag{2.78}$$

$$e=a\frac{y}{2}+c \tag{2.79}$$

$$f=b \tag{2.80}$$

$$g=a\left(x+\frac{y}{4}\right) \tag{2.81}$$

Usually, the steam injected is expressed as a mass fraction of the dry air. Thus, if Z denotes the mass fraction of steam (%) then the corresponding molar constituent of the injected steam is given by:

$$c=\frac{Z}{100}b\frac{MW_{air}}{MW_{H_2O}} \tag{2.82}$$

The mole fraction of nitrogen (y_{in,N_2}), oxygen (y_{in,O_2}) and argon ($y_{in,Ar}$) in dry air are assumed as 0.7809, 0.2095 and 0.0096. With the molar constituents of the products known, the mole fraction of each product was calculated as:

$$y_{CO_2}=\frac{d}{d+e+f-g} \tag{2.83}$$

$$y_{CO_2}=\frac{ax}{ax+a\frac{y}{2}+c+b-a(x+\frac{y}{4})} \tag{2.84}$$

$$y_{CO_2}=\frac{x}{x+\frac{y}{2}+\frac{c}{a}+\frac{b}{a}-(x+\frac{y}{4})} \tag{2.85}$$

$$y_{CO_2}=\frac{x}{x+\frac{y}{2}+\frac{\frac{Z}{100}b\frac{MW_{air}}{MW_{H_2O}}}{a}+\frac{b}{a}-(x+\frac{y}{4})} \tag{2.86}$$

$$y_{CO_2} = \frac{x}{x + \frac{y}{2} + \frac{Z}{100}\frac{b}{a}\frac{MW_{air}}{MW_{H_2O}} + \frac{b}{a} - (x + \frac{y}{4})} \tag{2.87}$$

$$y_{CO_2} = \frac{x}{x + \frac{y}{2} + \frac{b}{a}\left(\frac{Z}{100}\frac{MW_{air}}{MW_{H_2O}} + 1\right) - (x + \frac{y}{4})} \tag{2.88}$$

Equation (2.88) was developed at the molar level. However, the amount of air and the fuel supplied is usually presented as mass flow rates. The air-to-fuel ratio is expressed as:

$$AFR = \frac{\dot{m}_a}{\dot{m}_f} \tag{2.89}$$

Further the stoichiometric air-to-fuel ratio (AFR_{stoich}) is the amount of the air required for complete combustion of one mole of fuel. Thus, the ratio of the actual air-to-fuel ratio to the stoichiometric air-to-fuel-ratio is the excess dry air (DAR) in the combustion process and is:

$$DAR = \frac{AFR_{actual}}{AFR_{stoich}} \tag{2.90}$$

The moles of dry air used for complete combustion is:

$$= \frac{x + \frac{y}{4}}{y_{in,O_2}} \tag{2.91}$$

Thus, the amount of dry air used for actual combustion is:

$$= DAR\left(\frac{x + \frac{y}{4}}{y_{in,O_2}}\right) \tag{2.92}$$

However, the amount of dry air used for the combustion of a moles of fuel is $\frac{b}{a}$. Therefore, we get:

$$\frac{b}{a} = DAR\left(\frac{x + \frac{y}{4}}{y_{in,O_2}}\right) \tag{2.93}$$

Substituting, from equation (2.93) to (2.88) we get:

$$y_{CO_2} = \frac{x}{x + \frac{y}{2} + DAR\left(\frac{x + \frac{y}{4}}{y_{in,O_2}}\right)\left(\frac{Z}{100}\frac{MW_{air}}{MW_{H_2O}} + 1\right) - (x + \frac{y}{4})} \tag{2.94}$$

$$y_{CO_2} = \frac{1}{1 + \frac{y}{2x} + DAR\left(\frac{1 + \frac{y}{4x}}{y_{in,O_2}}\right)\left(\frac{Z}{100}\frac{MW_{air}}{MW_{H_2O}} + 1\right) - (1 + \frac{y}{4x})} \tag{2.95}$$

$\frac{y}{x}$ is the ratio of the hydrogen atoms to the carbon atoms in the fuel and defining it as *HbyCRatio* then equation (2.95) becomes:

$$y_{CO_2} = \frac{1}{1 + \frac{HbyCRatio}{2} + DAR\left(\frac{1 + \frac{HbyCRatio}{4}}{y_{in,O_2}}\right)\left(\frac{Z}{100}\frac{MW_{air}}{MW_{H_2O}} + 1\right) - (1 + \frac{HbyCRatio}{4})} \tag{2.96}$$

$$y_{CO_2} = \frac{1}{\left(\frac{2 + HbyCRatio}{2}\right) + DAR\left(\frac{\frac{4 + HbyCRatio}{4}}{y_{in,O_2}}\right)\left(\frac{Z}{100}\frac{MW_{air}}{MW_{H_2O}} + 1\right) - \left(\frac{4 + HbyCRatio}{4}\right)} \tag{2.97}$$

$$y_{CO_2} = \frac{1}{\left(\frac{HbyCRatio + 2}{2}\right) + DAR\left(\frac{\frac{HbyCRatio + 4}{4}}{y_{in,O_2}}\right)\left(\frac{Z}{100}\frac{MW_{air}}{MW_{H_2O}} + 1\right) - \left(\frac{HbyCRatio + 4}{4}\right)} \tag{2.98}$$

$$y_{CO_2} = \frac{1}{\left(\frac{HbyCRatio + 2}{2}\right) + \frac{HbyCRatio + 4}{4}\left(DAR\left(\frac{1}{y_{in,O_2}}\right)\left(\frac{Z}{100}\frac{MW_{air}}{MW_{H_2O}} + 1\right) - 1\right)} \tag{2.99}$$

$$y_{CO_2} = \frac{1}{\left(\frac{HbyCRatio + 2}{2}\right) + \frac{HbyCRatio + 4}{4}\left(\frac{DAR}{y_{in,O_2}}\left(\frac{Z}{100}\frac{MW_{air}}{MW_{H_2O}} + 1\right) - 1\right)} \tag{2.100}$$

If $\frac{HbyCRatio+4}{4}$ is designated as $SpentO_2$ then equation (2.100) becomes:

$$y_{out,CO_2} = \frac{1}{\left(\frac{HbyCRatio+2}{2}\right) + SpentO_2\left(\frac{DAR}{y_{in,O_2}}\left(\frac{Z}{100}\frac{MW_{air}}{MW_{H_2O}}+1\right)-1\right)} \tag{2.101}$$

Equation (2.101) gives the mole fraction of CO_2 in the product stream in terms of $HbyCRatio$, $SpentO_2$, and DAR.

The mole fraction of water vapor (y_{out,H_2O}) was:

$$y_{out,H_2O} = \frac{e}{d+e+f-g} \tag{2.102}$$

But,

$$d+e+f-g = \frac{d}{y_{out,CO_2}} \tag{2.103}$$

$$y_{out,H_2O} = \frac{e}{\frac{d}{y_{out,CO_2}}} \tag{2.104}$$

$$y_{out,H_2O} = \frac{e}{d} y_{out,CO_2} \tag{2.105}$$

$$y_{out,H_2O} = \frac{a\frac{y}{2}+c}{ax} y_{out,CO_2} \tag{2.106}$$

$$y_{out,H_2O} = \frac{\frac{y}{2}+\frac{c}{a}}{x} y_{out,CO_2} \tag{2.107}$$

$$y_{out,H_2O} = y_{out,CO_2}\left(\frac{\frac{Z}{100}\frac{b}{a}\frac{MW_{air}}{MW_{H_2O}}}{x} + \frac{y}{2x}\right) \tag{2.108}$$

$$y_{out,H_2O} = y_{out,CO_2}\left(\frac{y}{2x} + \frac{1}{x}\frac{Z}{100}\frac{b}{a}\frac{MW_{air}}{MW_{H_2O}}\right) \tag{2.109}$$

$$y_{out,H_2O} = y_{out,CO_2}\left(\frac{y}{2x} + \frac{1}{x}\frac{Z}{100}DAR\left(\frac{x+\frac{y}{4}}{y_{in,O_2}}\right)\frac{MW_{air}}{MW_{H_2O}}\right) \tag{2.110}$$

$$y_{out,H_2O} = y_{out,CO_2}\left(\frac{HbyCRatio}{2} + \frac{Z}{100}DAR\left(\frac{1+\frac{HbyCRatio}{4}}{y_{in,O_2}}\right)\frac{MW_{air}}{MW_{H_2O}}\right) \tag{2.111}$$

$$y_{out,H_2O} = y_{out,CO_2}\left(\frac{HbyCRatio}{2} + \frac{Z}{100}DAR\left(\frac{\frac{HbyCRatio+4}{4}}{y_{in,O_2}}\right)\frac{MW_{air}}{MW_{H_2O}}\right) \tag{2.112}$$

$$y_{out,H_2O} = y_{out,CO_2}\left(\frac{HbyCRatio}{2} + \frac{Z}{100}DAR\left(\frac{SpentO_2}{y_{in,O_2}}\right)\frac{MW_{air}}{MW_{H_2O}}\right) \tag{2.113}$$

Equation (2.113) provides the mole fraction of H_2O in the product stream in terms of $HbyCRatio$, $SpentO_2$, and DAR.

The purpose of expressing the mole fractions of the product stream in terms of $HbyCRatio$, $SpentO_2$, and DAR was to be able to make the modification in the C++ routine provided as part of the TPSI package to compute the product side enthalpy, entropy, and the combustor exit temperature. The original TPSI formulation did not allow for the injection of steam into combustor and thus the C++ routine needed modifications. The mole fractions of the excess air in the product stream, nitrogen and argon remained unchanged from the original formulation presented by Knopf (2011):

$$y_{out,Ar} = y_{out,CO_2}\frac{y_{in,Ar}}{y_{in,O_2}}SpentO_2 \tag{2.114}$$

$$y_{out,N_2} = y_{out,CO_2}\frac{y_{in,N_2}}{y_{in,O_2}}SpentO_2 \tag{2.115}$$

$$y_{out,N_2} = \frac{(DAR-1)\,y_{out,CO_2}SpentO_2}{y_{in,O_2}} \tag{2.116}$$

The fuel here was assumed to be pure methane and thus $x = 1$ and $y = 4$. The enthalpy at point 4 was used to calculate the combustor exit temperature. However, the temperature was additionally a function of DAR, $HbyCRatio$, and Z. Thus,

$$T_4 = f\left\langle P_4, \left(h_4 - h_{ref}\right), DAR, HbyCRatio, Z \right\rangle \tag{2.117}$$

And the entropy was, $s_4 = f\left\langle P_4, T_4, DAR, HbyCRatio, Z \right\rangle$ (2.118)

Thermodynamic performance model of the turbine

For the gas generator and power turbine combination assuming an isentropic expansion the isentropic entropy at state 5 was then known.

$$s_{5isen} = s_4 \tag{2.119}$$

The pressure at state 5 was obtained from using a known pressure drop across the gas side of the air preheater.

$$P_5 = \frac{P_6}{1 - \Delta p_{APH,g}} \tag{2.120}$$

The isentropic temperature and enthalpy were computed at state 5. These along with the isentropic efficiency of the turbine were then used to calculate the enthalpy at state 5. It may be recalled that the isentropic efficiency of the turbine was assumed as a decision variable.

$$T_{5isen} = f\left\langle s_{5isen}, P_5, DAR, HbyCRatio, Z \right\rangle \tag{2.121}$$

$$h_{5isen} = f\left\langle P_5, T_{5isen}, DAR, HbyCRatio, Z \right\rangle \tag{2.122}$$

$$h_5 = h_4 - \frac{h_4 - h_{5isen}}{\eta_{G\&PT}} \tag{2.123}$$

$$T_5 = f\left\langle h_5, P_5, DAR, HbyCRatio, Z \right\rangle \tag{2.124}$$

Thermodynamic performance model of the air preheater- gas side

An energy balance on the gas side of the air-preheater led to the following:

$$\dot{m}_a\left(h_3 - h_2\right) = \dot{m}_g\left(h_5 - h_6\right) \tag{2.125}$$

$$\dot{m}_a\left(h_3 - h_2\right) = \left(\dot{m}_a + \dot{m}_f + \dot{m}_{steaminject}\right)\left(h_5 - h_6\right) \tag{2.126}$$

$$h_6 = h_5 - \frac{\dot{m}_a \left(h_3 - h_2\right)}{\dot{m}_a + \dot{m}_f + \dot{m}_{steaminject}} \tag{2.127}$$

The pressure at state 6 was known from the pressure drop across the HRSG and the pressure to the stack which was assumed to be ambient.

$$P_6 = P_7 \left(1 - \Delta p_{HRSG}\right) \tag{2.128}$$

$$P_7 = P_1 \tag{2.129}$$

The logarithmic mean temperature difference for the air preheater ($LMTD_{APH}$) required for the cost model was:

$$LMTD_{APH} = \frac{\left(T_5 - T_3\right) - \left(T_6 - T_2\right)}{\ln\left[\frac{\left(T_5 - T_3\right)}{\left(T_6 - T_2\right)}\right]} \tag{2.130}$$

Thermodynamic performance model of heat recovery steam generator

In the heat recovery steam generator (HRSG), the exhaust gas first enters the evaporator section and then the economizer section. In the HRSG the additional parameters of interest are the pinch temperature difference and the approach temperature difference. In the economizer section water enters at conditions T_8 and P_8 and is heated to a temperature slightly less than the saturation temperature of the steam. The temperature to which the water is heated is known as the approach temperature. The difference between the approach temperature and the saturation temperature is the approach temperature difference ($\Delta T_{approach}$). On the evaporator side, the exhaust gas enters the HRSG at conditions T_6 and P_6 and exits the evaporator at a temperature higher than the saturation temperature of water. The difference between the temperature the gas exits the evaporator and the saturation temperature of water is the pinch temperature difference (ΔT_{pinch}). The temperatures at the pinch and approach point, T_{7p} and T_{8p} were calculated using a pre-defined approach and pinch temperature differences.

$$T_{8P} = T_9 - \Delta T_{approach} \tag{2.131}$$

$$T_{7P} = T_9 + \Delta T_{pinch} \tag{2.132}$$

The pressure at the pinch point (P_{7p}) was an average of the pressures at state 6, and 7 while the enthalpy was obtained from the modified TPSI package.

$$P_{7p} = \frac{P_7 + P_6}{2} \tag{2.133}$$

$$h_{7p} = f\left\langle T_{7p}, P_{7p}, DAR, HbyCRatio, Z \right\rangle \tag{2.134}$$

The heat lost by the evaporator was calculated as:

$$\dot{Q}_{eva} = \dot{m}_g \left(h_6 - h_{7p} \right) \tag{2.135}$$

$$\dot{Q}_{eva} = \left(\dot{m}_a + \dot{m}_f + \dot{m}_{steaminject} \right)\left(h_6 - h_{7p} \right) \tag{2.136}$$

The pressure at 8p was assumed to be the same as at 8, and 9. Thus,

$$P_{8p} = P_9 \tag{2.137}$$

$$P_8 = P_9 \tag{2.138}$$

An energy balance on the gas side and the steam side of the evaporator provided the rate of steam generation:

$$\dot{m}_s = \frac{\dot{Q}_{eva}}{h_9 - h_{8p}} \tag{2.139}$$

It may be recalled from the discussion earlier that the enthalpy h_9 is the enthalpy of superheated steam at the pressure P_9 and temperature T_9. The pressure P_9 and temperature T_9 are dictated by the plant requirements. The heat gained by the economizer was:

$$\dot{Q}_{eco} = \dot{m}_w \left(h_{8p} - h_8 \right) \tag{2.140}$$

The enthalpy and temperature at 7 were calculated from:

$$h_7 = h_{7p} - \frac{\dot{Q}_{eco}}{\dot{m}_a + \dot{m}_f + \dot{m}_{steaminject}} \tag{2.141}$$

$$T_7 = f\left\langle h_7, P_7, DAR, HbyCRatio, Z \right\rangle \tag{2.142}$$

The logarithmic mean temperature difference for the economizer ($LMTD_{eco}$) and the evaporator ($LMTD_{eva}$) required for the cost model were:

$$LMTD_{eco} = \frac{\left(T_{7P} - T_{8p} \right) - \left(T_7 - T_8 \right)}{\ln\left[\frac{\left(T_{7P} - T_{8p} \right)}{\left(T_7 - T_8 \right)} \right]} \tag{2.143}$$

$$LMTD_{eva} = \frac{\left(T_6 - T_9\right) - \left(T_{7p} - T_{8p}\right)}{\ln\left[\frac{\left(T_6 - T_9\right)}{\left(T_{7p} - T_{8p}\right)}\right]} \tag{2.144}$$

Thermodynamic performance model of the system

Finally, the compressor work required and the turbine power generated were calculated from:

$$W_C = \dot{m}_a \left(h_2 - h_1\right) \tag{2.145}$$

$$W_{G\&PT} = \left(\dot{m}_a + \dot{m}_f + \dot{m}_{steaminject}\right)\left(h_4 - h_5\right) \tag{2.146}$$

And the system work was:

$$W_{system} = W_{G\&PT} - W_C - Power_{IAC} \tag{2.147}$$

Degradation model

As seen earlier, the fundamental impact of degradation is loss of system output. Since, the system has to continuously meet the process constraints, therefore, the most optimal values of decision variables are not necessarily the same as time progresses. The operation and optimization model developed here was not a time dependent model so the influence of degradation over time could not be modeled directly. However, the determination of optimal system information can be done at different snapshots in time. For such a model, degradation factors that correct the performance of a new machine at different time intervals can be incorporated. The optimization would then provide new optimal values for the system performance which would include the degradation of the machine over time. The models to establish the suitable values of the correction factors would have to come from empirical data. The CTOOM-OPTIMIZE model includes degradation factors for compressor pressure ratio, compressor efficiency and turbine efficiency. When these degradation factors are set to 1, the evaluation is exactly as that of a new machine. When these variables have suitable values that are reflective of the current state of the machine then the optimal values determined are for a degraded machine. A simple model as explained above would allow the user of new machine to know and forecast the departure from the new machine optimal decision variable values as the machine is in service.

A slightly more sophisticated model would be to determine machine maintenance strategies that could recover some of the degradation. Figure 2-4 illustrates the performance decrease due to fouling over time (service hours) as presented by Diakunchak (1991). It can be seen that washing/cleaning of the machine can recover some of the degradation. Figure 2-4 does not show any numbers because these can vary widely from 8% loss of power over two weeks to 4.3% over six months (Diakunchak. 1991) of continuous operation for a compressor that was not cleaned.

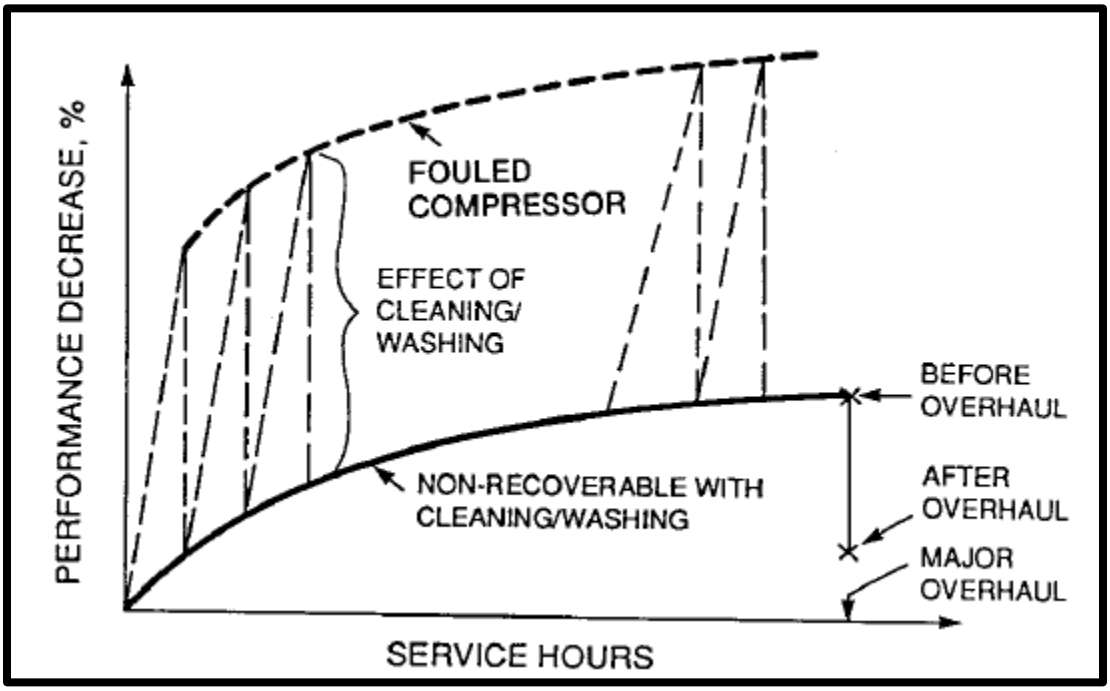

Figure 2-4 Effect of washing on a fouled compressor (Diakunchak. 1991)

However, 99.5% of the power short fall was recovered using a series of online water washes at reduced load (Diakunchak. 1991). Figure 2-4 shows the performance decrease to be an exponentially increasing function over time. On the contrary, as seen in Figure 2-5, Anonymous (2005) presents the performance decrease to be a linear function over time. In this work, a linear function (Figure 2-6) was assumed. Thus, considering the overall loss in performance at the end of 8000 hours of operation as 2.4% of the design performance, the loss recovery due to washing can be presented as a function of the frequency of both the on-line washing and the off-line washing. If the loss recovered due to the off-line washing is assumed to be a constant then the loss recovered due to the on-line washing is:

$$l_{totalreco} = l_{onlinereco} + l_{offlinereco} \tag{2.148}$$

$$l_{totalreco} = \left(-0.0071 * f_{onlinewashing} + 1.175\right) + l_{offlinereco} \quad (2.149)$$

In equation (2.149) $l_{offlinereco}$ is set at 1.3954%.

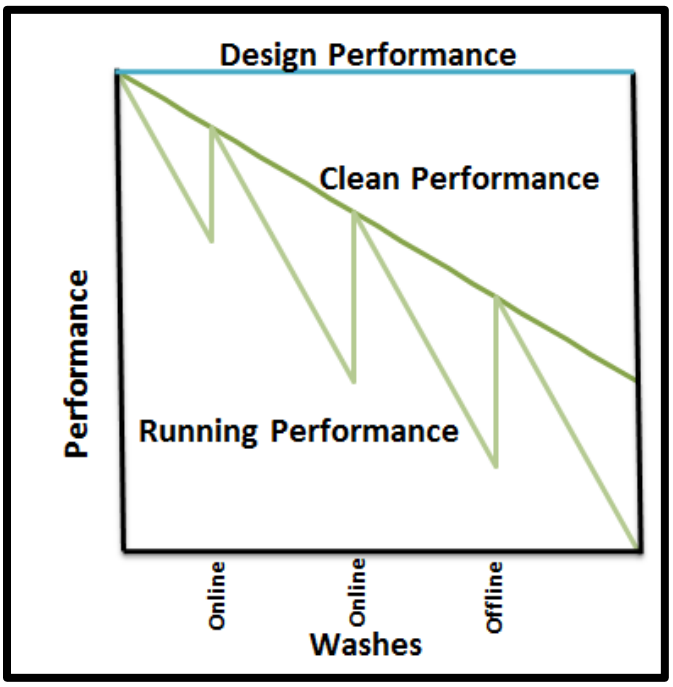

Figure 2-5 Effect of on-line and off-line washing on efficiency (Anonymous. 2005)

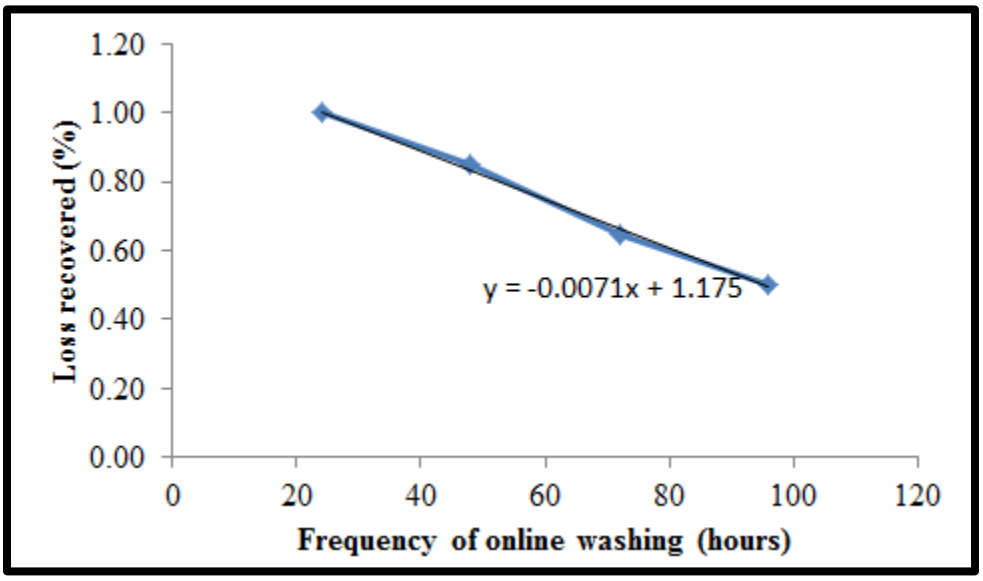

Figure 2-6 Loss recovery due to online washing

Emissions model

In this work the focus of emissions was on NO_x. Thus, only NO_x models are reviewed. The most fundamental NO_x prediction model, the Zeldovich model is obtained from the solution of the combustion equation with all relevant reaction mechanisms. However, from the optimization standpoint, a simpler correlation based emissions prediction model was a more suitable approach. From the CT standpoint, the five most widely accepted NO_x emission models (Lefebvre. 1984, Lewis. 1991, Odgers and Kretschmer. 1985, Rizk and Mongia. 1994, Rokke, et al. 1993) are presented below:

$$\dot{m}_{NOx} = \frac{9\times10^{-8} P^{1.25} V_c \exp\left(0.01 T_{st}\right)}{\dot{m}_a T_{pz}} \tag{2.150}$$

$$\dot{m}_{NOx} = 3.32\times10^{-6} \exp\left(0.008 T_c\right) P^{0.5} \tag{2.151}$$

$$\dot{m}_{NOx} = 29 \exp\left(\frac{-21670}{T_c}\right) P^{0.66} \left[1-\exp\left(-250\tau\right)\right] \tag{2.152}$$

$$\dot{m}_{NOx} = 15.1^{14} \left(t - 0.5 t_e\right) \exp\left(\frac{-71100}{T_{st}}\right) P^{-0.05} \left(\frac{\Delta P}{P}\right)^{-0.5} \tag{2.153}$$

$$\dot{m}_{NOx} = 18.1 P^{1.42} \dot{m}_a \left(FAR\right)^{0.72} \tag{2.154}$$

All the above models were based upon specific combustor geometry and are not necessarily universal models. However, for this work from the optimization standpoint, the objective was to implement a NO_x model, the suitability of which was dependent on the choice of decision variables. Equation (2.150) needed information about the combustion volume (V_c) and the primary zone temperature (T_{pz}). The combustion model implemented in this work was not a zone based model and thus, the primary zone temperature was not available. Therefore, this model was not found suitable. Equation (2.152) was more suitable for aircraft combustors and thus, was not considered as a candidate here. Equation (2.153) required the calculation of evaporation time (t_e) and the knowledge or assumption of the residence time (t) and was not considered to be a suitable choice. Equation (2.154) was expressed in terms of mass flow rate of air and the fuel-to-air ratio. However, in the problem set up since the cost of fuel was minimized wherein the solution always seeks the lowest fuel flow rate, therefore, any NO_x correlation based on air flow rate and the fuel-to-air ratio was not a suitable model. A NO_x model in terms of the

combustion temperature (T_c) as presented by Lewis (1991) in the equation (2.151) was the most suitable. The coefficient 0.008 was corrected to 0.108 to ensure reasonable values of NO_x for the dataset in consideration in this study. Thus, the NO_x model used for this work was:

$$\dot{m}_{NO_x} = 3.32 \times 10^{-6} \exp\left(0.108 T_c\right) P^{0.5} \tag{2.155}$$

The NO_x value obtained using equation (2.155) was in ppmv. This was converted to the emissions index (EI) using the rule of thumb suggested by (Lefebvre and Ballal. 2010) :

$$\dot{m}_{NO_x EI} = \frac{\dot{m}_{NO_x ppmv}}{12.1} \tag{2.156}$$

$$\dot{m}_{NO_x} = \frac{\dot{m}_{NO_x EI}}{1000} * \dot{m}_f \tag{2.157}$$

The emissions index (EI) is in grams of NO_x per kg of fuel. The conversion was necessary since the cost of environmental impact due to NO_x emissions in equation (2.22) was expressed in $/ kg of NO_x.

Optimization solver

The minimization of the objective function formulated above subject to process and thermodynamic constraints for seven decision variables is a classic multivariable non-linear optimization problem of a single objective function. There are many techniques to solve such a problem and a review of these techniques are available in Vanderplaats (2005) and Rao (2010). The technique used in this study was the Generalized Reduced Gradient (GRG) search algorithm. The solver is based on the sparse implementation of the GRG algorithm as provided by Drud (1994). The global optimum was determined using the algorithm presented by Lasdon, et al. (2002) which uses different starting points and solves each to a local optimum and then returns the best solution found. The solver used was available as a DLL plugin for MS EXCEL called What's Best! (Anonymous. 2011) supplied by LINDO systems. The advantage of using the plugin was the ability to use Excel to develop the model.

Chapter 3 - Component level turbomachinery models-Compressor

Aero-thermodynamic performance modeling

Aero-thermodynamic performance modeling of a turbomachine can be done using high fidelity 3D or 2D models or low fidelity 1D models. The 3D turbulent flow solution is a full blown CFD problem that is computationally expensive and was not a suitable option for this development of this tool. The next possible alternative was to use a 2D axisymmetric solution also known as the hub to shroud analysis. In a hub to shroud analysis the conservation equations in the differential form are solved numerically. Of significant interest is the conservation of momentum solution which provides the radial variation of axial velocity. To accomplish this, the annulus domain of interest is divided into number of stream tubes and the solution is carried out in each stream tube. Since the path of the streamtube is not known a priori hence computation is commenced with a guessed path and the mass conservation is used to correct the stream tube path in each iteration. The solution technique is presented by (Novak. 1966, Novak. 1973, Novak and Hearsey. 1976, Novak and Hearsey. 1976, Novak and Hearsey. 1977, Wu. 1952). However, a close examination of the scheme showed that apart from the radial distribution of the axial velocity no additional advantage was gained from the performance stand point. Furthermore, the performance characteristics were finally mass averaged over the passage. The 1D passage averaged solution technique uses non-linear algebraic equations as the mathematical model. These have been widely reported (Bathie. 1996, Farokhi. 2009, Mattingly. 1996) in the literature and were a suitable choice from an implementation standpoint for developing this tool. 1D model would provide sufficient correlation with actual tested performance data as long as the loss characterization is accurately done and therefore, a hub to shroud analysis does not provide any additional advantages over the 1D technique. Thus, the 1D method also known as the mean line or pitch line was chosen since it provided the appropriate combination of capturing sufficient details without sacrificing computational speed. Irrespective of the choice of 1D, 2D or 3D models the most fundamental concept in any turbomachinery are the Euler's equation and the velocity diagrams which have been reviewed next. The concepts are illustrated using a compressor but would apply to a turbine as well.

Compressor construction

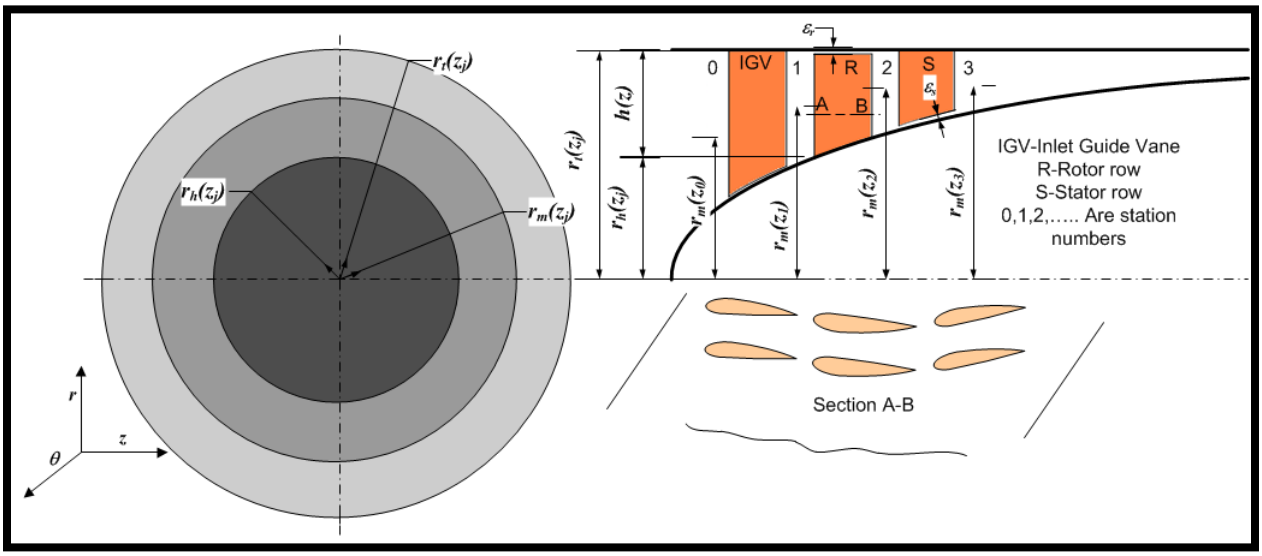

Figure 3-1 Cross section of a compressor

An axial compressor is a series of blade rows that are alternately either fixed to the casing or the hub and can be best visualized in the cross sectional view shown in Figure 3-1. The blade row fixed to the casing is called the stator while the one fixed to the hub is called the rotor. The hub of the axial compressor is mounted on a shaft (not shown in the Figure) that rotates and thus the rotor rows are the rotating set of blade rows while the stator rows are the stationary set. The combination of one rotor row and the subsequent stator row constitutes a stage of the compressor. Often, the rotor may be preceded by a stationary blade row called the inlet guide vane. The purpose of the inlet guide vane (IGV) is to provide the necessary swirl to the entering fluid. As seen in the Figure 3-1 the hub has a continuously increasing cross sectional area as traversed axially (in the z direction) while the casing has a fixed cross sectional area. This results in a continuously decreasing annulus area between the casing and the hub and is the most fundamental geometric parameter that influences the aero-thermodynamic performance of the compressor. From a modeling standpoint, the annulus areas of interest are the regions in between the blade rows. These regions are known as stations. Thus, as seen in Figure 3-1, station 0 represents the inlet to the IGV, station 1 represents the inlet to rotor row 1 and the exit of the IGV, station 2 is at the exit of the rotor row 1 and inlet of stator row 1, station 3 is at the exit of stator row 1 and so on. The annulus area at any station j is given by (Mattingly. 1996):

$$A_j = 2\pi * r_m\left\langle z_j \right\rangle * \left(r_t\left\langle z_j \right\rangle - r_h\left\langle z_j \right\rangle \right) \tag{3.1}$$

In the equation (3.1), $r_m\left\langle z_j\right\rangle$ is the mean radius at station j and is modeled as (Mattingly. 1996):

$$r_m\left\langle z_j\right\rangle = \frac{r_t\left\langle z_j\right\rangle + r_h\left\langle z_j\right\rangle}{2} \tag{3.2}$$

Apart from the annulus area the other parameters that influence the performance are the attributes of the blade geometry. Figure 3-2 illustrates each of these attributes. Figure 3-2 also shows the sign convention that was used for this work. Using the sign convention shown, the attributes θ, γ, κ_i, and κ_e are negative for the rotor row while they are positive for the stator row. It is customary to define the airfoil using the following ratios: solidity ($\frac{c}{s}$), maximum thickness-to-chord ($\frac{t_m}{c}$), trailing edge thickness-to-chord ($\frac{t_e}{c}$), point of maximum camber-to-chord ($\frac{a}{c}$), and throat opening-to-pitch ($\frac{o}{s}$). The blade pitch (s) is a function of the radius at which it is evaluated and the number of blades:

$$s = \frac{2\pi r_{eval}}{N_{blades}} \tag{3.3}$$

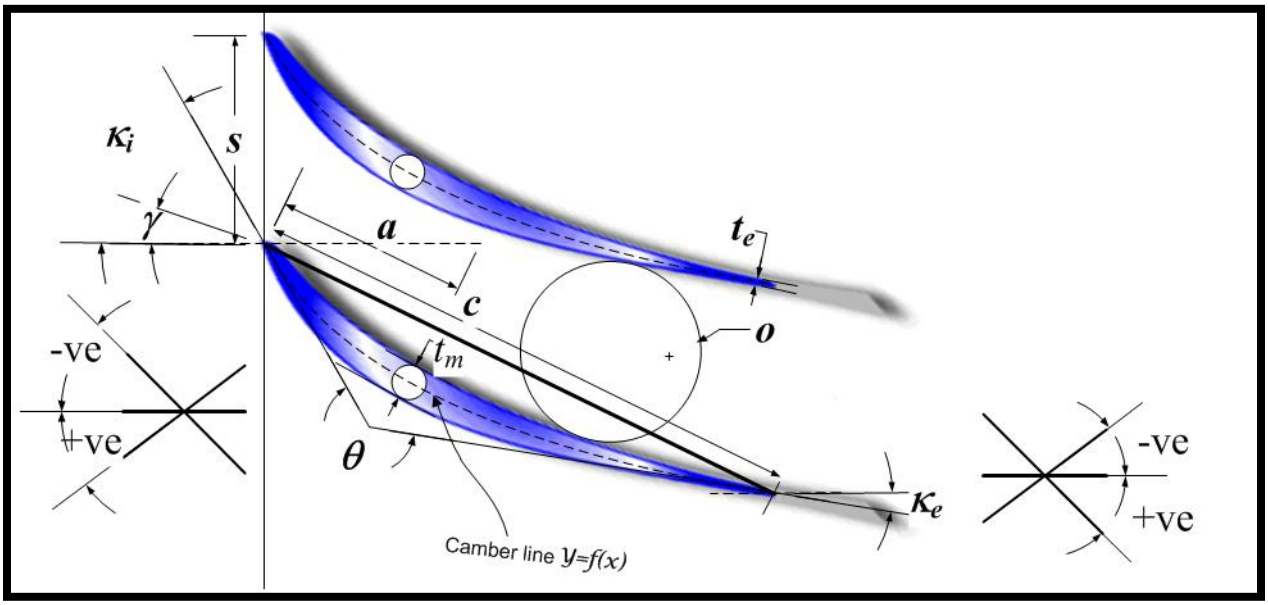

Figure 3-2 Blade geometry

Sometimes, as in the case of NACA 65 series, the airfoils are designated by their lift coefficient (C_{l0}) and maximum thickness-to-chord ratio ($\frac{t_b}{c}$). In such case, the blade camber angle θ is calculated from the lift coefficient C_{l0} by equation (3.4).

$$\tan\frac{\theta}{4} = 0.05515 C_{l0}\left(\frac{a}{c}\right) \tag{3.4}$$

Further, the blade metal angles at inlet and exit (κ_i and κ_e) are related to the blade stagger (γ) and camber angles (θ) by equations (3.5) and (3.6).

$$|\kappa_i| + |\kappa_e| = 2\gamma \tag{3.5}$$

$$|\kappa_i| - |\kappa_e| = \theta \tag{3.6}$$

The absolute values in equations (3.5) and (3.6) ensure that the same formulation can be also be used for the blade rows where these angles have a negative sign. As stated earlier, in this work the rotor row is that blade row. Thus, as long as any two of the four angles ($\kappa_i, \kappa_e, \gamma, \theta$) are known the other two can be determined. It has been seen earlier that θ can either be user defined or computed from a user defined value of C_{l0}. Furthermore, it is a common practice to specify γ instead of κ_i and κ_e. That is because in a compressor γ for stator rows is often allowed to be changed during operation to optimize the compressor performance. In CTOOMCOMP1DPERF the necessary input blade attributes are parameters N_{blades}, r_{eval}, $\frac{a}{c}$, c, γ, $\frac{t_b}{c}$, $\frac{t_e}{c}$, and either θ or C_{l0}. Finally, CTOOMCOMP1DPERF, being a mean-line analysis solver, the evaluation radius (r_{eval}) is the mean radius $r_m\left\langle z_j \right\rangle$ unless any other radius is explicitly user defined for evaluation.

The ratio ($\frac{o}{s}$) can be computed either by calculating the throat opening (o) directly or use an empirical model. The direct method utilizes the blade stagger angle, camberline and profile coordinates to locate the minimum distance between the blades i.e., the throat opening (o). The empirical model is obtained from the family of curves published by Dunavant et al., (1955) that relates the ratio ($\frac{o}{s}$) to the stagger angle and the lift coefficient.

$$\frac{o}{s}=\left\{1-\frac{t}{c}\sqrt{\sigma}\cos\left[\gamma\left(1-0.05C_{l0}^{1.5}\right)+5C_{l0}^{1.5}-2\right]\right\}^{\sqrt{\sigma}} \tag{3.7}$$

Velocity Triangles

In a compressor energy is removed from the fluid by the rotating components or the rotor row. The Euler's equation relates the change in angular momentum to the change in energy across the rotor row. In order to determine the change in angular momentum the velocity distribution in the flow field should be known. This is best characterized by velocity triangles. Figure 3-3 illustrates the velocity triangles on the $z-\theta$ plane for one stage of the compressor. The $z-\theta$ plane is at the evaluation radius (r_{eval}) between the hub and tip at a particular station. For a mean-line analysis the $z-\theta$ plane is at the mean radius ($r_m\langle z_j\rangle$) at each station. For 2D and 3D analyses the velocity triangles at different radii are necessary since analysis is done at more than one radius.

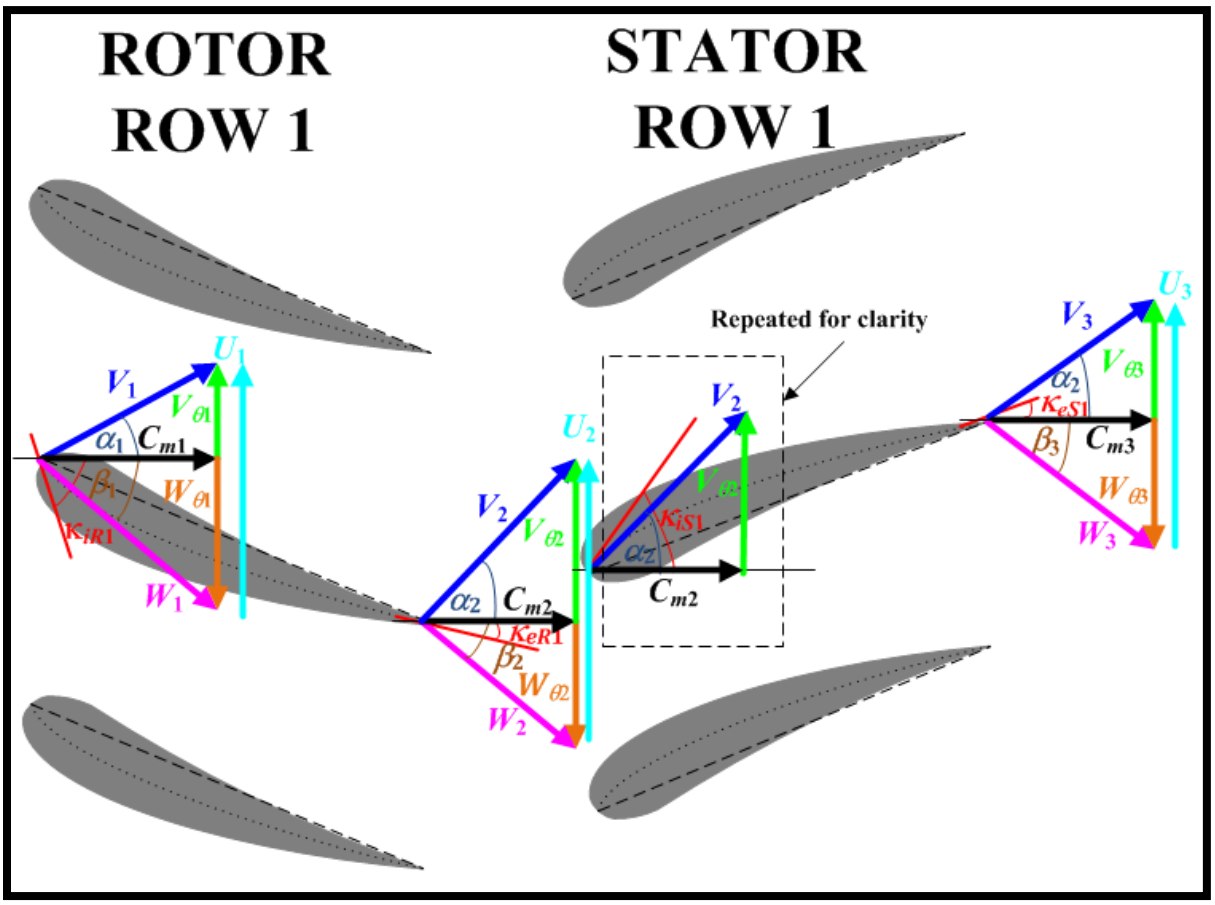

Figure 3-3 Velocity triangles in a compressor

At station 1, i.e., inlet to the rotor, the rotor blade has a tangential velocity U_1 due to the rotational speed N of the compressor and is calculated using:

$$U_1 = \frac{2\pi r_m \langle z_1 \rangle N}{60} \tag{3.8}$$

The fluid attacks the rotor blade with the relative velocity W_1 at an angle β_1 to the axial direction. W_1 is a consequence of the blade tangential velocity U_1 and the absolute velocity V_1 with which the fluid enters. As seen in the Figure 3-3, V_1 is at an angle α_1 to the axial direction. α_1 is called the swirl angle. In absence of the swirl i.e., $\alpha_1 = 0$, the fluid would enter the rotor axially. The swirl is an artifact of the IGV. From the modeling standpoint, either the IGV can be explicitly modeled or a swirl angle can be imposed at the rotor inlet. In this work a swirl angle was imposed at the rotor inlet.

If W_1 were along the tangent to the blade at inlet then its direction would correspond to the blade metal angle, κ_{iR1}, else it results in an angle of incidence ι_1 and is given by:

$$\iota_1 = \beta_1 - \kappa_{iR1} \tag{3.9}$$

The tangential components of W_1 and V_1 are related to U_1 by:

$$U_1 = V_{\theta 1} - W_{\theta 1} \tag{3.10}$$

Additionally, the tangential and axial components of W_1 and V_1 are related by the trigonometric entities:

$$V_{m1} = V_1 \cos\alpha_1 \tag{3.11}$$

$$V_{m1} = W_1 \cos\beta_1 \tag{3.12}$$

$$V_{\theta 1} = V_1 \sin\alpha_1 \tag{3.13}$$

$$W_{\theta 1} = W_1 \sin\beta_1 \tag{3.14}$$

At station 2, the fluid leaves the rotor blade with the relative velocity W_2 at an angle β_2 to the axial direction. As at the inlet, if W_2 were along the tangent to the blade then its direction would correspond to the blade metal angle, κ_{eR1}, else it results in an angle of deviation δ_2 which is given by:

$$\delta_2 = \beta_2 - \kappa_{eR1} \tag{3.15}$$

The remaining mathematical model at station 2 is identical to station 1 and thus equations (3.8), (3.10), (3.11), (3.12), (3.13), and (3.14) hold with only the suffix 1 changed to suffix 2. Thus, these equations are:

$$U_2 = \frac{2\pi r_m \langle z_2 \rangle N}{60} \tag{3.16}$$

$$U_2 = V_{\theta 2} - W_{\theta 2} \tag{3.17}$$

$$V_{m2} = V_2 \cos\alpha_2 \tag{3.18}$$

$$V_{m2} = W_2 \cos\beta_2 \tag{3.19}$$

$$V_{\theta 2} = V_2 \sin\alpha_2 \tag{3.20}$$

$$W_{\theta 2} = W_2 \sin\beta_2 \tag{3.21}$$

Station 2 is the interface between the rotor row 1 and stator row 1. At station 2 the velocity of fluid leaving the rotor W_2 and rotor blade tangential velocity U_2 result in the absolute fluid velocity V_2 and thus the fluid enters the stator row 1 with the absolute velocity V_2. Similar to the rotor, even in the case of the stator if velocity of fluid entering the stator (V_2) were along the tangent to the blade inlet then its direction would correspond to the blade metal angle κ_{iS1}, else the resulting angle of incidence ι_2 at station 2 is:

$$\iota_2 = \alpha_2 - \kappa_{iS1} \tag{3.22}$$

Finally, at station 3, the fluid exits the stator blade with the absolute velocity V_3. Similar to the rotor, the angle of deviation δ_3 would exist if V_3 is not the blade metal angle at exit κ_{eS1} and is given by:

$$\delta_3 = \alpha_3 - \kappa_{eS2} \tag{3.23}$$

The remaining mathematical model at station 3 would be identical to that of station 2 or station 1 unless station 3 is the last station. In such case any relative quantity would cease to exist due to the absence of downstream rotor row.

Thus, in summary the salient points of the velocity triangles are:

1. For the rotor blade, the relative flow angle β is associated with the calculation of the incidence angle ι and the deviation angle δ.

2. For the stator blade, the absolute flow angle α is associated with the calculation of ι and δ.
3. The sign for ι and δ depend on the numerical values of the associated flow angles in relation to the blade metal angles. Thus, ι and δ are positive if the flow angles are greater than the blade metal angles and are negative if otherwise. The sign convention of ι and δ are independent of the sign convention used for the flow angles and the blade metal angles. Thus, equations (3.9), (3.15), (3.22) and (3.23) can be recast using the absolute values of the flow and metal angles as:

$$\iota_1 = |\beta_1| - |\kappa_{iR1}| \tag{3.24}$$

$$\delta_2 = |\beta_2| - |\kappa_{eR1}| \tag{3.25}$$

$$\iota_2 = |\alpha_2| - |\kappa_{iS1}| \tag{3.26}$$

$$\delta_3 = |\alpha_3| - |\kappa_{eS2}| \tag{3.27}$$

Euler's equation for turbomachines

The change in angular momentum can now be calculated from the relevant velocity components known from the velocity triangles. Euler's pump equation relates the change in angular momentum to the change in energy across the rotor row and is given by (Mattingly. 1996):

$$h_{ta2} - h_{ta1} = \omega\left(r_2 C_{\theta 2} - r_1 C_{\theta 1}\right) \tag{3.28}$$

The equation (3.28) is applicable for stator, where $\omega = 0$ leads to:

$$h_{ta3} - h_{ta2} = 0 \tag{3.29}$$

Conservation of mass

The conservation of mass across the blade row applies to both the rotor row and the stator row and for the rotor row is:

$$\dot{m}_1 = \dot{m}_2 \tag{3.30}$$

where, the mass flow rate is:

$$\dot{m} = \rho A C_m \tag{3.31}$$

Conservation of Rothalpy

As noted earlier, the Euler's pump equation relates the change in angular momentum to the change in energy across the rotor row and leads to the classic turbomachinery conservation of rothalpy equation (Aungier. 2003, Cumpsty. 2004).

$$I_1 = I_2 \tag{3.32}$$

The rothalpy I in equation (3.32) is given by:

$$I = h_{ta} - UC_\theta \tag{3.33}$$

Alternately, I can also be expressed as:

$$I = h_{tr} - \frac{U^2}{2} \tag{3.34}$$

$$I = h_{st} + \frac{W^2}{2} - \frac{U^2}{2} \tag{3.35}$$

It is applicable for steady, adiabatic flow including the viscous regions except the casing region of the rotor. For the stator row since $U = 0$ in equation (3.33) the rothalpy simply corresponds to the absolute total enthalpy h_{ta} and thus the conservation of rothalpy is really the conservation of absolute total enthalpy.

$$h_{ta1} = h_{ta2} \tag{3.36}$$

Mathematical description of aero-thermodynamic properties at compressor rotor row inlet

At the rotor row inlet the blade velocity U_1 can be evaluated at the mean radius (r_{m1}) from the speed (N) of the turbomachine,

$$U_1 = \frac{2\pi N}{60} r_{m1} \langle z_1 \rangle \tag{3.37}$$

Then, for the known total absolute temperature (T_{ta1}) and pressure (P_{ta1}) the corresponding total absolute enthalpy (h_{ta1}) and the entropy (s_1) can be determined from the equation of state:

$$h_{ta1} = f\langle P_{ta1}, T_{ta1} \rangle \tag{3.38}$$

$$s_1 = f\langle P_{ta1}, T_{ta1} \rangle \tag{3.39}$$

At any given state point, the total absolute entropy (s_{ta}), the total relative entropy (s_{tr}) and the static entropy (s_{st}) are the same and thus is simply denoted by s (Mattingly. 1996).

The static enthalpy (h_{st}) is determined from the total absolute enthalpy and the absolute fluid velocity as:

$$h_{st1} = H_{ta1} - \frac{V_1^2}{2} \tag{3.40}$$

From the velocity triangles:

$$V_1 = \frac{C_{m1}}{\cos(\alpha_1)} \tag{3.41}$$

Thus, using equation (3.41), equation (3.40) can be re-written as:

$$h_{st1} = h_{ta1} - \frac{C_{m1}^2}{2\left[\cos(\alpha_1)\right]^2} \tag{3.42}$$

The fluid density ρ_{s1} can be determined from the static enthalpy h_{st1} and the entropy s_1 using the EOS:

$$\rho_{st1} = f\left\langle h_{st1}, s_1 \right\rangle \tag{3.43}$$

The mass flow rate ($\dot{m}_1$) at the rotor inlet is given by equation (3.31) and has been re-written below with inlet suffix (1) for clarity:

$$\dot{m}_1 = \rho_{st1} A_1 C_{m1} \tag{3.44}$$

Similarly, the rothalpy (I_1) at the rotor inlet is given by equation (3.33) and has been re-written below with inlet suffix (1) for clarity:

$$I_1 = h_{ta1} - U_1 V_{\theta 1} \tag{3.45}$$

Once again, from the velocity triangles,

$$V_{\theta 1} = C_{m1} \tan(\alpha_1) \tag{3.46}$$

Thus, combining equations (3.45) and (3.46), we get,

$$I_1 = h_{ta1} - U_1 C_{m1} \tan(\alpha_1) \tag{3.47}$$

The aero-thermodynamic conditions at the rotor inlet can be completely described by equations (3.42), (3.43), (3.44) and (3.47). The four unknowns being evaluated are $h_{st1}, \rho_{st1}, C_{m1}$ and I_1. However, the equation for I_1 does not need to be solved simultaneously with the other

equations. Thus, at rotor inlet, a simultaneous solution of the three equations (3.42), (3.43), (3.44) provide the requisite information. The remaining variables are known either from the geometry (A_1) or the operating inlet conditions (h_{ta1} and s_1 from P_{ta1} and T_{ta1}) or from a combination of the geometry and the operating characteristic (U_1 from N and r_{m1}). The only other variable, the swirl angle α_1, is either specified by the user, or assumed equal to zero for an inlet with no swirl or can be determined using an inlet guide vane model. Using this scheme some of the properties at the rotor row inlet do not get calculated as they are not a part of the system of equations. These are β_1, ι_1, P_{tr1}, T_{tr1}, a_1, V_1, W_1, P_{s1}, T_{s1}, M_{a1} and M_{r1}. These are independently evaluated after the system is solved and are:

$$\beta_1 = \arctan\left(\tan(\alpha_1) - \frac{U_1}{C_{m1}}\right) \tag{3.48}$$

$$\iota_1 = |\beta_1| - |\kappa_{iR1}| \tag{3.49}$$

$$V_1 = \frac{C_{m1}}{\cos(\alpha_1)} \tag{3.50}$$

$$W_1 = \frac{C_{m1}}{\cos(\beta_1)} \tag{3.51}$$

P_{tr1}, T_{tr1}, a_1, P_{s1}, T_{s1} come from the EOS and is given by:

$$P_{tr1} = f\langle h_{tr1}, s_1\rangle \tag{3.52}$$

$$T_{tr1} = f\langle h_{tr1}, s_1\rangle \tag{3.53}$$

$$P_{st1} = f\langle h_{st1}, s_1\rangle \tag{3.54}$$

$$T_{st1} = f\langle h_{st1}, s_1\rangle \tag{3.55}$$

$$a_1 = f\langle h_{st1}, s_1\rangle \tag{3.56}$$

M_{a1} and M_{r1} can be calculated from:

$$M_{a1} = \frac{V_1}{a_1} \tag{3.57}$$

$$M_{r1} = \frac{W_1}{a_1} \tag{3.58}$$

Mathematical description of aero-thermodynamic properties at the compressor rotor row exit

Analogous to the compressor rotor inlet, the system of equations at the compressor rotor exit is:

$$U_2 = \frac{2\pi N}{60} r_{m2} \tag{3.59}$$

$$I_2 = h_{tr2} - \frac{U_2^2}{2} \tag{3.60}$$

$$h_{st2} = h_{tr2} - \frac{W_2^2}{2} \tag{3.61}$$

$$W_2 = \frac{C_{m2}}{\cos(\beta_2)} \tag{3.62}$$

$$h_{st2} = h_{tr2} - \frac{C_{m2}^2}{2\left[\cos(\beta_2)\right]^2} \tag{3.63}$$

$$\dot{m}_2 = \rho_{st2} A_2 C_{m2} \tag{3.64}$$

$$\rho_{st2} = f\left\langle h_{st2}, s_2 \right\rangle \tag{3.65}$$

The closure for I_2 and $\dot{m}_2$ can be obtained from the conservation of rothalpy and mass,

$$I_2 = I_1 \tag{3.66}$$

$$\dot{m}_2 = \dot{m}_1 \tag{3.67}$$

Equations (3.60) allows the calculation of h_{tr2} and then equations (3.63), (3.64), and (3.65) can be solved to determine the three unknowns i.e., h_{st2}, ρ_{st2}, and C_{m2}.

However, the outlet flow angle β_2 in the equation (3.63) and the entropy at rotor row exit s_2 in the equation (3.65) are also unknown. The outlet flow angle β_2 is a function of the blade metal angle at exit κ_{eR1} and is given by:

$$\beta_2 = \kappa_{eR1} - \delta_2 \tag{3.68}$$

where, δ_2 is the angle of deviation. If δ_2 is assumed to be zero, then the equation (3.68) reduces to:

$$\beta_2 = \kappa_{eR1} \tag{3.69}$$

If the compression process across the rotor row was isentropic then:

$$s_2 = s_1 \tag{3.70}$$

Thus, with the assumptions of an isentropic compression process and $\delta_2 = 0$ equations (3.69) and (3.70) will result in closure for the blade row exit. Equation (3.70) automatically ensures the following

$$P_{tr2} = P_{tr1} \tag{3.71}$$

Thus, at the rotor exit the simultaneous solution of three independent equations with associated boundary conditions would suffice. In case of a non-isentropic solution, i.e., a system with losses, equation (3.70) no longer is suitable. On the contrary, s_2 needs to be calculated from the EOS for a known value of P_{tr2} and is:

$$s_2 = f\left\langle P_{tr2}, h_{tr2} \right\rangle \tag{3.72}$$

However, P_{tr2} is unknown and is expressed as a function of the loss parameter, ϖ_{R1}, and the pressure loss due to blade row clearances, ΔP_{clR1}, and given by:

$$P_{tre2} = P_{tr1} - \varpi_{R1} * \left(P_{tr1} - P_{s1}\right) - \Delta P_{clR1} \tag{3.73}$$

Therefore, if the loss parameter and the clearance losses are known then the simultaneous solution of five independent equations (3.63), (3.64), (3.65), (3.72), (3.73) with associated boundary conditions would provide the aero-thermodynamic properties. The methodology to model the loss parameter ϖ_{R1}, the clearance loss ΔP_{clR1} and the deviation angle δ_1 is covered in the section "Loss characterization in compressor".

Mathematical description of aero-thermodynamic properties at compressor stator row inlet

The properties at the stator row inlet are the same as that of the rotor row exit. I_2, P_{tr2}, s_2, h_{st2}, ρ_{st2}, C_{m2} and h_{tr2} are already known and no additional simultaneous solution is required. In order to continue the calculations further downstream of the stator h_{ta2} should be known which can be calculated from (3.33) and is re-stated in a re-arranged form here for clarity.

$$h_{ta2} = I_2 + U_2 C_{\theta 2} \tag{3.74}$$

Though no other property is necessary for downstream calculations, it is useful to compute the remaining properties i.e., α_2, ι_2, P_{tr2}, T_{tr2}, P_{ta2}, T_{ta2}, P_{st2}, T_{st2}, a_2, V_2, W_2, M_{a2}, and M_{r2} prior to the stator row exit. α_2 and ι_2 are calculated from the following:

$$\alpha_2 = \arctan\left(\tan(\beta_2) + \frac{U_2}{C_{m2}}\right) \tag{3.75}$$

$$\iota_2 = |\beta_2| - |\kappa_{iS1}| \tag{3.76}$$

P_{ta2} and T_{ta2} come from the EOS:

$$P_{ta2} = f\langle h_{ta2}, s_2\rangle \tag{3.77}$$

$$T_{ta2} = f\langle h_{ta2}, s_2\rangle \tag{3.78}$$

The remainder of the properties listed above can be determined using exactly the same equations (3.50) through (3.58) with the subscripts changed from 1 to 2.

Mathematical description of aero-thermodynamic properties at compressor stator row exit

The conservation of rothalpy as applied to the stator row results in the conservation of total absolute enthalpy:

$$h_{ta3} = h_{ta2} \tag{3.79}$$

Once h_{ta3} is known then the stator exit properties can be determined using the following five equations:

$$h_{st3} = h_{ta3} - \frac{C_{m3}^2}{2\left[\cos(\alpha_3)\right]^2} \tag{3.80}$$

$$\dot{m}_3 = \rho_{st3} A_3 C_{m3} \tag{3.81}$$

$$\rho_{st3} = f\langle h_{st3}, s_3\rangle \tag{3.82}$$

$$s_3 = f\langle P_{ta3}, h_{ta3}\rangle \tag{3.83}$$

$$P_{ta3} = P_{ta2} - \varpi_{S1} * (P_{ta2} - P_{st2}) - \Delta P_{clS2} \tag{3.84}$$

The exit flow angle α_3 in equation (3.80) can be obtained from the following:

$$\alpha_3 = \kappa_{eS1} - \delta_3 \tag{3.85}$$

δ_3 can be calculated from the deviation angle model while ϖ_{S1} and ΔP_{clS1} from the loss parameter model and the clearance loss model respectively, and the same are described in the next section. Similar to the treatment used for the rotor row inlet, rotor row exit and the stator row inlet additional properties not calculated so far at the stator row exit were done here.

Loss characterization in compressor

Characterizing a non-isentropic process requires modeling the pressure losses across each individual blade row. This is closely tied to determining the deviation angle at blade row exit. Both the pressure loss across the blade row and the deviation angle at exit are functions of the incidence angle (the design incidence and the actual incidence) at the blade row inlet. The subsequent sections describe the models used to characterize the design incidence angle, the pressure loss and the deviation angles.

Design incidence angle

The design incidence angle defines a near-optimum or minimum loss incidence angle for any blade row. The design incidence angle model is an empirical model obtained from two-dimensional cascade tests done by Emery, et al. (1958). Figure 3-5 presents the data from Emery, et al. (1958). Figure 3-5 plots the design angle of attack against the blade solidity for nine different NACA 65 series blade types with $\frac{t_b}{c} = 0.1$ and $\frac{a}{c} = 0.5$. The angle of attack is related to the incidence angle by:

$$\iota = \alpha + \gamma - \kappa_i \tag{3.86}$$

Lieblein (1960), also presented in NASA SP-36 (Johnsen and Bullock. 1965), extends Emery's design angle of attack chart to other blade profile types and other thickness-to-chord ratio by applying correction factors to the design angle of attack for zero camber angle. The blade profile correction factor (K_{sh}) is 0.7 for double circular arc profile, 1.1 for C4-series profile and quite obviously 1.0 for the NACA profile itself. The blade thickness correction factor ($K_{t,\iota}$) is provided graphically in Johnsen and Bullock (1965) and is reproduced here in the Figure 3-4. Aungier (2003) provides a mathematical correlation for Figure 3-4:

$$K_{t,\iota} = \left(10\frac{t_b}{c}\right)^q \tag{3.87}$$

Where,

$$q = \frac{0.28}{0.1 + \left(\frac{t_b}{c}\right)^{0.3}} \tag{3.88}$$

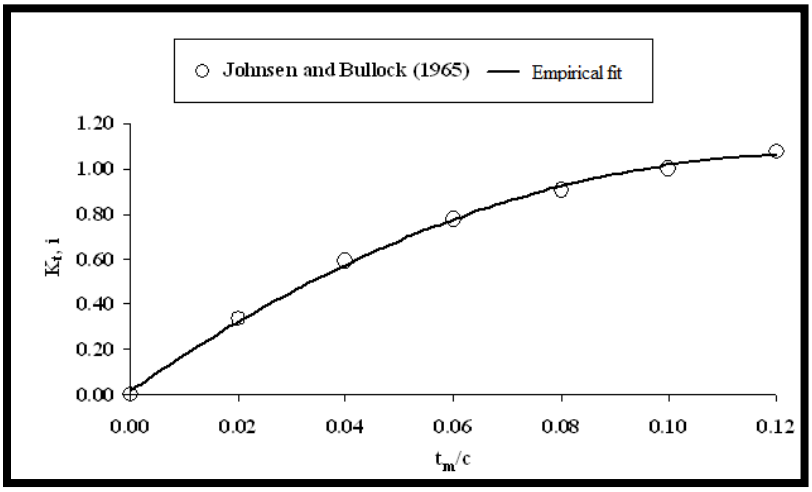

Figure 3-4 Blade thickness correction factor for design incidence angle

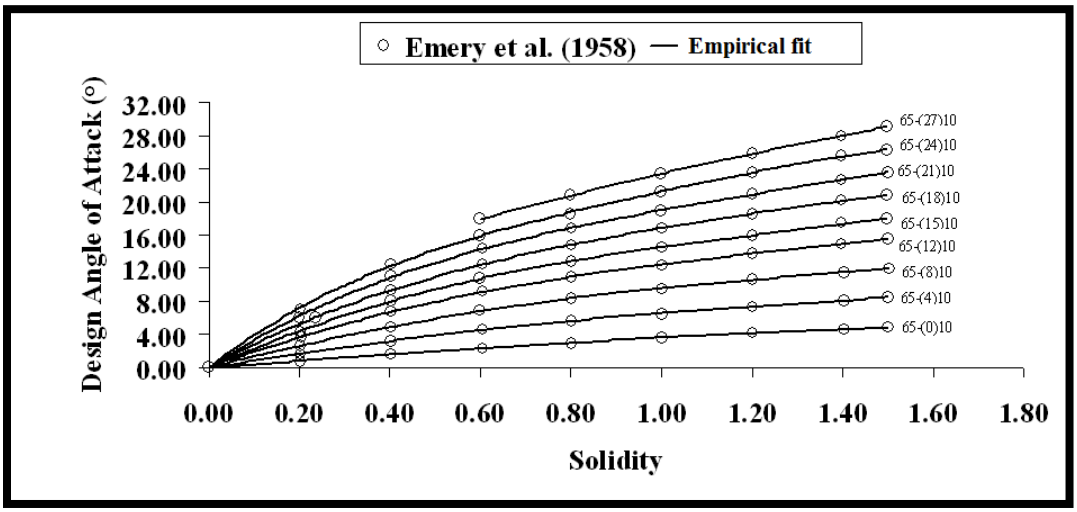

Figure 3-5 Design angle of attack

Furthermore, Aungier (2003) provides the empirical model (equation (3.89)) for the design angle of attack which is a mathematical correlation for Emery's chart in Figure 3-5. The model incorporates Lieblein's blade profile correction factor (K_{sh}) and blade thickness correction factor ($K_{t,t}$) to expand usability of the chart for all the blade types. Additionally, the

blade attribute $\frac{a}{c}$ was incorporated into the model to extend the correlation to include NACA A_4K_6 inlet guide vanes.

$$\alpha^* = \left[3.6K_{sh}K_{t,t} + 0.3532\theta\left(\frac{a}{c}\right)^{0.25} \right]\sigma^e \tag{3.89}$$

Where, $$e = 0.65 - 0.002\theta \tag{3.90}$$

Once α^* is calculated from equation (3.89), the design incidence angle ι^* can be calculated using equation (3.86). It can be seen from the equations (3.86) and (3.89) that the design incidence angle is purely a function of the blade geometry.

Design deviation angle

The empirical model for design deviation angle corresponding to the operation at design incidence angle is available originally in Lieblein (1959) and reported again in NASA SP-36 (Johnsen and Bullock. 1965). The model is mathematically expressed as:

$$\delta^* = K_{sh}K_{t,t}\left(\delta_0^*\right)_{10} + m\theta \tag{3.91}$$

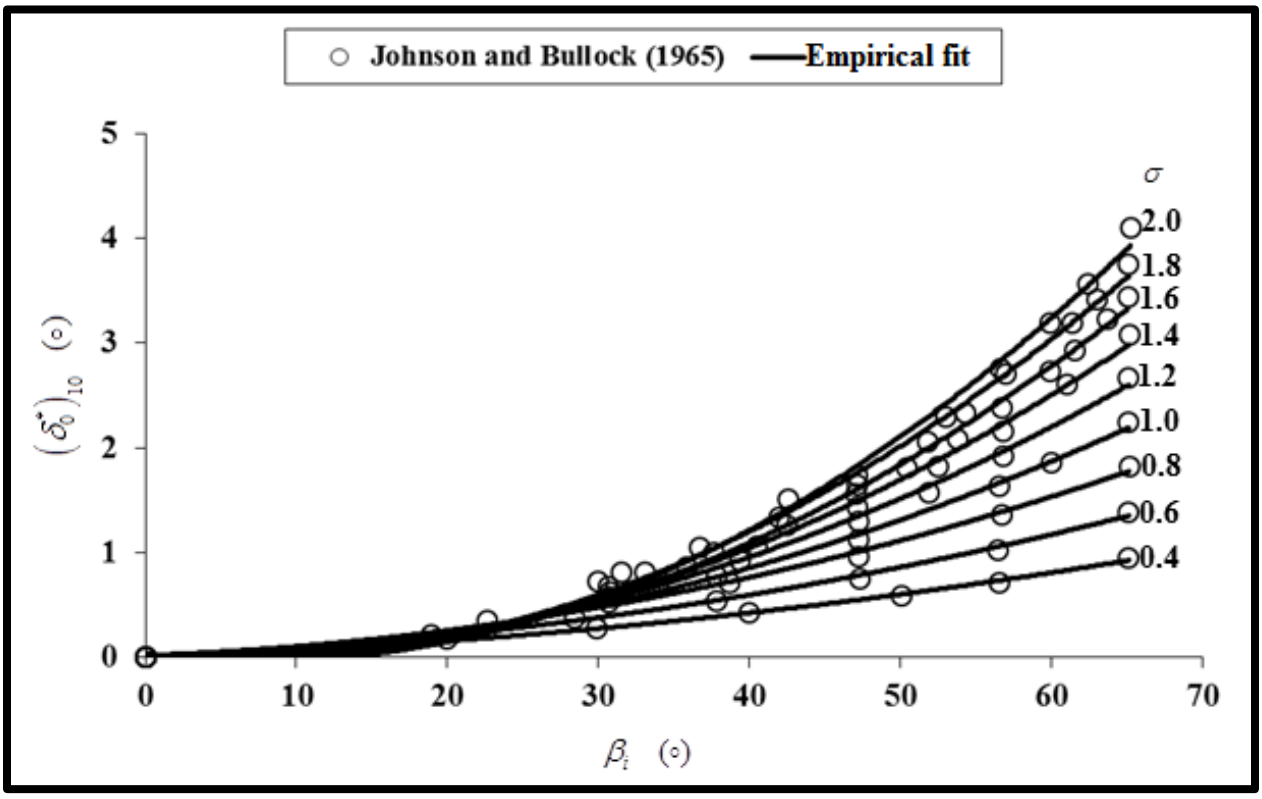

Figure 3-6 Zero camber deviation angle

In equation (3.91) $\left(\delta_0^*\right)_{10}$ is the design deviation angle for a 10% thick blade, i.e., $\frac{t_b}{c} = 0.1$ and with zero camber. The empirical model for $\left(\delta_0^*\right)_{10}$ is obtained from the low speed cascade testing results and is a relationship between the inlet flow angle (β_i) and the blade solidity (σ).

$$\left(\delta_0^*\right)_{10} = 0.01\sigma\beta_i + \left(0.74\sigma^{1.9} + 3\sigma\right)\left(\frac{\beta_i}{90}\right)^{1.67+1.09\sigma} \tag{3.92}$$

Further, in equation (3.91) K_{sh} is the profile correction factor and already explained earlier while $K_{t,\delta}$ is the thickness correction factor to incorporate other blade thicknesses and was modeled as a simple second order polynomial from the graphical data of (Johnsen and Bullock. 1965).

$$K_{t,\delta} = 6.25\left(\frac{t_b}{c}\right) + 37.5\left(\frac{t_b}{c}\right)^2 \tag{3.93}$$

The last correction parameter (m) in equation (3.91) allows to extend the correlation to blades of other camber angles apart from zero camber and is given by

$$m = \frac{m_{1.0}}{\sigma^b} \tag{3.94}$$

In equation (3.94), the numerator $m_{1.0}$ was determined for a solidity of 1 and the denominator allows it to be extended to other blade solidities. The term $m_{1.0}$ was modeled as a second order polynomial for NACA 65-series blades using the empirical relationship

$$m_{1.0} = 0.17 - 0.0333\frac{\beta_i}{100} + 0.333\left(\frac{\beta_i}{100}\right)^2 \tag{3.95}$$

In contrast, for circular-arc camberlines it was modeled as a third order polynomial and given by

$$m_{1.0} = 0.249 + 0.074\frac{\beta_i}{100} - 0.132\left(\frac{\beta_i}{100}\right)^2 + 0.316\left(\frac{\beta_i}{100}\right)^3 \tag{3.96}$$

The exponent b is also a third order polynomial function of the inlet flow angle (β_i) and was expressed as

$$m_{1.0} = 0.9625 - 0.17\frac{\beta_i}{100} - 0.85\left(\frac{\beta_i}{100}\right)^3 \tag{3.97}$$

Equations (3.95), (3.96), and (3.97) are the mathematical representations of the graphical relationships presented in NASA SP-36 (Johnsen and Bullock. 1965).

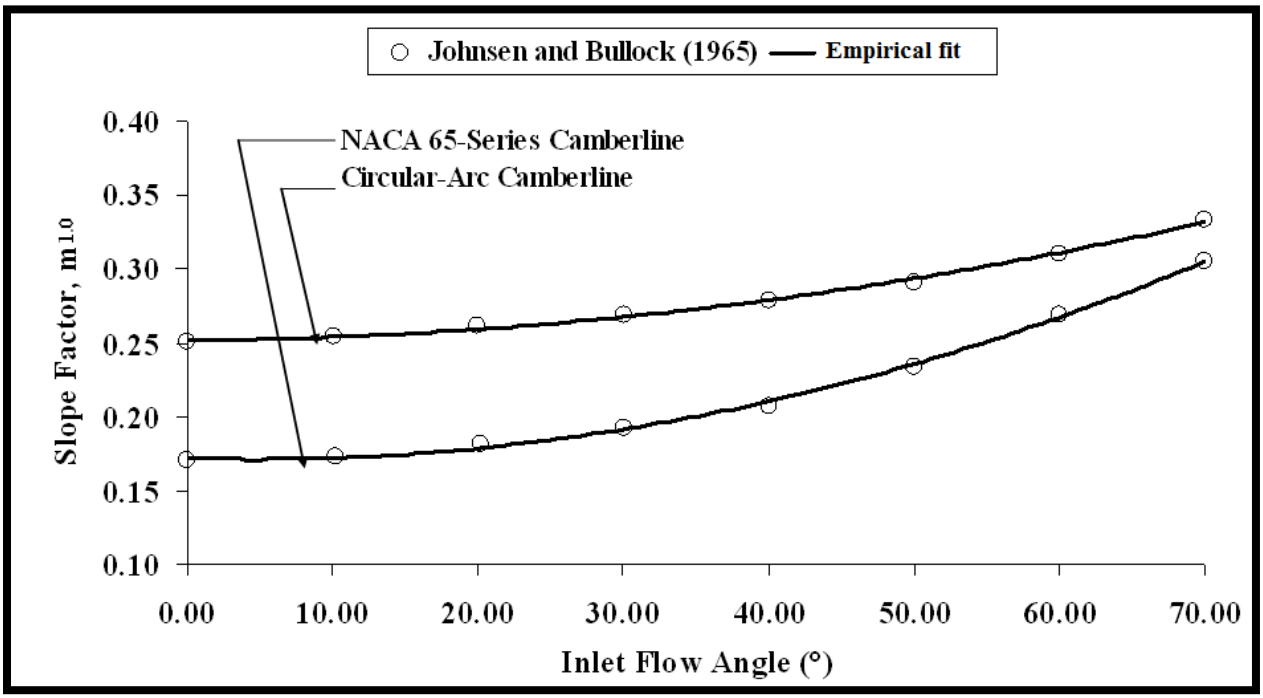

Figure 3-7 Variation of parameter $m_{1.0}$ with inlet flow angle

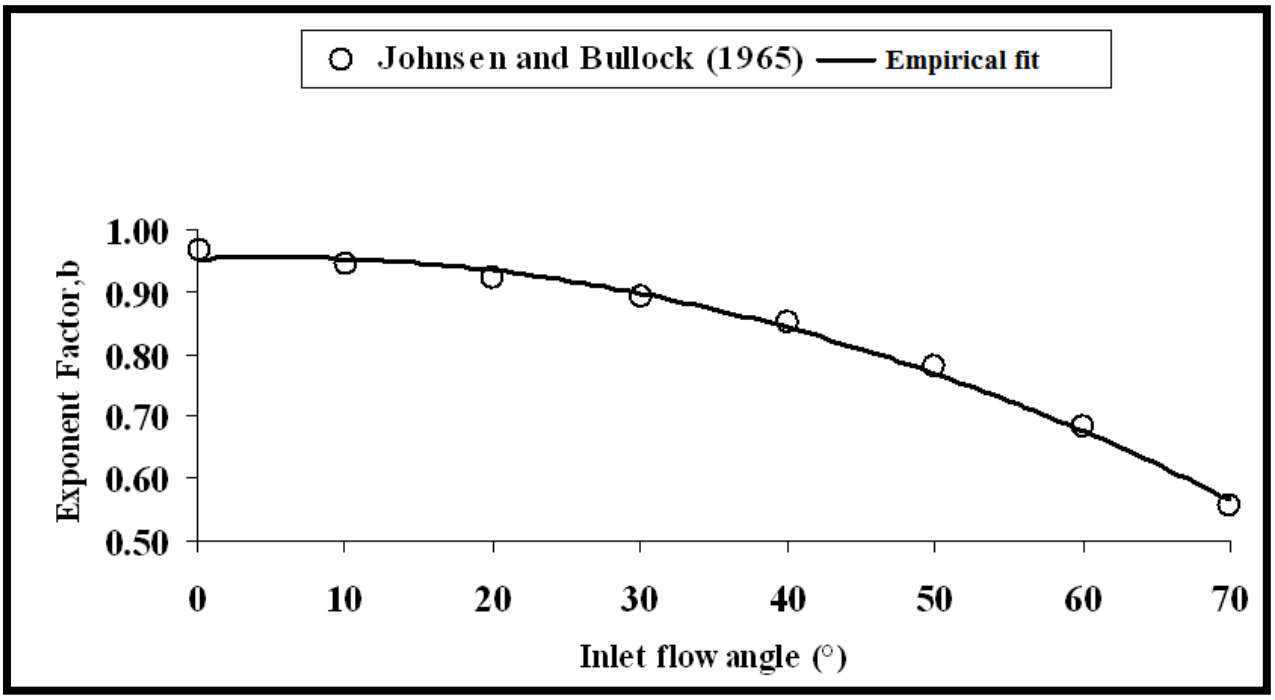

Figure 3-8 Variation of parameter b with blade solidity

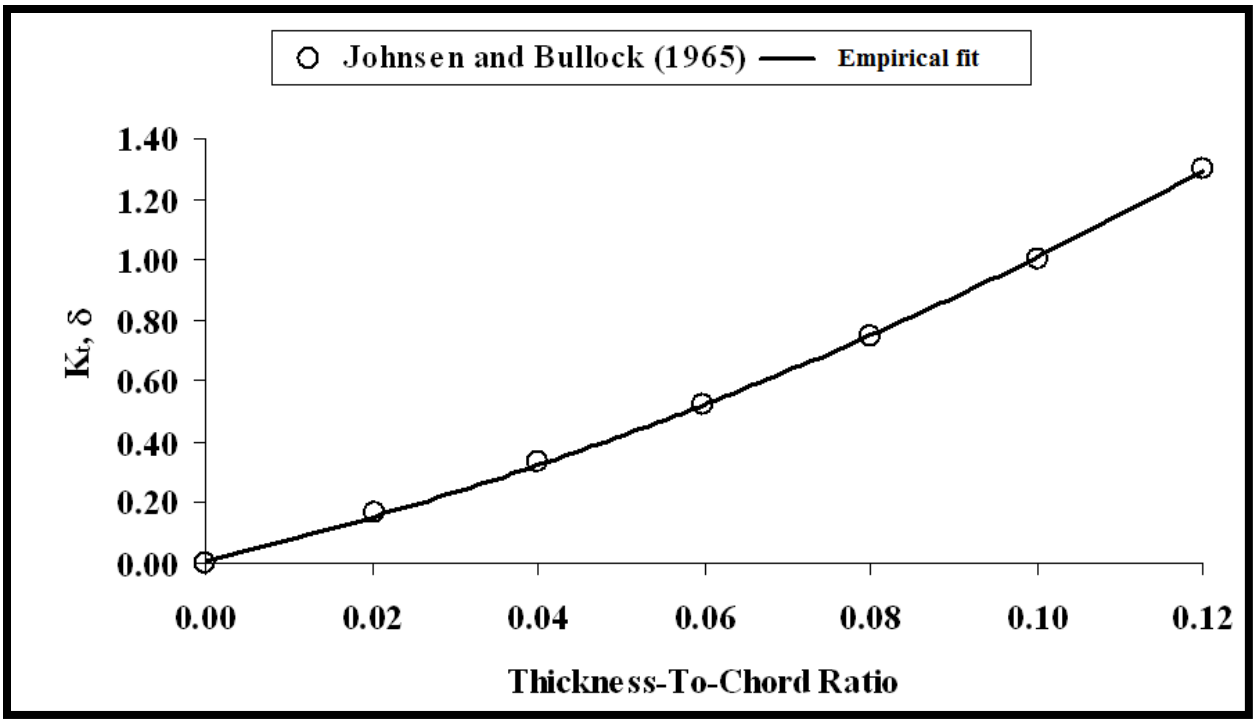

Figure 3-9 Blade thickness correction factor for design deviation angle

Compressor losses

Pressure losses in a compressor are classified into profile loss and blade tip clearance loss. Profile loss as determined from the low speed cascade testing is a function of the wake momentum thickness, blade geometry, and inlet and exit velocities (total relative). Profile loss is represented by a profile loss coefficient (ϖ).

$$\varpi = 2\frac{\theta_w}{c}\frac{\sigma}{\cos(\beta_e)}\left(\frac{W_e}{W_i}\right)^2 \tag{3.98}$$

The parameter $\frac{\theta_w}{c}$ can be correlated to another parameter called the diffusion factor D (Johnsen and Bullock. 1965). In such a case the loss coefficient should also correlate with the diffusion factor which consequently would result in the following:

$$\frac{\varpi\cos(\beta_e)}{2\sigma}\left(\frac{W_i}{W_e}\right)^2 = f(D) \tag{3.99}$$

Or ,

$$\frac{\varpi \cos\left(\beta_e\right)}{2\sigma} = f\left(D\right) \tag{3.100}$$

Thus, as long as the correlation for $f\left(D\right)$ is known the ϖ profile loss coefficient can be determined. $f\left(D\right)$ has the profile as shown in Figure 3-10 reported in Johnsen and Bullock (1965). The corresponding empirical model is:

$$f(D) \equiv 0.0035\left(1+3.5D+37D^4\right) \tag{3.101}$$

However, Figure 3-10 is only suitable for design incidence angles (Aungier. 2003) and thus for the off-design operations the corresponding design diffusion factor is represented by D^* which would result in the following modifications to equations (3.101) and (3.100):

$$f(D^*) \equiv 0.0035\left(1+3.5D^*+37\left(D^*\right)^4\right) \tag{3.102}$$

$$\frac{\varpi^* \cos\left(\beta_e^*\right)}{2\sigma} = f\left(D^*\right) \tag{3.103}$$

or,
$$\frac{\varpi^* \cos\left(\beta_e^*\right)}{2\sigma} = 0.0035\left(1+3.5D^*+37\left(D^*\right)^4\right) \tag{3.104}$$

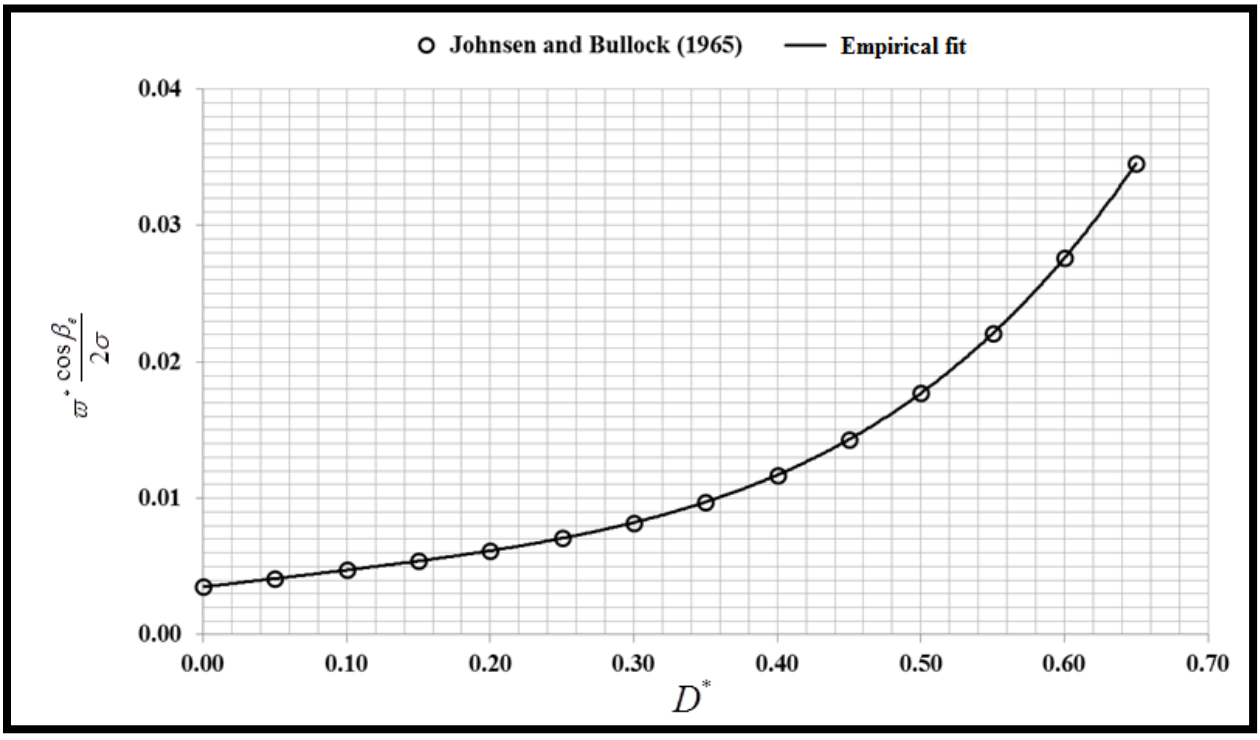

Figure 3-10 Loss coefficient as a function of the design diffusion factor D^*

Furthermore, Aungier (2003) suggests that Figure 3-10 is suitable only for design diffusion factors less than 0.6. Lieblein (1959) proposed a modification to the diffusion factor D and presents it as an equivalent diffusion factor D_{eq}. The evolution of D_{eq} is well illustrated in Aungier (2003) and is not explained here. From its usage standpoint the more important aspect is that D_{eq} allows the Figure 3-10 to be extended well beyond 0.6, in fact to 2.4 and the same is shown in the Figure 3-11. It can be seen from Figure 3-11 that beyond $D_{eq} = 2.0$ the loss coefficient rapidly increases and Lieblein (1960) suggested to limit the use of Figure 3-11 to $D_{eq} = 2.0$. It should be recalled that similar to the case of D, D_{eq} is also suitable for design incidence angles only and thus in the Figure 3-11, D_{eq} is represented as D_{eq}^*.

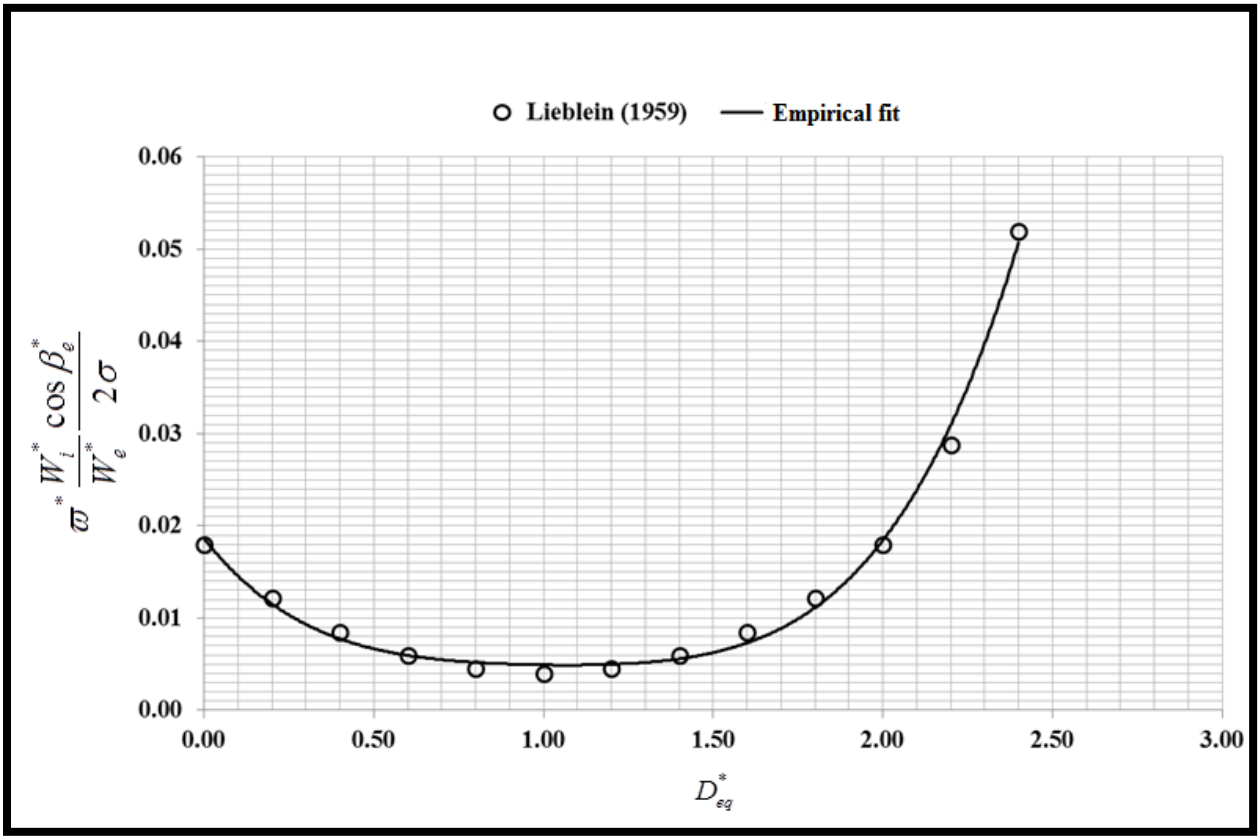

Figure 3-11 Loss coefficient as a function of the design diffusion factor D_{eq}^*

The functional form of D_{eq}^* is empirically represented as:

$$f\left(D_{eq}^*\right) = 0.004\left[1 + 3.1\left(D_{eq}^* - 1\right)^2 + 0.4\left(D_{eq}^* - 1\right)^8\right] \tag{3.105}$$

Thus, the loss coefficient is then given by:

$$\varpi^* \frac{\cos\left(\beta_e^*\right)}{2\sigma}\left(\frac{W_i^*}{W_e^*}\right)^2 = 0.004\left[1+3.1\left(D_{eq}^*-1\right)^2+0.4\left(D_{eq}^*-1\right)^8\right] \tag{3.106}$$

Comparing equations (3.106) with (3.104), it can be seen that the change from using D^* to D_{eq}^* results in a slight modification as to how the loss coefficient is represented. The additional term $\frac{W_i^*}{W_e^*}$ adds to more complexity in the model but provides better fit to the cascade data. Aungier (2003) suggests that the coefficient 0.004 and the constant 1 in equation (3.106) can be used as model constants to allow the model to fit a variety of axial compressor designs. Thus, using Aungier's proposition, equation (3.106) was modified as:

$$\varpi^* \frac{\cos\left(\beta_2^*\right)}{2\sigma}\left(\frac{W_i^*}{W_e^*}\right)^2 = K_1\left[K_2+3.1\left(D_{eq}^*-1\right)^2+0.4\left(D_{eq}^*-1\right)^8\right] \tag{3.107}$$

In equation (3.107), the model constants K_1 and K_2 were used to perform a sensitivity study on the NASA 10 stage compressor case study.

At this point, if the value of D_{eq}^* is known then the design loss coefficient can be calculated. Lieblein (1960) proposed the evaluation of D_{eq}^* as:

$$D_{eq}^* = \left(\frac{W_{\max}}{W_i}\right)^* \frac{\cos\beta_e^*}{\cos\beta_i^*}\left(\frac{C_{mi}}{C_{me}}\right) \tag{3.108}$$

Where,
$$\left(\frac{W_{\max}}{W_i}\right)^* = 1.12+0.61\frac{\cos^2\beta_i^*}{\sigma}\left(\tan\beta_i^*-\tan\beta_e^*\right) \tag{3.109}$$

Finally, β_i^* and β_2^* can be calculated equation (3.15) for a known δ^*.

So far, models to compute the design incidence angle, the design deviation angle and the design loss coefficient have been reviewed. The goal of this work is to also determine off-design performance characteristics. Lieblein (1960) proposed a modification to (3.109) to extend its use for off-design cases and is:

$$\frac{W_{\max}}{W_i} = 1.12+0.61\frac{\cos^2\beta_i}{\sigma}\left(\tan\beta_i-\tan\beta_e\right)+\mathfrak{V}\left(\imath-\imath^*\right)^{1.43} \tag{3.110}$$

Where, $\mho = 0.0117$ for NACA 65 series blades and $\mho = 0.007$ for circular arc camber line cases. A further modification was presented in Lieblein (1960) which allowed extending the equation (3.110) to rotating cascades with non-constant axial velocity and radius.

$$\frac{W_{\max}}{W_i} = 1.12 + 0.61\frac{\cos^2\beta_i}{\sigma}\left(\frac{r_i V_{\theta i} - r_e V_{\theta e}}{r_i C_{mi}}\right) + \mho\left(\iota - \iota^*\right)^{1.43} \tag{3.111}$$

However, Lieblein (1960) limits the use of the equation (3.110) and consequently equation (3.111) to situations where $\iota \geq \iota^*$. On account of this limitation neither of the equations have not been used for the model here. Instead, equation (3.109) was chosen which is primarily applicable for only determining the design loss coefficient and then other modeling approaches outlined below were used to correct it for off-design performance. In order to make the corrections, computing the stall incidence angle is mandatory.

Stall angle calculation and off-design corrections for incidence angle and loss coefficient

In order to understand the stall angle calculation the loss profile pattern as a function of the incidence angle needs to be examined. Figure 3-12 presents the same. It is seen that the loss profile has a reverse bell shape (parabolic) nature about the design incidence angle. The loss coefficient is the least at the design incidence angle and rises continuously with departure from the design incidence angle. It is a standard practice to limit the loss coefficient value to twice the minimum value and thus on the curve there are two incidence angles with a loss coefficient of 2ϖ. The negative value is the negative stall incidence angle ι_c while the positive value corresponds to the positive stall incidence angle ι_s. Operating at incidence angles beyond the positive and negative stall values is not recommended. It is thus critical in an off-design performance evaluation to determine both the stall limits.

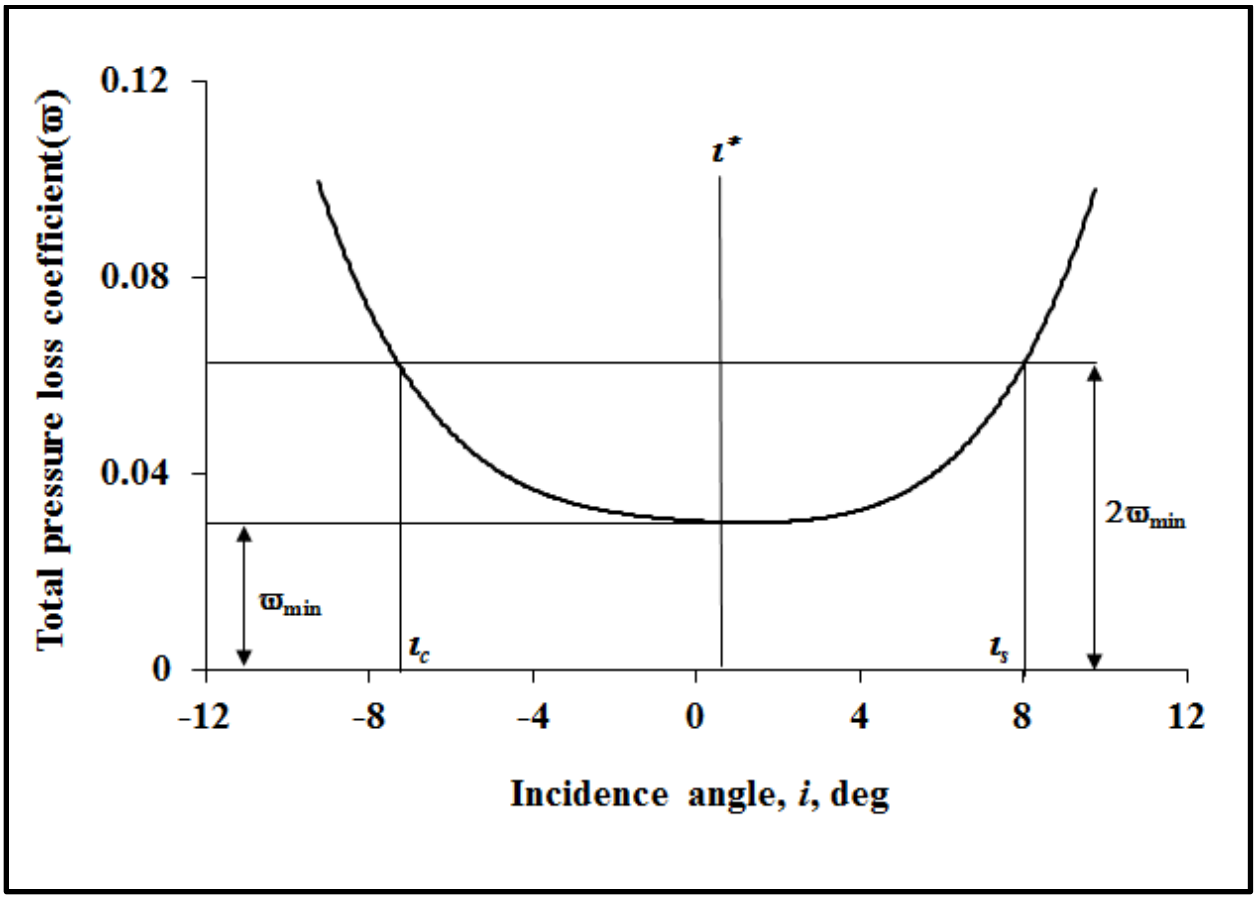

Figure 3-12 Loss coefficient profile

The stall limits are provided by Emery, et al. (1958) graphically out of a low speed cascade test for NACA 65 series blades. The mathematical models for the Herrig's chart as given by Aungier (2003) are:

$$\alpha_c - \alpha^* = -9 + \left[1 - \left(\frac{30}{\beta_{ic}}\right)^{0.48}\right]\frac{\theta}{4.176} \tag{3.112}$$

$$\alpha_s - \alpha^* = 10.3 + \left[2.92 + \left(\frac{\beta_{is}}{15.6}\right)^{0.48}\right]\frac{\theta}{8.2} \tag{3.113}$$

Since α is a function of β_i each of the equations (3.112) and (3.113) have to be iteratively solved to determine the corresponding $\alpha - \alpha^*$ value.

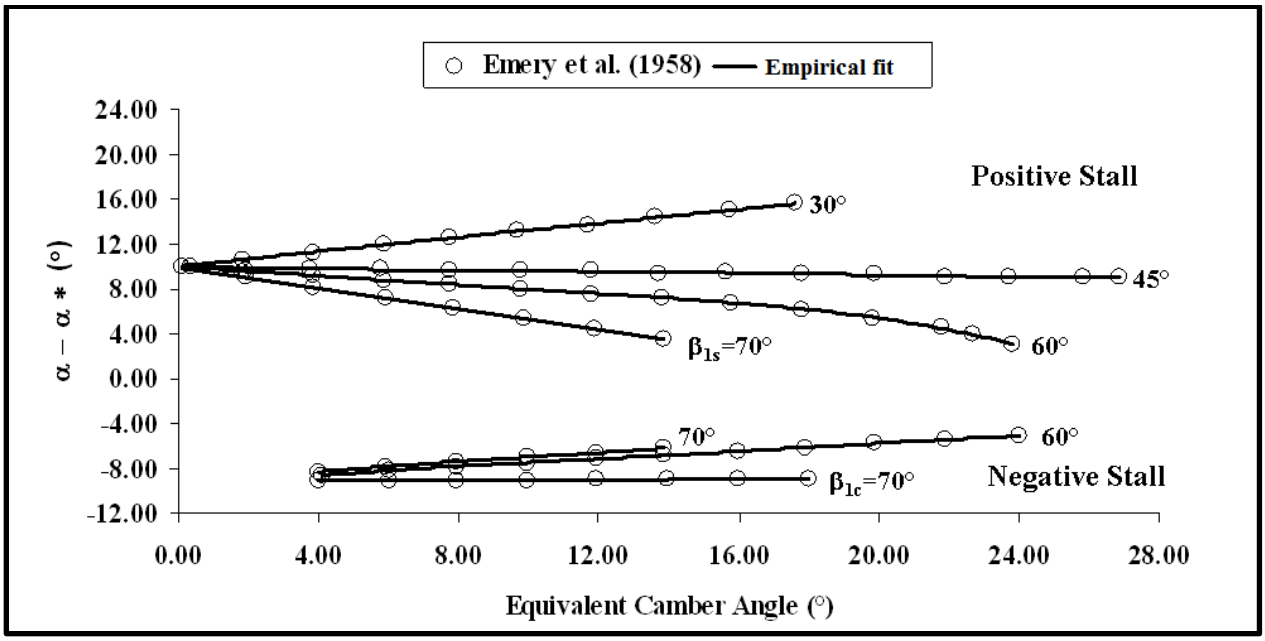

Figure 3-13 Positive and negative stall angle of attack as function of camber angle

Though, the above models are for NACA blades, Aungier (2003) reports that the same correlations have been successfully applied to other blade types as well, except for the NACA A4K6 camberline profile. In this work the NACA 65 series blade has been the primary focus of development. Modifications for other blade types can be subsequently added when requisite information is available. Once $\alpha_c - \alpha^*$ and $\alpha_s - \alpha^*$ is known ι_c and ι_s can be determined from equation (3.86). During the performance analysis the actual incidence angle (ι) is determined directly from equation (3.9) for rotor row and equation (3.22) for the stator row. The knowledge of ι_c and ι_s provides an exit criterion for the code to stop if the stall angles exceed the incidence angle. Aungier (2003) also provides a mechanism to correct the stall angles for the Mach number and the empirical models are:

$$\iota_{ccor} = \iota^* - \frac{\iota^* - \iota_c}{1 + 0.5 M_i^3} \tag{3.114}$$

$$\iota_{scor} = \iota^* + \frac{\iota_s - \iota^*}{1 + 0.5\left(K_{sh} M_i\right)^3} \tag{3.115}$$

The corrected stall angles can then be used to determine a minimum loss angle of incidence (ι_m) as below (Aungier. 2003):

$$\iota_m = \iota_c + \frac{(\iota_s - \iota_c)\left(\iota^* - \iota_c\right)}{\left(\iota^* - \iota_c\right) + \left(\iota_s - \iota^*\right)} \tag{3.116}$$

Further, the design loss coeffiecient ϖ^* can be corrected to the minimum loss coefficient (ϖ_m) using the following correlation (Aungier. 2003):

$$\varpi_m = \varpi^* \left[1 + \frac{\left(\iota_m - \iota^*\right)^2}{\left(\iota_s - \iota^*\right)^2} \right] \tag{3.117}$$

Off-design correction for deviation angle

The design deviation angle calculation explained earlier needs a correction for off-design performance evaluation. An empirical model for the slope of the off-design angle (Figure 3-14) is available in Johnsen and Bullock (1965) as a family of curves for different blade solidity and inlet flow angles. The mathematical model is given by:

$$\frac{\partial \delta}{\partial \iota} = \frac{1 + \left(\sigma + 0.25\sigma^4\right)\left(\frac{\beta_i}{53}\right)^{2.5}}{e^{3.1\sigma}} \tag{3.118}$$

Aungier (2003) then provides a model to compute the off-design deviation angle using the deviation angle slope and the same is:

$$\delta = \delta^* + \left(\frac{\partial \delta}{\partial \iota}\right)^* \left(\iota - \iota^*\right) + 10\left(1 - \frac{C_{mi}}{C_{me}}\right) \tag{3.119}$$

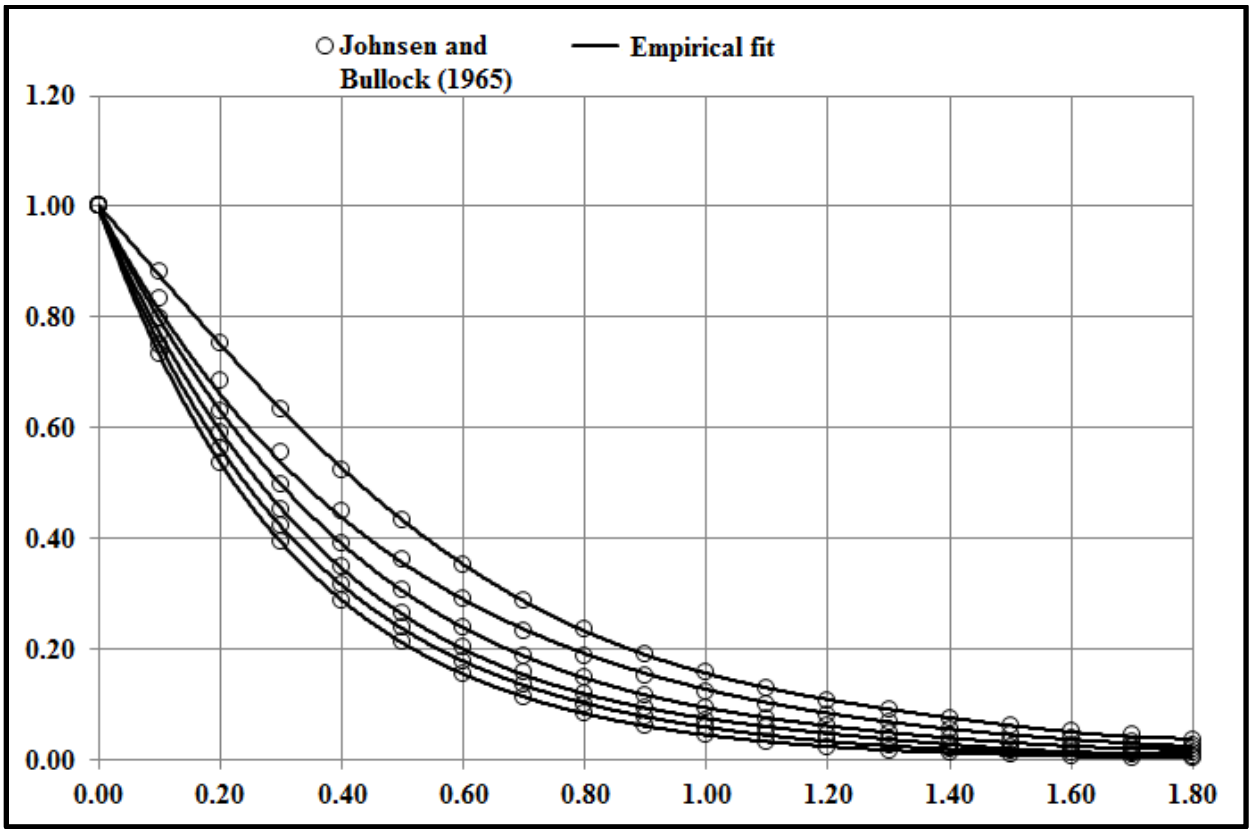

Figure 3-14 Off-design deviation angle slope

Off design loss coefficient

Once, all the above information is known the off-design loss coefficient can be calculated using Aungier's proposed model (Aungier. 2003):

$$\varpi = \varpi_s + \varpi_m \left(1+\xi^2\right); -2 \le \xi \le 1 \tag{3.120}$$

$$\varpi = \varpi_s + \varpi_m \left[5-4\left(\xi+2\right)\right]; \xi < -2 \tag{3.121}$$

$$\varpi = \varpi_s + \varpi_m \left[2+2\left(\xi-1\right)\right]; \xi \ge 1 \tag{3.122}$$

$$\xi = \frac{\imath - \imath_m}{\imath_s - \imath_m}; \imath \ge \imath_m \tag{3.123}$$

$$\xi = \frac{\imath - \imath_m}{\imath_m - \imath_c}; \imath < \imath_m \tag{3.124}$$

Clearance loss

As indicated earlier apart from the profile loss the tip clearance loss is of importance. In case of the rotor row it is usually known as the tip clearance loss while in case of the stator row the clearance losses would depend on if the stator row is shrouded or non-shrouded (Figure 3-15).

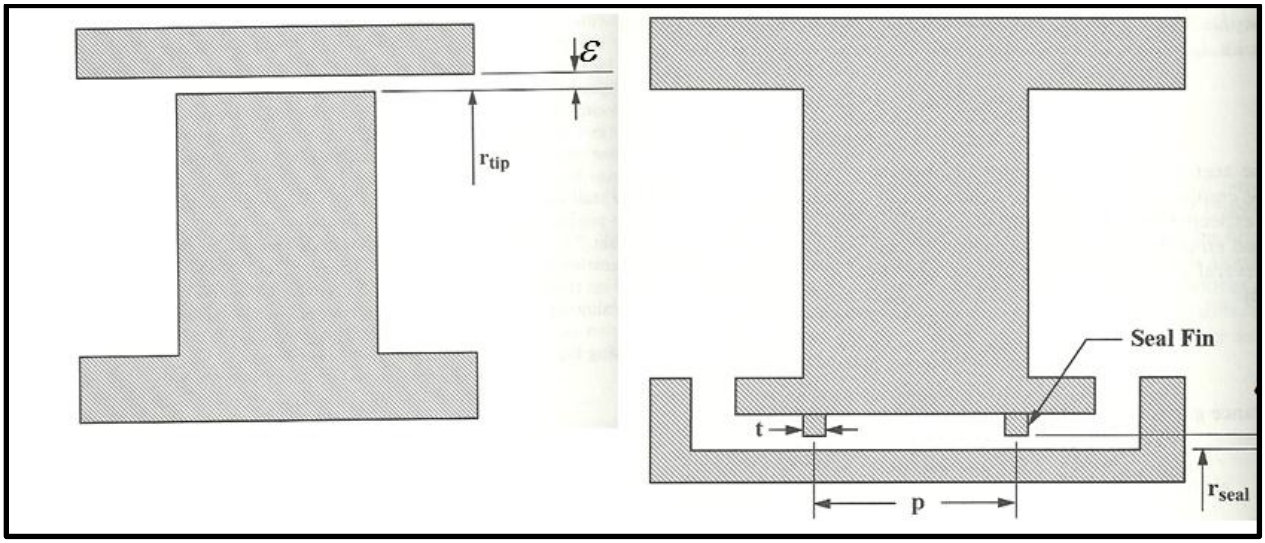

Figure 3-15 Blade tip types (unshrouded on left and shrouded on right)

If the stator row tip is shrouded then the shroud model is used while if it is un-shrouded then the tip clearance model is used. In this work, it was assumed that the stator row is un-shrouded and thus the un-shrouded tip clearance model is covered in this section. The tip clearance model was first presented for centrifugal compressor performance modeling (Aungier. 2000) and later extended to the axial compressor (Aungier. 2003). The model is based on the philosophy that the pressure difference across the blade row must balance the blade torque. For the rotor row the blade torque is expressed as:

$$\tau = \pi \varepsilon_R \left[\left(r \rho C_m \right)_i + \left(r \rho C_m \right)_e \right] \left[\left(r V_\theta \right)_e - \left(r V_\theta \right)_i \right] \tag{3.125}$$

The average pressure difference across the blade row is given by:

$$\Delta P = \frac{\tau}{N_b r_{tip} \varepsilon_R c \cos \gamma} \tag{3.126}$$

The fluid velocity of the leakage flow can then be estimated from:

$$U_{cl} = \frac{0.816\sqrt{\frac{2\Delta P}{\bar{\rho}}}}{N_{row}^{0.2}} \tag{3.127}$$

An explanation for $\bar{\rho}$ is not provided by Aungier and it was assumed to be the average of the inlet and exit densities. N_{row} is the blade row number and it accounts for the reduction of the leakage flow as one traverses downstream across the multistage compressor. This has been determined from measured performance data. The leakage mass flow rate is then expressed as:

$$\dot{m}_{cl} = \bar{\rho} U_c N_b \varepsilon_R c \cos\gamma \tag{3.128}$$

The clearance gap total pressure loss is then given by:

$$\Delta P_{cl} = \Delta P \frac{\dot{m}_{cl}}{\dot{m}} \tag{3.129}$$

Summary of loss modeling for off-design performance

1. Calculate the design incidence angle- It is a function of the blade geometry alone.
2. Calculate the design deviation angle- It is also a function of the blade geometry alone.
3. Use design incidence and deviation angles to calculate the design flow angles at inlet and exit.
4. Use the design flow angles and the axial velocities to determine equivalent design diffusion factor.
5. Use the diffusion factor to determine the design loss coefficient.
6. Correct the design loss coefficient to determine the minimum loss coefficient. This is achieved by determining the stall angles (positive and negative), correcting the stall angles for Mach number, using the corrected stall angles to compute a minimum loss incidence angle and then using the minimum loss incidence angle to determine the minimum loss coefficient.
7. Use the minimum loss coefficient to determine the off-design coefficient by using a normalized incidence angle parameter.
8. Correct the design deviation angle for off-design by determining the deviation angle slope.

Equation of state model

The equation of state (EOS) package REFPROP developed at NIST was used here for the property data (Lemmon, et al. 2010). REFPROP implements three models for the thermodynamic properties of pure fluids: equations of state explicit in Helmholtz energy, the modified Benedict-Webb-Rubin equation of state, and an extended corresponding states (ECS) model. Mixture calculations employ a model that applies mixing rules to the Helmholtz energy of the mixture components; it uses a departure function to account for the departure from ideal mixing.

Chapter 4 - Component level turbomachinery models-Turbine

Turbine construction

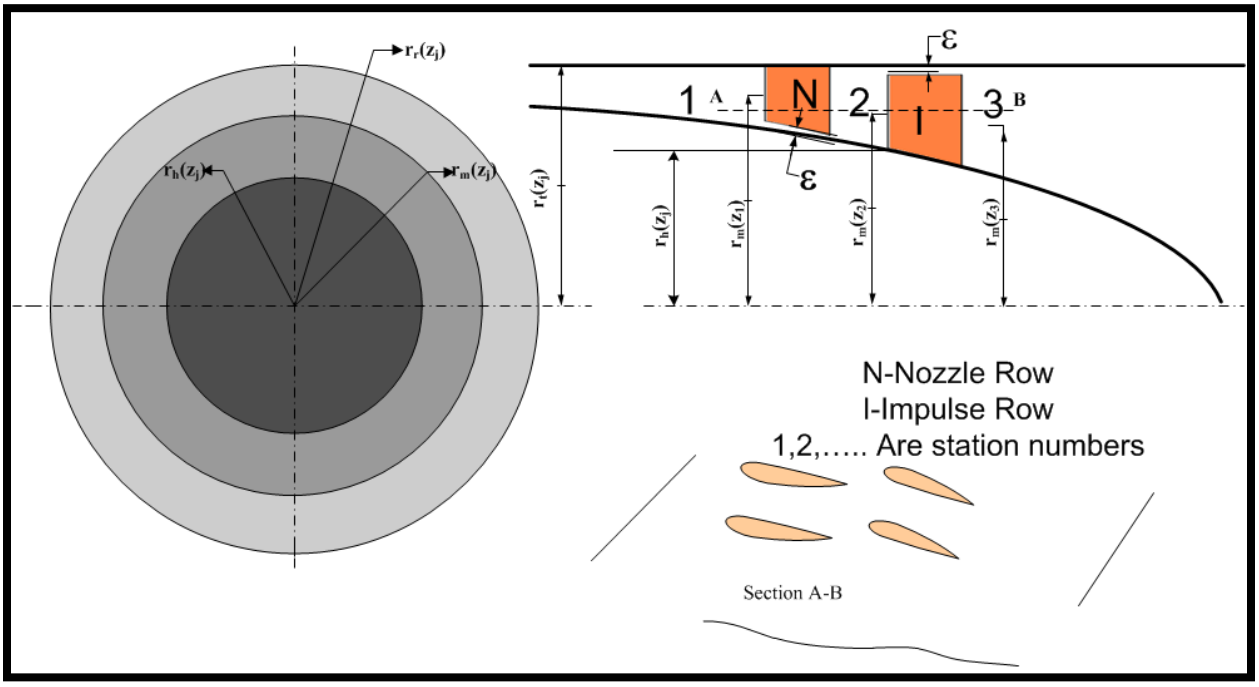

Figure 4-1 Cross section of a turbine

An axial turbine is the opposite of a compressor in terms of both the construction and the performance. Figure 4-1 shows the cross-section of a turbine. Similar to the compressor, it also has a series of blade rows that are alternately either fixed to the casing or the hub. The blade row fixed to the casing is called the stator but more often as nozzle while the one fixed to the hub is called the rotor. Similar to the compressor, the combination of a nozzle row and the rotor row constitute a stage. From the construction stand point there are two fundamental differences between the turbine and the compressor. The turbine has a consistently increasing cross-sectional area while the compressor has a decreasing cross-section. Also, the turbine stage has nozzle (stator) followed by the rotor, unlike the compressor where the rotor precedes the stator. Since the evolution of turbine sections in a CT is more from the steam turbine area rather than from the compressor so the terminology and blade sign convention is slightly different. To ensure consistent mathematical formulation for this work much of the compressor conventions are used. As an example, in the steam turbine world all angles are measured against the tangential

direction and references in the gas turbine area also follow the same. In this work however, the angles are measured against the axial direction similar to the compressor described earlier. As seen in Figure 4-1, station 1 represents the inlet to the nozzle row 1, station 2 represents the inlet to rotor row 1 and the exit of the nozzle row 1, station 3 is at the exit of the rotor row 1 and so on. The annulus area at any station j is given by equation (3.1) (Mattingly. 1996).

The remaining geometry parameters that influence the turbine performance are attributes of the blade (airfoil) such as the profile shape given by the camber line distribution (shown as $y = f(x)$ in the Figure 3-2), the blade stagger angle (γ), the blade camber angle (θ), the blade metal inlet and exit angles (κ_i and κ_e), the blade chord (c), the blade pitch (s), the blade maximum thickness (t_m), the location of the blade maximum thickness along the chord (a), the trailing edge thickness (t_e) and the throat opening (o). Detailed definitions and explanations of the blade geometry are available in number of references (Aungier. 2006, Bathie. 1996, Farokhi. 2009, Mattingly. 1996). Figure 4-2 illustrates each of these attributes. It also shows the sign convention that was used for this work. The stagger angle γ is set positive for all rows unlike in the case of the compressor and consequently the blade angles κ_i, and κ_e are positive for all the blade rows. It is customary to define the airfoil using the following ratios: solidity ($\frac{c}{s}$), maximum thickness-to-chord ($\frac{t_m}{c}$), trailing edge thickness-to-chord ($\frac{t_e}{c}$), point of maximum camber-to-chord ($\frac{a}{c}$), throat opening-to-pitch ($\frac{o}{s}$). The blade pitch (s) is a function of the radius at which it is evaluated and the number of blades and is given by equation (3.3). In the turbine $\frac{o}{s}$ is an important parameter and leads to the well-known gauging angle:

$$\beta_g = \arccos\left(\frac{o}{s}\right) \tag{4.1}$$

If the stagger is set to positive then the gauging angle is always set as negative. Unlike in the case of the NACA-65 series compressor airfoils, the literature reviewed in the turbine section did not provide any relationship between the blade metal angles and the stagger angle. Thus, the blade metal angles at the inlet and exit would be used as input parameters for the performance

evaluation. Thus, in CTOOMTURB1DPERF the necessary input blade attributes are parameters N_{blades}, r_{eval}, $\frac{a}{c}$, c, γ, $\frac{t_b}{c}$, $\frac{t_e}{c}$, κ_i, κ_i, and $\frac{o}{s}$. Finally, CTOOMTURB1DPERF, being a mean-line analysis solver, the evaluation radius (r_{eval}) is the mean radius $r_m\langle z_j \rangle$ unless any other radius is explicitly user defined for evaluation.

Velocity triangles for turbine

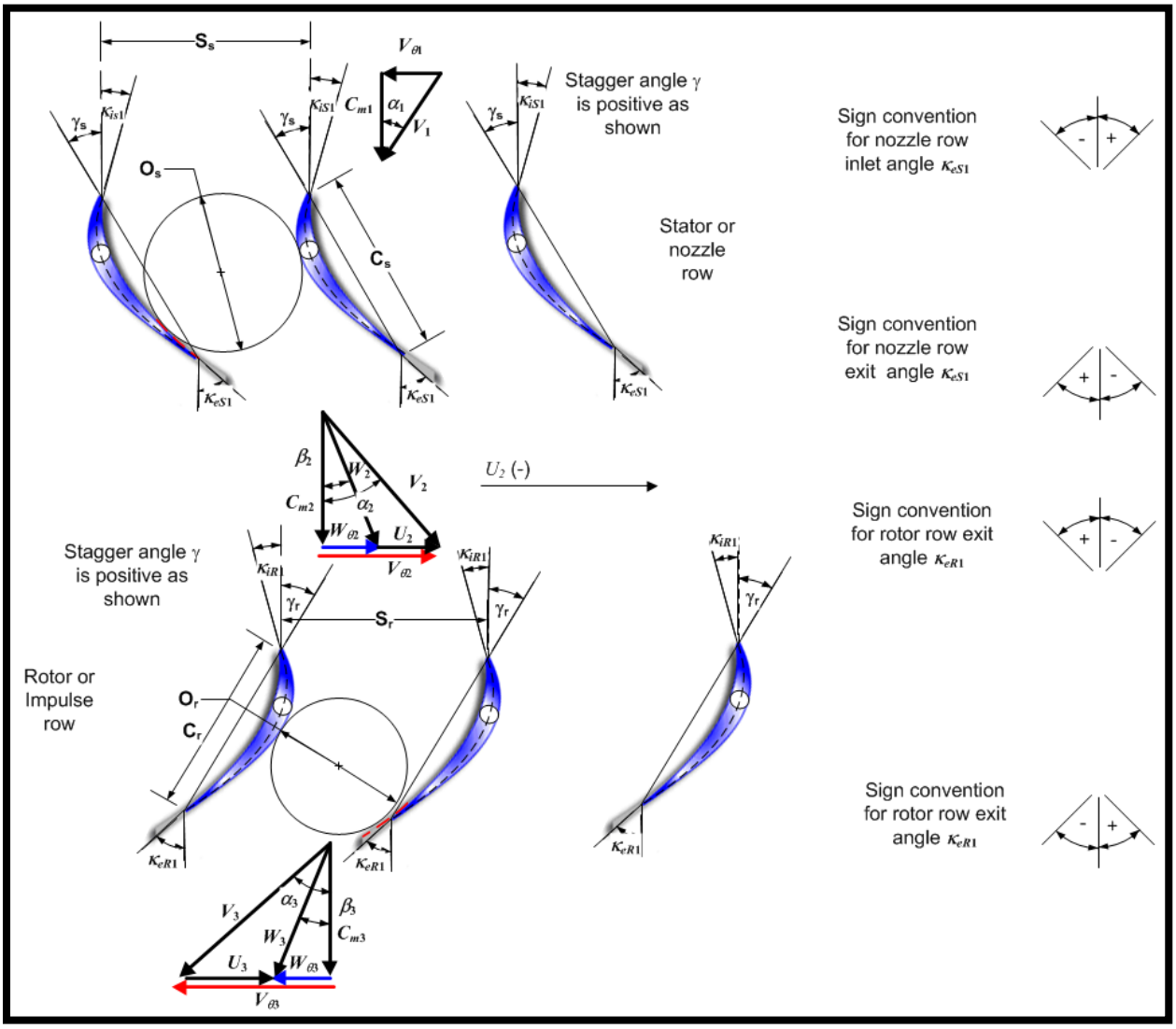

Figure 4-2 Velocity triangles in a turbine

The velocity triangles for the turbine are quite similar to the compressor. At the nozzle row inlet there is no relative velocity since the nozzle is stationary. The inlet velocity V_1 makes an angle α_1 with the axial direction. The velocity components are:

$$C_{m1} = V_1 \cos \alpha_1 \tag{4.2}$$

$$V_{\theta 1} = V_1 \sin \alpha_1 \tag{4.3}$$

If the inlet flow angle $\alpha_1 = 0$, then

$$C_{m1} = V_1 \tag{4.4}$$

At the nozzle row exit, the gas leaves at an angle α_2 and the velocity triangle gives:

$$C_{m2} = V_2 \cos \alpha_2 \tag{4.5}$$

$$V_{\theta 2} = V_2 \sin \alpha_2 \tag{4.6}$$

In the equation (4.5) and (4.6) α_2 is unknown. As seen in the compressor section, the gas exit flow angle is related to the blade metal angle at exit and a known angle of deviation. In the turbine the exit flow angle is called the gas efflux angle and is strongly correlated to the gauging angle:

$$\alpha_2 = f\left\langle \beta_{gS1} \right\rangle \tag{4.7}$$

The other half of the velocity triangle is expressed as:

$$C_{m2} = W_2 \cos \beta_2 \tag{4.8}$$

$$W_{\theta 2} = W_2 \sin \beta_2 \tag{4.9}$$

$$U_2 = V_{\theta 2} - W_{\theta 2} \tag{4.10}$$

At station 3, the gas efflux angle β_3 can be determined from the rotor row gauging angle (β_{gR1}) and relevant equations then are:

$$C_{m3} = W_3 \cos \beta_3 \tag{4.11}$$

$$W_{\theta 3} = W_3 \sin \beta_3 \tag{4.12}$$

$$C_{m3} = V_3 \cos \alpha_3 \tag{4.13}$$

$$V_{\theta 3} = V_3 \sin \alpha_3 \tag{4.14}$$

$$U_3 = V_{\theta 3} - W_{\theta 3} \tag{4.15}$$

Note that the rotor blade has a tangential velocity U_2 due to the rotational speed N of the compressor and is calculated using:

$$U_2 = \frac{2\pi r_m \langle z_2 \rangle N}{60} \tag{4.16}$$

Equation (4.16) remains valid for computing U_3 by changing the subscripts from 2 to 3.

Mathematical models for nozzle inlet, nozzle exit, rotor inlet and rotor exit

The mathematical model for the turbine components is similar to that of the compressor and the equations are listed below. At the nozzle row inlet the following three equations are solved simultaneously:

$$h_{st1} = h_{ta1} - \frac{C_{m1}^2}{2\left[\cos(\alpha_1)\right]^2} \tag{4.17}$$

$$\dot{m}_1 = \rho_{st1} A_1 C_{m1} \tag{4.18}$$

$$\rho_{st1} = f\langle h_{st1}, s_1 \rangle \tag{4.19}$$

In the equations (4.18) $\dot{m}_1$, α_1 and A_1 are user specified. h_{ta1} and s_1 can be calculated a priori from the user specified values of P_{ta1} and T_{ta1}. Nozzle inlet model is complete only when the variables ι_1, a_1, V_1, P_{st1}, T_{st1}, M_{a1} are computed. Relevant equations for these variables have been documented earlier in the compressor section.

At the nozzle row exit the equations are:

$$h_{st2} = h_{ta2} - \frac{C_{m2}^2}{2\left[\cos(\alpha_2)\right]^2} \tag{4.20}$$

$$\dot{m}_2 = \rho_{st2} A_2 C_{m2} \tag{4.21}$$

$$\rho_{st2} = f\langle h_{st2}, s_2 \rangle \tag{4.22}$$

$$s_2 = f\langle h_{ta2}, P_{ta2} \rangle \tag{4.23}$$

$$P_{ta2} = \frac{P_{ta1} + Y_{S1} P_{s2}}{1 + Y_{S1}} - \Delta P_{cl} \tag{4.24}$$

Equation (4.24) is derived from the definition of the turbine loss coefficient (Y) which is:

$$Y = \frac{P_{t1} - P_{t2}}{P_{t2} - P_{s2}} \tag{4.25}$$

Equation (4.24) adds another unknown P_{st2}, hence for closure an additional equation is necessary, which is:

$$P_{st2} = f\left\langle h_{st2}, s_2 \right\rangle \tag{4.26}$$

Thus unlike the compressor stator exit where only five equations were sufficient to describe the system, at the turbine stator exit six equations are necessary. However, there are two additional unknowns in the system of equations i.e., efflux angle and loss coefficient. As long as these are modeled separately and specified the above system can be solved. It should be recalled that the stator exit is also the rotor inlet which then gets fully described. In equation (4.25) the suffixes for absolute or relative quantities have been dropped in the description of total pressure to provide a generalized model. For nozzle row the quantities are absolute while they are relative for the rotor row. Re-arranging equation (4.25) to solve for P_{t2} would provide the first term of equation (4.24). The second term is simply added to account for the clearance losses if the clearance losses are modeled separately. In the classic Ainley-Matheison-Durham-Came (AMDC) loss model the clearance losses are tied into the secondary losses and the second term then is dropped. For completeness the remaining variables a_2, V_2, W_2, P_{st2}, T_{st2}, M_{a1}, M_{r1}, β_2, I_2 , H_{tr2} , P_{tr2}, T_{tr2} at the stator exit are computed. Finally, at the rotor exit six equations to be solved simultaneously are:

$$h_{st3} = H_{tr3} - \frac{C_{m3}^2}{2\left[\cos\left(\beta_3\right)\right]^2} \tag{4.27}$$

$$\dot{m}_3 = \rho_{st3} A_3 C_{m3} \tag{4.28}$$

$$\rho_{st3} = f\left\langle h_{st3}, s_3 \right\rangle \tag{4.29}$$

$$s_3 = f\left\langle h_{tr3}, P_{tr3} \right\rangle \tag{4.30}$$

$$P_{tr3} = \frac{P_{tr2} + Y_{R1} P_{st3}}{1 + Y_{R1}} - \Delta P_{cl} \tag{4.31}$$

$$P_{st3} = f\left\langle h_{st3}, s_3 \right\rangle \tag{4.32}$$

Turbine losses are usually categorized into profile losses, secondary losses and clearance losses. The clearance losses could be modeled separately (Aungier. 2006) or they could be modeled as part of the secondary losses (Ainley & Mathieson. 1951). The Ainley-Mathieson model is presented here.

Profile loss coefficient

Ainley and Mathieson (1951) published graphical correlations for loss coefficient for both nozzle blades and the impulse blades. Aungier (2006) provides the analytical form for it. For the Ainley-Mathieson correlations low speed cascade testing was done for $\frac{t_e}{s} = 0.02$ and hence all of the below is applicable only for the same. Ainley and Mathieson used the axial direction as the reference for measuring all angles and the same is done here. Aungier, however, uses the tangential direction as the reference. Thus, in order to use Aungier's analytical model the first step is to do a reference coordinate transformation. This was accomplished as below:

$$\alpha_{et} = 90 - \alpha_e \tag{4.33}$$

In equation (4.33) α_e denotes the gas flow efflux angle i.e., the flow angle at exit. For the nozzle row it would be α_2 while for the impulse row it would be β_3.

Nozzle row profile loss coefficient

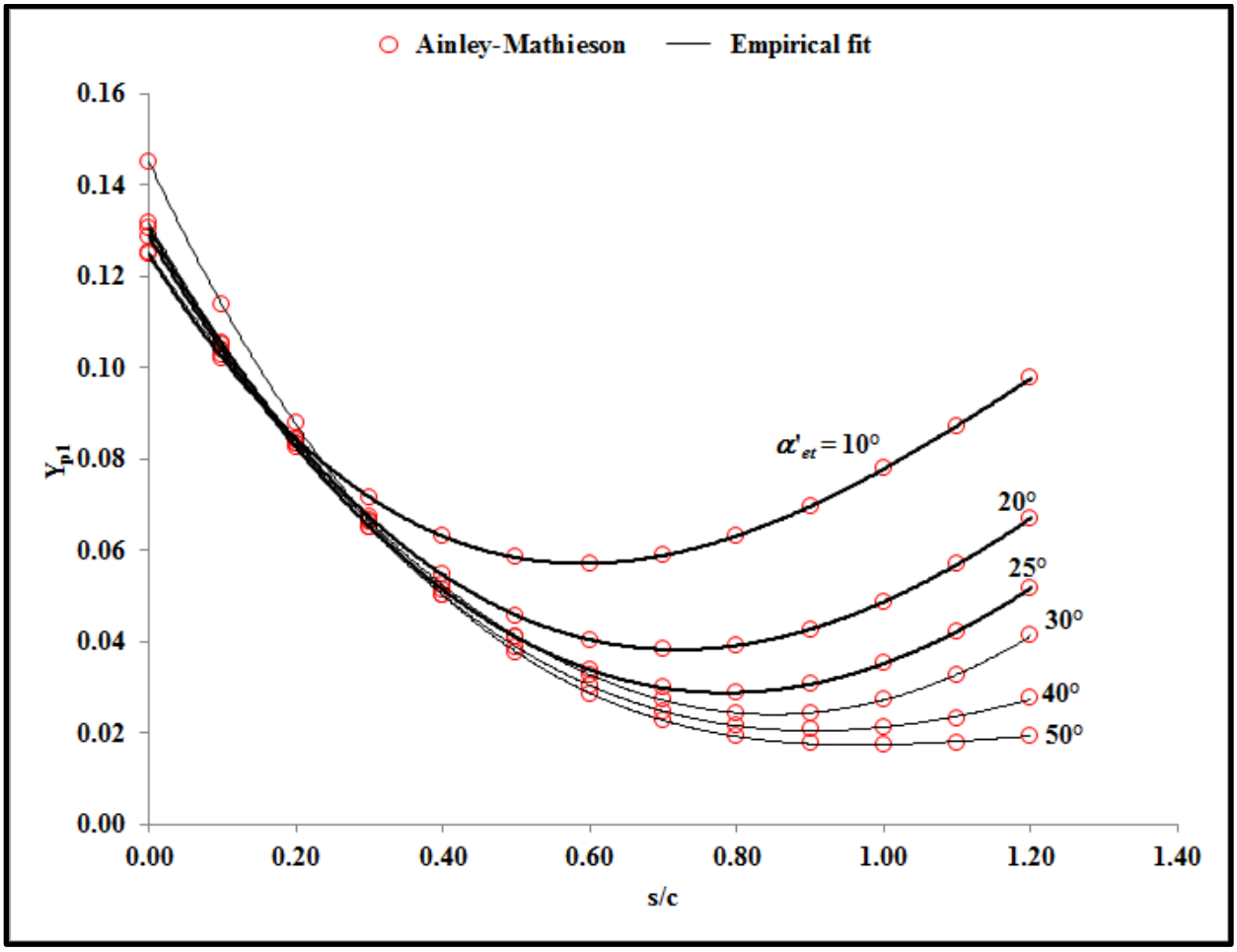

Figure 4-3 Nozzle row profile loss coefficient

Figure 4-3 provides the nozzle row profile coefficient. It is a modification by Aungier of the original Ainley-Mathieson model, the modification being the reference transformation from axial to tangential. A generalized one equation does not fit very well for the entire set of curves and thus the graph has been split into two pieces one for $\alpha_{et} > 30^{\circ}$ and the other for $\alpha_{et} \le 30^{\circ}$. α_{et} is the exit flow angle in the tangential direction. The loss coefficient can then be approximated as follows:

$$Y_{p1} = A_N + B_N X^2 + C_N X^3; \qquad \alpha_{et} \le 30^{\circ} \tag{4.34}$$

$$Y_{p1} = A_N + B_N |X|^n; \qquad \alpha_{et} > 30^{\circ} \tag{4.35}$$

where,

$$X = \frac{s}{c} - \left(\frac{s}{c}\right)_{\min} \tag{4.36}$$

and $$\left(\frac{s}{c}\right)_{\min} = 0.46 + \frac{\alpha_{et}}{77} \qquad ;\alpha_{et} \le 30^{\circ} \tag{4.37}$$

$$\left(\frac{s}{c}\right)_{\min} = 0.46 + \frac{\alpha_{et}}{77} \qquad ;\alpha_{et} > 30^{\circ} \tag{4.38}$$

While the values of the coefficients are

$$A_N = 0.025 + \frac{27 - \alpha_{et}}{530} \qquad ;\alpha_{et} \le 27^{\circ} \tag{4.39}$$

$$A_N = 0.025 + \frac{27 - \alpha_{et}}{3085} \qquad ;\alpha_{et} > 27^{\circ} \tag{4.40}$$

$$B_N = 0.1583 - 1640 \qquad ;\alpha_{et} \le 30^{\circ} \tag{4.41}$$

$$C_N = 0.08\left[\left(\frac{\alpha_{et}}{30}\right)^2 \text{-1}\right] \tag{4.42}$$

$$n = 1 + \frac{\alpha_{et}}{30} \tag{4.43}$$

The Ainley-Mathieson correlations were developed for the blade angle $\kappa_i = 0^{\circ}$ which represents $\kappa_i = 90^{\circ}$ for the Aungier modification.

Impulse blade row profile loss coefficient

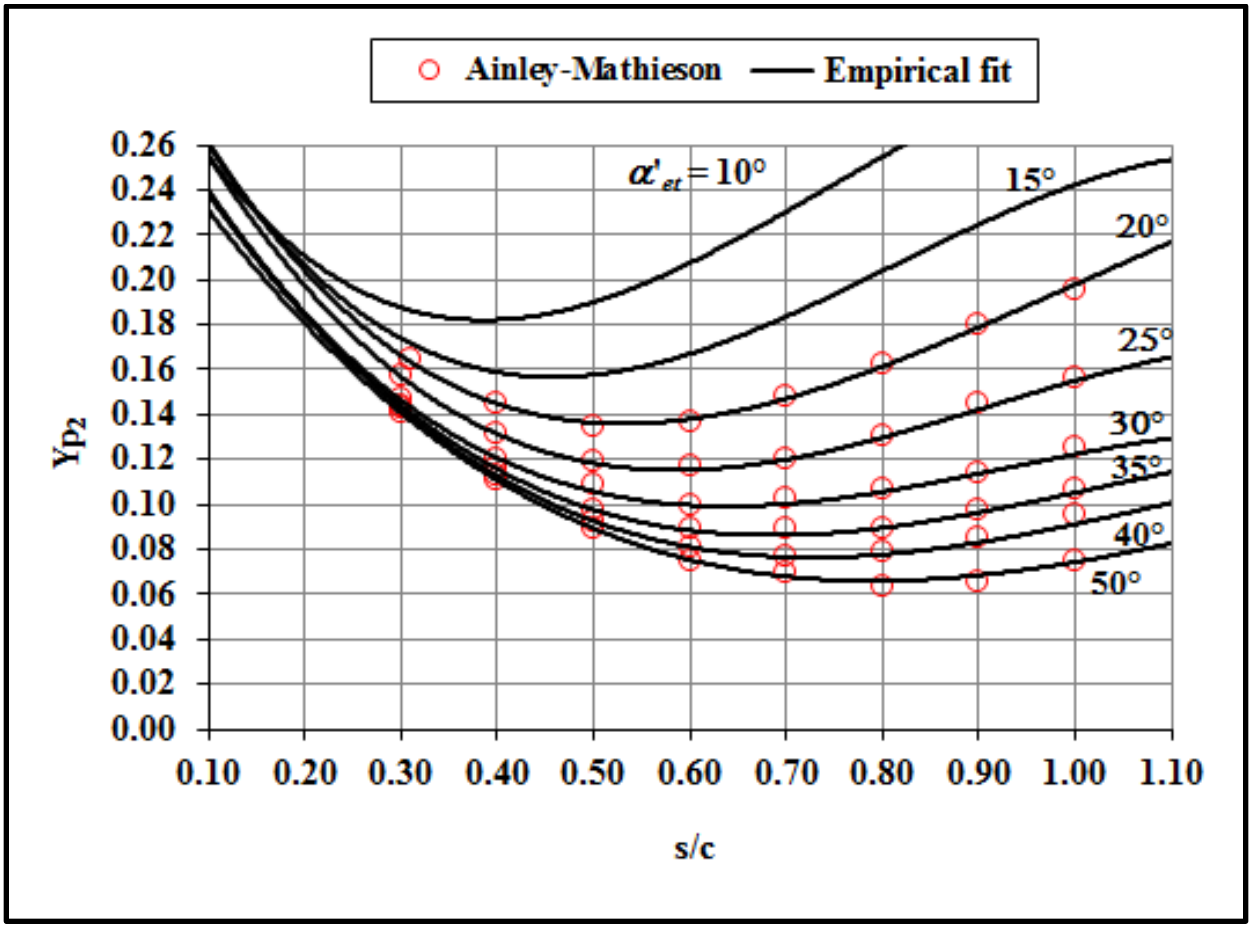

Figure 4-4 Impulse row profile loss coefficient

Figure 4-4 provides the impulse row profile coefficient plots. It is a modification by Aungier of the original Ainley-Mathieson model, the modification being the reference transformation from axial to tangential. Even in this case a generalized one equation does not fit very well for the entire set of curves and thus the graph has been split into two pieces one for $\alpha_{et} > 30^{\circ}$ and the other for $\alpha_{et} \le 30^{\circ}$. The loss coefficient can then be approximated as follows:

$$Y_{p2} = A_I + B_I X^2 - C_I X^3 \tag{4.44}$$

where,
$$X = \frac{s}{c} - \left(\frac{s}{c}\right)_{\min} \tag{4.45}$$

and
$$\left(\frac{s}{c}\right)_{\min} = 0.224 + 1.575\left(\frac{\alpha_{et}}{90}\right) - \left(\frac{\alpha_{et}}{90}\right)^2 \tag{4.46}$$

While the values of the coefficients are

$$A_I = 0.242 - \frac{\alpha_{et}}{151} + \left(\frac{\alpha_{et}}{127}\right)^2 \tag{4.47}$$

$$B_I = 0.3 + \frac{(30 - \alpha_{et})}{50} \quad ; \alpha_{et} \leq 30^\circ \tag{4.48}$$

$$B_I = 0.3 + \frac{(30 - \alpha_{et})}{275} \quad ; \alpha_{et} > 30^\circ \tag{4.49}$$

$$C_I = 0.88 - \frac{\alpha_{et}}{42.4} + \left(\frac{\alpha_{et}}{72.8}\right)^2 \tag{4.50}$$

These impulse row correlations were developed for $\alpha_{et} = \kappa_i$.

Overall profile loss coefficient

The nozzle row profile loss coefficient (Y_{p1}) and the impulse row profile loss coefficient (Y_{p2}) can be combined to compute the overall profile loss coefficient (Y_p):

$$Y_p = \left[Y_{p1} + \xi\left(Y_{p2} - Y_{p1}\right)\right]\left(5\frac{t_m}{c}\right)^{\xi} \tag{4.51}$$

In case of the nozzle row alone the Y_{p2} is zero while in case of evaluating the impulse blade both the Y_{p1} and Y_{p2} terms are used.

Incidence angle correction

An incidence angle correction is required for determining the off-design incidence loss coefficient. In order to determine that first the stall incidence angle needs to be calculated.

Stall incidence angle

The stalling incidence angle as presented by Ainley-Mathieson (1959) is a function of α_e, ξ and $\frac{s}{c}$. Ainley-Mathieson's graphs revised by Aungier (2006) are presented in Figure 4-5.

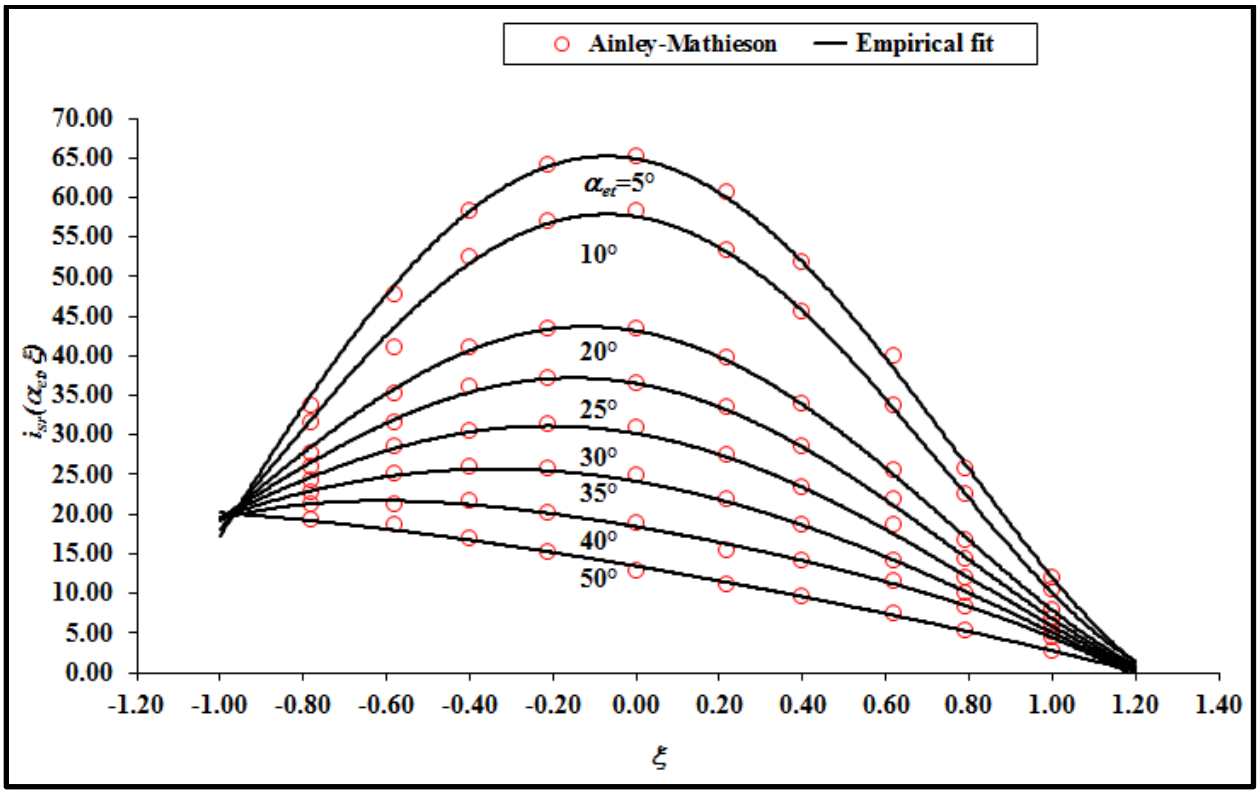

Figure 4-5 Stall angle of incidence for $\frac{s}{c}=0.75$

The graphical relationship is specific for $\frac{s}{c}=0.75$. The Ainley-Mathieson model is applicable for $\alpha_{et}\le 40^{\circ}$. The empirical equation for the model is:

$$\iota_{sr}\left(\alpha_{et},\xi\right)=\iota_{s0}+A_{stall}-B_{stall}\xi^{2}+C_{stall}\xi^{3}+D_{stall}\xi^{4};\quad \alpha_{et}\le 40^{\circ} \tag{4.52}$$

$$\iota_{s0}=20-\frac{\xi+1}{0.11} \tag{4.53}$$

$$A_{stall}=61.8-\left(1.6-\frac{\alpha_{et}}{165}\right)\alpha_{et} \tag{4.54}$$

$$B_{stall}=71.9-1.69\alpha_{et} \tag{4.55}$$

$$C_{stall}=7.8-\left(0.28-\frac{\alpha_{et}}{320}\right)\alpha_{et} \tag{4.56}$$

$$D_{stall}=14.2-\left(0.16-\frac{\alpha_{et}}{160}\right)\alpha_{et} \tag{4.57}$$

Aungier (2006) suggests that the model can be extrapolated beyond $\alpha_{et} > 40^{\circ}$ and furnishes an analytical model for the extrapolation as:

$$\iota_{sr}\left(\alpha_{et},\xi\right) = \iota_{s0} + \frac{\left|\iota_{sr}\left(40,\xi\right) - \iota_{s0}\right|\left|55 - \alpha_{et}\right|}{15}; \qquad \alpha_{et} > 40^{\circ} \tag{4.58}$$

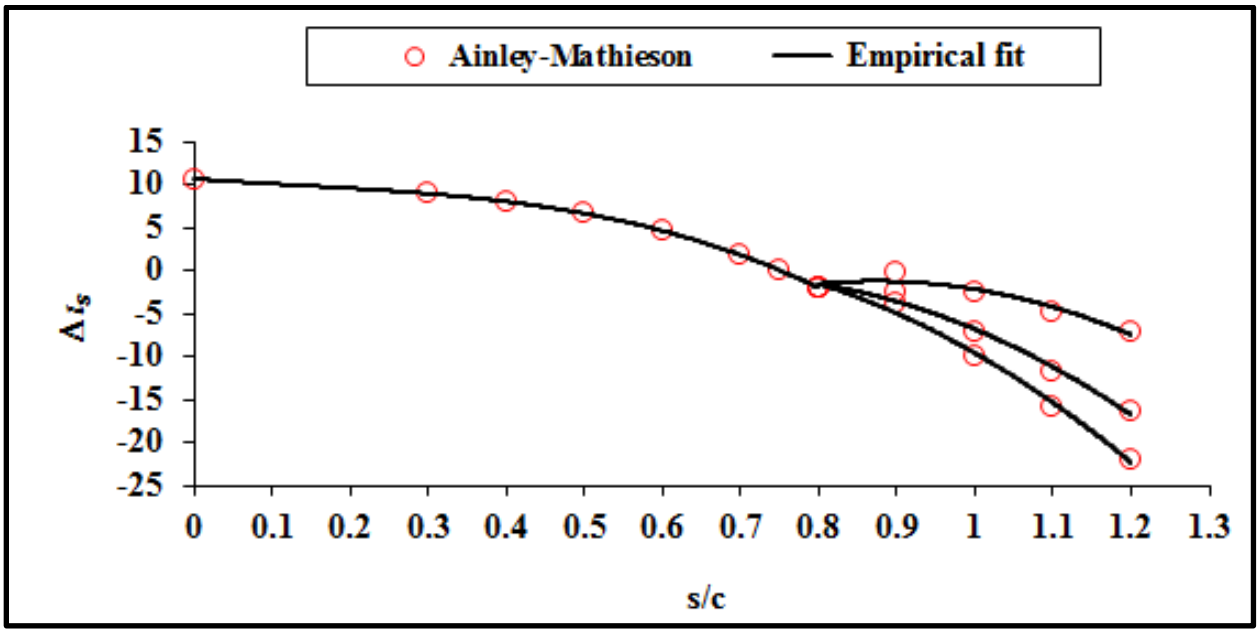

Figure 4-6 Stall angle correction factor

The equations (4.52) and (4.58) provide a reference stall incidence angle, $\iota_{sr}\left(\alpha_{et},\xi\right)$, for the problem specific α_{et} and ξ but for $\frac{s}{c} = 0.75$. Thus, a correction factor of $\Delta\iota_s\left(\alpha_{et},\frac{s}{c}\right)$ is added to the reference stall incidence angle to determine the problem specific stall angle, ι_s. The correction factor is modeled as:

$$\Delta\iota_s = -38\left(\frac{s}{c} - 0.75\right) - 53.5\left(\frac{s}{c} - 0.75\right)^2 - 29\left(\frac{s}{c} - 0.75\right)^3; \qquad \frac{s}{c} \le 0.8 \tag{4.59}$$

$$\Delta\iota_s = 2.0374 - \left(\frac{s}{c} - 0.8\right)\left[69.58 - \left(\frac{\alpha_{et}}{14.48}\right)^{3.1}\right]; \qquad \frac{s}{c} > 0.8 \tag{4.60}$$

Thus, the problem specific stall angle can now be calculated using:

$$\iota_s = \iota_{sr}\left(\alpha_{et},\xi\right) + \Delta\iota_s\left(\alpha_{et},\frac{s}{c}\right) \tag{4.61}$$

Incidence angle correction factor

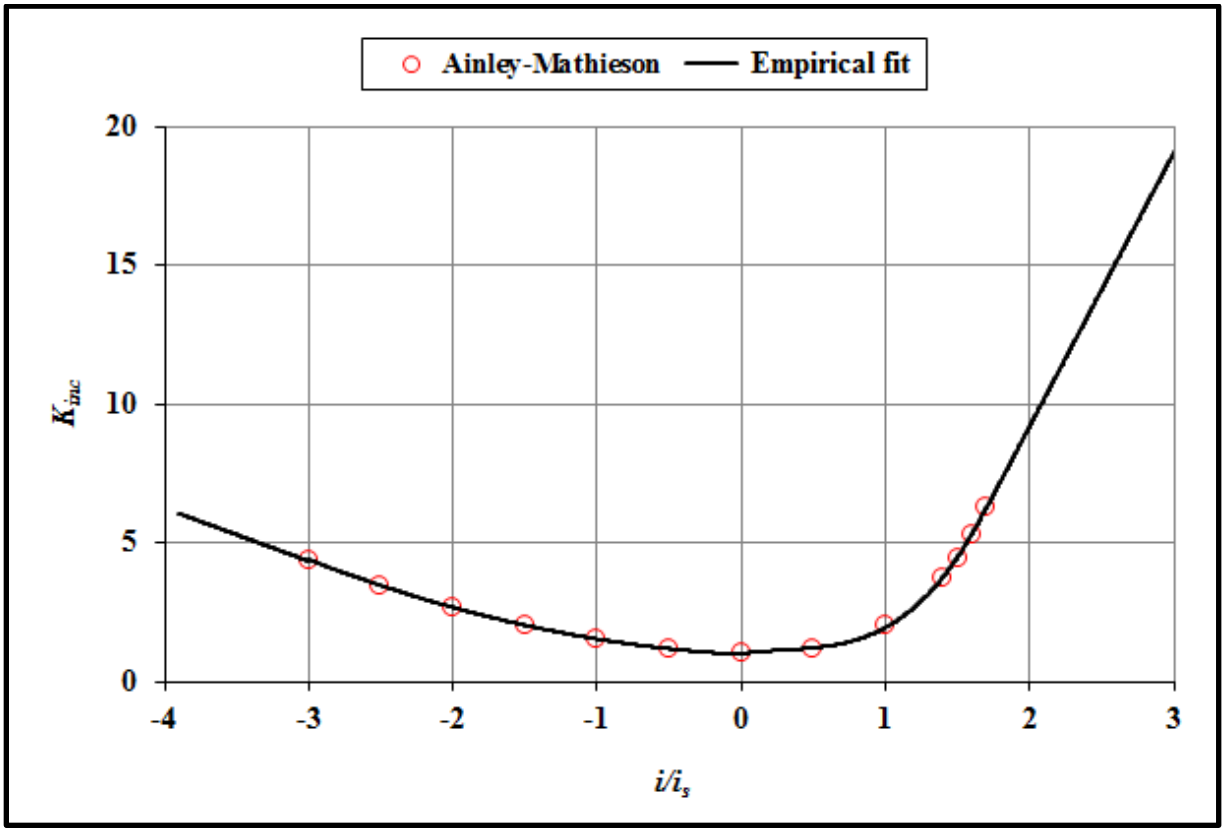

Figure 4-7 Stall angle of incidence for $\frac{s}{c} = 0.75$

The incidence angle correction factor for off-design incidences is presented in Figure 4-7 as proposed by Ainley-Mathieson. Since a single empirical model cannot satisfy the curve four separate models for portions of the curve are:

$$K_{inc} = -1.39214 - 1.90738\left(\frac{\iota}{\iota_s}\right); \quad \frac{\iota}{\iota_s} < -3^\circ \tag{4.62}$$

$$K_{inc} = 1 + 0.52\left|\frac{\iota}{\iota_s}\right|^{1.7}; \quad -3^\circ \le \frac{\iota}{\iota_s} < 0^\circ \tag{4.63}$$

$$K_{inc} = 1 + \left(\frac{\iota}{\iota_s}\right)^{\left(2.3+0.5\frac{\iota}{\iota_s}\right)}; \quad 0^\circ \le \frac{\iota}{\iota_s} < 1.7^\circ \tag{4.64}$$

$$K_{inc} = 6.23 - 9.8577\left(\frac{\iota}{\iota_s} - 1.7\right); \quad \frac{\iota}{\iota_s} > 1.7^\circ \tag{4.65}$$

Secondary flow loss coefficient

The secondary flow loss is a function of the lift and the lift coefficient and defined as:

$$C_L = 2\left(\tan\alpha_i - \tan\alpha_e\right)\frac{s}{c}\cos\alpha_m \tag{4.66}$$

where,

$$\alpha_m = \arctan\left(\frac{\tan\alpha_i + \tan\alpha_e}{2}\right) \tag{4.67}$$

The Ainley loading parameter is defined as:

$$Z = \left(\frac{C_L}{\frac{s}{c}}\right)^2 \frac{\cos^2\alpha_e}{\cos^2\alpha_m} \tag{4.68}$$

Then, the secondary flow loss coefficient is:

$$Y_s = \lambda Z \tag{4.69}$$

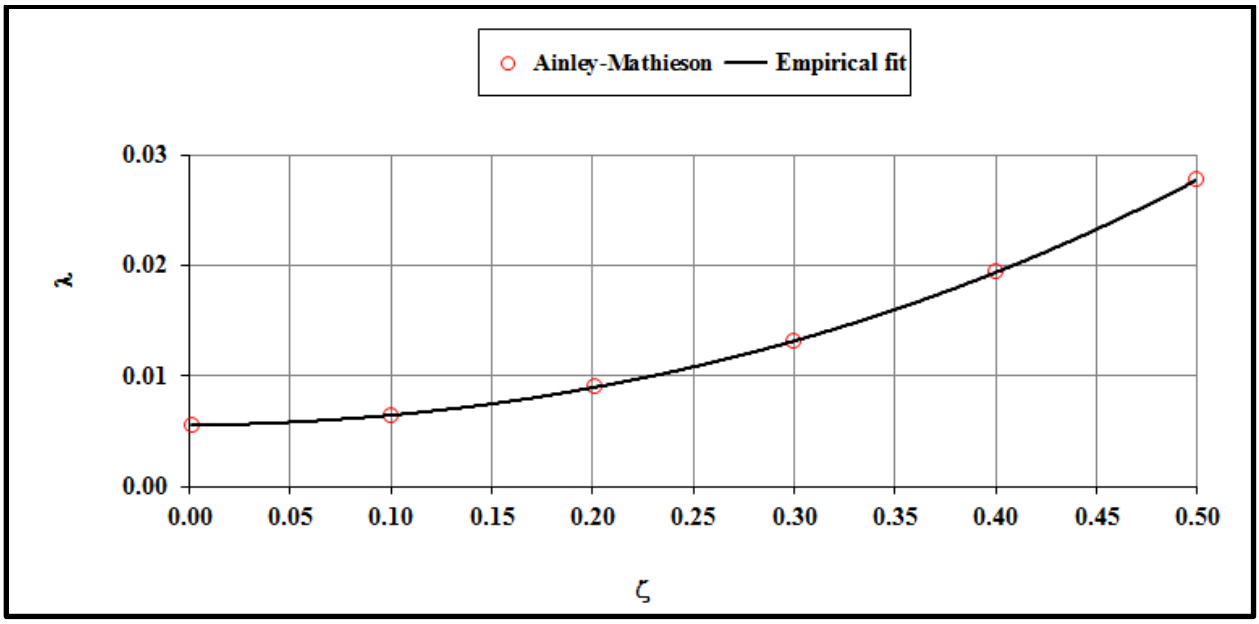

Figure 4-8 λ parameter for secondary losses

λ is a function of the area expansion correction parameter ζ which is:

$$\zeta = \frac{\left(\frac{A_e}{A_i}\right)^2}{1+\frac{r_h}{r_t}} \tag{4.70}$$

$$\lambda = 0.0367\zeta^3 + 0.0663\zeta^2 + 0.0023\zeta + 0.0055 \tag{4.71}$$

Tip Clearance loss

Tip clearance losses are associated with either shrouded or unshrouded blades. Ainley and Mathieson (1951) presented a general purpose model covering both the types. Dunham and Came (1970) offer an improvement to this model for unshrouded blades only while Aungier uses Egli's labyrinth seal contraction theory to model shrouded tip clearances separately. For this work, the shrouded seal data was not available and hence the same has not been included.

Ainley-Mathieson model is a function of the blade height and the tip clearance:

$$Y_L = ZB\frac{\varepsilon}{h} \tag{4.72}$$

where, $B = 1.35$ for radial tip clearances or 0.7 for shrouded blades.

Dunham and Came (1970) propose a correction by introducing the blade chord into the model as below:

$$Y_L = 0.47Z\frac{c}{h}\left(\frac{\varepsilon}{c}\right)^{0.78} \tag{4.73}$$

Total loss coefficient and associated correction

The total loss coefficient is now modeled as:

$$Y = Y_p + Y_s + Y_L \tag{4.74}$$

It has been indicated earlier that all of the above models are applicable only for $\frac{t_e}{s} = 0.02$ and hence the same needs correction. Ainley-Mathieson provided a tip thickness correction model (Figure 4-9). The value of Y can be corrected using the same.

$$\frac{Y}{Y_{\frac{t_e}{s}=0.02}} = 16.196\left(\frac{t_e}{s}\right)^2 + 4.5903\left(\frac{t_e}{s}\right) + 0.9082 \tag{4.75}$$

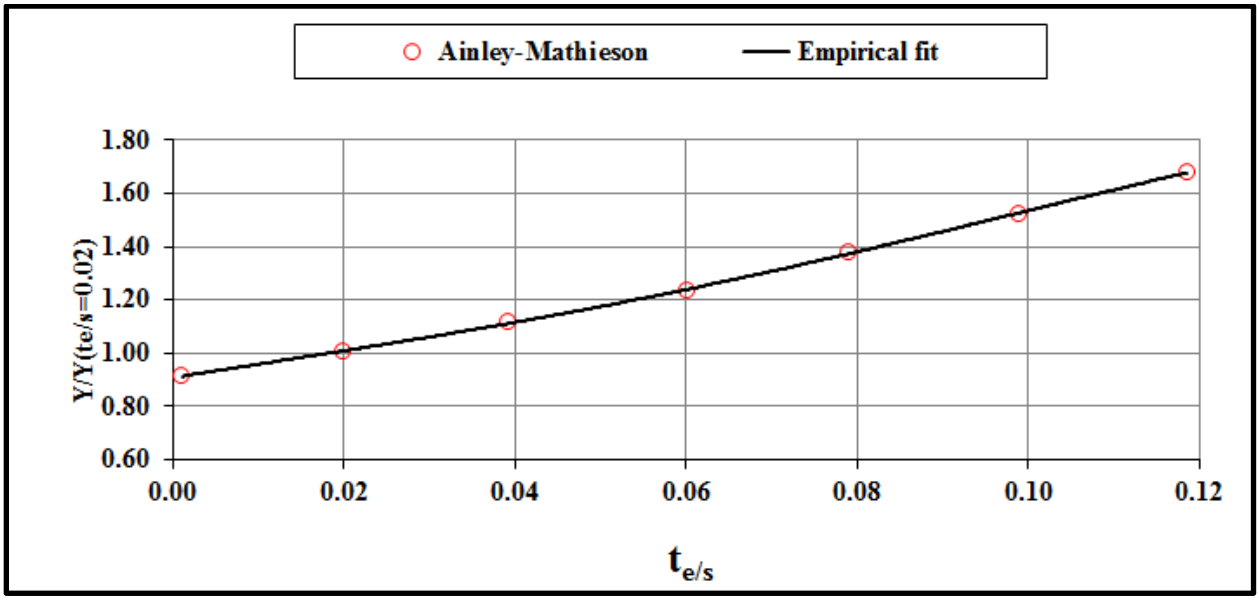

Figure 4-9 Tip thickness correction

Deviation angle correlation

Ainley and Mathieson (1951) provided correlations for the deviation angle information for different gauging angle as a function of the Mach number. However, it drops significantly

between Mach numbers 0.5 to 1.0. For Mach number values less than 0.5, the deviation angle expressed as a function of the deviation angle is:

$$\delta_0 = \arcsin\left\{\frac{o}{s}\left[1+\left(1-\frac{o}{s}\right)\left(\frac{90-\beta_g}{90}\right)^2\right]\right\}-\left(90-\beta_g\right) \tag{4.76}$$

For Mach numbers greater than, 0.5 the deviation angle is:

$$\delta = \delta_0\left[1-10\left(M_e-0.5\right)^3+15\left(M_e-0.5\right)^4-6\left(M_e-0.5\right)^5\right] \tag{4.77}$$

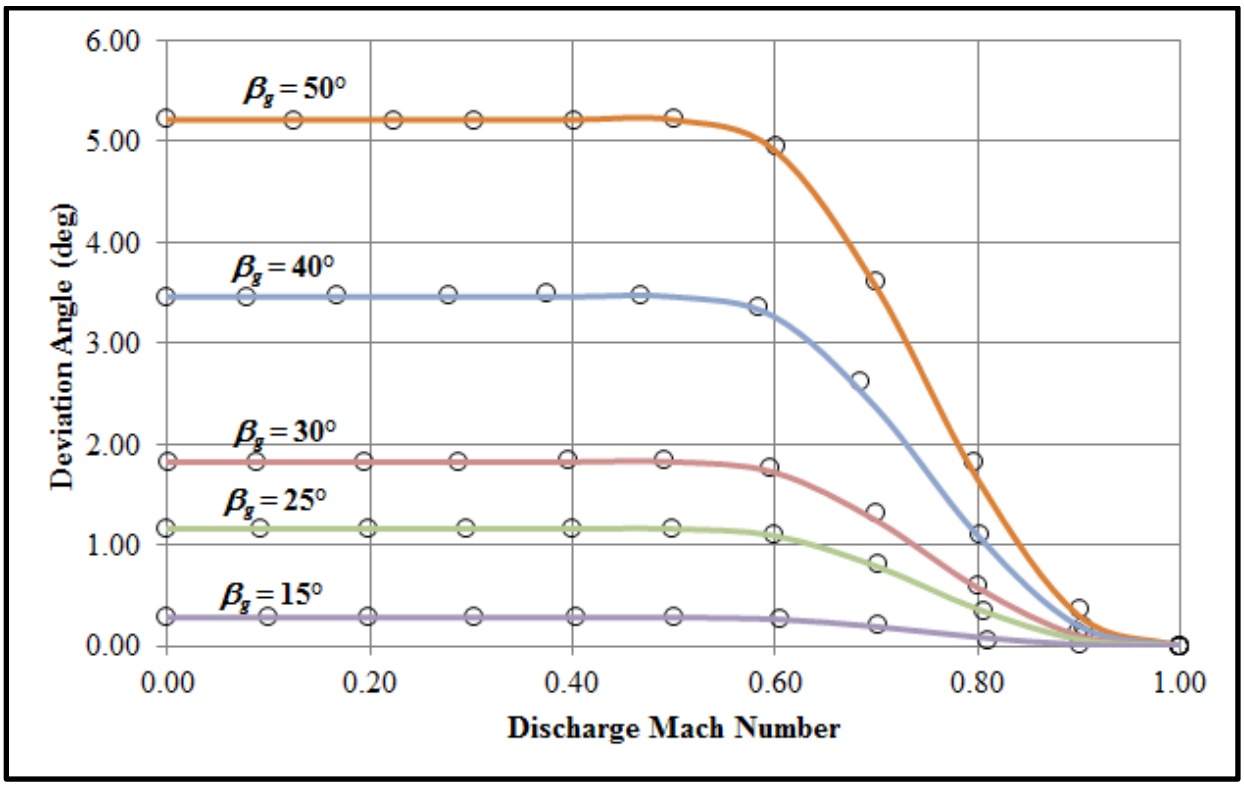

Figure 4-10 Deviation angle

Chapter 5 - Computer program development

Optimization model program architecture and interface

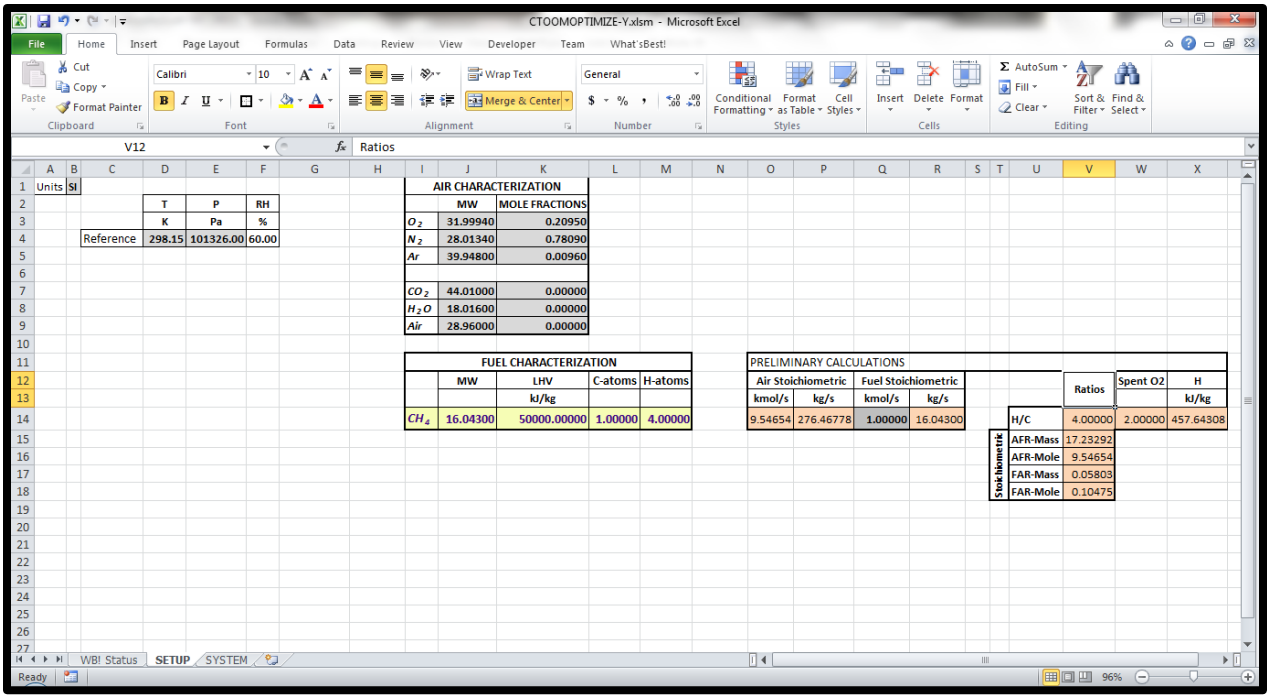

Figure 5-1 Screen shot of MS Excel workbook – Setup sheet

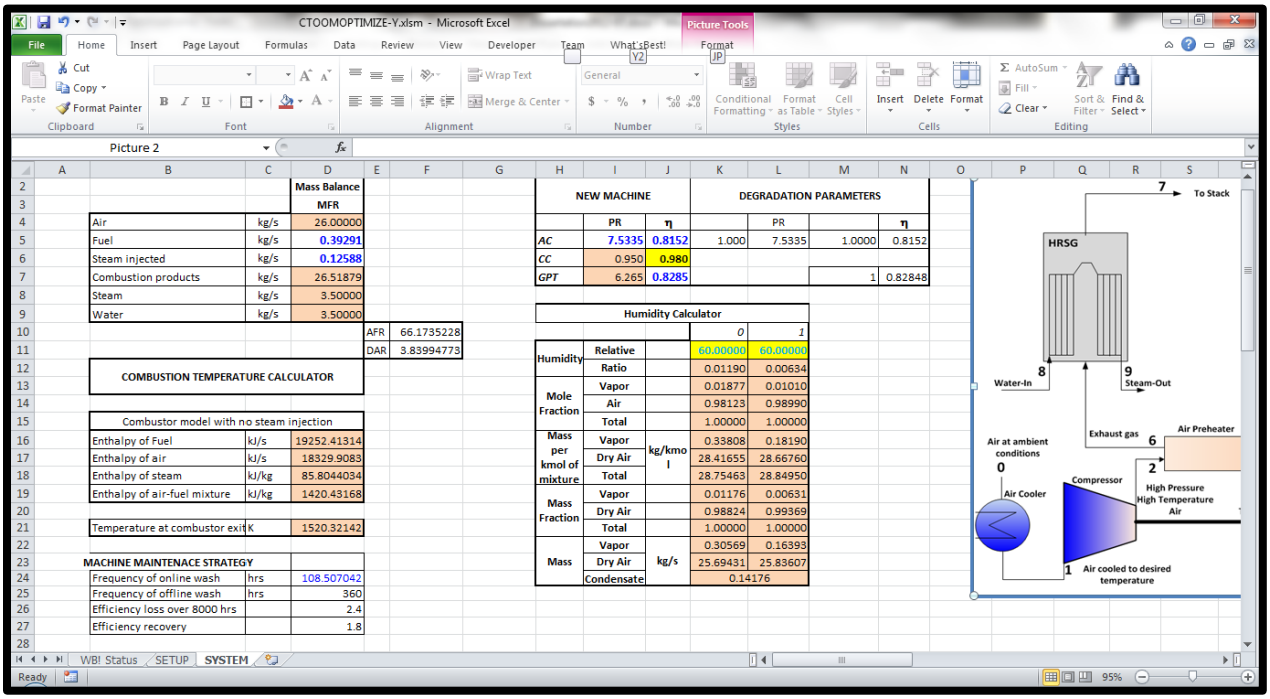

Figure 5-2 Screen shot of MS Excel workbook- SYSTEM worksheet (1)

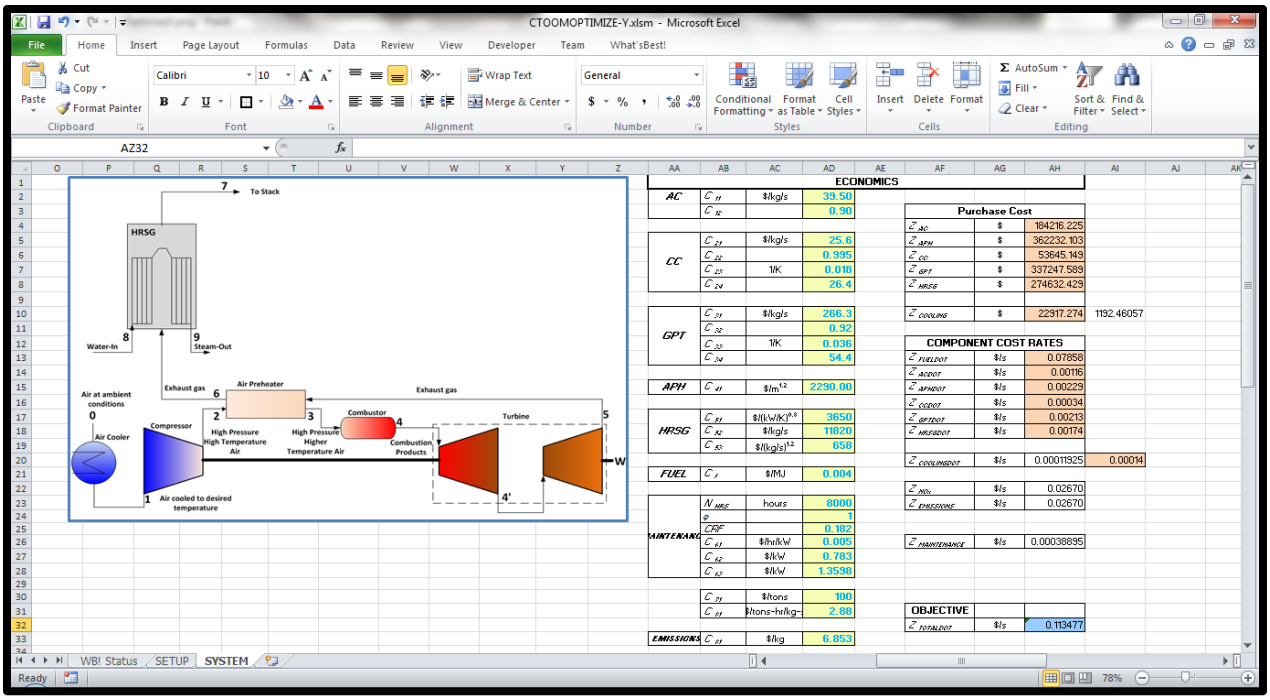

Figure 5-3 Screen shot of MS Excel workbook – SYSTEM worksheet (2)

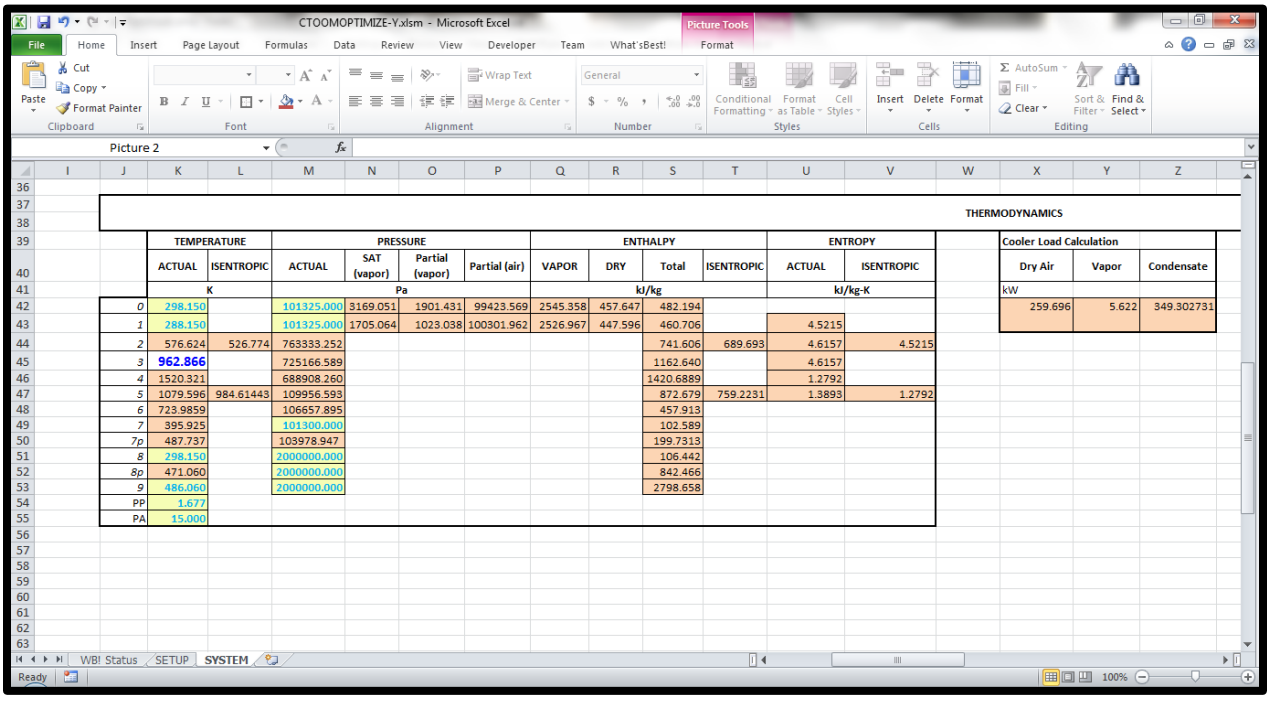

Figure 5-4 Screen shot of MS Excel workbook- SYSTEM worksheet (3)

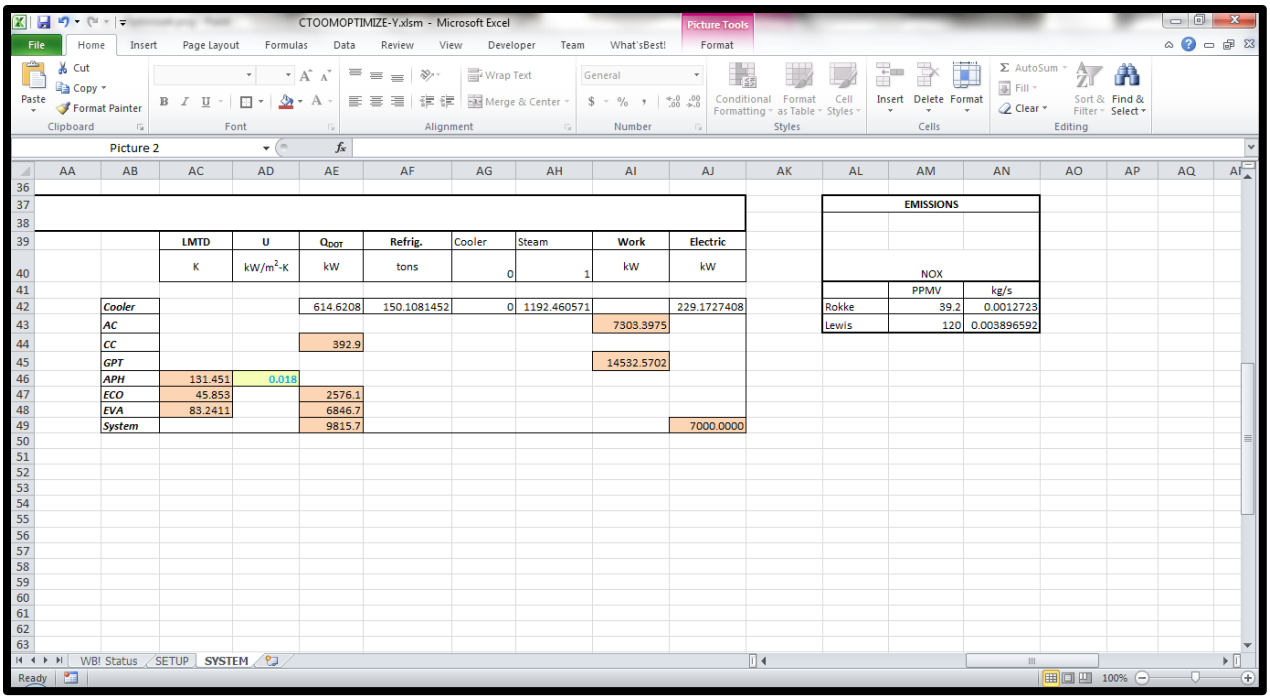

	LMTD	U	Q_{DOT}	Refrig.	Cooler	Steam	Work	Electric
	K	kW/m^2-K	kW	tons	0	1	kW	kW
Cooler			614.6208	150.1081452	0	1192.460571		229.1727408
AC							7303.3975	
CC			392.9					
GPT							14532.5702	
APH	131.451	0.018						
ECO	45.853		2576.1					
EVA	83.2411		6846.7					
System			9815.7					7000.0000

EMISSIONS		
NOX		
	PPMV	kg/s
Rokke	39.2	0.0012723
Lewis	120	0.003896592

Figure 5-5 Screen shot of MS Excel workbook- SYSTEM worksheet (4)

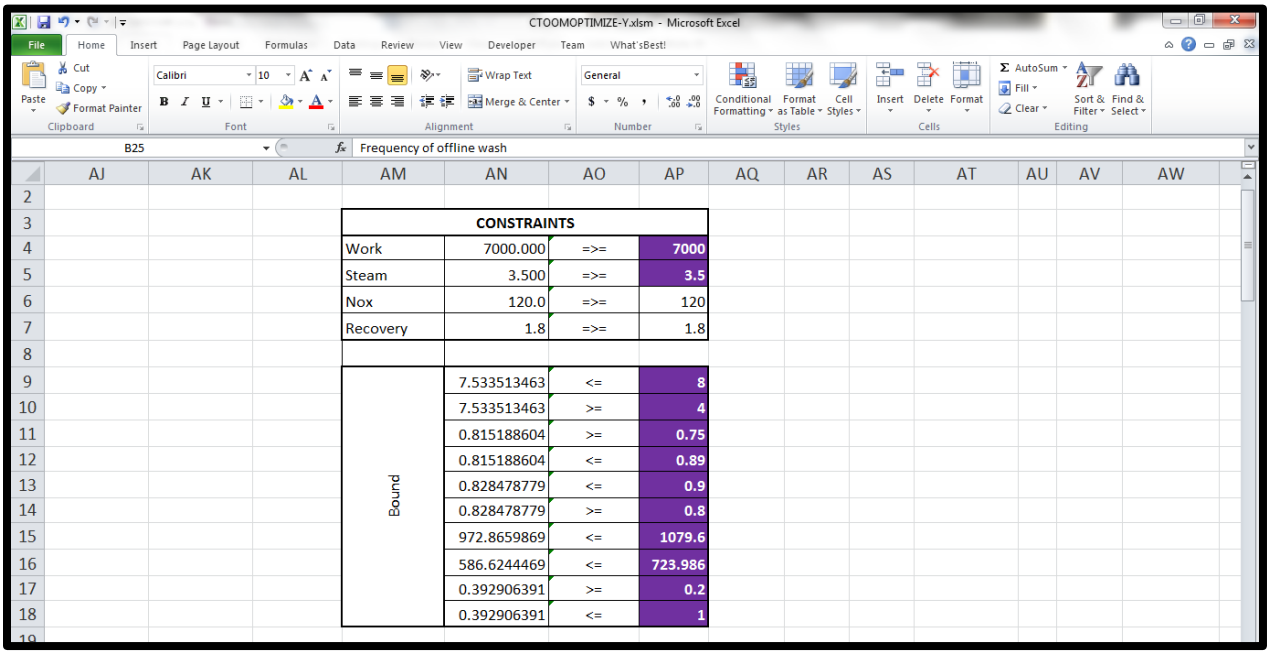

CONSTRAINTS			
Work	7000.000	=>=	7000
Steam	3.500	=>=	3.5
Nox	120.0	=>=	120
Recovery	1.8	=>=	1.8
Bound	7.533513463	<=	8
	7.533513463	>=	4
	0.815188604	>=	0.75
	0.815188604	<=	0.89
	0.828478779	<=	0.9
	0.828478779	>=	0.8
	972.8659869	<=	1079.6
	586.6244469	<=	723.986
	0.392906391	>=	0.2
	0.392906391	<=	1

Figure 5-6 Screen shot of MS Excel workbook- SYSTEM worksheet (5)

The MS Excel workbook in which the optimization model was set up comprises of two sheets i.e., SETUP and SYSTEM. Figure 5-1 shows the screen shot of the sheet SETUP while Figure 5-2, Figure 5-3, Figure 5-4, Figure 5-5, and Figure 5-6 demonstrate the worksheet SYSTEM. The worksheet SYSTEM was the engine of the optimization model and was

exhaustive in the number of rows and columns used. Therefore, the five different screen shots of the worksheet are used for illustration. The SETUP worksheet has four distinct regions – the reference data region, the air characterization region, the fuel characterization region, and the preliminary calculation region. The reference data region has the reference temperature, pressure and relative humidity. The reference temperature and pressure are required for the combustor calculations. The air characterization region has the molecular weights of the constituents of dry air and the products. The air characterization region also has the mole fractions of the dry air. The fuel characterization region lists the molecular weight of the fuel, the lower heating value, the number of carbon atoms in the fuel and the number of hydrogen atoms in the fuel. If a different fuel is used then the user can simply modify the information in the fuel characterization region. The preliminary calculation region calculates some preliminary information necessary for the calculations to proceed. These are the mass and molar flow rates for stoichiometric air and fuel required for combustion, the stoichiometric air-to-fuel ratio and fuel-to-air ratio on both mass and molar basis. The other parameters computed here are the $HbyCRatio$, the $SpentO_2$ and the $h_{air,ref}$ i.e. the enthalpy of air at reference temperature and pressure.

Figure 5-2 illustrates one sixth of the entire worksheet SYSTEM. There are six sections in the region i.e., Mass balance, Combustion temperature calculator, Machine maintenance strategy, New Machine, Degradation parameters and Humidity calculator. The region Mass balance provides the mass flow rates of air ($\dot{m}_a$), fuel ($\dot{m}_f$), steam injected ($m_{steaminject}$), combustion products ($\dot{m}_g$), process steam ($\dot{m}_s$) and water in the condenser section of HRSG ($\dot{m}_w$). In the mass balance section the flow rates of fuel ($\dot{m}_f$) and steam injected ($m_{steaminject}$) are in dark blue and these are two of the seven decision variables. The user can start off with an assumed value here. The section on the immediate right of the "Mass Balance" section is the "New Machine" section. This section has the pressure ratio and efficiency information for the compressor, combustion chamber and the turbine. The efficiency of the combustion chamber is set at some user defined value. For this work it is set at 98%. The pressure ratio of the compressor, the efficiency of the compressor and the efficiency of the gas and power turbine are the three additional decision variables. These are again shown in dark blue. The section to the right of the "New Machine" section is the "Degradation Parameters" section. In this section the user can enter some know loss in efficiency or pressure ratio for the compressor and the gas and

power turbine. If the value is set to 1 then the optimal value calculations are for a new machine. However, if the user uses some other value less than 1 then the solution converges for a degraded machine where the influence of degradation has been defined by the user.

The section on the bottom of the "Degradation Parameters" section is the "Humidity Calculator". This section is applicable if inlet air cooling is used. The mole fractions, mass fractions, and the mass of the dry air, vapor and condensate due to cooling if any are calculated here. The relative humidity at state 0 and state 1 are the input parameters that the user can modify. Below the "Mass Balance" section is the "Combustion temperature calculator" section. This section does a simple energy balance around the combustor to determine the combustor exit temperature for known fuel, air, and steam injected flow rates. There are no user inputs in this section. Immediately, below the "Combustion temperature calculator" section is the "Machine maintenance strategy" section. This section includes the sixth decision variable i.e. the frequency of the online washing. The other parameters are the maximum loss recovery and the required loss recovery in percentages. The required loss recovery can be set by the user. This is used to determine the optimal washing frequency.

Figure 5-3 describes another portion of the same worksheet SYSTEM. This portion primarily includes the Economics. The cost coefficients are all user inputs. The purchase cost and the component cost rates all are computed here for a final input to the objective function which is also listed in this section. Figure 5-4 illustrates the section "Thermodynamics". Most of this section is self-explanatory. Calculations are done at all the states from 0 through 9. States 7p and 8p are the pinch points corresponding to 7 and 8. PP and PA are the user defined pinch and approach temperatures. The cooler load calculation happens automatically only if the temperatures at 0 and 1 differ. If the temperatures do not differ then the cooler load is calculated as 0. Once the cooling load is established the user then can choose to either run the model with inlet air cooling or steam injection as desired for power boosting. The last of the decision variables is listed in this section i.e. the temperature at point 3. Figure 5-5 shows the remainder of the "Thermodynamics" section where the system power, the heat transferred between the economizer and the evaporator, the heat lost by the combustion chamber, the logarithmic mean temperature differences for the air preheater, economizer, and the evaporator are calculated. Figure 5-6 shows the final section of the worksheet SYSTEM. This section includes the

constraints on the optimization system. The first four constraints are the system constraints while the remainders are the bound constraints.

Component model program architecture

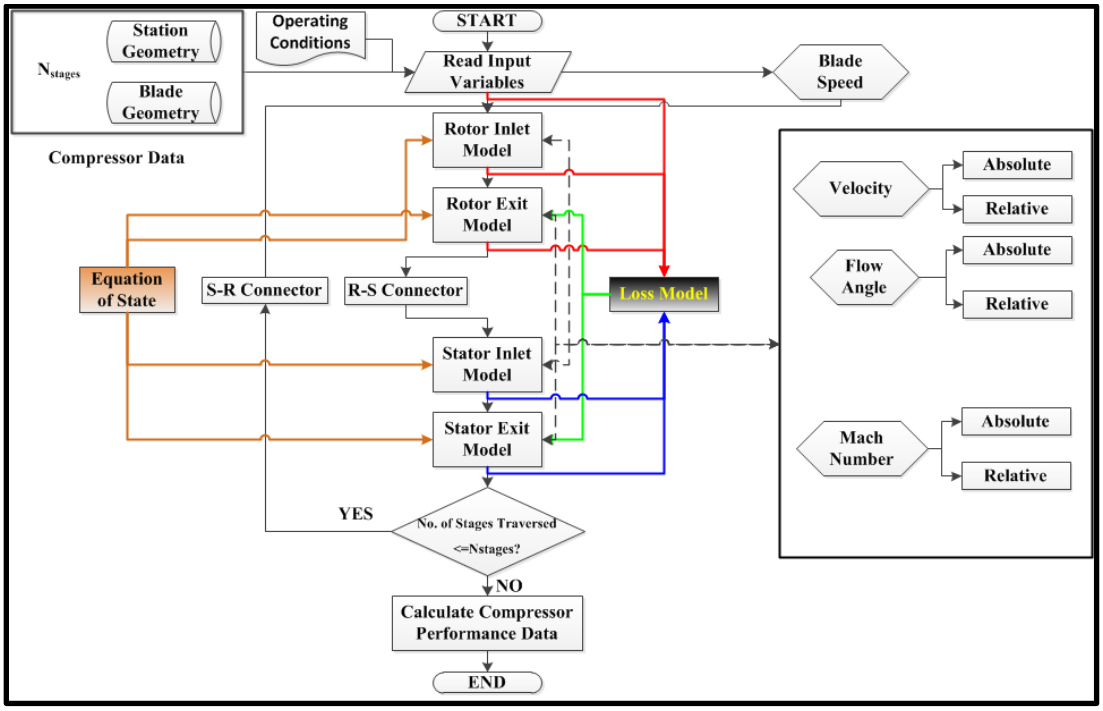

Figure 5-7 Compressor flow chart

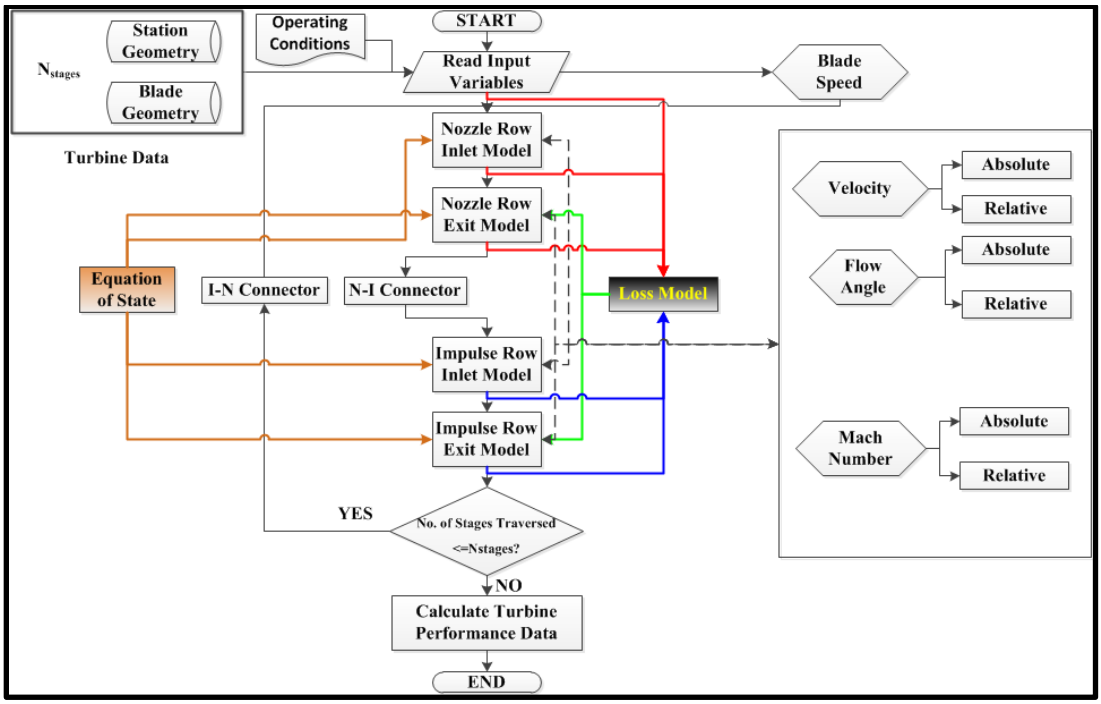

Figure 5-8 Turbine flow chart

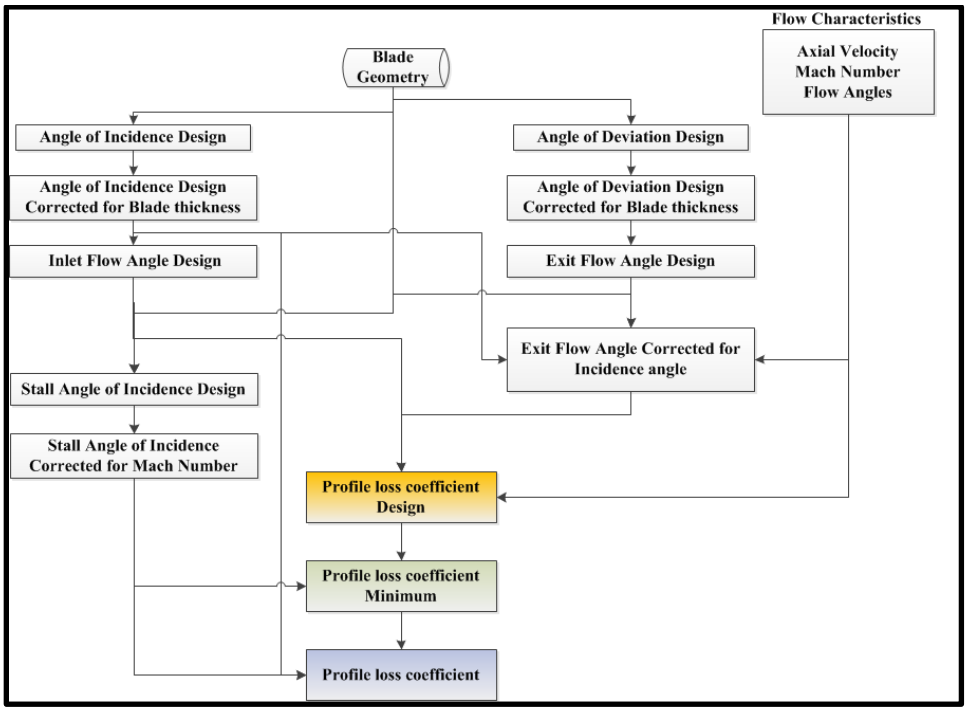

Figure 5-9 Compressor loss chart

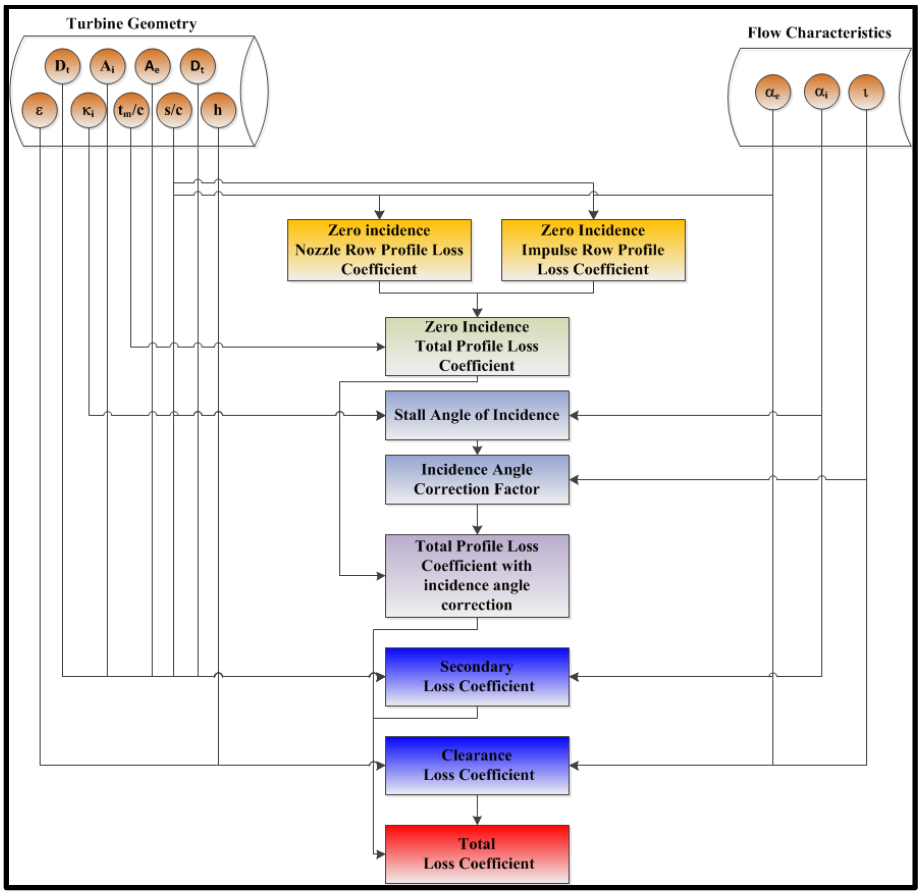

Figure 5-10 Turbine loss chart

The program architecture for the two component models are illustrated in Figure 5-7 and Figure 5-8 for the CTOOMCOMP1DPERF (compressor) and the CTOOMTURB1DPERF (turbine) separately and the flow charts are self-explanatory. The most important aspect is that the NR solver is called once independently in the rotor inlet, rotor exit, and the stator exit models for the compressor while it is never called in the stator inlet in the first stage. In the subsequent stages only the rotor exit and the stator exit models call the NR solver. Information from the rotor to stator flows using the "RS connector" while from the stator to rotor flows using the "SR connector". The difference between the compressor and the turbine algorithms is that the NR solver is never called for the rotor inlet for the first turbine stage. The "NI connector" is used to pass information from nozzle to impulse blade while the "IN connector" is used to pass information from impulse to nozzle blade. The loss models are called only in the exit models while the EOS DLL is called multiple times every time a property is required. Figure 5-9 and Figure 5-10 present the loss characterization algorithms. It can be seen that both for the

compressor and the turbine the incidence and deviation angles are computed first. A generalized loss coefficient is evaluated at zero incidence or design incidence as the case may be and then the same is corrected for the problem specific incidence angle. Other corrections for the blade thickness, solidity, trailing edge thickness are applied as necessary along with corrections for Mach number.

Programming details

The entire computer program development was done in Fortran 90 using Intel Visual Fortran 2011 compiler. The equation of state model source code as obtained from NIST was in Fortran 77. Consequently, it was converted into a dynamic link library (DLL) and the DLL is called within the main code.

The fundamental feature of an object oriented programming is encapsulation of the abstract data. Fortran 90 offers the use of “Module” which allows data encapsulation. Data declared inside the “Module” are available outside the “Module” with a “Use” statement. Operations on the variables are performed inside the “Module” and the “Module” can be independently compiled prior to it being called by the main program. Fortran 90 has the “Type” declaration statement for the variables. The combination of the “Module” in conjunction with the “Type” statement can be understood as a class in the object oriented language parlance. As an illustration of the same the “Module Class_BLDRow” is examined in detail below.

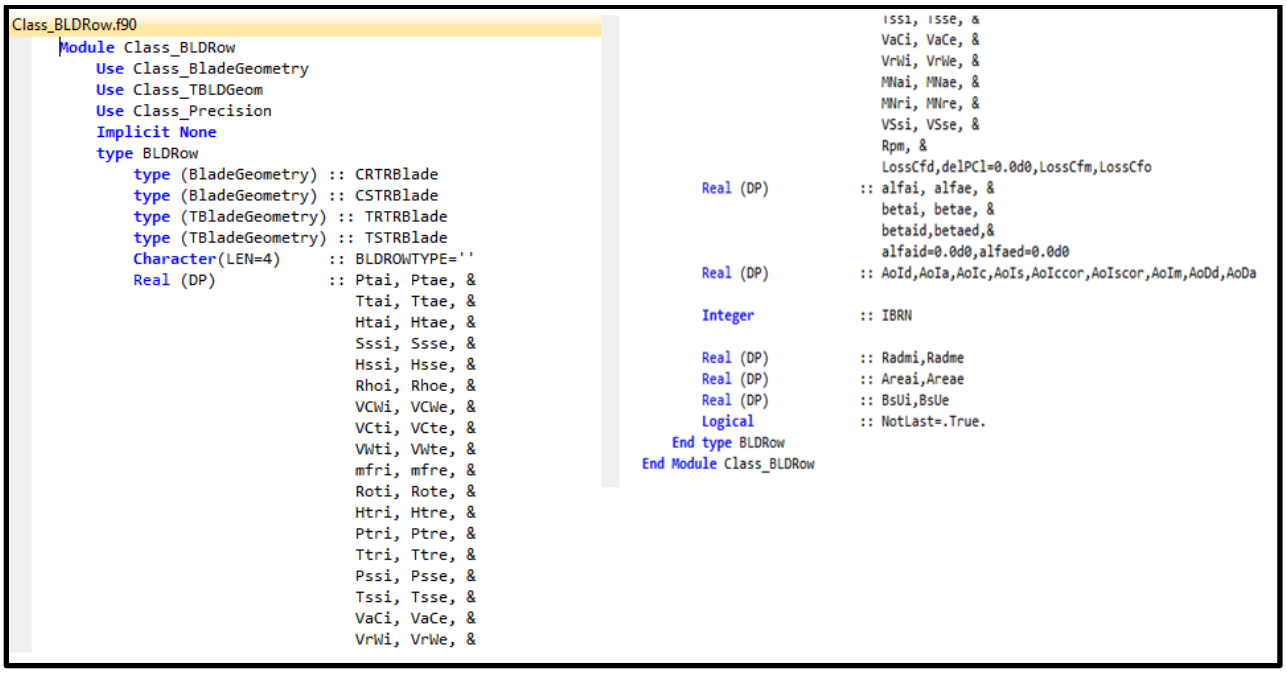

```
Class_BLDRow.f90
    Module Class_BLDRow
        Use Class_BladeGeometry
        Use Class_TBLDGeom
        Use Class_Precision
        Implicit None
        type BLDRow
            type (BladeGeometry) :: CRTRBlade
            type (BladeGeometry) :: CSTRBlade
            type (TBladeGeometry) :: TRTRBlade
            type (TBladeGeometry) :: TSTRBlade
            Character(LEN=4)     :: BLDROWTYPE=''
            Real (DP)            :: Ptai, Ptae, &
                                    Ttai, Ttae, &
                                    Htai, Htae, &
                                    Sssi, Ssse, &
                                    Hssi, Hsse, &
                                    Rhoi, Rhoe, &
                                    VCWi, VCWe, &
                                    VCti, VCte, &
                                    VWti, VWte, &
                                    mfri, mfre, &
                                    Roti, Rote, &
                                    Htri, Htre, &
                                    Ptri, Ptre, &
                                    Ttri, Ttre, &
                                    Pssi, Psse, &
                                    Tssi, Tsse, &
                                    VaCi, VaCe, &
                                    VrWi, VrWe, &
                                    Tssi, Tsse, &
                                    VaCi, VaCe, &
                                    VrWi, VrWe, &
                                    MNai, MNae, &
                                    MNri, MNre, &
                                    VSsi, VSse, &
                                    Rpm, &
                                    LossCfd,delPCl=0.0d0,LossCfm,LossCfo
            Real (DP)            :: alfai, alfae, &
                                    betai, betae, &
                                    betaid,betaed,&
                                    alfaid=0.0d0,alfaed=0.0d0
            Real (DP)            :: AoId,AoIa,AoIc,AoIs,AoIccor,AoIscor,AoIm,AoDd,AoDa

            Integer              :: IBRN

            Real (DP)            :: Radmi,Radme
            Real (DP)            :: Areai,Areae
            Real (DP)            :: BsUi,BsUe
            Logical              :: NotLast=.True.
        End type BLDRow
    End Module Class_BLDRow
```

Figure 5-11 Module Class_BLDRow [Figure goes from top to bottom on left and continues right]

The Figure 5-11 shows the program details of the Module Class_BLDRow. The first three lines are the “Use” statements that allow this module to access some other modules. Of specific interest is the fifth statement “type BLDRow”. Following the fifth statement there are many more statements till the penultimate statement “End type BLDRow”. All the data that has been declared between the fifth statement and the penultimate statement are assigned the type “BLDRow”. Once a data type is declared multiple derived data types can now be easily declared. In this work four different derived data types CRTRRow, CSTRRow, TSTRRow, TRTRRow were declared. If “BLDRow” could be thought of as class then these are the derived classes. A derived class will possess all the attributes of the base class and any other individual attributes can be added.

```
Class_CRTRRow.f90
    Module Class_CRTRRow
        Use Class_Precision
        Use Class_BLDRow
        Use Class_BladeGeometry
        Use Class_CPERFCORR
        Use Class_VelocityTriangle
        Use Class_StnGeom
        Use Class_SysInfo
        Type CRTRRow
            Type (BLDRow)           :: thisCRTRRow
            Type (StnGeom)          :: thatStnGeom
            Real (DP)               :: Ptrenl=25.0d0,RTRPR,RTRTR,delEnth,betaenl,alfaenl,delEnthnl,Htaenl,Efficiency,Ptaenl,Ttaenl,RTRPRnl,RTRTRnl
        End Type CRTRRow
        Interface
            Real(KIND=8)Function PropCalc(cip,cop,p1,p2)
                Real(KIND=8),Intent(in) ::p1,p2
                Character(LEN=01)  :: cop
                Character(LEN=02)  :: cip
            End Function
        End Interface
    Contains
```

Figure 5-12 Module Class_CRTRRow

Figure 5-12 shows the Module Class_ CRTRRow. In order to access all the variables assigned to the "BLDRow" statement 10 "Type (BLDRow) :: thisCRTRRow" is used. This could be thought of something like creating an object "thisCRTRRRow" of the class BLDRow. Statement 14 is "Interface" which explicitly specifies any external function to be accessed. In this case the EOS is accessed. Furthermore, statement 12 declares some additional real variables. These variables are attributes of CRTRRow but not of BLDRow. Unlike some other programming environments there are no specific syntaxes to declare objects or derived classes. The fundamental advantage of being able to use the "Type" is that the object "thisCRTRRow" can directly be passed to any subroutine or function and the entire structure gets passed. This was very useful in implementing the loss models. In the procedural scheme using Fortran 77 that was developed earlier (Sengupta, et al. 2008) it was programmatically cumbersome to pass seventeen different variables (both geometry and other operating data). In this revised program simply passing "thisCRTRRow" and "thatSTNGeom" pass the rotor row properties and the station geometry information. This allowed developing a more elegant and re-usable program.

The input file format and workbench

The work bench is primarily a MS Excel spreadsheet. Populating the spreadsheet and hitting the "Run" button essentially generates input files in ASCII file format that is read by the compiled program. Alternately, the user can manually populate the ASCII files and thus details of the same are given below. There are five input files: SystemInformation, CompressorBlade Geometry, CompressorStationGeometry, TurbineBladeGeometry, TurbineStationGeometry.

The system information input file has five lines

Line 1- Input is Logical [True/False]: It determines if a system is evaluated or only individual components (compressor or turbine) are evaluated.

Lines 2, 3, 4, 5 also have Logical inputs for evaluating the compressor, combustor, gas generator turbine and the power turbine in the stated chronology. A “False” would skip evaluating that particular component.

To evaluate the compressor, Line 2 can be set to “True” while all other lines can be set to “False”.

The compressor blade geometry can be specified in the input file “CompressorBladeGeometry”. It has three lines

Blade Row Number, Blade Row Type

Blade Profile Type, Number of blades, Number of streamlines, Lift Coefficient / Camber angle Identifier, Blade tip clearance

Geometry specification Radius, Blade chord, Blade throat to pitch ratio, Ratio-Maximum blade thickness to chord, Ratio- throat to pitch, Stagger Angle and Lift coefficient or Camber Angle.

Line 1: Blade Row Number- Integer value identifying the Blade row. Thus, a 10 stage compressor has 20 blade rows.

Line 1: Blade Row Type: Takes the character string “CSTR” or “CRTR” denoting stator or rotor row.

Line 2: Blade profile type: Takes a character string between “NACA”, “DCAP” denoting either a NACA profile or Double circular arc profile.

Line 2: Number of blades: Integer specifying the number of blades on the blade row.

Line 2: Number of streamlines: It is currently set to 1 always. It is left to enable extending the program to a streamline code.

Line 2: Lift coefficient/Camber angle identifier: It takes a logical value to determine whether the user specifies the lift coefficient or the camber angle.

Line 3: All the variables are self-explanatory.

The “CompressorStationGeometry” file has three columns. The first column specifies the axial distance location, the second column specifies the hub radius while the last column specifies the tip radius.

The blade geometry input file for the turbine is similar to the compressor except for the line 3 where the blade stagger and camber angle are specified. This is replaced by the blade inlet and exit angles. Furthermore, on line 2 an additional value for trailing edge thickness to pitch ratio is specified.

Chapter 6 - Case studies, system integration and discussion

Optimization case studies

A cogeneration system with one emission control technology i.e. steam injection for NO_x abatement, two power boosting technologies i.e. inlet air cooling and steam injection and a machine maintenance schedule was analyzed. The process requirements were to generate 7 MW of power, deliver 3.5 kg/s steam, control NO_x at 64 ppmv [approx.], and apply a user-defined recovery efficiency at 1.8%.

Thus, the relevant process constraints were:

$$W_{system} \geq 7000 \text{ kW} \tag{6.1}$$

$$\dot{m}_{steam} \geq 3.5 \text{ kg/s} \tag{6.2}$$

$$\eta_{reco} \leq 1.8 \text{ \%} \tag{6.3}$$

$$NO_x \leq 64\text{ppmv} \tag{6.4}$$

The remaining constraints were the lower bound and upper bound on the variables. These bounds were either on the decision variables or some other computed variable. The bounds were an artifact of either computational constraints or physical constraints. The following were the bound constraints:

$$4 \leq PR_C \leq 8 \tag{6.5}$$

$$0.50 < \eta_C < 0.90 \tag{6.6}$$

$$0.50 < \eta_{G\&PT} < 0.92 \tag{6.7}$$

$$T_3 < T_5 \tag{6.8}$$

$$T_2 < T_6 \tag{6.9}$$

$$T_5 < 1500\text{K} \tag{6.10}$$

$$T_7 < 400\text{K} \tag{6.11}$$

The upper bound on the compressor pressure ratio was to ensure that the optimization results could be used in the component level analysis. The upper bounds on the compressor and turbine efficiencies were an artifact of computational constraints resulting from the formulation of the capital cost models for each. The bounds on the temperatures T_2 and T_3 expressed by equations (6.8) and (6.9) stem from the physics of the air preheater. To ensure a solution the two constraints were modified as below:

$$T_3 + 10 < T_5 \tag{6.12}$$

$$T_2 + 10 < T_6 \tag{6.13}$$

The constraint on the turbine exit temperature (T_5) was a result of the material used for turbine construction while the constraint on the gas delivered to the stack (T_7) was to preclude the formation of sulfuric acid.

Table 6-1 Cost model coefficients for optimization case study

Component	Coefficient	Units	Value
AC	C_{11}	\$/kg/s	39.5000
	C_{12}	None	0.9000
CC	C_{21}	\$/kg/s	25.6000
	C_{22}	None	0.9950
	C_{23}	1/K	0.0180
	C_{24}	None	26.4000
GPT	C_{31}	\$/kg/s	266.3000
	C_{32}	None	0.9200
	C_{33}	1/K	0.0360
	C_{34}	None	54.4000
APH	C_{41}	$\$/m^{1.2}$	2290.0000

Component	Coefficient	Units	Value
HRSG	C_{51}	$/(kW/K)$^{0.8}$	3650.0000
	C_{52}	$/kg/s	11820.0000
	C_{53}	$/(kg/s)$^{1.2}$	658.0000
FUEL	C_f	$/MJ	0.0004
MAINTENANCE	N_{HRS}	hours	8000.0000
	ϕ_m	None	1.0000
	CRF	None	0.1820
	C_{61}	$/hr/kW	0.0005
	C_{62}	$/kW	0.7830
	C_{63}	$/kW	1.3598
COOLING	C_{71}	$/tons	100.0000
	C_{81}	$/tons-hr/kg/s	2.8800
EMISSIONS	C_{91}	$/kg	6.8530

Table 6-2 Results of CTOOM-OPTIMIZE Baseline case, Modification 1 and 2

Variable	Units	Baseline	Modification 1	Modification 2
$\dot{m}_f$	kg/s	0.3878(±0.0007)	0.3878(±0.0007)	0.3878(±0.0007)
$\dot{m}_{steaminject}$	kg/s	0.0	0.0	0.0
PR_C		6.566(±0.009)	7.790(±0.011)	6.566(±0.009)
η_C	%	82.4(±0.082)	85.4(±0.085)	82.4(±0.082)
$\eta_{G\&PT}$	%	86.0(±0.086)	89.0(±0.089)	86.0(±0.086)
T_3	K	902.6(±0.7)	790.63(±0.7)	902.6(±0.7)
$f_{onlinewashing}$	hrs	109(±4)	109(±4)	109(±4)

Variable	Units	Baseline	Modification 1	Modification 2
T_4	K	1468 (±1.1)	1371 (±1)	1468 (±1.1)
W_C	kW	6570 (±110)	7120 (±120)	6570 (±110)
$W_{G\&PT}$	kW	13570(±230)	14120 (±240)	13570(±230)
W_{system}	kW	7000(±170)	7000(±170)	7000(±170)
$\dot{m}_s$	kg/s	3.50(±0.05)	3.50(±0.05)	3.50(±0.05)
$\dot{m}_{NO_x}$	ppmv	64.1 (±0.8)	24.3(±0.3)	64.1 (±0.8)
$\dot{C}_t$	$/hr	304(±7)	330 (±8)	355(±9)

The first case analyzed was the baseline case with no steam injection. Thus, the mass flow rate of steam in ($\dot{m}_{steaminject}$) was zero. Thus, it was not a decision variable either and the baseline case had only six decision variables. Furthermore, the environmental impact was also not considered in the baseline case. Therefore, the objective function did not include the cost rate of emissions. Consequently, the constraint on the mass flow rate of NO_x was removed. There was not inlet air cooling as well and the inlet air temperature was 288.15K. Table 6-2 provides the results obtained from the optimization study of the baseline system. Table 6-2 illustrates the optimal value of the fuel flow rate as 0.3878 kg/s and the mass flow rate of NO_x was 64.1 ppmv.

The next case analyzed referred to as "Modification 1" included the environmental impact in the objective function. Since the cost rate of emissions is a function of the mass flow rate of NO_x, minimizing the objective function automatically also seeks to find the lowest possible value of NO_x. As seen in Table 6-2 the new optimal values obtained in Modification-1 were significantly different from the optimal values obtained in the baseline case. The fuel flow rate did not show a significant change but the remaining decision variables varied vastly from the baseline case. Also, the flow rate of NO_x was 24.3 ppmv. Therefore, a constraint on NO_x was necessary. This is in line with the basic formulation of the objective function where the emission

was included as a constraint. Thus, in Modification-2, NO_x was constrained at 64.1 ppmv and it was observed that the values of the decision variables were similar to the ones in the baseline case.

Table 6-3 Results of CTOOM-OPTIMIZE – Cases Modifications 3, 4, and 5

Variable	Units	Modification 3	Modification 4	Modification 5
$\dot{m}_f$	kg/s	0.3878(±0.0007)	0.3878(±0.0007)	0.392(±0.0007)
$\dot{m}_{steaminject}$	kg/s	0.130 (±0.007)	0.00	0.00
PR_C		6.566(±0.009)	6.566(±0.009)	6.95(±0.01)
η_C	%	82.4(±0.082)	82.4(±0.082)	83.0(±0.083)
$\eta_{G\&PT}$	%	86.0(±0.086)	86.0(±0.086)	86.7(±0.086)
T_3	K	902.6(±0.7)	902.6(±0.7)	892.4(±0.7)
$f_{onlinewashing}$	hrs	109(±4)	109(±4)	109(±4)
T_4	K	1461 (±1.1)	1469 (±1.1)	1466 (±1.1)
W_C	kW	6570 (±110)	6860(±120)	6790 (±110)
$W_{G\&PT}$	kW	13610 (±230)	13580(±230)	14020 (±240)
W_{system}	kW	7040 (±170)	6720(±160)	7000(±170)
$\dot{m}_s$	kg/s	3.47(±0.06)	3.50(±0.06)	3.50(±0.06)
$\dot{m}_{NO_x}$	ppmv	59.1(±0.7)	64.1(±0.8)	64.1(±0.8)
$\dot{C}_t$	$/hr	350 (±9)	355(±9)	361(±9)

The next case analyzed was Modification-3 where the optimized solution of Modification-2 was examined for steam injection. Results obtained from Modification-3 are documented in the Table 6-3. The steam injected was set at 0.5% of the air flow rate. The primarily influence of the injected steam was a decrease in the combustor exit temperature from

1469K to 1461K. As a result of the decrease in combustor exit temperature the flow rate of NO_x also decreased from 64.1 ppmv to 59.1 ppmv. Furthermore, the system power increased from 7000 kW to 7040 kW. All these three effects were as anticipated. This demonstrated that the model was capable of correctly characterizing the influence of steam injection. It also exhibited that steam injection is a suitable power boosting technique apart from being a NO_x abatement technique. The next case analyzed was Modification-4 where the injected steam was set to zero. This was basically reverting to the case Modification-2. However, the inlet temperature was increased from 288.15K to 298.15K. This resulted in a drop in system power from 7000 kW to 6720 kW. This demonstrated the impact of increased inlet temperature was a loss in system power.

The case Modification-5 was analyzed with inlet air cooling where the cooling load was used to compute the cost of cooling and was included in the objective function. The new optimal values with an inlet air cooling showed that the total cost rate increased from 355 $/hr to 361 $/hr. Furthermore, as seen in the Table 6-3, the increase lies within the uncertainty band. It would be seem that since the new cost rate with inlet air cooling is within the uncertainty band, there is really no additional cost of using an inlet air cooler. However, such a conclusion would be inappropriate since, the cost of inlet air cooling is a function of the cost coefficient. For this work a due to lack of appropriate manufacturer's data a reasonable assumption was made. Any increase in that cost coefficient would result in a higher value of cost rate and that could be larger than the uncertainty band. There was also a 1.2% increase in the fuel flow rate which also contributed to the increased total cost rate.

Table 6-4 Results of CTOOM-OPTIMIZE – Cases Modifications 6, 11, and 12

Variable	Units	Modification 6	Modification 11	Modification 12
$\dot{m}_f$	kg/s	0.3936(±0.0007)	0.3936(±0.0007)	0.3936(±0.0007)
$\dot{m}_{steaminject}$	kg/s	0.52 (±0.03)	0.52 (±0.03)	0.52(±0.03)
PR_C		6.657(±0.009)	6.657(±0.009)	6.657(±0.009)

Variable	Units	Modification 6	Modification 11	Modification 12
η_C	%	81.28(±0.08)	81.28(±0.08)	81.28(±0.08)
$\eta_{G\&PT}$	%	85.20(±0.09)	85.20(±0.09)	85.20(±0.09)
T_3	K	927.3(±0.07)	927.3(±0.07)	927.3(±0.07)
$f_{onlinewashing}$	hrs	109(±4)	80(±3)	52(±2)
T_4	K	1468(±1.1)	1468(±1.1)	1468(±1.1)
W_C	kW	6730(±110)	6730(±110)	6730(±110)
$W_{G\&PT}$	kW	13730(±240)	13730(±240)	13730(±240)
W_{system}	kW	7000(±170)	7000(±170)	7000(±170)
$\dot{m}_s$	kg/s	3.50 (±0.06)	3.50 (±0.06)	3.50 (±0.06)
$\dot{m}_{NO_x}$	ppmv	64.1(±0.8)	64.1(±0.8)	64.1(±0.8)
$\dot{C}_t$	$/hr	359(±9)	360(±9)	361(±9)

Modification-6 examined the use of steam injection as an alternative to inlet air cooling for boosting power. Thus, the mass of steam injected was now a decision variable and the solution sought optimal values of all the decision variables including the amount of steam injected to offset the power lost due to higher inlet air temperature. It may be noted that the NO_x was constrained at 64.1 ppmv and the amount of steam injection required for power boosting was 0.5163 kg/s. Modification-7, 8, 9, and 10 were studies done for determining the influence of decreasing NO_x on two decision variables. The results of the same are plotted for two of the decision variables i.e., fuel flow rate and compressor pressure ratio against different values of NO_x (Figure 6-1 and Figure 6-2). It can be seen that the pressure ratio increases with reducing NO_x while the fuel flow rate remains the same. The fuel flow rate does change in the numerical value but the change is not significant. This is concluded from the uncertainity bars that have been indicated in the Figure 6-1. The uncertainity bar indicated on the Figure is obtained from a

detailed uncertainity analysis outlined in the Appendix A. The uncertainity value on the fuel flow rate is ± 0.182%. On the contrary the influence of constraining NO_x on the pressure ratio is quite different. It can be seen from the Figure 6-2 that the pressure ratio changes significantly as NO_x is constrained from 60 ppmv to 45 ppmv. To ensure that a reasonable conclusion on the change of pressure ratio can be drawn a similar uncertainity analysis was done to determine the uncertainty of the pressure ratio. This was determined to be 0.1% and is illustrated using the uncertainty bar in Figure 6-2. Thus, it can be seen that to achieve a reduction in NOx, a higher pressure ratio is required. Table 6-4 also documents the results of two more case studies Modification-11 and Modification-12. In these cases the loss recovery was changed from the original 1.8% to 2.0% and 2.2% to determine new values of frequency of online washing. It was observed that with increasing recovery requirement, the frequency of online washing increased which also resulted in a marginal increase of the total cost rate. This seems reasonable since online washing alone would not greatly affect the total cost rate. However, as earlier the washing unit cost coefficients have been assumed for developing the model and a reasonable conclusion can be drawn only after validating the cost coefficients against field data.

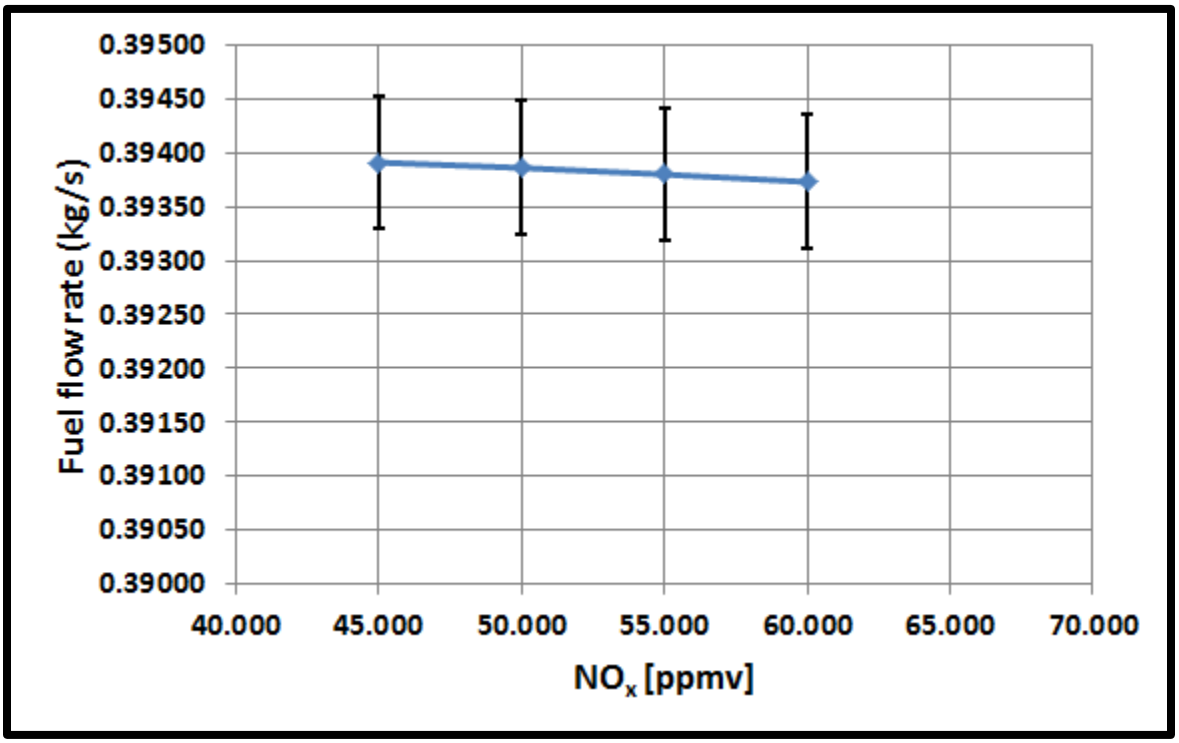

Figure 6-1 Pareto optimal values of fuel flow rate against NO_x

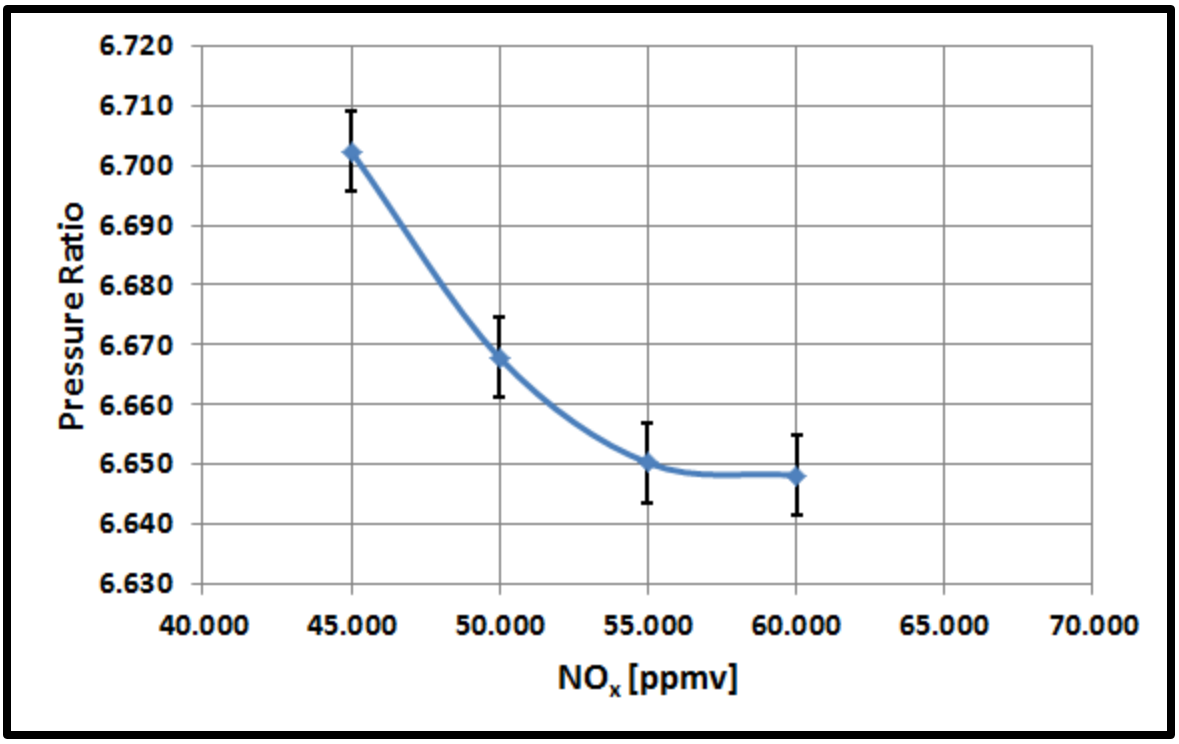

Figure 6-2 Pareto optimal values of compressor pressure ratio against NO_x

Validation of the optimization model

The optimization model developed as part of the CTOOM-OPTIMIZE was validated against the classic CGAM problem. The CGAM problem is named after the four authors C. Frangopoulos, G. Tsatsaronis, A. Valero and M. von Spakovsky, who compared their methodologies by solving a predefined optimization problem. The process requirements for the CGAM problem were to generate 30 MW of power, deliver 14 kg/s steam, with no NO_x control and machine maintenance. Thus, the constraints for the validation study were:

$$W_{system} \geq 30000 \text{ kW} \tag{6.14}$$

$$\dot{m}_{steam} \geq 14 \text{ kg/s} \tag{6.15}$$

The constraints on the loss recovery (l_{reco}) and NO_x control ($\dot{m}_{NO_x}$) were removed. The CGAM problem uses a constant maintenance factor ($\phi_{m,i}$) of 1.06 for all components. Thus, the CTOOM-OPTIMIZE model was modified to incorporate that. Consequently, equations 2.17, 2.18, 2.19 were modified to:

$$\dot{C}_{c\&m,C} = \frac{C_C (CRF_C)\phi_{m,C}}{3600 N_{hrs}} \tag{6.16}$$

$$\dot{C}_{c\&m,CC} = \frac{C_{CC} (CRF_{CC})\phi_{m,CC}}{3600 N_{hrs}} \tag{6.17}$$

$$\dot{C}_{c\&m,G\&PT} = \frac{C_{G\&PT} (CRF_{G\&PT})\phi_{m,G\&PT}}{3600 N_{hrs}} \tag{6.18}$$

Furthermore, $C_{wash,C,CC,G\&PT}$ in equation 2.20 was set to 0 and c_{NO_x} in equation 2.23 was also set to 0. This ensured that washing and NO_x were not part of the cost model. Similarly, cost coefficients C_{71} and C_{81} in equations 2.29 and 2.30 were set to 0 to disable the cost of power boosting. The decision variables for steam injection flow rate ($\dot{m}_{steaminject}$) and the frequency of online washing ($f_{onlinewashing}$) were now treated as regular variables and not decision variables. The value of $\dot{m}_{steaminject}$ was set to 1E-05 since it could not be set exactly to zero on account of divide by zero error problem.

$$\dot{m}_{steaminject} = 0.00001 \tag{6.19}$$

The temperature at the cooler exit T_2 was set equal to the temperature at the cooler inlet T_1. Setting the two temperatures as equal automatically disables the cooler load calculation routine.

$$T_2 = T_1 \tag{6.20}$$

The other necessary modifications were those to the bound constraint on the compressor pressure ratio and the mass flow rate of air was increased to match that in the CGAM problem. These were:

$$5 \le PR_C \le 20 \tag{6.21}$$

$$\dot{m}_a = 99.4559 \text{ kg/s} \tag{6.22}$$

Table 6-5 Comparison of the CTOOM-OPTIMIZE to the CGAM solution

Decision Variable	Units	CGAM solution	CTOOM-OPTIMIZE
PR_C		8.5234	8.3535
η_C		0.8648	0.8474
T_3	K	914.28	913.5019
$\eta_{G\&PT}$		0.8786	0.8785
T_4	K	1492.63	1494.4174
			(Not a decision variable)
$\dot{m}_f$	kg/s	1.6274	1.5309
		(Not a decision variable)	

Table 6-5 presents the comparison between the CTOOM-OPTIMIZE solution and the classic CGAM solution. The compressor pressure ratio (PR_C), and the fuel flow rates ($\dot{m}_f$) predicted by CTOOM-OPTIMIZE are 2% and 6% lower than that predicted by the classic CGAM solution. The difference between the two algorithms is that in the classic CGAM solution the combustor exit temperature (T_4) was considered to be a decision variable and the fuel flow rate ($\dot{m}_f$) was calculated while in the CTOOM-OPTIMIZE model the fuel flow rate was the decision variable ($\dot{m}_f$) that was used to calculate the combustor exit temperature (T_4). Another difference was that CTOOM-OPTIMIZE used the real gas formulation with a higher order equation of state package to compute the various state properties while the classic CGAM solution used the ideal gas model with constant values of specific heat of air ($c_{p,a}$), specific heat of combustion products ($c_{p,g}$), the ratio of specific heats for air (γ_a), and the ratio of specific heats for combustion products (γ_g). It should also be noted that the amount of steam injected was not set exactly to 0 but a very small value of 1E-05 for reasons described earlier. In order to

obtain more confidence in the solution algorithm, the original CGAM problem was solved exactly as outlined by Valero, et al. (1994). The mathematical model of CTOOM-OPTIMIZE was modified to model the original CGAM problem. For the compressor, the conditions were calculated from (Mattingly. 1996).

$$P_2 = P_1 * PR_C \tag{6.23}$$

$$T_2 = T_1\left[1+\frac{1}{\eta_C}\left(PR_C^{\frac{\gamma_a-1}{\gamma_a}}-1\right)\right] \tag{6.24}$$

The combustion chamber was modeled using the mass and energy balance and the resulting equations were (Knopf. 2011):

$$\dot{m}_a + \dot{m}_f = \dot{m}_g \tag{6.25}$$

$$\dot{m}_a\left(h_3 - h_{a,ref}\right) + \dot{m}_f LHV = \dot{m}_g\left(h_4 - h_{g,ref}\right) + \dot{Q}_{cc} \tag{6.26}$$

The enthalpies $h_{a,ref}$ and $h_{g,ref}$ were evaluated at the reference condition, based on the definition of the lower heating value of fuel (LHV), which was 25°C and 1 atm (101.325 kPa). For an ideal gas with constant specific heats equation (6.26) can be recast as:

$$\dot{m}_a c_{p,a}\left(T_3 - T_{air,ref}\right) + \dot{m}_f LHV = \dot{m}_g c_{p,g}\left(T_4 - T_{g,ref}\right) + \dot{Q}_{cc} \tag{6.27}$$

Since, $T_{a,ref} = T_{g,ref} = T_{ref}$, equation (6.27) can be re-written as:

$$\dot{m}_a c_{p,a}\left(T_3 - T_{ref}\right) + \dot{m}_f LHV = \dot{m}_g c_{p,g}\left(T_4 - T_{ref}\right) + \dot{Q}_{cc} \tag{6.28}$$

From equation (6.25) in equation (6.28), we get:

$$\dot{m}_a c_{p,a}\left(T_3 - T_{ref}\right) + \dot{m}_f LHV = \left(\dot{m}_a + \dot{m}_f\right) c_{p,g}\left(T_4 - T_{ref}\right) + \dot{Q}_{cc} \tag{6.29}$$

Further, the heat lost by the combustor ($\dot{Q}_{cc}$) is expressed as:

$$\dot{Q}_{CC} = \dot{m}_f LHV\left(1-\eta_{CC}\right) \tag{6.30}$$

With relevant substitutions the equation (6.29) can be modified to give the fuel flow rate:

$$\dot{m}_a c_{p,a}\left(T_3 - T_{ref}\right) + \dot{m}_f LHV = \left(\dot{m}_a + \dot{m}_f\right) c_{p,g}\left(T_4 - T_{ref}\right) + \dot{m}_f LHV\left(1 - \eta_{CC}\right) \quad (6.31)$$

$$\dot{m}_f LHV - \dot{m}_f LHV\left(1 - \eta_{CC}\right) = \left(\dot{m}_a + \dot{m}_f\right) c_{p,g}\left(T_4 - T_{ref}\right) - \dot{m}_a c_{p,a}\left(T_3 - T_{ref}\right) \quad (6.32)$$

$$\dot{m}_f LHV - \dot{m}_f LHV\left(1 - \eta_{CC}\right) - \dot{m}_f c_{p,g}\left(T_4 - T_{ref}\right) = \dot{m}_a c_{p,g}\left(T_4 - T_{ref}\right) - \dot{m}_a c_{p,a}\left(T_3 - T_{ref}\right) \quad (6.33)$$

$$\dot{m}_f LHV\eta_{CC} - \dot{m}_f c_{p,g}\left(T_4 - T_{ref}\right) = \dot{m}_a c_{p,g}\left(T_4 - T_{ref}\right) - \dot{m}_a c_{p,a}\left(T_3 - T_{ref}\right) \quad (6.34)$$

$$\dot{m}_f \left[LHV\eta_{cc} - c_{p,g}\left(T_4 - T_{ref}\right)\right] = \dot{m}_a c_{p,g}\left(T_4 - T_{ref}\right) - \dot{m}_a c_{p,a}\left(T_3 - T_{ref}\right) \quad (6.35)$$

$$\dot{m}_f = \frac{\dot{m}_a c_{p,g}\left(T_4 - T_{ref}\right) - \dot{m}_a c_{p,a}\left(T_3 - T_{ref}\right)}{\left[LHV\eta_{CC} - c_{p,gas}\left(T_4 - T_{ref}\right)\right]} \quad (6.36)$$

Thus, equation (6.36) gives the fuel flow rate determined from the mass and energy balance of the combustion chamber. The lower heating value (LHV) of methane is 50,000 kJ/kg, the reference temperature (T_{ref}) is 25°C and the combustion efficiency (η_{CC}) is 98%. It may be recalled that the temperatures T_3 and T_4 were decision variables and will be known either as initial guess values or will get modified as the solution progresses. The other unknown at this point was the pressure at the combustor exit (P_4) and was calculated from:

$$P_4 = P_3\left(1 - \Delta p_{CC}\right) \quad (6.37)$$

In equation (6.37), Δp_{cc} is the pressure drop across the combustion chamber and was assumed to be 5%. The pressure at the combustion chamber inlet (P_3) was evaluated from a known pressure drop across the air side of the air preheater ($\Delta p_{APH,a}$) and was given as:

$$P_3 = P_2\left(1 - \Delta p_{APH,a}\right) \quad (6.38)$$

In equation (6.38), $\Delta p_{APH,air}$ was assumed as 5%. The turbine performance was characterized by determining the turbine discharge temperature (T_5) (Mattingly, 1995):

$$T_5 = T_4\left[1+\eta_{G\&PT}\left(\left(\frac{1}{PR_{G\&PT}}\right)^{\frac{\gamma_a-1}{\gamma_a}}-1\right)\right] \tag{6.39}$$

Where, $$PR_{G\&PT} = \frac{P_4}{P_5} \tag{6.40}$$

And, $$P_5 = \frac{P_6}{1-\Delta p_{APH,g}} \tag{6.41}$$

In equation (6.41), $\Delta p_{APH,g}$ represents the pressure drop across points air preheater on the gas side. This was assumed as 3%. The air preheater model provided the condition at state 6, i.e., on the exit of the gas side of the air preheater from an energy balance across the air-preheater:

$$\dot{m}_a\left(h_3-h_2\right) = \left(\dot{m}_a+\dot{m}_f\right)\left(h_5-h_6\right) \tag{6.42}$$

For ideal gas assumption both for air and the combustion products equation (6.42) can be recast as:

$$\dot{m}_a c_{p,a}\left(T_3-T_2\right) = \left(\dot{m}_a+\dot{m}_f\right)c_{p,g}\left(T_5-T_6\right) \tag{6.43}$$

i.e., $$T_6 = T_5 - \frac{\dot{m}_a c_{p,a}\left(T_3-T_2\right)}{\left(\dot{m}_a+\dot{m}_f\right)c_{p,g}} \tag{6.44}$$

The other state property at point 6 was the pressure (P_6) that can be expressed with reference to the pressure drop across points 6 and 7:

$$P_6 = \frac{P_7}{1-\Delta p_{HRSG}} \tag{6.45}$$

The equations governing the HRSG pinch and approach temperatures were:

$$T_{8P} = T_9 - \Delta T_{approach} \tag{6.46}$$

$$T_{7P} = T_9 + \Delta T_{pinch} \tag{6.47}$$

In equations (6.46) and (6.47), the $\Delta T_{approach}$ and ΔT_{pinch} are specified as 1.64K and 15K respectively and T_9 was known since the steam conditions required were known. Further, the exhaust pressure (P_7) and the pinch point pressure (P_{7p}) were:

$$P_7 = P_{amb} \tag{6.48}$$

$$P_{7p} = \frac{P_7 + P_6}{2} \tag{6.49}$$

And the heat lost by the evaporator was:

$$\dot{Q}_{eva} = \dot{m}_g \left(h_6 - h_{7p} \right) \tag{6.50}$$

which for an ideal gas was:

$$\dot{Q}_{eva} = \dot{m}_g c_{p,g} \left(T_6 - T_{7p} \right) \tag{6.51}$$

The pressure at 8p was assumed to be the same as at 8, and 9. Thus,

$$P_{8p} = P_9 \tag{6.52}$$

$$P_8 = P_9 \tag{6.53}$$

An energy balance on the gas side and the steam side of the evaporator provided the rate of steam generation:

$$\dot{m}_s = \frac{\dot{Q}_{eva}}{h_9 - h_{8p}} \tag{6.54}$$

The enthalpy (h_9) was the enthalpy of superheated steam at the pressure (P_9) and temperature (T_9). The pressure P_9 and temperature T_9 were dictated by the plant requirement at which steam was desired and was assumed to be 20 bar and 486.06K (converted from the 875°R).

The heat gained by the economizer was given by:

$$\dot{Q}_{eco} = \dot{m}_w \left(h_{8p} - h_8 \right) \tag{6.55}$$

The enthalpy h_8 was of the water as liquid at the inlet temperature of $T_8 = 298.15$ K and pressure $P_8 = 20$ bar while the enthalpy h_{8p} was at the condition T_{8p} and P_{8p}. The relevant models to compute these conditions have been explained above.

The system power W_{system}:

$$W_{system} = W_{G\&PT} - W_C \tag{6.56}$$

where, $$W_C = \dot{m}_a \left(h_2 - h_1 \right) \tag{6.57}$$

i.e.. for ideal gas $$W_C = \dot{m}_a c_{p,a} \left(T_2 - T_1 \right) \tag{6.58}$$

where, $$W_{G\&PT} = \dot{m}_g \left(h_4 - h_5 \right) \tag{6.59}$$

i.e., for ideal gas, $$W_{G\&PT} = \dot{m}_g c_{p,g} \left(T_4 - T_5 \right) \tag{6.60}$$

or, $$W_{G\&PT} = \left(\dot{m}_a + \dot{m}_f \right) c_{p,g} \left(T_4 - T_5 \right) \tag{6.61}$$

The following were the values were used in the original CGAM solution and the same were used here for the validation purpose as well:

$$c_{p,a} = 1.004 \tag{6.62}$$

$$c_{p,g} = 1.170 \tag{6.63}$$

$$\gamma_a = 1.40 \tag{6.64}$$

$$\gamma_a = 1.33 \tag{6.65}$$

Table 6-6 Comparison of the CTOOM-OPTIMIZE IDEAL model optimal values of the decision variables to the CGAM solution

Decision Variable	Units	CGAM solution	CTOOM-OPTIMIZE Ideal
PR_C		8.5234	8.5070

η_C		0.8648	0.8468
T_3	K	914.28	914.1661
$\eta_{G\&PT}$		0.8786	0.8787
T_4	K	1492.63	1492.4713
$\dot{m}_f$	kg/s	1.6274	1.6273
		(Not a decision variable)	(Not a decision variable)

It can be seen from the Table 6-6 that the CTOOM-OTPIMIZE IDEAL solution matches very closely with the original CGAM solution.

Table 6-7 Comparison of the CTOOM-OPTIMIZE IDEAL solution cost values to the CGAM solution

Description	CGAM		CTOOM-OPTIMIZE IDEAL	
	Cost ($)	Cost Rate ($/s)	Cost ($)	Cost Rate ($/s)
Compressor	1,348,000	Not Reported	1,311,638	0.00879
Combustor	146,900	Not Reported	146,057	0.00098
Turbine	1,927,000	Not Reported	1,882,245	0.01261
Air Preheater	827,700	Not Reported	834,089	0.00559
HRSG	1,202,000	Not Reported	883,510	0.00592
Investment	Not Reported	0.03625	Not Calculated	0.02796
Fuel	Not Reported	0.32548	Not Calculated	0.32594
Total	Not Reported	0.36200	Not Calculated	0.35982

Validation of the inlet cooler model

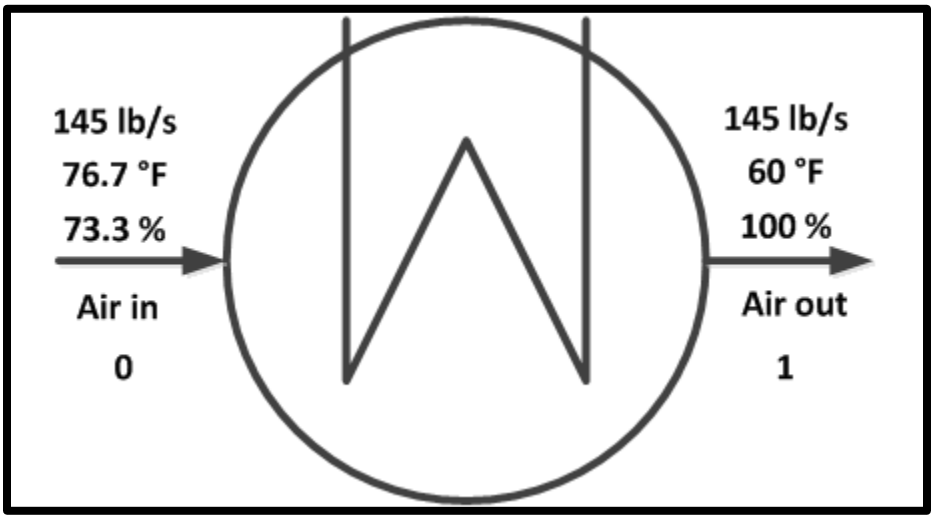

Figure 6-3 Validation data for cooling load

The inlet cooling model described above was validated against the data presented by Knopf (2010). The conditions at state 0 and 1 are shown in Figure 6-3. It is observed from Table 6-7 that the CTOOM-OPTIMIZE-REAL results match reasonably with the data presented by Knopf (2010).

Table 6-8 Comparison of results obtained from CTOOM-OPTIMIZE with Knopf (2010) for the cooling model

	Description	Knopf (2010)				CTOOM-OPTIMIZE	
		Original data in British Units		Data converted to SI units			
Input	Pressure at inlet (absolute)	14.696	psi	101325.00	Pa	101325.00	Pa
	Temperature at inlet	76.70	°F	297.9833	K	297.9833	K
	Relative Humidity at inlet	73.30		73.30		73.30	
	Mass flow rate at inlet	145.00	lb/s	65.7709	kg/s	65.7709	kg/s
	Pressure at exit (absolute)	14.696	psi	101325.00	Pa	101325.00	Pa
	Temperature at exit	60.00	°F	288.705	K	288.705	K
	Relative Humidity at exit	100.00		100.00		100.00	
	Mass flow rate at exit	145.000	lb/s	65.7709	kg/s	65.7709	kg/s
Output	Mass flow rate of dry air at inlet	143.911	lb/s	65.277	kg/s	64.831	kg/s
	Mass flow rate of water vapor at inlet	2.0787	lb/s	0.947	kg/s	0.9315	kg/s
	Mass flow rate of dry air at exit	143.911	lb/s	65.277	kg/s	65.0528	kg/s
	Mass flow rate of water vapor at exit	1.5889	lb/s	0.721	kg/s	0.7180	kg/s

Description	Knopf (2010)				CTOOM-OPTIMIZE	
	Original data in British Units		Data converted to SI units			
Mass flow rate of the condensate	0.4897	lb/s	0.226	kg/s	0.213468	kg/s
Cooling load for cooling the dry air	577.17	BTU/s	608.9	kW	606.889	kW
Cooling load for cooling the vapor	15.45	BTU/s	16.3	kW	15.983	kW
Condensation load	518.87	BTU/s	547.4	kW	525.887	kW

Validation of the combustor model

The combustor model that was developed as part of this CTOOM-OPTIMIZE routine was validated against data in the solved example 5.8 presented by Bathie (1996). Table 6-9 provides the comparison between the results obtained from the validation study done for the combustor model against the data provided by Bathie (1996). The combustor temperature determined using CTOOM-OPTIMIZE differed only by 1K approximately as compared to the Bathie's data. Thus, CTOOM-OPTIMIZE has a simple but robust combustor model that can compute the combustor exit temperatures for different fuel flow rates and different fuel. The difference between the two models is that CTOOM-OPTIMIZE determines the combustor exit temperature using a known fuel flow rate while Bathie's model determines the fuel flow rate using a known combustor temperature. Furthermore, the data presented by Bathie was for liquid octane. It was not a difficulty to change the fuel in CTOOM-OPTIMIZE as the code has been structured for any hydrocarbon.

Table 6-9 Comparison of results obtained from CTOOM-OPTIMIZE with Bathie (1996) for the combustor model

Description	Bathie (1996)				CTOOM-OPTIMIZE	
	British Units		Converted to SI units			
Pressure of air at combustor inlet (absolute)	176.40000	psi	1216.23518	kPa	1216.23518	kPa
Temperature of air at combustor inlet	1122.00000	R	623.33333	K	623.33333	K
Pressure of fuel into combustor inlet (absolute)	176.40000	psi	1216.23518	kPa	1216.23518	kPa
Temperature of fuel into combustor inlet	537.00000	R	298.15000	K	298.15000	K
Pressure of steam injected into combustor (absolute)	200.00000	psi	1378.95146	kPa	1378.95146	kPa
Temperature of steam injected into combustor	1175.00000	R	652.77778	K	652.77778	K
Pressure of products at combustor exit (absolute)	176.40000	psi	1216.23518	kPa	1216.23518	kPa
Temperature of products at combustor exit	2520.0000	R	1400.00000	K	***1398.93210***	K
Mass flow rate of air	1.00000	lb/s	0.45359	kg/s	0.45359	kg/s
Mass flow rate of fuel	0.02252	lb/s	0.01022	kg/s	0.01022	kg/s
Mass flow rate of steam	0.02500	lb/s	0.01134	kg/s	0.01134	kg/s
Mass flow rate of products	1.04752	lb/s	0.47515	kg/s	0.47515	kg/s

Component level models-Compressor case study

A 10 stage axial compressor was chosen for model validation since this was the most completely characterized axial compressor available in open literature. The design data was available from Johnsen (1952) while the performance data was obtained from Budinger and Thompson (1952). Further, Aungier (2008) also provided the same information on both the design and the performance data in a far more easily usable format rather than the original work, although certain modifications were necessary for suitable inputs to CTOOMCOMP1DPERF. Tested data was available for three different speeds i.e., at 9959 rpm which represents 100% of the design speed, 8963 rpm (90% of the design speed) and 7967 (70% of the design speed). The analysis was carried out for an inlet total pressure of 101311.56 Pa (14.694 psi) and an inlet total temperature of 287.778K (518.7°R). The requisite compressor geometry is divided into two parts: the row by row blade geometry and the station geometry. The blade geometry has been very well described at five different radii from hub to tip as seen in Table 6-10. For a mean line analysis the blade geometry at station mean line is of primary interest. The same was extracted and the relevant geometry information necessary as an input for CTOOMCOMP1DPERF is presented in Table 6-10. The station geometry on the other hand was useable in exactly the same format as available in the literature and is presented in Table 6-12, Table 6-13, Table 6-14, Table 6-15, Table 6-16, Table 6-17, Table 6-18, Table 6-19, Table 6-20, Table 6-21, Table 6-22, and Table 6-23. The design point mass flow rate was not clarified in the literature and hence every mass flow rate was analyzed with the off-design corrections. If the design point were known then that point alone would not have an off-design correction. However, evaluating every mass flow rate with off-design corrections would not significantly impact the results and the conclusions from this study.

Table 6-10 Blade geometry for case study 1

Row	Chord	t/c	Lift Coefficient	Stagger Angle	Camber Angle	Metal Angles		c/s	o/s
			C_{l0}	γ	θ	κ_i	κ_e		
	m			°	°	°	°		
Rotor 01	0.039370	0.10	-0.910	-39.40	-22.93	-50.86	-27.94	0.6167	0.7461
Stator01	0.039370	0.10	0.910	38.36	22.93	49.82	26.90	0.6661	0.7456
Rotor02	0.038354	0.10	-0.930	-37.80	-23.43	-49.51	-26.09	0.6729	0.7485
Stator02	0.038354	0.10	0.930	36.38	23.43	48.09	24.67	0.6969	0.7556
Rotor03	0.037211	0.10	-0.950	-35.86	-23.93	-47.82	-23.90	0.7228	0.7545
Stator03	0.037211	0.10	1.025	34.41	25.80	47.31	21.51	0.7694	0.7555
Rotor04	0.036068	0.10	-1.110	-33.71	-27.92	-47.67	-19.75	0.7684	0.7582
Stator04	0.036068	0.10	1.110	32.68	27.92	46.64	18.72	0.7910	0.7623
Rotor05	0.035052	0.10	-1.120	-32.34	-28.17	-46.42	-18.26	0.8126	0.7609
Stator05	0.035052	0.10	1.120	31.43	28.17	45.51	17.35	0.8566	0.7608
Rotor06	0.033782	0.10	-1.120	-30.73	-28.17	-44.81	-16.65	0.8679	0.7644
Stator06	0.033782	0.10	1.200	28.91	30.16	43.99	13.83	0.9102	0.7689
Rotor07	0.032512	0.10	-1.280	-28.58	-32.14	-44.65	-12.51	0.9167	0.7670
Stator07	0.032512	0.10	1.280	27.62	32.14	43.69	11.55	0.9371	0.7714
Rotor08	0.031115	0.10	-1.300	-26.94	-32.64	-43.26	-10.62	0.9163	0.7785
Stator08	0.031115	0.10	1.300	26.17	32.64	42.49	9.85	0.9553	0.7789
Rotor09	0.029845	0.10	-1.300	-25.66	-32.64	-41.98	-9.34	0.9537	0.7829
Stator09	0.029845	0.10	1.300	24.81	32.64	41.13	8.49	0.9911	0.7844
Rotor10	0.028448	0.10	-1.300	-24.46	-32.64	-40.78	-8.14	0.9982	0.7861
Stator10	0.028448	0.10	1.300	23.38	32.64	39.70	7.06	1.0517	0.7877
EGV	0.028448	0.10	0.660	5.00	16.65	13.33	-3.33	1.0517	0.8900

Table 6-11 Station Geometry

Station Number	Axial Distance (Z_j)		Hub Radius ($r_h(Z_j)$)		Tip Radius ($r_t(Z_j)$)	
	in	m	in	m	in	m
1	3.86	*0.098044*	5.500	*0.139700*	10.00	*0.254000*
2	5.78	*0.146812*	5.822	*0.147879*	10.00	*0.254000*
3	7.12	*0.180848*	6.131	*0.155727*	10.00	*0.254000*
4	9.04	*0.229616*	6.420	*0.163068*	10.00	*0.254000*
5	10.58	*0.268732*	6.696	*0.170078*	10.00	*0.254000*
6	12.51	*0.317754*	6.952	*0.176581*	10.00	*0.254000*
7	13.96	*0.354584*	7.197	*0.182804*	10.00	*0.254000*
8	15.81	*0.401574*	7.424	*0.188570*	10.00	*0.254000*
9	17.37	*0.441198*	7.639	*0.194031*	10.00	*0.254000*
10	19.03	*0.483362*	7.838	*0.199085*	10.00	*0.254000*
11	20.58	*0.522732*	8.026	*0.203860*	10.00	*0.254000*
12	22.21	*0.564134*	8.199	*0.208255*	10.00	*0.254000*
13	23.50	*0.596900*	8.361	*0.212369*	10.00	*0.254000*
14	25.26	*0.641604*	8.508	*0.216103*	10.00	*0.254000*
15	26.64	*0.676656*	8.647	*0.219634*	10.00	*0.254000*
16	28.30	*0.718820*	8.771	*0.222783*	10.00	*0.254000*
17	29.55	*0.750570*	8.885	*0.225679*	10.00	*0.254000*
18	31.10	*0.789940*	8.988	*0.228295*	10.00	*0.254000*
19	32.35	*0.821690*	9.085	*0.230759*	10.00	*0.254000*
20	33.87	*0.860298*	9.174	*0.233020*	10.00	*0.254000*
21	35.15	*0.892810*	9.262	*0.235255*	10.00	*0.254000*
22	36.35	*0.923290*	9.262	*0.235255*	10.00	*0.254000*

Table 6-12 Blade data for case study 1 (all rows)

Row	No. of blades	a/c		s/h		h/c		Tip Clearance (ε)	
		in	m	in	m	in	m	in	m
Rotor01	25	0.5000	*0.01270*	0.4536	*0.01152*	2.7994	*0.07110*	0.0400	*0.001016*
Stator01	27	0.5000	*0.01270*	0.4620	*0.01173*	2.5958	*0.06593*	0.0400	*0.001016*
Rotor02	28	0.5000	*0.01270*	0.4903	*0.01245*	2.4666	*0.06265*	0.0400	*0.001016*
Stator02	29	0.5000	*0.01270*	0.5211	*0.01324*	2.2795	*0.05790*	0.0400	*0.001016*
Rotor03	31	0.5000	*0.01270*	0.5368	*0.01363*	2.1679	*0.05506*	0.0400	*0.001016*
Stator03	33	0.5000	*0.01270*	0.5556	*0.01411*	1.9969	*0.05072*	0.0400	*0.001016*
Rotor04	34	0.5000	*0.01270*	0.5947	*0.01511*	1.8940	*0.04811*	0.0400	*0.001016*
Stator04	35	0.5000	*0.01270*	0.6375	*0.01619*	1.7384	*0.04416*	0.0400	*0.001016*
Rotor05	37	0.5000	*0.01270*	0.6660	*0.01692*	1.6388	*0.04163*	0.0400	*0.001016*
Stator05	39	0.5000	*0.01270*	0.6985	*0.01774*	1.4986	*0.03806*	0.0400	*0.001016*
Rotor06	41	0.5000	*0.01270*	0.7353	*0.01868*	1.4192	*0.03605*	0.0400	*0.001016*
Stator06	43	0.5000	*0.01270*	0.7765	*0.01972*	1.2923	*0.03282*	0.0400	*0.001016*
Rotor07	45	0.5000	*0.01270*	0.8221	*0.02088*	1.2230	*0.03106*	0.0400	*0.001016*
Stator07	46	0.5000	*0.01270*	0.8919	*0.02265*	1.1113	*0.02823*	0.0400	*0.001016*
Rotor08	47	0.5000	*0.01270*	0.9687	*0.02460*	1.0539	*0.02677*	0.0400	*0.001016*
Stator08	49	0.5000	*0.01270*	1.0300	*0.02616*	0.9567	*0.02430*	0.0400	*0.001016*
Rotor09	51	0.5000	*0.01270*	1.0968	*0.02786*	0.9051	*0.02299*	0.0400	*0.001016*
Stator09	53	0.5000	*0.01270*	1.1711	*0.02975*	0.8200	*0.02083*	0.0400	*0.001016*
Rotor10	56	0.5000	*0.01270*	1.2328	*0.03131*	0.7772	*0.01974*	0.0400	*0.001016*
Stator10	59	0.5000	*0.01270*	1.3086	*0.03324*	0.6982	*0.01773*	0.0400	*0.001016*
EGV	59	0.5000	*0.01270*	1.3898	*0.03530*	0.6589	*0.01674*	0.0400	*0.001016*

Table 6-13 Blade data for case study 1 (Stage 1 – Rotor Row 1 and Stator Row 1)

Row	Radius		Chord		t/c	Lift Coefficient	Stagger Angle	Camber Angle	Metal Angle		c/s	o/s
						C_{l0}	γ	θ	κ_i	κ_e		
	in	m	in	m			°	°	°	°		
Rotor01	5.5000	*0.13970*	1.5500	*0.03937*	0.1000	-0.9100	-13.6600	-22.9300	-25.1200	-2.2000	1.1213	0.8547
	6.6250	*0.16828*	1.5500	*0.03937*	0.1000	-0.9100	-19.1200	-22.9300	-30.5800	-7.6600	0.9309	0.8458
	7.7500	*0.19685*	1.5500	*0.03937*	0.1000	-0.9100	-24.8000	-22.9300	-36.2600	-13.3400	0.7958	0.8252
	8.8750	*0.22543*	1.5500	*0.03937*	0.1000	-0.9100	-31.2900	-22.9300	-42.7500	-19.8300	0.6949	0.7951
	10.0000	*0.25400*	1.5500	*0.03937*	0.1000	-0.9100	-39.4000	-22.9300	-50.8600	-27.9400	0.6167	0.7461
Stator01	5.8220	*0.14788*	1.5500	*0.03937*	0.1000	0.9100	14.2600	22.9300	25.7200	2.8000	1.1440	0.8497
	6.8660	*0.17440*	1.5500	*0.03937*	0.1000	0.9100	19.4900	22.9300	30.9500	8.0300	0.9701	0.8395
	7.9110	*0.20094*	1.5500	*0.03937*	0.1000	0.9100	24.9200	22.9300	36.3800	13.4600	0.8419	0.8186
	8.9550	*0.22746*	1.5500	*0.03937*	0.1000	0.9100	31.0200	22.9300	42.4800	19.5600	0.7438	0.7894
	10.0000	*0.25400*	1.5500	*0.03937*	0.1000	0.9100	38.3600	22.9300	49.8200	26.9000	0.6661	0.7456

Table 6-14 Blade data for case study 1 (Stage 2 – Rotor Row 2 and Stator Row 2)

Row	Radius		Chord		t/c	Lift Coefficient	Stagger Angle	Camber Angle	Metal Angles		c/s	o/s
						C_{l0}	γ	θ	κ_i	κ_e		
	in	m	in	m			°	°	°	°		
Rotor02	6.1310	*0.1557*	1.5100	*0.0384*	0.1000	-0.9300	-15.7100	-23.4300	-27.4200	-4.0000	1.0975	0.8470
	7.0980	*0.1803*	1.5100	*0.0384*	0.1000	-0.9300	-20.4700	-23.4300	-32.1800	-8.7600	0.9480	0.8351
	8.0650	*0.2049*	1.5100	*0.0384*	0.1000	-0.9300	-25.5600	-23.4300	-37.2700	-13.8500	0.8344	0.8143
	9.0320	*0.2294*	1.5100	*0.0384*	0.1000	-0.9300	-31.1200	-23.4300	-42.8300	-19.4100	0.7450	0.7878
	10.0000	*0.2540*	1.5100	*0.0384*	0.1000	-0.9300	-37.8000	-23.4300	-49.5100	-26.0900	0.6729	0.7485
Stator02	6.4200	*0.1631*	1.5100	*0.0384*	0.1000	0.9300	15.9400	23.4300	27.6500	4.2300	1.0856	0.8470
	7.3150	*0.1858*	1.5100	*0.0384*	0.1000	0.9300	20.4200	23.4300	32.1300	8.7100	0.9528	0.8349
	8.2100	*0.2085*	1.5100	*0.0384*	0.1000	0.9300	25.1700	23.4300	36.8800	13.4600	0.8489	0.8152
	9.1050	*0.2313*	1.5100	*0.0384*	0.1000	0.9300	30.3200	23.4300	42.0300	18.6100	0.7654	0.7904
	10.0000	*0.2540*	1.5100	*0.0384*	0.1000	0.9300	36.3800	23.4300	48.0900	24.6700	0.6969	0.7556

Table 6-15 Blade data for case study 1 (Stage 2 – Rotor Row 2 and Stator Row 2)

Row	Radius		Chord		t/c	Lift Coefficient	Stagger Angle	Camber Angle	Metal Angles		c/s	o/s
						C_{l0}	γ	θ	κ_i	κ_e		
	in	m	in	m			°	°	°	°		
Rotor02	6.1310	*0.1557*	1.5100	*0.0384*	0.1000	-0.9300	-15.7100	-23.4300	-27.4200	-4.0000	1.0975	0.8470
	7.0980	*0.1803*	1.5100	*0.0384*	0.1000	-0.9300	-20.4700	-23.4300	-32.1800	-8.7600	0.9480	0.8351
	8.0650	*0.2049*	1.5100	*0.0384*	0.1000	-0.9300	-25.5600	-23.4300	-37.2700	-13.8500	0.8344	0.8143
	9.0320	*0.2294*	1.5100	*0.0384*	0.1000	-0.9300	-31.1200	-23.4300	-42.8300	-19.4100	0.7450	0.7878
	10.0000	*0.2540*	1.5100	*0.0384*	0.1000	-0.9300	-37.8000	-23.4300	-49.5100	-26.0900	0.6729	0.7485
Stator02	6.4200	*0.1631*	1.5100	*0.0384*	0.1000	0.9300	15.9400	23.4300	27.6500	4.2300	1.0856	0.8470
	7.3150	*0.1858*	1.5100	*0.0384*	0.1000	0.9300	20.4200	23.4300	32.1300	8.7100	0.9528	0.8349
	8.2100	*0.2085*	1.5100	*0.0384*	0.1000	0.9300	25.1700	23.4300	36.8800	13.4600	0.8489	0.8152
	9.1050	*0.2313*	1.5100	*0.0384*	0.1000	0.9300	30.3200	23.4300	42.0300	18.6100	0.7654	0.7904
	10.0000	*0.2540*	1.5100	*0.0384*	0.1000	0.9300	36.3800	23.4300	48.0900	24.6700	0.6969	0.7556

Table 6-16 Blade data for case study 1 (Stage 3 – Rotor Row 3 and Stator Row 3)

Row	Radius		Chord		t/c	Lift Coefficient	Stagger Angle	Camber Angle	Metal Angles		c/s	o/s
						C_{l0}	γ	θ	κ_i	κ_e		
	in	m	in	m			°	°	°	°		
Rotor03	6.6960	*0.1701*	1.4650	*0.0372*	0.1000	-0.9500	-17.5100	-23.9300	-29.4700	-5.5500	1.0795	0.8387
	7.5220	*0.1911*	1.4650	*0.0372*	0.1000	-0.9500	-21.5500	-23.9300	-33.5100	-9.5900	0.9609	0.8261
	8.3480	*0.2120*	1.4650	*0.0372*	0.1000	-0.9500	-25.8100	-23.9300	-37.7700	-13.8500	0.8658	0.8079
	9.1740	*0.2330*	1.4650	*0.0372*	0.1000	-0.9500	-30.5100	-23.9300	-42.4700	-18.5500	0.7879	0.7849
	10.0000	*0.2540*	1.4650	*0.0372*	0.1000	-0.9500	-35.8600	-23.9300	-47.8200	-23.9000	0.7228	0.7545
Stator03	6.9520	*0.1766*	1.4650	*0.0372*	0.1000	1.0250	17.0600	25.8000	29.9600	4.1600	1.1068	0.8364
	7.7140	*0.1959*	1.4650	*0.0372*	0.1000	1.0250	20.9900	25.8000	33.8900	8.0900	0.9975	0.8230
	8.4760	*0.2153*	1.4650	*0.0372*	0.1000	1.0250	24.9100	25.8000	37.8100	12.0100	0.9078	0.8060
	9.2380	*0.2346*	1.4650	*0.0372*	0.1000	1.0250	29.1600	25.8000	42.0600	16.2600	0.8329	0.7852
	10.0000	*0.2540*	1.4650	*0.0372*	0.1000	1.0250	34.4100	25.8000	47.3100	21.5100	0.7694	0.7555

Table 6-17 Blade data for case study 1 (Stage 4 – Rotor Row 4 and Stator Row 4)

Row	Radius		Chord		t/c	Lift Coefficient	Stagger Angle	Camber Angle	Metal Angles		c/s	o/s
						C_{l0}	γ	θ	κ_i	κ_e		
	in	m	in	m			°	°	°	°		
Rotor04	7.1970	*0.1828*	1.4200	*0.0361*	0.1000	-1.1100	-18.3600	-27.9200	-32.3200	-4.4000	1.0677	0.8295
	7.8980	*0.2006*	1.4200	*0.0361*	0.1000	-1.1100	-21.8500	-27.9200	-35.8100	-7.8900	0.9729	0.8161
	8.5990	*0.2184*	1.4200	*0.0361*	0.1000	-1.1100	-25.3600	-27.9200	-39.3200	-11.4000	0.8936	0.8009
	9.3000	*0.2362*	1.4200	*0.0361*	0.1000	-1.1100	-29.3400	-27.9200	-43.3000	-15.3800	0.8262	0.7816
	10.0000	*0.2540*	1.4200	*0.0361*	0.1000	-1.1100	-33.7100	-27.9200	-47.6700	-19.7500	0.7684	0.7582
Stator04	7.4240	*0.1886*	1.4200	*0.0361*	0.1000	1.1100	18.5700	27.9200	32.5300	4.6100	1.0655	0.8284
	8.0680	*0.2049*	1.4200	*0.0361*	0.1000	1.1100	21.8000	27.9200	35.7600	7.8400	0.9804	0.8156
	8.7120	*0.2213*	1.4200	*0.0361*	0.1000	1.1100	25.0500	27.9200	39.0100	11.0900	0.9079	0.8013
	9.3560	*0.2376*	1.4200	*0.0361*	0.1000	1.1100	28.6900	27.9200	42.6500	14.7300	0.8454	0.7836
	10.0000	*0.2540*	1.4200	*0.0361*	0.1000	1.1100	32.6800	27.9200	46.6400	18.7200	0.7910	0.7623

Table 6-18 Blade data for case study 1 (Stage 5 – Rotor Row 5 and Stator Row 5)

Row	Radius		Chord		t/c	Lift Coefficient	Stagger Angle	Camber Angle	Metal Angles		c/s	o/s
						C_{l0}	γ	θ	κ_i	κ_e		
	in	m	in	m			°	°	°	°		
Rotor05	7.6390	*0.1940*	1.3800	*0.0351*	0.1000	-1.1200	-19.6100	-28.1700	-33.6900	-5.5300	1.0638	0.8214
	8.2300	*0.2090*	1.3800	*0.0351*	0.1000	-1.1200	-22.6000	-28.1700	-36.6800	-8.5200	0.9874	0.8090
	8.8200	*0.2240*	1.3800	*0.0351*	0.1000	-1.1200	-25.6100	-28.1700	-39.6900	-11.5300	0.9214	0.7952
	9.4100	*0.2390*	1.3800	*0.0351*	0.1000	-1.1200	-28.8200	-28.1700	-42.9000	-14.7400	0.8636	0.7796
	10.0000	*0.2540*	1.3800	*0.0351*	0.1000	-1.1200	-32.3400	-28.1700	-46.4200	-18.2600	0.8126	0.7609
Stator05	7.8380	*0.1991*	1.3800	*0.0351*	0.1000	1.1200	19.8200	28.1700	33.9000	5.7400	1.0928	0.8172
	8.3790	*0.2128*	1.3800	*0.0351*	0.1000	1.1200	22.6200	28.1700	36.7000	8.5400	1.0223	0.8050
	8.9190	*0.2265*	1.3800	*0.0351*	0.1000	1.1200	25.3400	28.1700	39.4200	11.2600	0.9604	0.7924
	9.4600	*0.2403*	1.3800	*0.0351*	0.1000	1.1200	28.2700	28.1700	42.3500	14.1900	0.9055	0.7778
	10.0000	*0.2540*	1.3800	*0.0351*	0.1000	1.1200	31.4300	28.1700	45.5100	17.3500	0.8566	0.7608

Table 6-19 Blade data for case study 1 (Stage 6 – Rotor Row 6 and Stator Row 6)

Row	Radius		Chord		t/c	Lift Coefficient	Stagger Angle	Camber Angle	Metal Angles		c/s	o/s
						C_{l0}	γ	θ	κ_i	κ_e		
	in	m	in	m			°	°	°	°		
Rotor06	8.0260	*0.2039*	1.3300	*0.0338*	0.1000	-1.1200	-20.4900	-28.1700	-34.5700	-6.4100	1.0813	0.8138
	8.5200	*0.2164*	1.3300	*0.0338*	0.1000	-1.1200	-22.9700	-28.1700	-37.0500	-8.8900	1.0186	0.8029
	9.0130	*0.2289*	1.3300	*0.0338*	0.1000	-1.1200	-25.4100	-28.1700	-39.4900	-11.3300	0.9629	0.7916
	9.5070	*0.2415*	1.3300	*0.0338*	0.1000	-1.1200	-28.0000	-28.1700	-42.0800	-13.9200	0.9129	0.7787
	10.0000	*0.2540*	1.3300	*0.0338*	0.1000	-1.1200	-30.7300	-28.1700	-44.8100	-16.6500	0.8679	0.7644
Stator06	8.1990	*0.2083*	1.3300	*0.0338*	0.1000	1.2000	19.4300	30.1600	34.5100	4.3500	1.1101	0.8146
	8.6500	*0.2197*	1.3300	*0.0338*	0.1000	1.2000	21.7300	30.1600	36.8100	6.6500	1.0523	0.8044
	9.1000	*0.2311*	1.3300	*0.0338*	0.1000	1.2000	24.0900	30.1600	39.1700	9.0100	1.0002	0.7932
	9.5500	*0.2426*	1.3300	*0.0338*	0.1000	1.2000	26.3600	30.1600	41.4400	11.2800	0.9531	0.7822
	10.0000	*0.2540*	1.3300	*0.0338*	0.1000	1.2000	28.9100	30.1600	43.9900	13.8300	0.9102	0.7689

Table 6-20 Blade data for case study 1 (Stage 7 – Rotor Row 7 and Stator Row 7)

Row	Radius		Chord		t/c	Lift Coefficient	Stagger Angle	Camber Angle	Metal Angles		c/s	o/s
						C_{l0}	γ	θ	κ_i	κ_e		
	in	m	in	m			°	°	°	°		
Rotor07	8.3610	*0.2124*	1.2800	*0.0325*	0.1000	-1.2800	-20.2800	-32.1400	-36.3500	-4.2100	1.0964	0.8061
	8.7710	*0.2228*	1.2800	*0.0325*	0.1000	-1.2800	-22.3200	-32.1400	-38.3900	-6.2500	1.0452	0.7971
	9.1810	*0.2332*	1.2800	*0.0325*	0.1000	-1.2800	-24.3200	-32.1400	-40.3900	-8.2500	0.9985	0.7880
	9.5910	*0.2436*	1.2800	*0.0325*	0.1000	-1.2800	-26.4300	-32.1400	-42.5000	-10.3600	0.9558	0.7778
	10.0000	*0.2540*	1.2800	*0.0325*	0.1000	-1.2800	-28.5800	-32.1400	-44.6500	-12.5100	0.9167	0.7670
Stator07	8.5080	*0.2161*	1.2800	*0.0325*	0.1000	1.2800	20.1800	32.1400	36.2500	4.1100	1.1014	0.8063
	8.8810	*0.2256*	1.2800	*0.0325*	0.1000	1.2800	21.8800	32.1400	37.9500	5.8100	1.0552	0.7992
	9.2540	*0.2351*	1.2800	*0.0325*	0.1000	1.2800	23.7900	32.1400	39.8600	7.7200	1.0126	0.7901
	9.6270	*0.2445*	1.2800	*0.0325*	0.1000	1.2800	25.7100	32.1400	41.7800	9.6400	0.9734	0.7809
	10.0000	*0.2540*	1.2800	*0.0325*	0.1000	1.2800	27.6200	32.1400	43.6900	11.5500	0.9371	0.7714

Table 6-21 Blade data for case study 1 (Stage 8 – Rotor Row 8 and Stator Row 8)

Row	Radius		Chord		t/c	Lift Coefficient	Stagger Angle	Camber Angle	Metal Angles		c/s	o/s
						C_{l0}	γ	θ	κ_i	κ_e		
	in	m	in	m			°	°	°	°		
Rotor08	8.6470	*0.2196*	1.2250	*0.0311*	0.1000	-1.3000	-20.3100	-32.6400	-36.6300	-3.9900	1.0597	0.8087
	8.9860	*0.2282*	1.2250	*0.0311*	0.1000	-1.3000	-21.9600	-32.6400	-38.2800	-5.6400	1.0197	0.8015
	9.3420	*0.2373*	1.2250	*0.0311*	0.1000	-1.3000	-23.5200	-32.6400	-39.8400	-7.2000	0.9809	0.7949
	9.6620	*0.2454*	1.2250	*0.0311*	0.1000	-1.3000	-25.1600	-32.6400	-41.4800	-8.8400	0.9484	0.7872
	10.0000	*0.2540*	1.2250	*0.0311*	0.1000	-1.3000	-26.9400	-32.6400	-43.2600	-10.6200	0.9163	0.7785
Stator08	8.7710	*0.2228*	1.2250	*0.0311*	0.1000	1.3000	20.2200	32.6400	36.5400	3.9000	1.0892	0.8063
	9.0790	*0.2306*	1.2250	*0.0311*	0.1000	1.3000	21.7000	32.6400	38.0200	5.3800	1.0522	0.7998
	9.3860	*0.2384*	1.2250	*0.0311*	0.1000	1.3000	23.2400	32.6400	39.5600	6.9200	1.0178	0.7927
	9.6930	*0.2462*	1.2250	*0.0311*	0.1000	1.3000	24.6700	32.6400	40.9900	8.3500	0.9856	0.7861
	10.0000	*0.2540*	1.2250	*0.0311*	0.1000	1.3000	26.1700	32.6400	42.4900	9.8500	0.9553	0.7789

Table 6-22 Blade data for case study 1 (Stage 9 – Rotor Row 9 and Stator Row 9)

Row	Radius		Chord		t/c	Lift Coefficient	Stagger Angle	Camber Angle	Metal Angles		c/s	o/s
						C_{l0}	γ	θ	κ_i	κ_e		
	in	m	in	m			°	°	°	°		
Rotor09	8.8850	*0.2257*	1.1750	*0.0298*	0.1000	-1.3000	-20.4300	-32.6400	-36.7500	-4.1100	1.0734	0.8064
	9.1640	*0.2328*	1.1750	*0.0298*	0.1000	-1.3000	-21.6700	-32.6400	-37.9900	-5.3500	1.0407	0.8013
	9.4430	*0.2399*	1.1750	*0.0298*	0.1000	-1.3000	-23.0600	-32.6400	-39.3800	-6.7400	1.0100	0.7948
	9.7220	*0.2469*	1.1750	*0.0298*	0.1000	-1.3000	-24.4100	-32.6400	-40.7300	-8.0900	0.9810	0.7886
	10.0000	*0.2540*	1.1750	*0.0298*	0.1000	-1.3000	-25.6600	-32.6400	-41.9800	-9.3400	0.9537	0.7829
Stator09	8.9880	*0.2283*	1.1750	*0.0298*	0.1000	1.3000	20.1500	32.6400	36.4700	3.8300	1.1027	0.8054
	9.2410	*0.2347*	1.1750	*0.0298*	0.1000	1.3000	21.2600	32.6400	37.5800	4.9400	1.0725	0.8007
	9.4940	*0.2411*	1.1750	*0.0298*	0.1000	1.3000	22.4500	32.6400	38.7700	6.1300	1.0440	0.7953
	9.7470	*0.2476*	1.1750	*0.0298*	0.1000	1.3000	23.6300	32.6400	39.9500	7.3100	1.0169	0.7899
	10.0000	*0.2540*	1.1750	*0.0298*	0.1000	1.3000	24.8100	32.6400	41.1300	8.4900	0.9911	0.7844

Table 6-23 Blade data for case study 1 (Stage 10 – Rotor Row 10 and Stator Row 10 & EGV)

Row	Radius		Chord		t/c	Lift Coefficient	Stagger Angle	Camber Angle	Metal Angles		c/s	o/s
						C_{l0}	γ	θ	κ_i	κ_e		
	in	m	in	m			°	°	°	°		
Rotor10	9.0850	*0.2308*	1.1200	*0.0284*	0.1000	-1.3000	-20.2900	-32.6400	-36.6100	-3.9700	1.0988	0.8049
	9.3140	*0.2366*	1.1200	*0.0284*	0.1000	-1.3000	-21.2400	-32.6400	-37.5600	-4.9200	1.0717	0.8009
	9.5430	*0.2424*	1.1200	*0.0284*	0.1000	-1.3000	-22.3100	-32.6400	-38.6300	-5.9900	1.0460	0.7961
	9.7720	*0.2482*	1.1200	*0.0284*	0.1000	-1.3000	-23.4100	-32.6400	-39.7300	-7.0900	1.0215	0.7910
	10.0000	*0.2540*	1.1200	*0.0284*	0.1000	-1.3000	-24.4600	-32.6400	-40.7800	-8.1400	0.9982	0.7861
Stator10	9.1740	*0.2330*	1.1200	*0.0284*	0.1000	1.3000	19.6700	32.6400	35.9900	3.3500	1.1464	0.8044
	9.3810	*0.2383*	1.1200	*0.0284*	0.1000	1.3000	20.6100	32.6400	36.9300	4.2900	1.1211	0.8003
	9.5870	*0.2435*	1.1200	*0.0284*	0.1000	1.3000	21.4700	32.6400	37.7900	5.1500	1.0970	0.7966
	9.7940	*0.2488*	1.1200	*0.0284*	0.1000	1.3000	22.4500	32.6400	38.7700	6.1300	1.0738	0.7921
	10.0000	*0.2540*	1.1200	*0.0284*	0.1000	1.3000	23.3800	32.6400	39.7000	7.0600	1.0517	0.7877
EGV	9.2620	*0.2353*	1.1200	*0.0284*	0.1000	0.6600	5.0000	16.6500	13.3300	-3.3300	1.1355	0.8815
	9.3810	*0.2383*	1.1200	*0.0284*	0.1000	0.6600	5.0000	16.6500	13.3300	-3.3300	1.1211	0.8830
	9.5870	*0.2435*	1.1200	*0.0284*	0.1000	0.6600	5.0000	16.6500	13.3300	-3.3300	1.0970	0.8854
	9.7940	*0.2488*	1.1200	*0.0284*	0.1000	0.6600	5.0000	16.6500	13.3300	-3.3300	1.0738	0.8878
	10.0000	*0.2540*	1.1200	*0.0284*	0.1000	0.6600	5.0000	16.6500	13.3300	-3.3300	1.0517	0.8900

Performance characterization terminology and definition

In describing the compressor performance a number of new parameters not covered earlier needed to be used and the same are introduced here. The foremost being the pressure rise ratio more commonly known as the pressure ratio. The pressure ratio as defined using the absolute total pressures:

$$PR = \frac{P_{tae}}{P_{tai}} \tag{6.66}$$

The pressure rise ratio can be defined for the compressor or for individual stages, but the definition remains the same. On similar lines the temperature rise ratio can be defined as:

$$TR = \frac{T_{tae}}{T_{tai}} \tag{6.67}$$

The adiabatic efficiency of the compressor is defined as the ratio of the ideal work per unit mass to the actual work per unit mass between the same total pressures and is given by:

$$\eta = \frac{H_{taeisen} - H_{tai}}{H_{tae} - H_{tai}} \tag{6.68}$$

For this work during the evaluation of the efficiency, it was assumed that the gas was calorically perfect. This allowed a simplified model for determining the efficiency and the isentropic enthalpy need not be tracked from stage to stage. With the assumption of calorically perfect gas, equation (6.68) becomes:

$$\eta = \frac{PR^{\frac{\gamma-1}{\gamma}} - 1}{TR - 1} \tag{6.69}$$

The work required per stage was determined from:

$$Work_{stage} = \left(H_{tae} - H_{tai}\right)_{stage} \tag{6.70}$$

The total work required per stage was then determined from:

$$Work_{total} = \sum_{stage=1}^{last} Work_{stage} \tag{6.71}$$

The degree of reaction (R_c) is defined as the ratio of the static enthalpy rise across the rotor to the static enthalpy rise across the stage.

$$R_c = \frac{\left(h_{se} - h_{si}\right)_{rotor}}{\left(h_{se} - h_{si}\right)_{stage}} \tag{6.72}$$

The flow coefficient is defined as the ratio of the axial velocity to the rotor tangential velocity:

$$\Phi = \frac{C_m}{U} \tag{6.73}$$

The stage loading coefficient is defined as the ratio of the stage work to the square of the rotor tangential velocity:

$$\psi = \frac{\left(H_{tae} - H_{tai}\right)_{stage}}{U^2} \tag{6.74}$$

Evaluation-1: Isentropic Performance evaluation at 100% speed

The first evaluation study illustrated an isentropic solution done at 9959 rpm which corresponds to 100% of the design speed. An isentropic solution is a solution with no losses across the compressor and indicates the maximum possible pressure rise across the compressor or the minimum work required. It provided a framework to examine the influence of different losses in the compressor.

Table 6-24 Test data at 100% design speed (9959 rpm)

Mass flow rate		PR	EFF
lb/s	kg/s		
53.700	24.380	7.640	0.828
54.800	24.879	7.350	0.838
55.200	25.061	6.970	0.831
55.800	25.333	6.750	0.826
55.900	25.379	6.560	0.825
56.000	25.424	6.240	0.810
56.100	25.469	5.560	0.771

To determine which flow rates would be examined, the test data at 9959 rpm shown in Table 6-24 was first examined. The flow rates varied from 53.70 lb/s to 56.10 lb/s. Thus, evaluations were done for flow rates ranging from 53.5 lb/s to 56.5 at regular intervals of 0.5 lb/s. Evaluations always commenced from the largest flow (near choke) to the smallest flow (surge). If for a pre-determined mass flow rate choke was encountered then that data point was dropped from the solution presentation.

It may be recalled from the mathematical model that system closure was obtained by specifying the exit flow angle. The exit flow angle is a function of the blade exit angle and an angle of deviation which is the function of the flow characteristics such as the angle of incidence and the blade geometry. In an isentropic solution the case where the flow angle at exit corresponded with the blade exit angle i.e. with zero deviation was first examined. Next, the influence of the flow angle models on the solution was evaluated. The results of the same are presented in Figure 6-4 along with the test data.

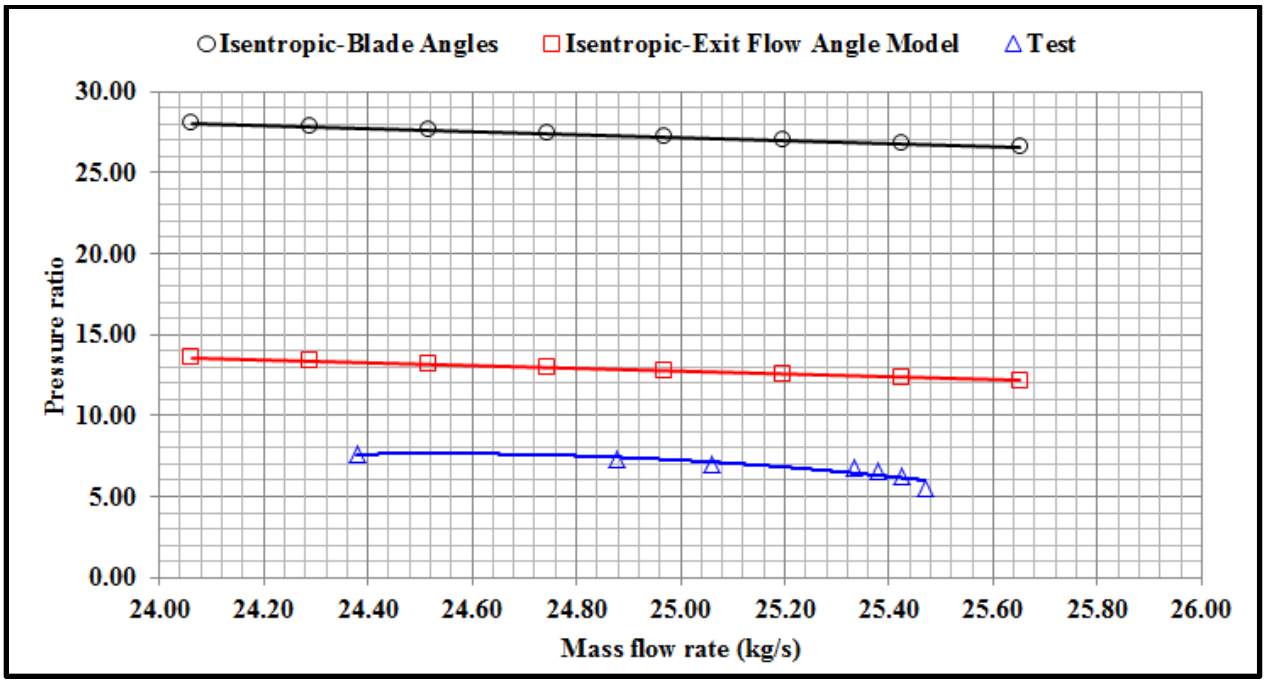

Figure 6-4 Pressure ratio vs. mass flow rate for 9959 rpm-Evaluation 1

The isentropic solution with exit flow angles corresponding with the exit blade metal angles is identified as "Isentropic-Blade Angles" in the Figure 6-4 while the solution that uses the exit flow angle model is identified as "Isentropic-Exit Flow Angle Model". It is apparent from the Figure 6-4 that the highest theoretical pressure ratios were achieved if the exit deviation was set to zero. The pressure ratio varied from 26.5 to 28 over the range of flow rates examined. However, this is approximately four times the pressure ratios measured during testing. By incorporating the flow angle model the pressure ratio dropped significantly, though it still was about twice the test data. It can be inferred from the above that a well described exit flow angle model can substantially improve model correlation with actual performance. It can also been seen from the Figure 6-4 the pressure ratio continuously drops with increasing flow rate. This trend is absolutely in congruence with the actual compressor performance. However, it is noteworthy that test data exhibits a drooping characteristic while the isentropic solutions are fairly flat. As a matter of fact, a linear curve was very easily fitted for the isentropic solutions in the Figure 6-4 since the data was flat. Further improvements to the modeled data can now be accomplished only with the loss characterization model.

For generating the data set in Figure 6-4 a swirl angle of 29° was used. The inlet swirl data was not found in the literature and hence it was iteratively determined to best correspond the test data. The next evaluation discusses the influence of inlet swirl angle on the solution.

Evaluation-2: Influence of inlet swirl angle

This study was also done for 100% design speed. The isentropic case with the flow angle model was used for this study.

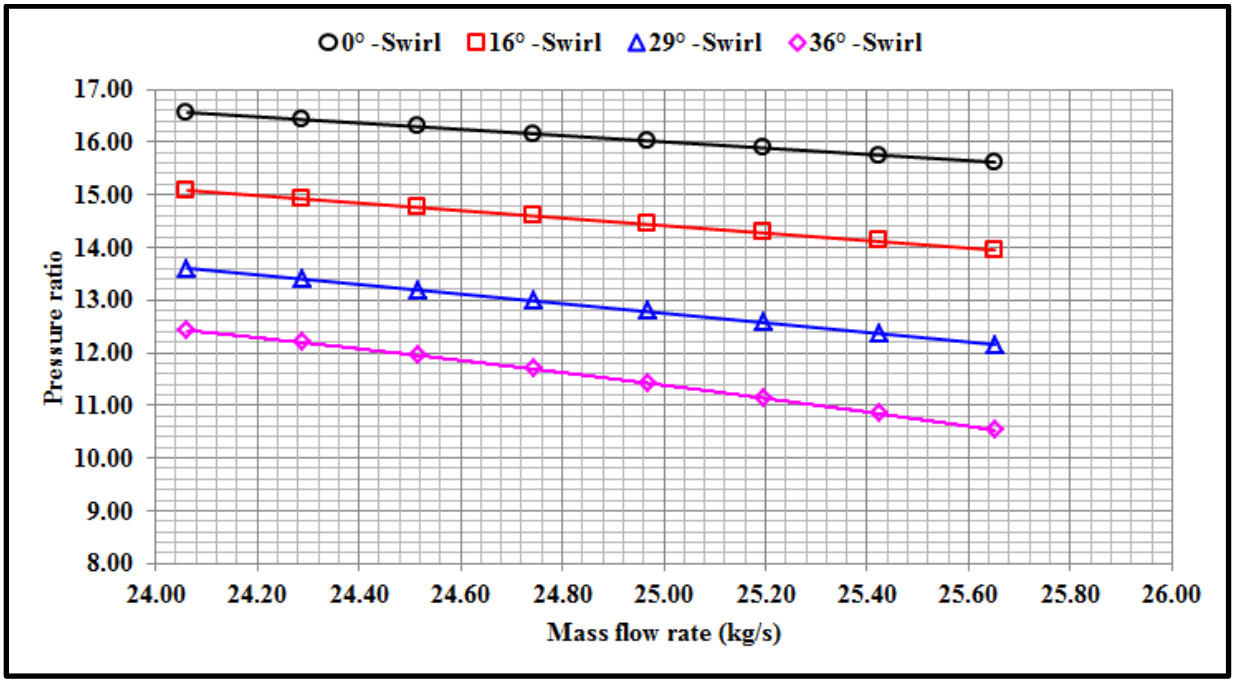

Figure 6-5 Pressure ratio vs. mass flow rate for 9959 rpm with varying inlet swirl

Figure 6-5 shows the performance curves for four different inlet swirl angles. It can be seen that with increasing swirl the pressure ratio decreased. But most importantly the flow characteristic also started to have a more drooping trend. A second order polynomial was fitted as the trend line for swirl angle of 36° with a R^2 value of 1 whereas a linear fit resulted in a R^2 value of 0.977. The second order curve fit is the one shown in the Figure 6-5 for the swirl angle of 36°. The 29° and 36° swirl angle solutions were closer to the tested data set and were thus used further in the models with loss characterization and the other two swirl angles were dropped.

Evalution-3: Performance evaluation with losses at 9959 rpm

In the compressor loss modeling chapter it was indicated that the coefficients K_1 and K_2 were performance loss model constants. Lieblien (1959) presented these coefficients as 0.004 and 1.0 respectively. However, Aungier (2003) reported greater success using the values 0.004 and 4.0 respectively for the two constants. In this evaluation, Aungier's proposed coefficients have been used.

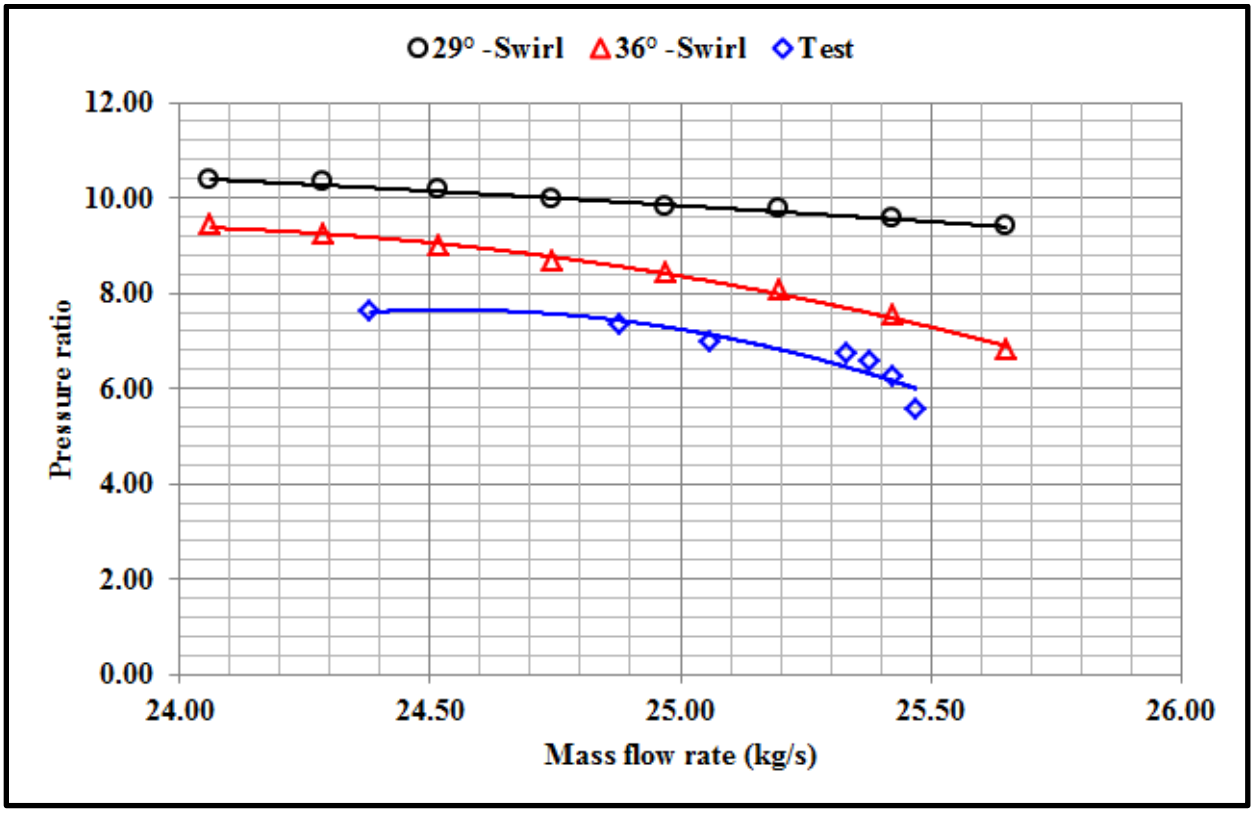

Figure 6-6 Pressure ratio vs. mass flow rate for 9959 rpm with losses and two inlet swirls

In the Figure 6-6 the pressure ratio versus flow rate has been plotted for swirl angles of 29° and 36° along with the test data. It is seen that the generalized loss model implemented here works very effectively. The curve for 36° swirl provided a better representation of the test data although it provided a slightly higher prediction.

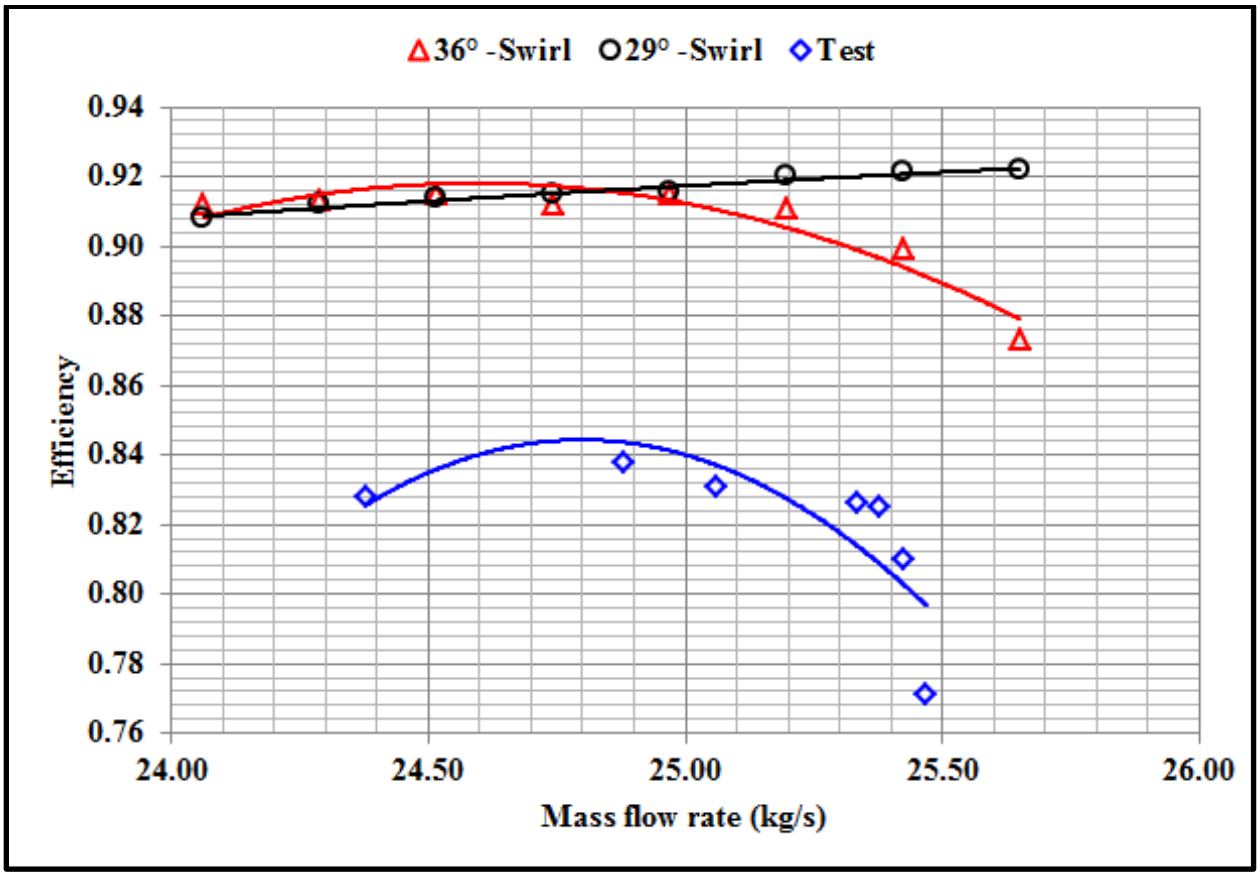

Figure 6-7 Efficiency vs. mass flow rate for 9959 rpm with losses and two inlet swirls

Figure 6-7 a comparison of the efficiency versus mass flow rate data for the 29° and 36° swirl angles along with the test data is done. The efficiency data for the 29° swirl angle case shows an increasing trend. On the contrary the 36° swirl angle case seems to follow the same trend as the test data except that it over predicts. It is apparent from the investigation so far that the 36° inlet swirl angle is best suited to characterize the performance, although there is some level of over-prediction. It is intuitive from the discussion above that using an inlet swirl of 36° would provide a good fit for the data. However, it was observed from tracking the stage performance data that the pressure rise in the first stage rotor for all the flow rates varied from 1.030 to 1.045. Consequently, stage efficiencies were of the order of 50%. When the same data for 29° swirl angle case was examined it was found that the pressure rise was about 1.12 to 1.14 with the first stage efficiency around 90% or higher. This was the case with smaller swirl angles. It was observed that larger the swirl angle the lower was the first stage performance. The drop in first stage performance was marginal up to 29° but then a rapid deterioration of performance was observed. Thus, the 36° inlet swirl angle was abandoned and 29° was used for further evaluation.

Evalution-3: Performance evaluation with losses at 9959 rpm and aerodynamic blockage factor

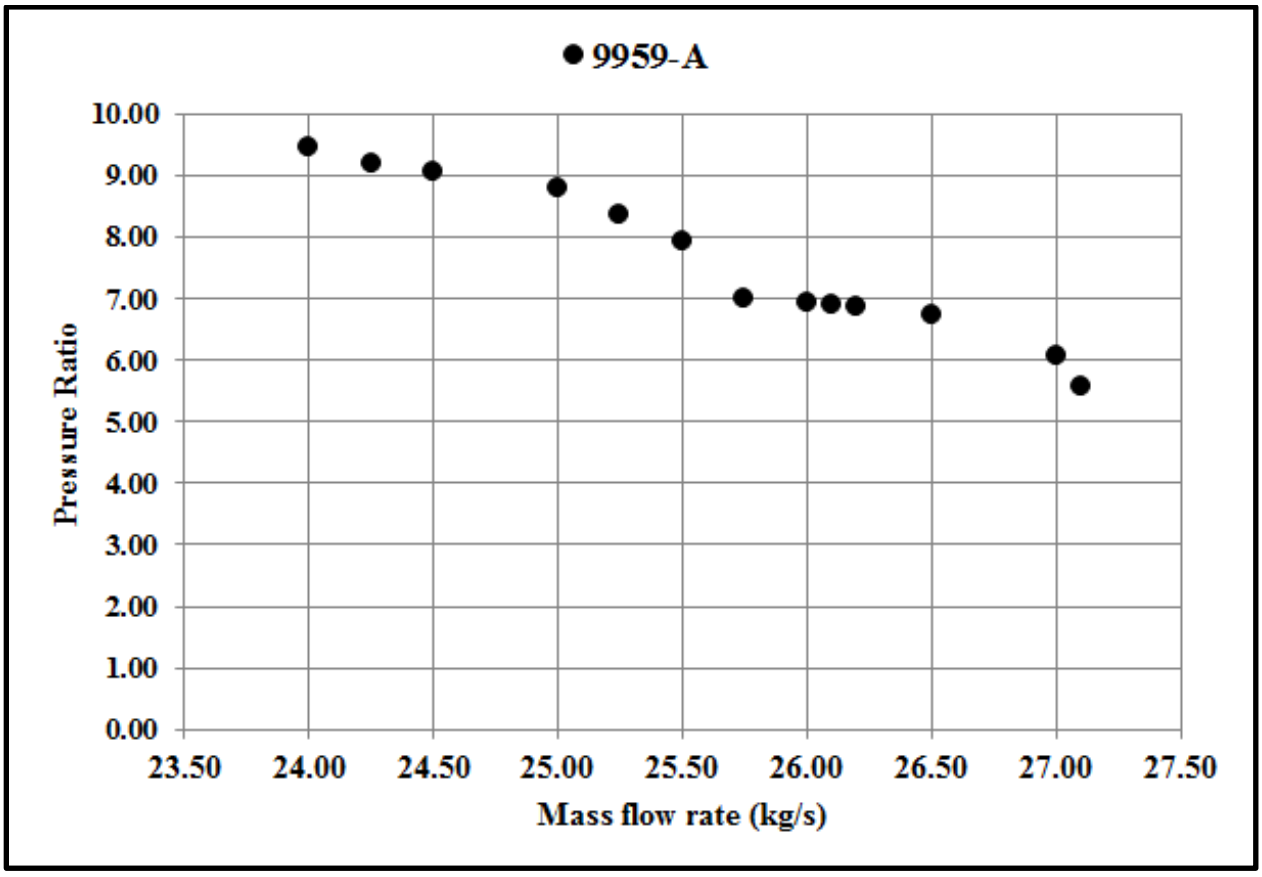

Figure 6-8 Pressure ratio versus mass flow rate at 9959 with $K_1 = 0.006$ (9959-A)

It has been presented earlier that the model constants K_1 and K_2 could be varied for determining improved correlation with test data. In this evaluation model constant K_1 was set to 0.006 and the case study is labeled as 9959-A. A detailed analysis on the influence of model constants is presented later. Further, since all the analysis was done in SI units it was inconvenient to run the analysis at steps of 0.5 lb/s. Hence, the analysis was commenced from a flow rate of 27.5 kg/s and continued to 24 kg/s at intervals of 0.25 kg/s. This change does not alter the analysis but makes it more reasonable to understand and track in SI units. Figure 6-8 shows the pressure rise performance data.

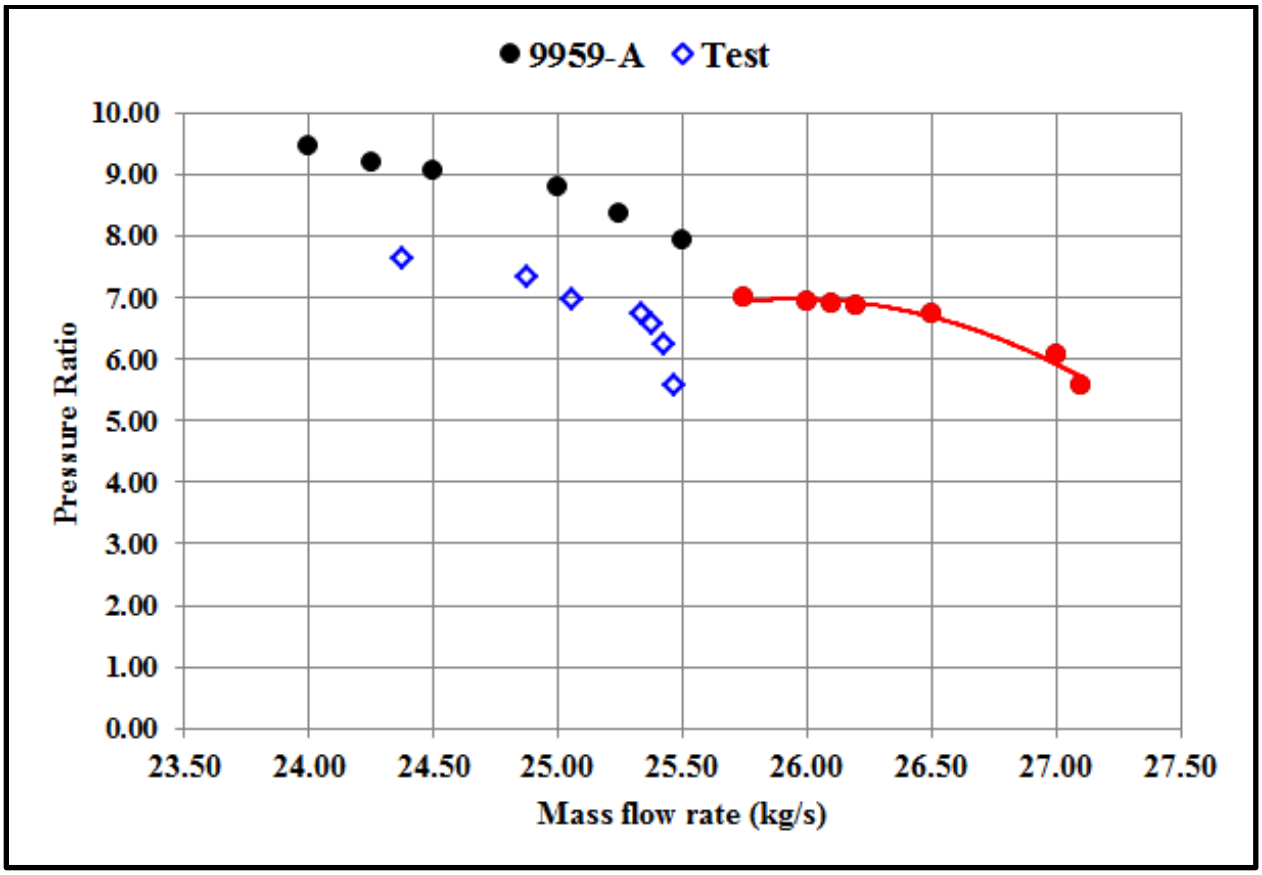

Figure 6-9 Pressure ratio versus mass flow rate with surge indicated for case 9959-A

At 27.5 kg/s choke was encountered and same was the case at 27.25 kg/s. Thus, these two data points are missing in the Figure 6-8. The first solution was obtained at 27.1 kg/s. From there on a continuously rising performance was observed till 26.00 kg/s after which the curve was flat. Subsequently, there was another set of data points from 25.5 kg/s but a discontinuity in the trend was observed. The primary surge criterion is to terminate the performance curve where the derivative of the curve tends to zero. Figure 6-9 demonstrates a curve plotted through the data set from choke (27.2 kg/s) to surge (25.75 kg/s). Furthermore, a comparison with the test data showed that the modeled data was shifted to the right.

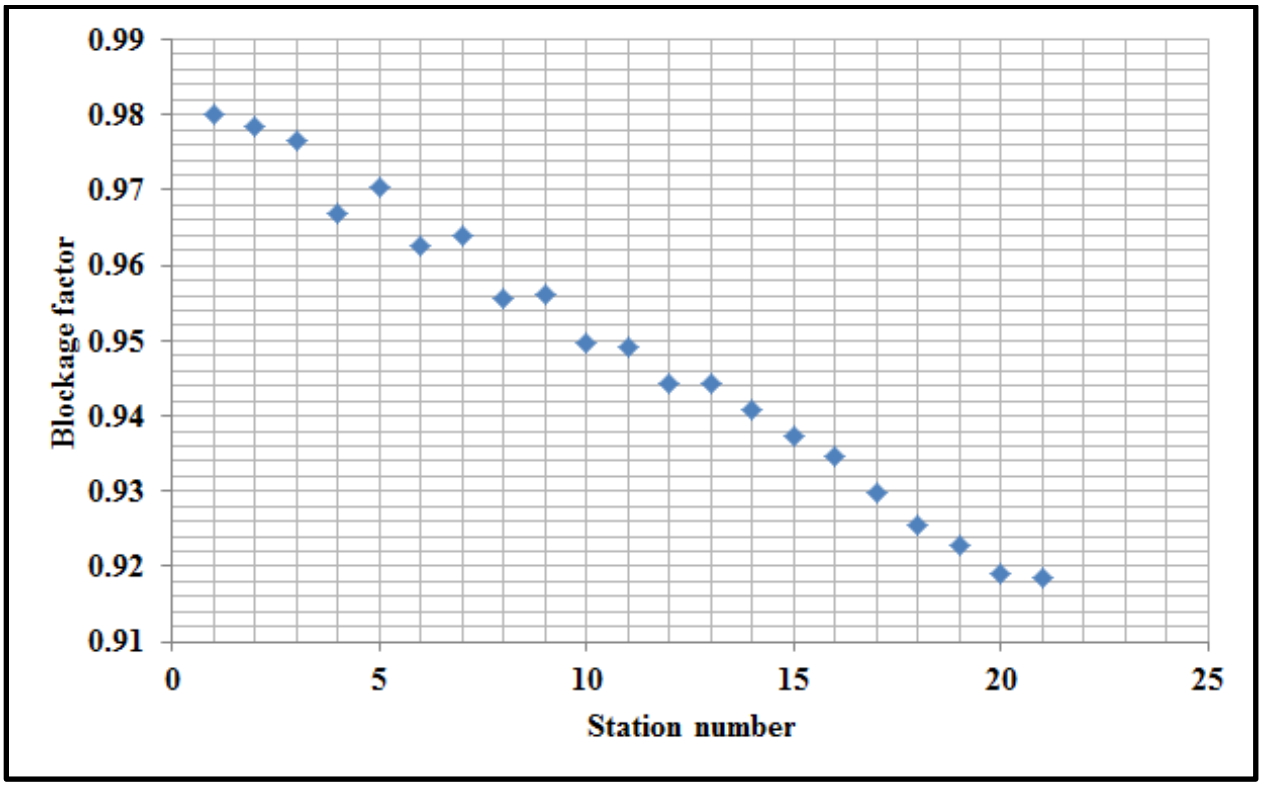

Figure 6-10 Blockage factor Aungier (2008)

Aungier (2003) and Veres (2009) indicate the use of aerodynamic blockage in their models. Aerodynamic blockage is an area correction factor and Aungier's proposed correction coefficients are presented graphically Figure 6-10. The graph helps demonstrate that the blockage factor value reduces as we traverse downstream which essentially means that the aerodynamic blockage increases or the annulus area that can be used for flow calculation reduces. The performance analysis of 9959-A was repeated with the blockage correction and the evaluation study is labeled as case 9959-B.

The analysis results are plotted in Figure 6-11. At the outset it is observed that the performance shifts left by including the aerodynamic blockage. This provides a significant improvement over the 9959-A evaluation when compared with the test data. A consequence of the plot shifting left is that choked flow is found at lower flow rate of 26.2 kg/s. Further, as before the surge is determined using the surge criterion of the derivative of curve tending to zero which results in the curve being terminated at a flow rate between 24.25 kg/s and 24.5 kg/s. The tested data surge is at 24.3 kg/s and thus the surge prediction by the model seems to be consistent with the test data.

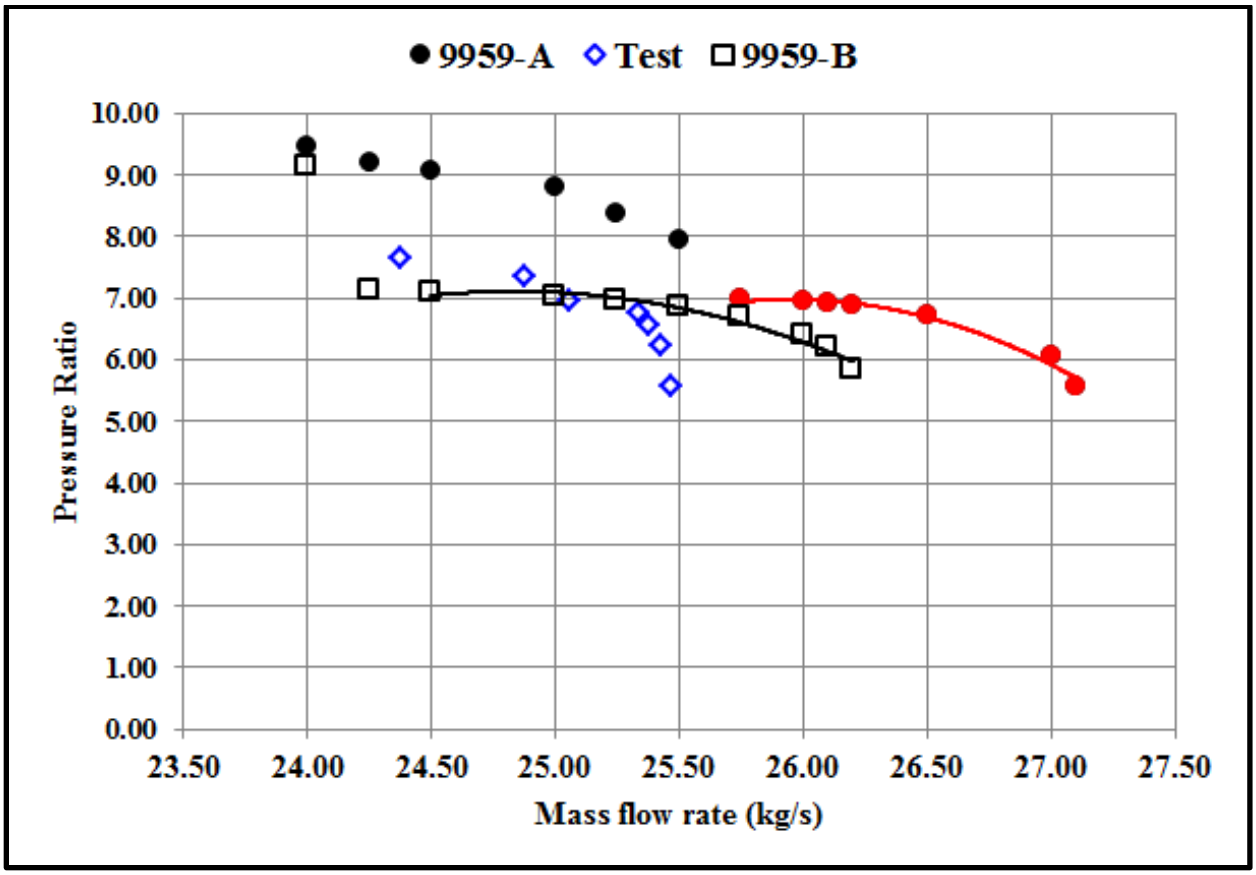

Figure 6-11 Pressure ratio versus mass flow rate with surge indicated for case 9959-A and 9959-B

The exact performance profile does not match completely with the test data. The goal of this study is not to specifically develop correlations for a particular machine rather it is to develop a generalized algorithm for performance modeling and understand the influence of loss models and the influence of some of the modifications that can be made to the machine. A performance analysis is incomplete without presenting the efficiency data against the flow rate. Data is plotted for the case 9959-A (without blockage model), 9959-B (with blockage model) and test data. The modeled data in both 9959-A and 9959-B exhibit satisfactory profile i.e., a continuously rising trend from surge reaching a maximum followed by a dropping characteristic to choke. The modeled data is shifted to the right as compared to the test data but that was already seen in the pressure ratio curve.

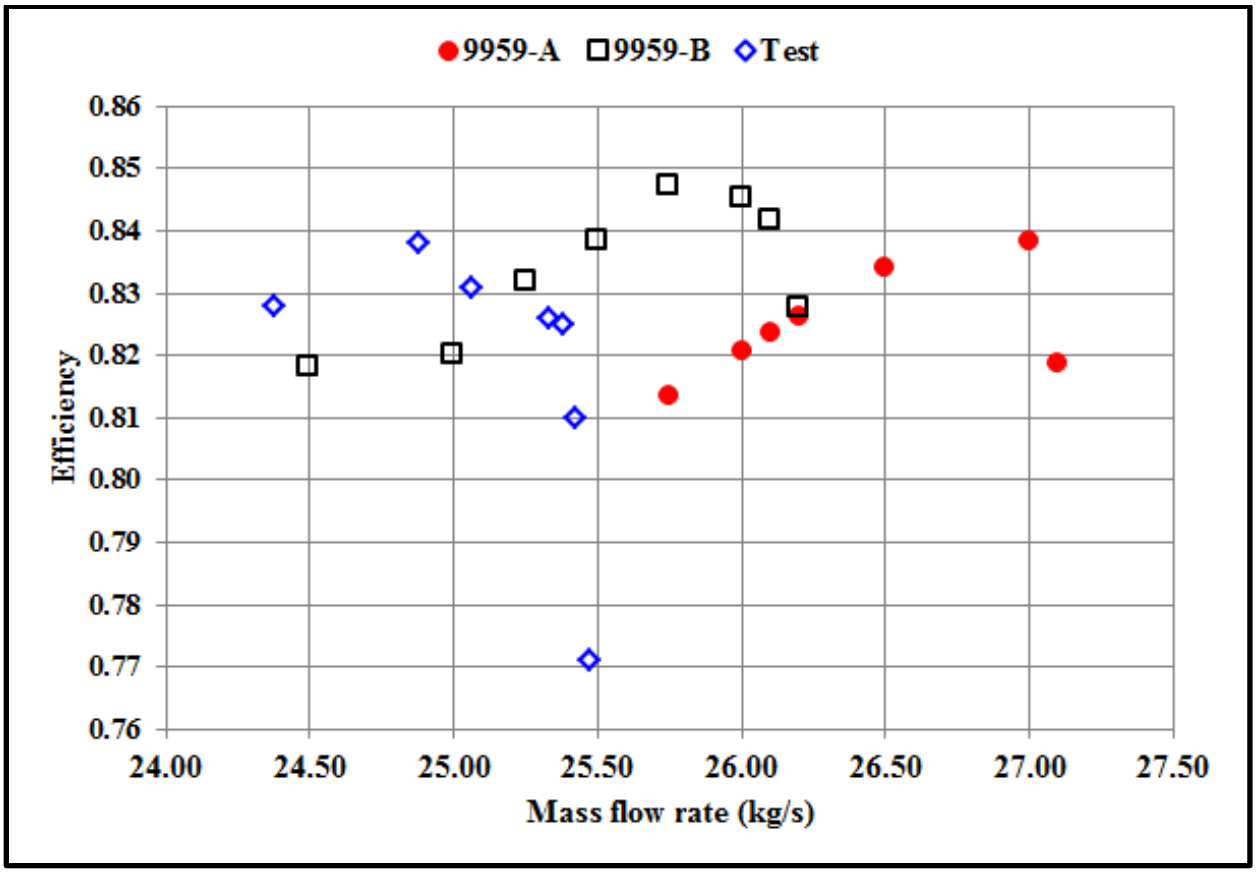

Figure 6-12 Efficiency versus mass flow rate for case 9959-A and 9959-B

Evalution-4: Understanding the influence of changing stagger angle

In a compressor the stagger angle of the stator blades can be changed to modify its performance. Thus, a performance analysis tool should be able to determine what the influence of such a modification would be. Using CTOOMCOMP1DPERF it is possible to accomplish that. As the next case study, the blade stagger angles of all the stator blades were changed by +1°, +2°, -1°, and -2°. Evaluation was carried out for mass flow rates from 24.25 kg/s to 26.2 kg/s since these were the original surge and choke limits. All of the data including the original case are plotted in Figure 6-13 and Figure 6-14.

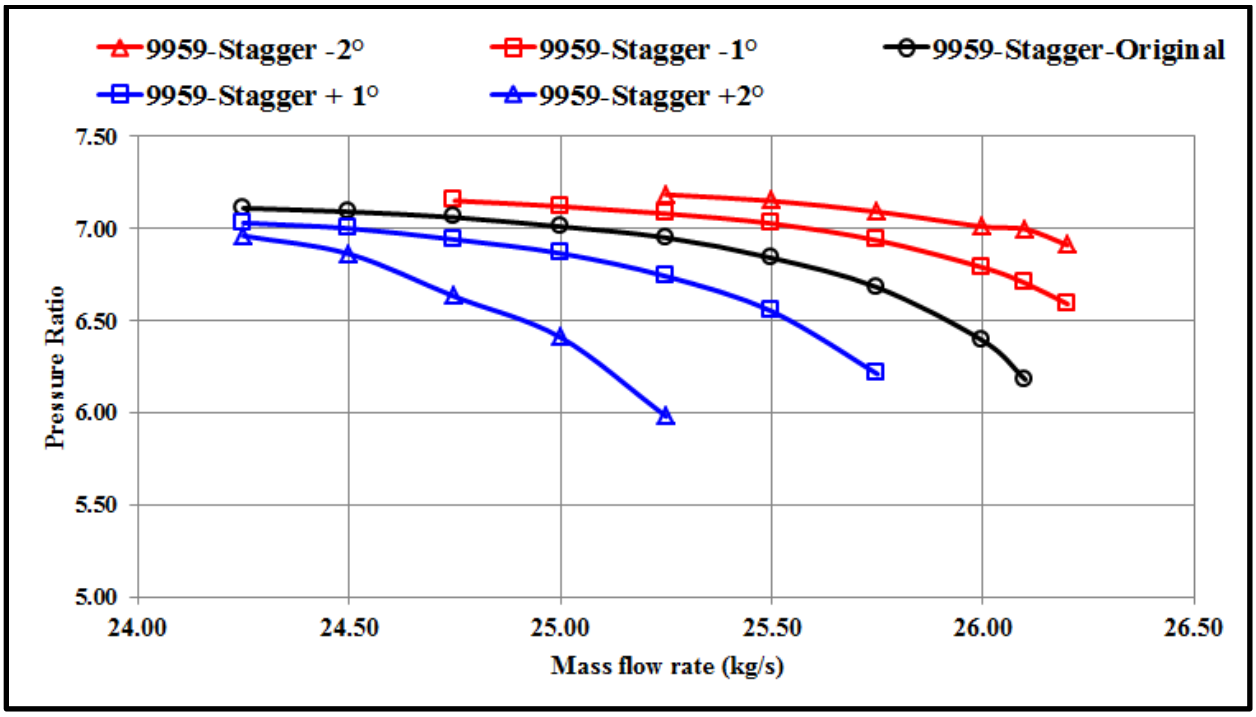

Figure 6-13 Pressure ratio versus mass flow rate for 5 different stagger angles (9959 rpm)

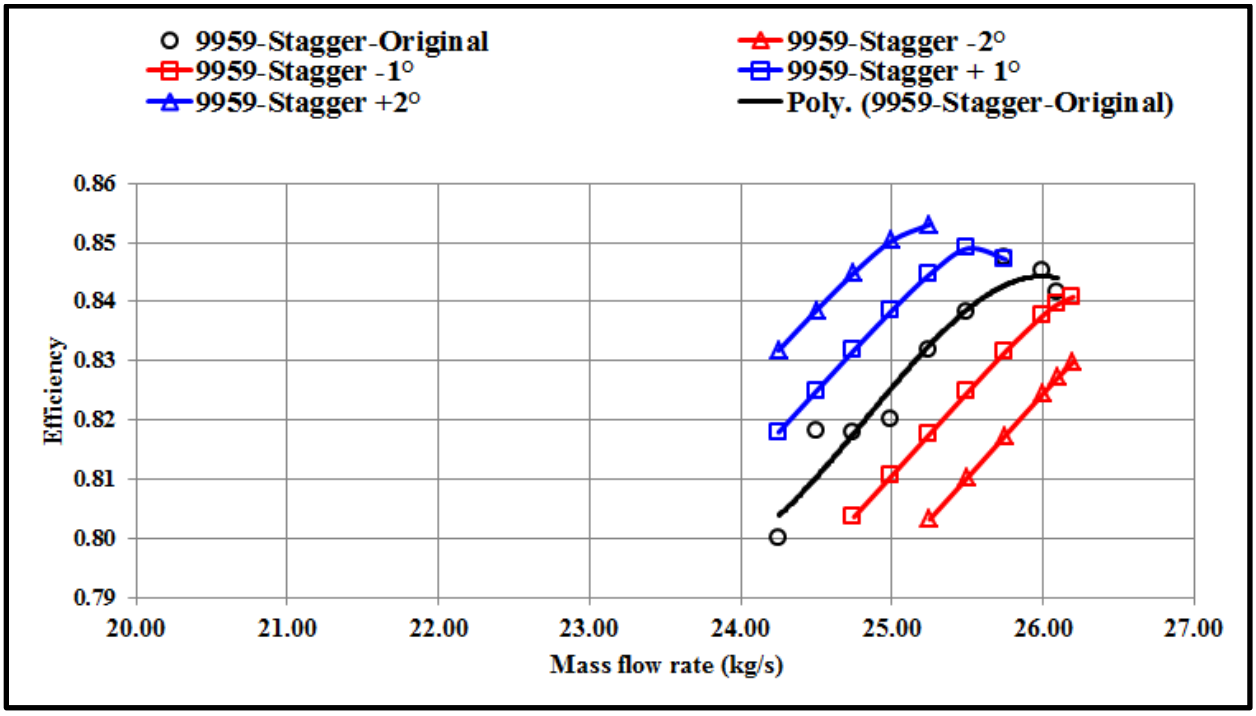

Figure 6-14 Efficiency versus mass flow rate for 5 different stagger angles (9959 rpm)

It can be seen that as a result of increasing the stagger angle the performance curve shifts to the left. The choked flow values are lesser than that of the original case and it is likely that the surge point also shifts to the left but is not known clearly since additional data point

beyond 24.25 kg/s was not run. However, observing the curve profile (Line segments to join the data points were used to establish the curve profile) it is very evident that the surge point would definitely shift to the left especially for the +2° stagger case which exhibits a rising characteristic. On the contrary, decreasing the stagger angle shifts the curve to the right. It is seen that the surge point was reached for the -2° and -1° cases while the choke condition was still not attained. This is further clear on the efficiency plot (Figure 6-14) where it can be seen that the efficiency curve shows a rising trend and the drooping part of the efficiency curve is not yet achieved for the cases where stagger angle was increased. On the efficiency plot a polynomial curve fit was used for the 9959-Original stagger case, while the remaining curves were not trend lines.

Evalution-5: Modeling the clearance losses

The effect of clearance losses is intuitive. Increased clearances during operation will increase the pressure drop and reduce efficiency. Using CTOOMCOMP1DPERF one can quantify the loss. In this evaluation study a baseline case was first established with zero clearance loss and then three different clearances were examined, the original clearance, three times the original clearance and eight times the original clearance.

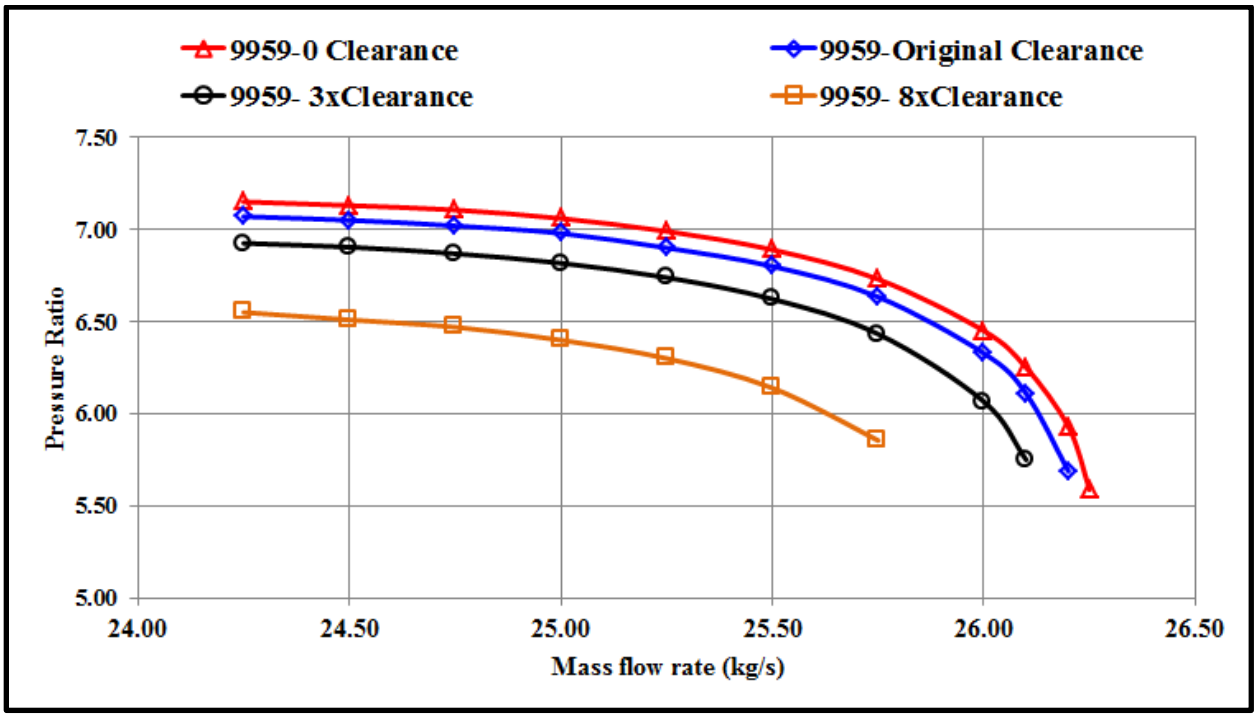

Figure 6-15 Pressure ratio versus mass flow rate for 4 different clearances (9959 rpm)

Figure 6-15 and Figure 6-16 present the performance characteristic of the compressor with different clearances. It was observed that with increasing clearances both the pressure ratio and the compressor efficiency dropped. Increased clearances are the most common occurrence during operation of the machine and loss in compressor performance influences the CT system on the whole increasing the fuel consumption. From an operational standpoint, the choice is to change the tip seals which would require opening the machine. Alternately, the machine can be re-staggered (change the stagger angle of the stator rows). This is usually accomplished without opening the machine as these machines usually have a built-in linkage mechanism to change the stagger angle. The fundamental question is the extent of re-staggering and CTOOMCOMP1DPERF can be used to evaluate that. A wider variety of re-staggering combinations can be evaluated using this tool which would allow the machine operator to recover lost performance.

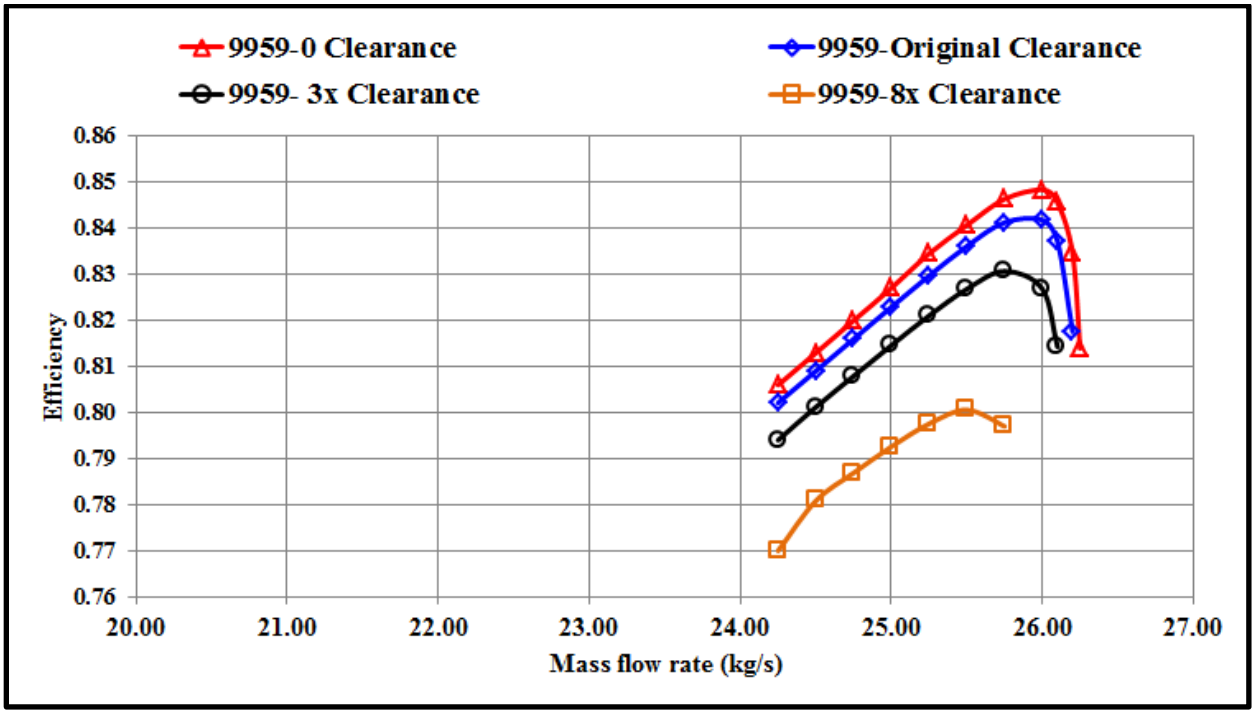

Figure 6-16 Efficiency versus mass flow rate for 4 different clearances (9959 rpm)

So far, all evaluations were done at 100% design speed with a blockage factor proposed by Aungier the performance evaluation constant K_1 set to 0.006. The influence of changing this constant was examined and is presented next.

Evalution-6: Performance evaluation with losses at 9959 rpm and modified model constant K_1

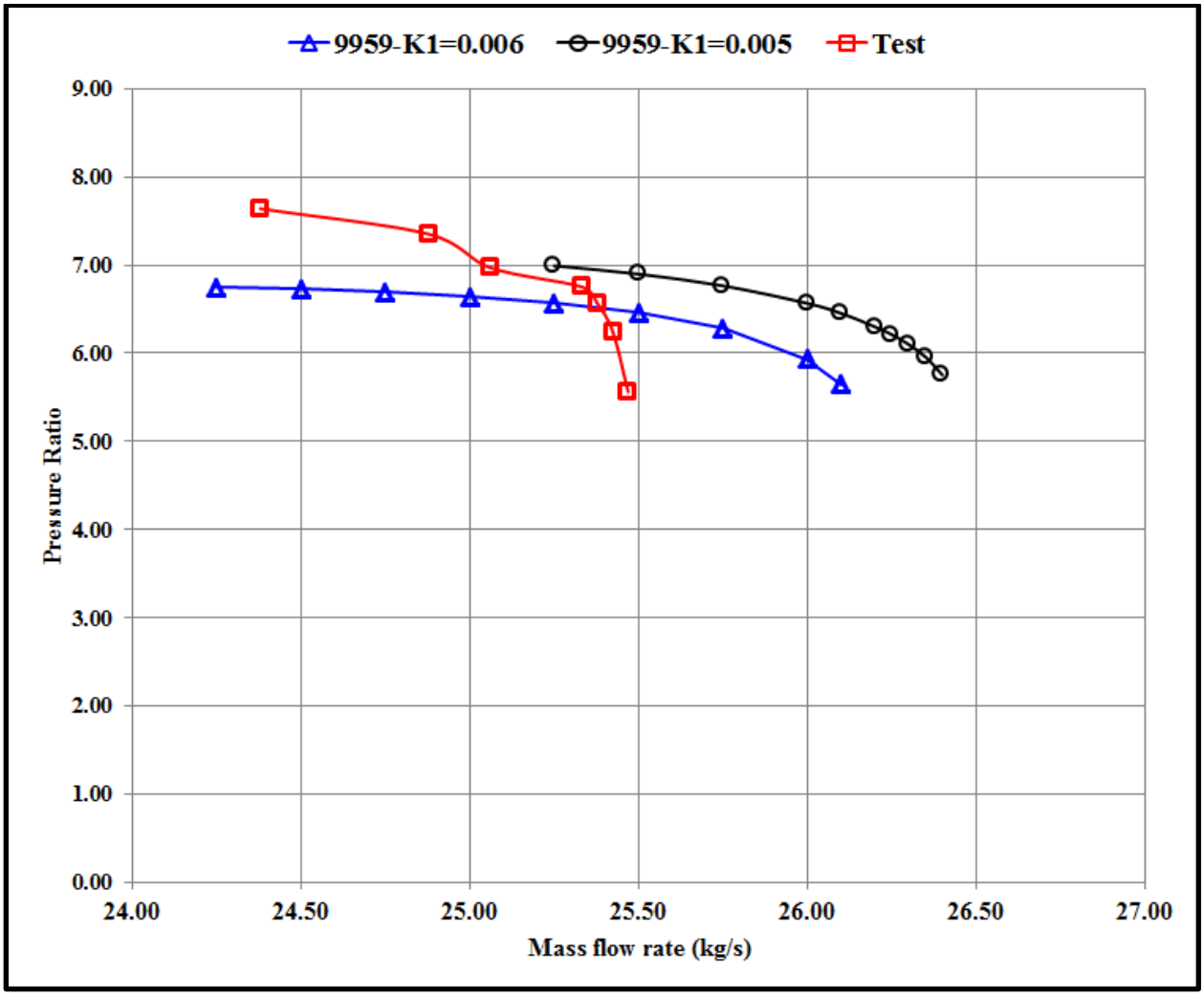

Figure 6-17 Pressure ratio vs. mass flow rate for 9959 rpm with two different values of K_1

Figure 6-17 and Figure 6-18 present the performance characteristics at 100% design speed (9959 rpm) for $K_1 = 0.005$ and $K_1 = 0.006$. It is observed that increasing the coefficient reduces the pressure ratio and the efficiency. This part is rather intuitive from the way the model is set up. It was observed that changing the constant had an impact on the surge and choke flow points i.e., the curve shifted to the left with increasing value of K_1. Thus, the effect of changing the constant is not linear. If it were then the curve would have simply shifted below. This is because the constant influences not only the design loss coefficient directly but also the off-design loss coefficient which is a polynomial function of the design loss coefficient.

Furthermore, a small change in the off-design loss coefficient value influences the subsequent stage incidence angles and thereafter there are a multitude of parameters that influence the loss calculation. Thus, we see a shift in the performance curve.

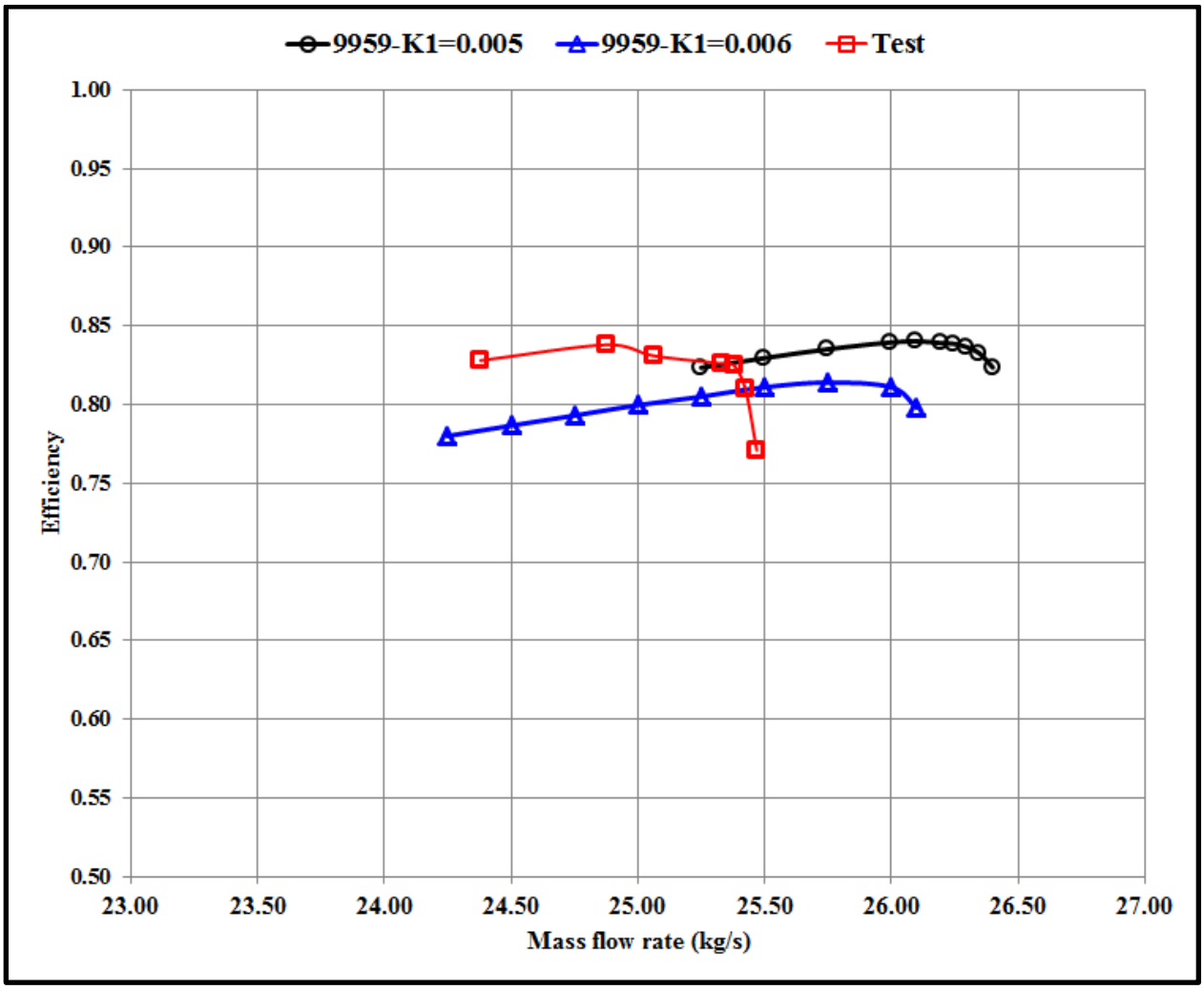

Figure 6-18 Efficiency vs. mass flow rate for 9959 rpm with two different values of K_1

Evalution-7: Performance evaluation with losses at 8963 rpm and 7967 rpm

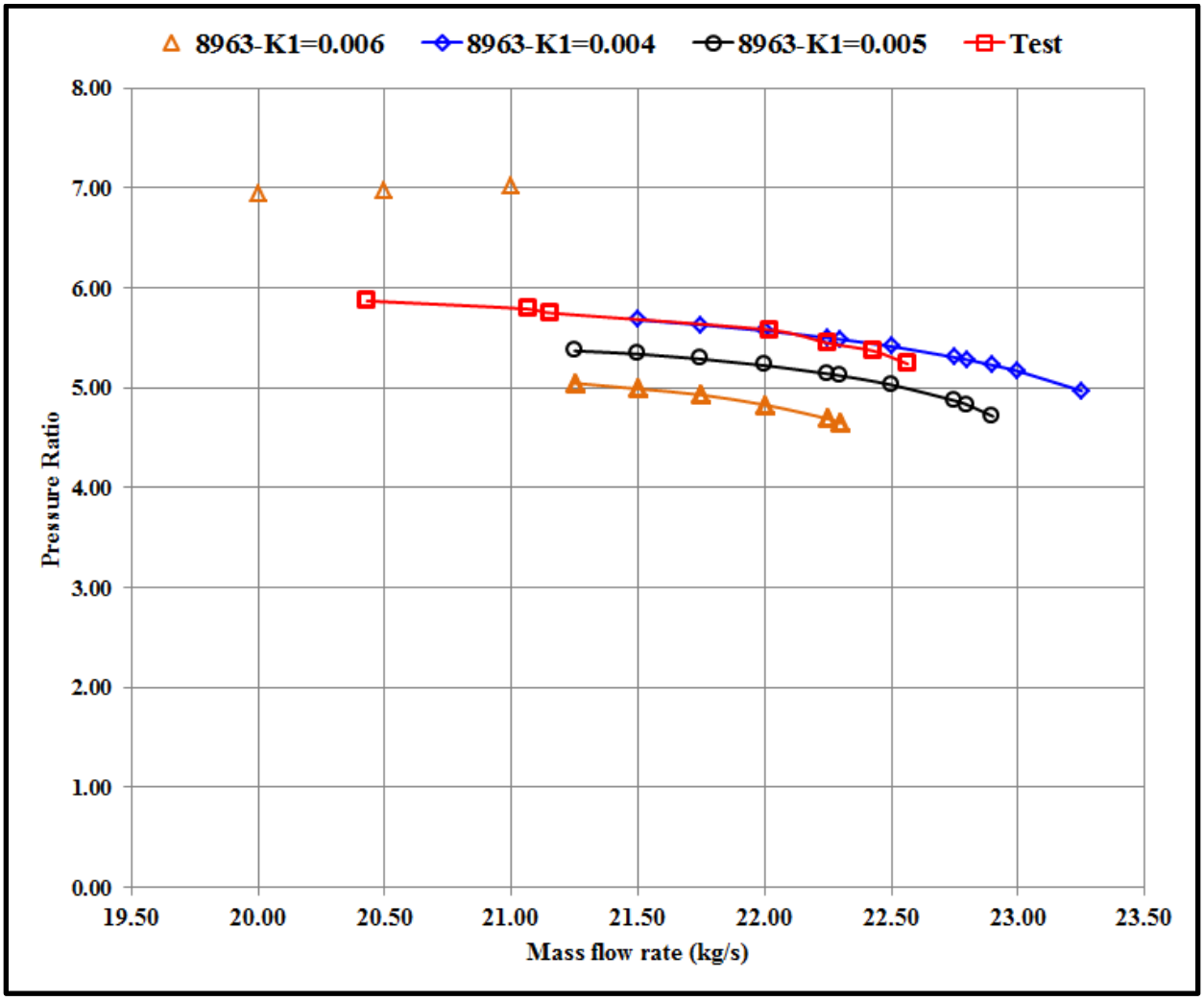

Figure 6-19 Pressure ratio vs. mass flow rate for 8963 rpm with three different values of K_1

Figure 6-18 and Figure 6-19 present the performance characteristics at 80% design speed (8963 rpm) for $K_1 = 0.004$, $K_1 = 0.005$ and $K_1 = 0.006$ along with the test data. It can be seen that $K_1 = 0.004$ provided the best correlation as far as the pressure ratio curve was concerned and increasing the coefficient only degraded the performance. The modeled efficiencies were comparable to the test data with a slight over prediction for $K_1 = 0.004$ while using $K_1 = 0.005$ and $K_1 = 0.006$ led to under-prediction. For the curve with $K_1 = 0.006$ the points used to represent the performance were connected using line segments while the three data points beyond the surge point are also shown simply to provide an understanding of how surge was

determined using the surge criterion. The same philosophy was used for the other modeled data as well but the details are not indicated.

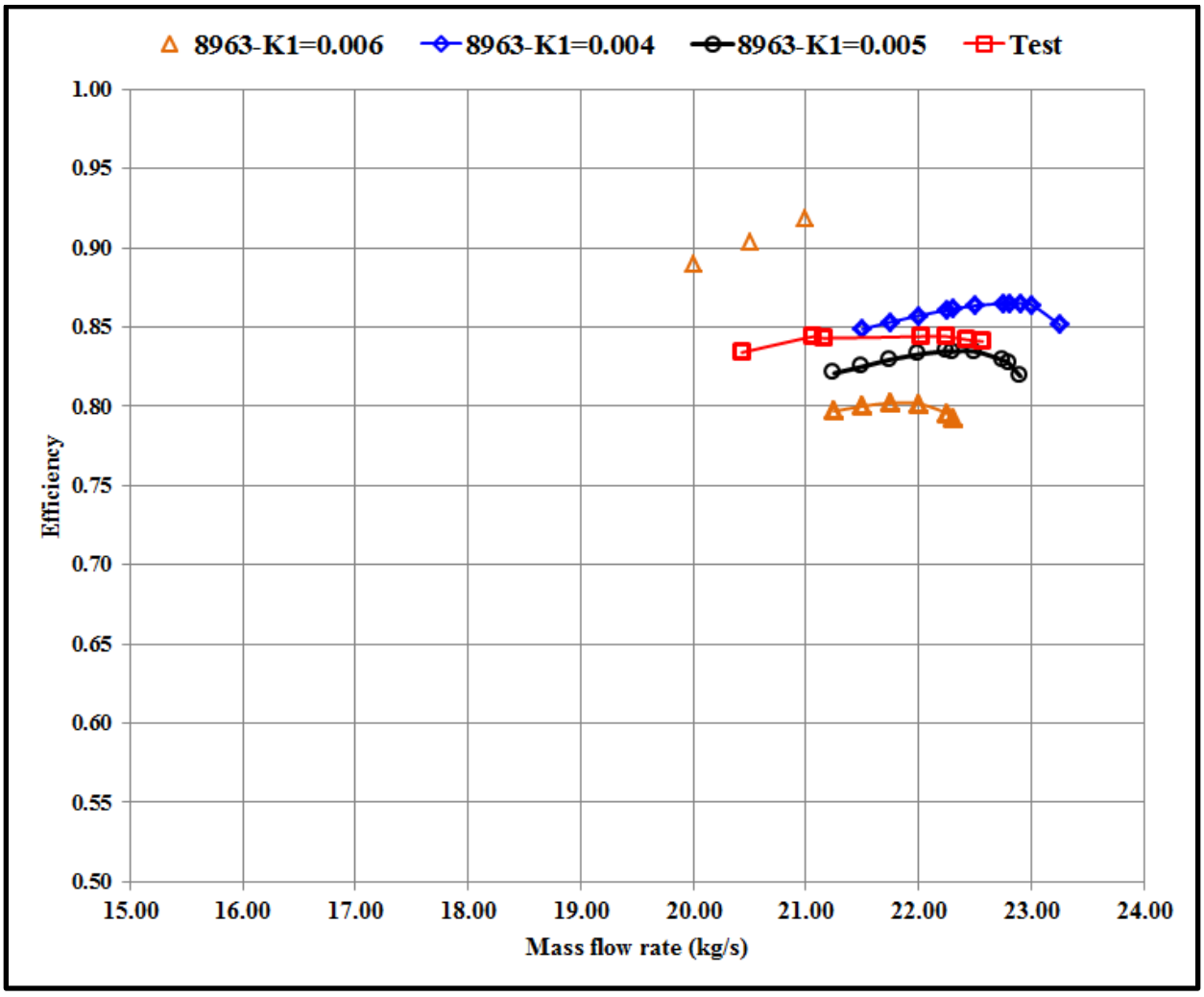

Figure 6-20 Efficiency vs. mass flow rate for 8963 rpm with three different values of K_1

A similar treatment was done for the final speed line at 80% of the performance (7967 rpm). The K_1 values chosen were 0.005, 0.006, and 0.007. The choice of the constants was to try and get the best possible fit with test data. Figure 6-21 and Figure 6-22 show that the modeled data over predicts the performance and larger constants probably would provide better fit.

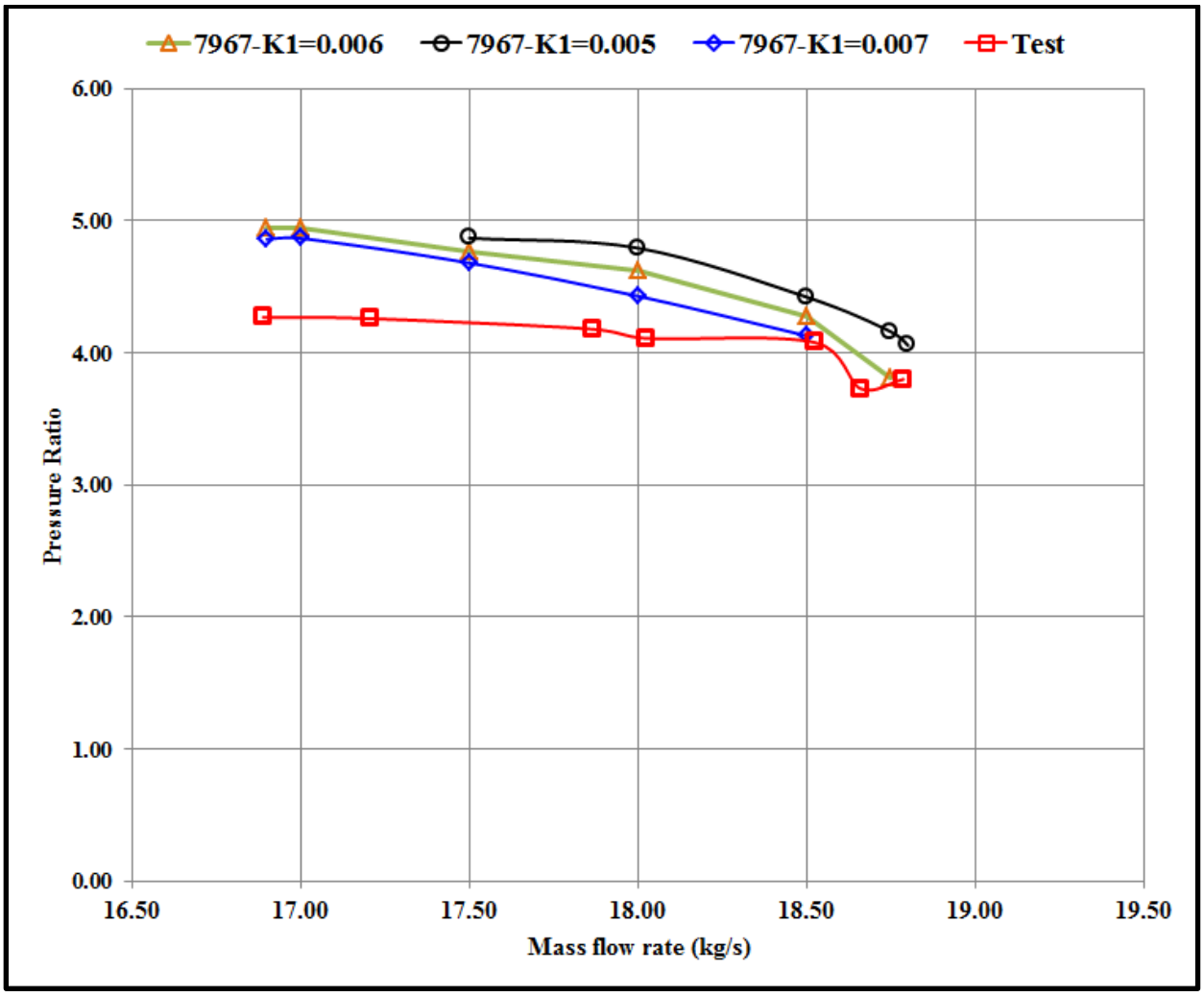

Figure 6-21 Pressure ratio vs. mass flow rate for 7967 rpm with three different values of K_1

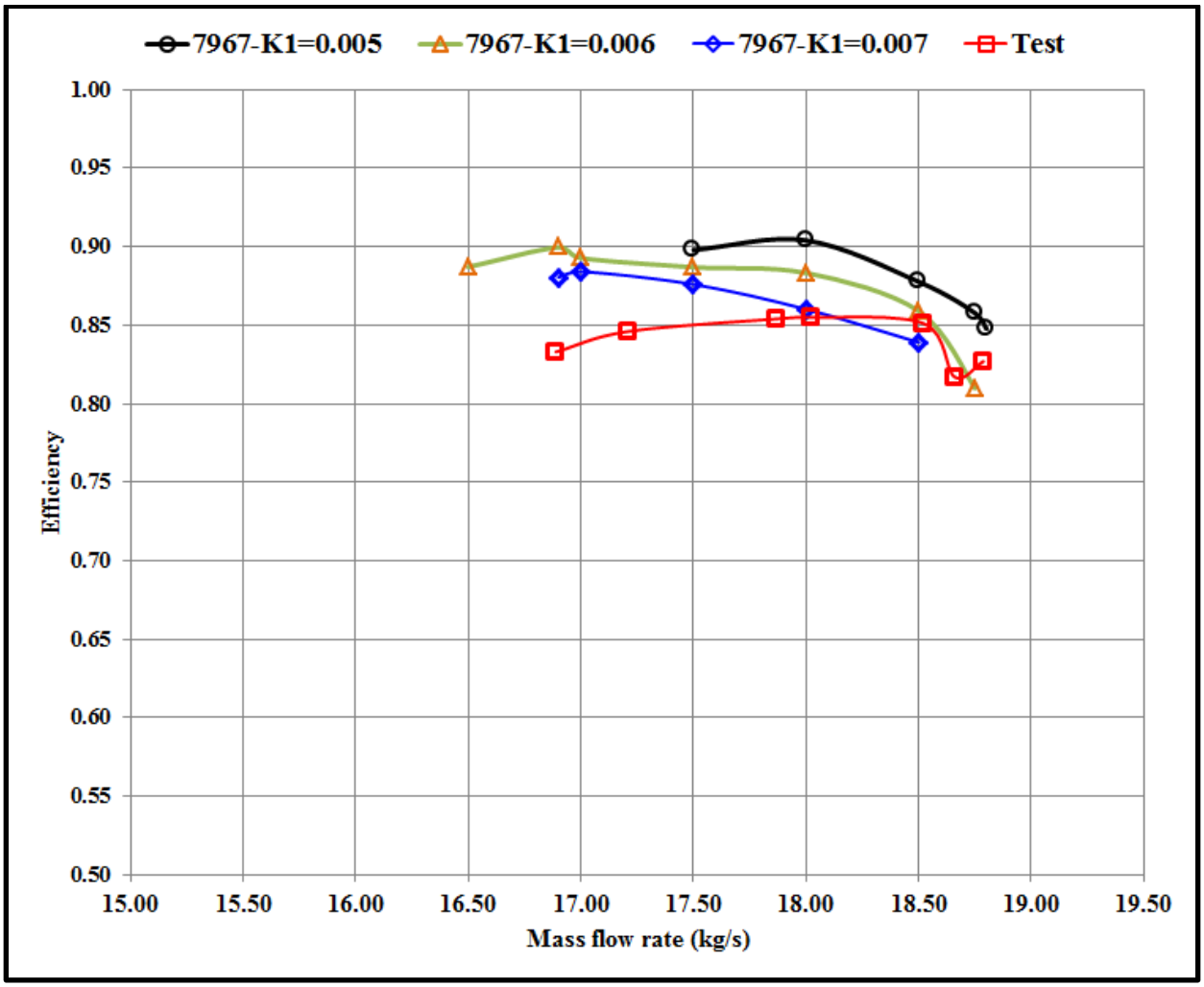

Figure 6-22 Efficiency vs. mass flow rate for 7967 rpm with three different values of K_1

Compressor performance map

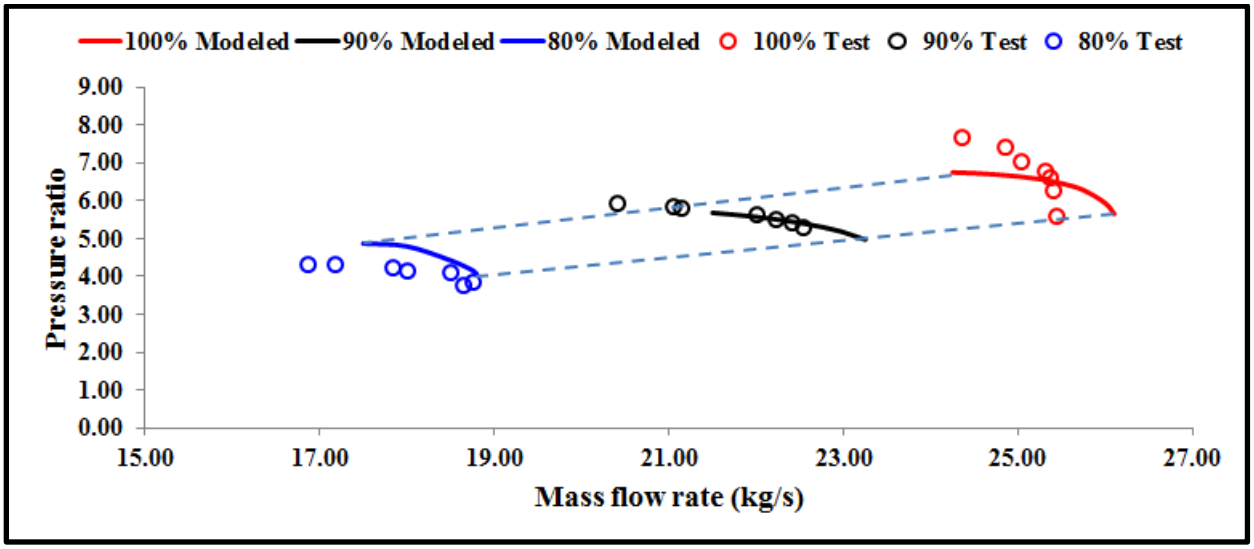

Figure 6-23 Compressor performance map (Pressure ratio versus mass flow rate)

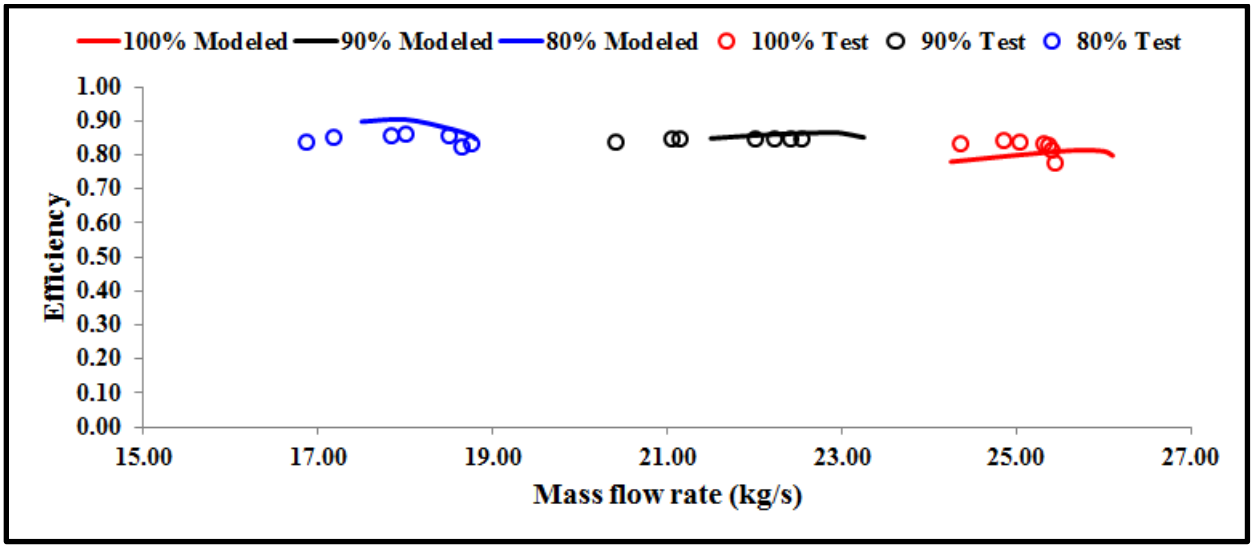

Figure 6-24 Compressor performance map (Pressure ratio versus mass flow rate)

Figure 6-23 and Figure 6-24 show the compressor performance map for the 10 stage compressor along with the tested performance data. The modeled data provides a fair correlation with the tested data. Undoubtedly, model improvements can be made by examining some of the models in greater detail or adding newer models. Some of the models not implemented here are the Reynolds number correction and the shock loss models. Furthermore, the value of the constant K_2 can be modeled separately using Howell's (Howell, 1942, 1945) secondary flow

drag coefficient model presented as a function of the blade height, the blade solidity and the inlet and exit flow angles.

Detailed performance data

Table 6-25 Row by row performance data at 26 kg/s

Row	*PR*	*TR*	*EFF*
1	1.099	1.031	0.884
2	1.087	1.031	0.783
3	1.303	1.089	0.885
4	1.290	1.089	0.851
5	1.559	1.153	0.886
6	1.543	1.153	0.864
7	1.921	1.231	0.888
8	1.899	1.231	0.871
9	2.366	1.315	0.887
10	2.339	1.315	0.874
11	2.908	1.403	0.885
12	2.872	1.403	0.872
13	3.622	1.506	0.879
14	3.558	1.505	0.865
15	4.490	1.616	0.870
16	4.406	1.616	0.857
17	5.512	1.730	0.861
18	5.404	1.730	0.849
19	6.710	1.848	0.852
20	6.566	1.848	0.839
Overall	***6.566***	***1.848***	***0.839***
Total Power			***6467 kW***

Table 6-25 presents the row by row performance data for the data point at 26 kg/s. The pressure rise ratio (PR) and temperature rise ratio (TR) are measured with reference to the inlet total conditions. Across the first stage rotor there is a pressure rise and a temperature rise. There is no total temperature rise across the stator so that remains the same as seen in the table. And on account of the loss model there is a drop in the pressure rise computed across rows 1 and 2 as compared to the rise computed across row one alone. This pattern is reflected right through each

and every stage of the compressor. The efficiency value also reflects the same trend. The overall characteristics along with total power required are also documented.

Table 6-26 Stage by stage performance data at 26 kg/s

Stage	Φ	ψ	R_c
1	0.9217	0.2127	0.1966
2	0.9222	0.3669	0.5093
3	0.8955	0.3787	0.5013
4	0.8786	0.4383	0.5113
5	0.8578	0.4460	0.5176
6	0.8539	0.4539	0.5093
7	0.8637	0.5070	0.5039
8	0.8842	0.5333	0.5159
9	0.9174	0.5401	0.5217
10	0.9731	0.5514	0.5382

Table 6-26 presents the stage performance parameters the flow coefficient Φ, the stage loading coefficient ψ and the degree of reaction R_c. These are important parameters from the design standpoint and the knowledge of this would help in making judicious choices while trying to evaluate different modification case scenarios. Furthermore, these are included in the code since some minor alterations to the code can make it run in design mode and then these parameters are usually applied as constraints during design. As an example, it is seen that the degree of reaction R_c for the first stage is very low while for the remaining stages it is about 0.5. The degree of reaction is the measure of the distribution of flow diffusion between the rotor and stator and a value of 0.5 means that the rotor and stator rows will "share the burden" of increasing enthalpy of the flow. Thus, when utilizing the code to evaluate the performance by making changes to the stagger angle, the stagger angle could be changed in a manner that the degree of reaction for the first stage is 0.5.

Turbine case study

A one stage axial turbine case study was performed. The turbine geometry selected was available from Ainley & Matheison (1951). Table 6-27, Table 6-28, Table 6-29 provide the necessary input parameters required for the analysis.

Table 6-27 Turbine station Geometry

Station Number	Hub Radius ($r_h\left(Z_j\right)$)		Tip Radius ($r_t\left(Z_j\right)$)	
	in	m	in	m
1	9.50	*0.12065*	13.00	*0.16510*
2	9.50	*0.12065*	13.00	*0.16510*
3	9.50	*0.12065*	13.00	*0.16510*

Table 6-28 Turbine blade data for case study (Stage 1 – Stator Row 1 and Rotor Row 1)

Row	No. of blades	$\frac{t}{c}$	$\frac{t_e}{s}$	$\frac{\varepsilon}{h}$
Stator01	36	0.20	0.02	0.0000
Rotor01	50	0.15	0.01	0.01715

Table 6-29 Turbine blade data for case study (Stage 1 – Stator Row 1 and Rotor Row 1)

Row	Radius		Chord		Metal Angle		$\frac{s}{c}$	$\frac{o}{s}$
					κ_i	κ_e		
	in	m	in	m	°	°		
Stator01	5.6250	*0.14287*	1.3300	*0.033782*	0.0000	70.0000	0.7390	0.4370
Rotor01	5.6250	*0.14287*	0.9500	*0.02413*	-36.0000	-53.1100	0.7490	0.6280

The Ainley-Matheison performance data was available for a rotational speed of 14427 rpm. For this particular study, this speed was considered as 100% speed and thus to generate the map two more additional speeds at 93% and 107% were generated. Data for these two speeds were not available in the Ainley-Matheison performance information. Figure 6-25 and Figure 6-26 provide the turbine performance map data for the flow rates against pressure ratio and efficiency respectively. The choked flow condition was at the flow rate 5.25 kg/s. This was iteratively determined as for the compressor where the slope of the pressure ratio vs. flow rate curve is infinity. The efficiency is modeled as:

$$\eta_t = \frac{1 - TR}{1 - PR^{\frac{\gamma - 1}{\gamma}}} \tag{6.75}$$

Figure 6-27 and Figure 6-28 show the same plots as Figure 6-25 and Figure 6-26 with the Ainley-Matheison data plotted along with the data from the current work. It can be seen that the pressure ratio curve is shifted to the left as compared to the data modeled in this work. The other difference was that the efficiency values were significantly higher. The difference in the pressure ratio curve is an artifact of the incidence angle. Thus, incidence angles calculated by CTOOM1DTURBPERF were different from those computed by Ainley and Matheison. The difference in the efficiency values were an artifact of both incidence angles and the fluid model used. For this analysis the fluid used is air and thus the value of γ for the performance evaluation is 1.4.

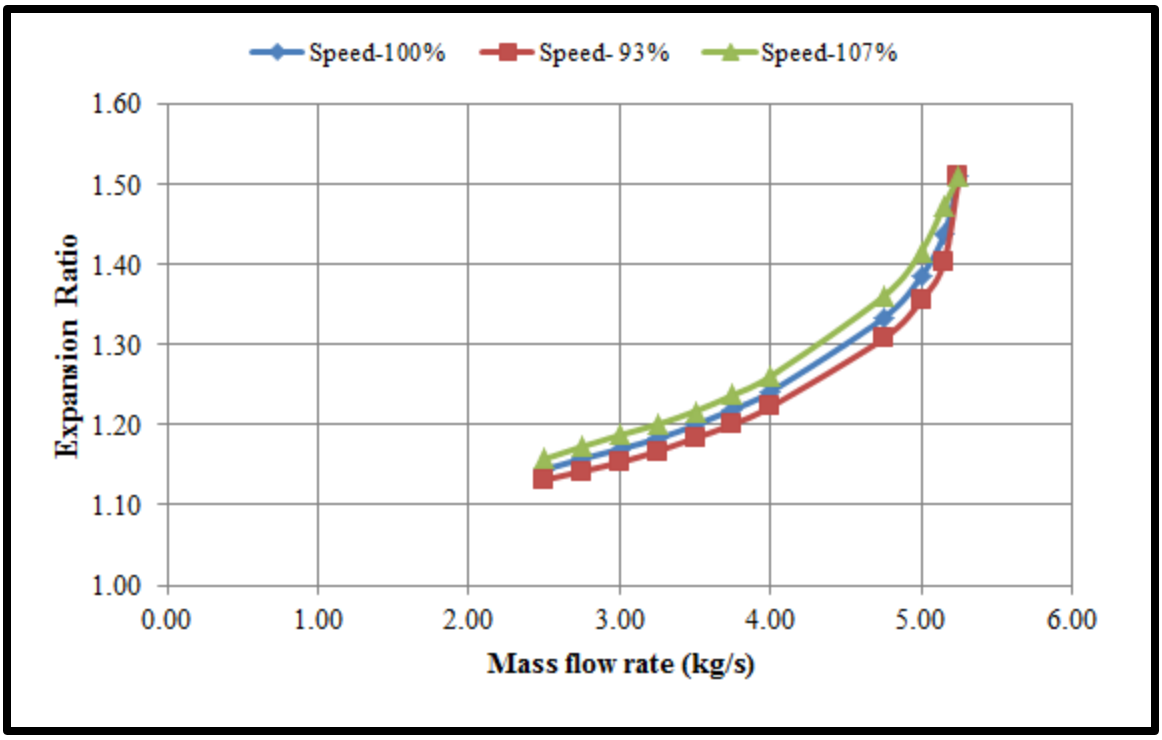

Figure 6-25 Turbine performance map [Flow rate vs. pressure ratio]

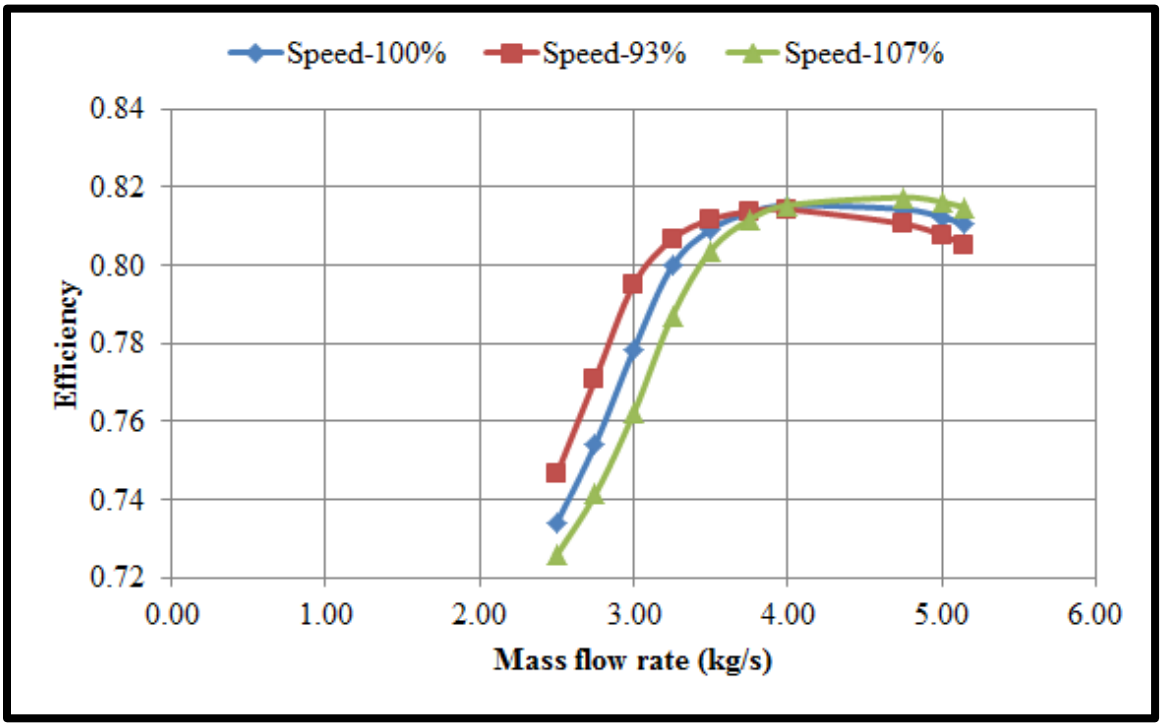

Figure 6-26 Turbine performance map [Efficiency vs. pressure ratio]

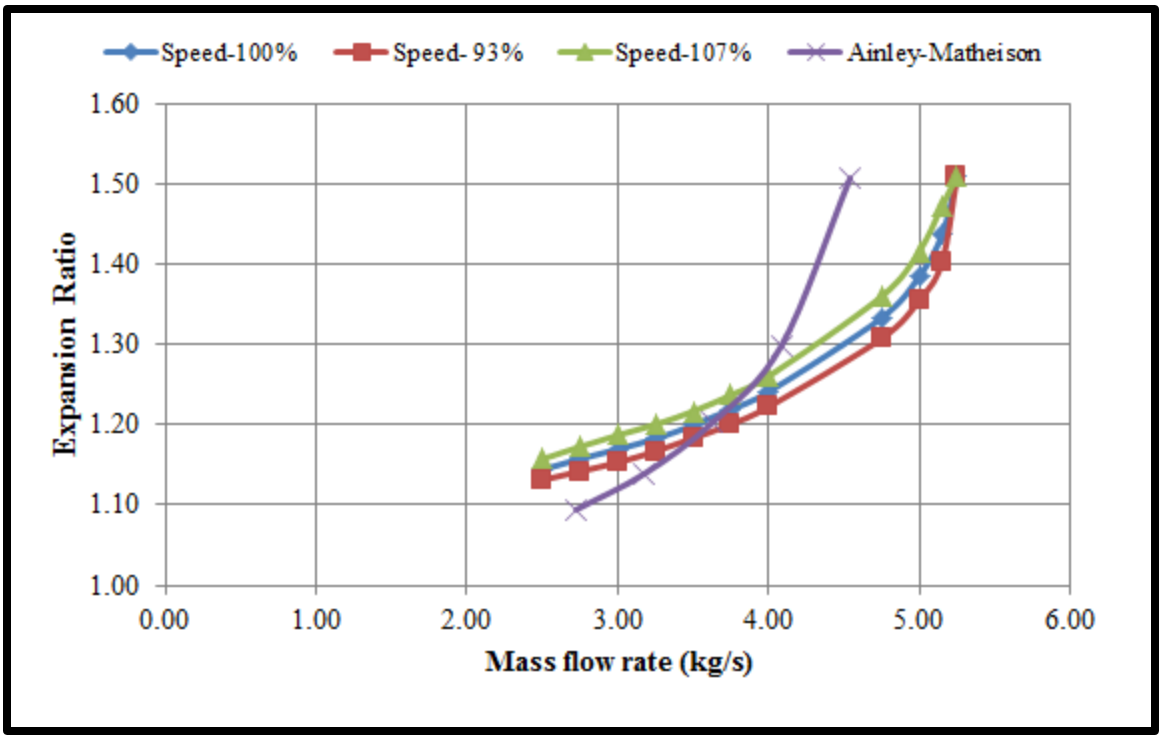

Figure 6-27 Turbine performance map [Flow rate vs. pressure ratio]

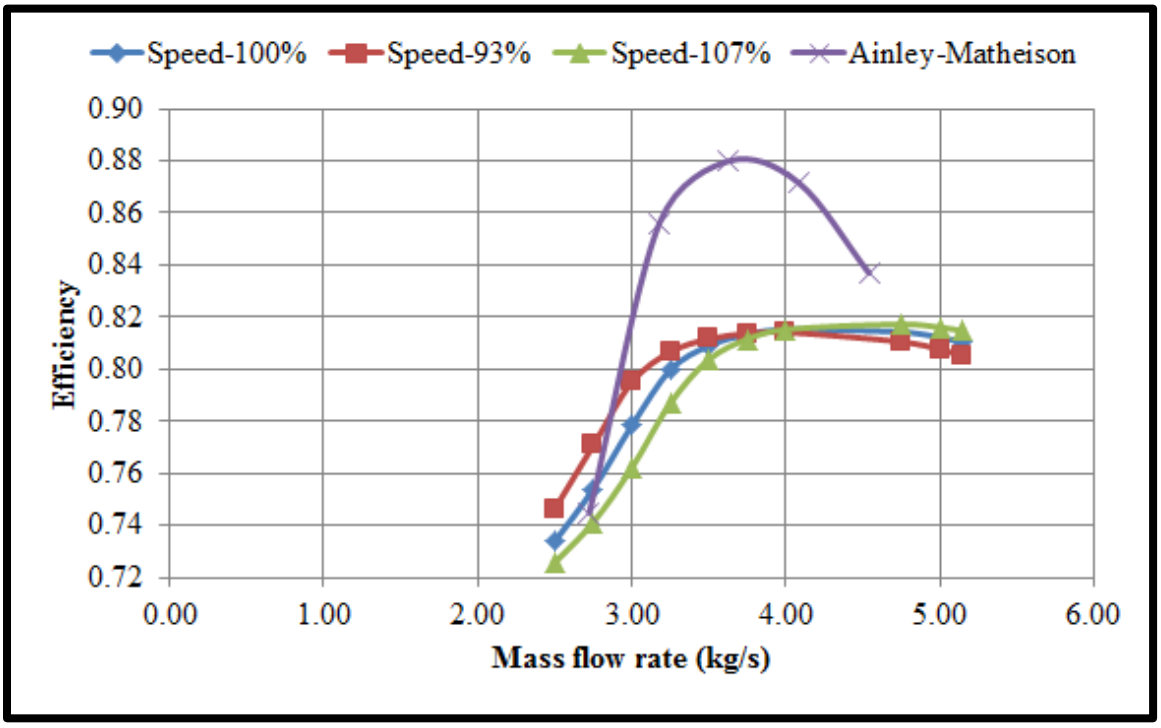

Figure 6-28 Turbine performance map [Efficiency vs. pressure ratio]

This differs significantly from the Ainley-Matheison data where the value of γ is 1.33. If the value of γ would be changed from 1.4 to 1.33 then the values of the efficiency would be significantly higher in the range of 0.89 as against 0.81 as seen in Figure 6-26. However, this would inconsistent with the enthalpy and entropy evaluations which were done for air as the working fluid and thus was not pursued with. The goal of this work was not to necessarily reproduce Ainley-Matheison's data using their algorithm of an ideal gas fluid with constant properties. This was already done as an initial investigation by Sengupta, et al. (2008). The goal here was to improve that model using real fluids and use a property calculation package.

Uncertainty analysis as carried out for the system level solution was not done for the component level models. The primary reason being that generalized loss models were used to capture the essence of pressure loss in the machines. Since the losses were not machine specific uncertainty analysis was not deemed as a reasonable exercise. However, once the models are calibrated against machine specific data-set, it would be useful to consider a detailed uncertainty analysis for the developed model.

Integration of the component models with the system model

The optimization model CTOOM-OPTIMIZE is essentially a thermodynamic model. The advantages of such a model were that a more general purpose model could be established and an efficient algorithm could be developed. This will allow the user to focus on the optimization decision variables and its influence on the system rather than on the more intricate details of the components. However, the thermodynamic modeling approach has its shortcomings. As an example, the speed of the compressor and the turbine are not system variables. Thus, from the optimization model, in its current form alone, it is impossible to determine what speed the machine is operating at. Speed is an important variable since speed control can be used to alter the operating point of the CT rotating components. Thus, integrating the individual component models established in this work would effectively mitigate some of the shortcomings of the thermodynamic system model. However, it should be recalled that once that is accomplished then the system becomes machine specific and the elegance of using the optimization model for evaluating different case studies is lost. As an illustration of the same, it can be seen from the compressor map that the flow rates for the compressor that was modeled varies from 17 kg/s to 26.5 kg/s, i.e. from the surge to choke. Thus, if this component model was tightly integrated into

the system level model, then any air flow rates outside the specified range would not be suitable any longer for doing a system level evaluation. Therefore, integrating the components would be counterproductive to having a general purpose optimization tool. Though, there are advantages of having an integrated tool-kit the loss of generality could be a reason to sacrifice the direct integration. Instead, the information established from the optimization model can be then used in conjunction with the component maps to determine component level modifications necessary to meet the optimal system variables. The other challenge in the system level integration was that the turbine model established here was for a one stage turbine with a flow rate of around 3 kg/s. Since the compressor and the turbine do not have similar operating regimes a direct integration of the component models was not feasible in any case. The alternative choice was to integrate either the compressor model or the turbine model. At the outset, it would seem more plausible to integrate the compressor model since the system level air flow rate falls within the compressor operating regime. However, as other components such as the turbine cannot be integrated into the system therefore partial integration of components into the system level model would not add value to this work. Hence the same was not pursued with.

On the contrary, the information obtained from executing the optimization model can be used in conjunction with machine specific maps to determine component level modifications that can be done to meet optimal operating conditions. As an illustration of the same, the optimal values obtained for the compressor pressure ratio in the system level case studies Modification 2 and 5 were examined for determining suitable re-staggering of the compressor stator vanes. It can be seen between Modification-2 and Modification-5 that the optimal value of the compressor pressure ratio changes from 6.56 to 6.95. These are the required optimal pressure ratios. However, for the compressor to operate at a different pressure ratio it should be accompanied by a change in either the flow rate or speed. But, if both have to be retained then the other standard practice is to change the compressor stator stagger angle setting. This is known as compressor re-staggering.

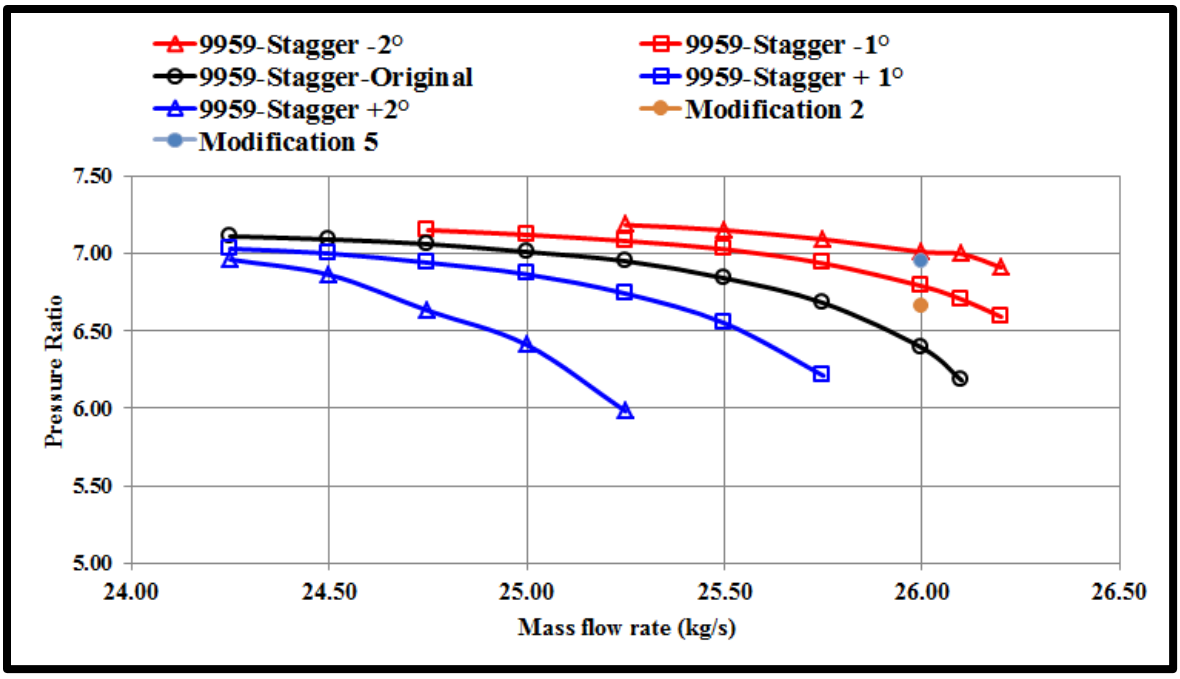

Figure 6-29 Re-staggering of compressor stator vanes to meet optimal pressure ratio

This is illustrated in the Figure 6-29 where the pressure ratio of Modification-2 and Modification-5 are plotted on the stagger angle graph. It can be seen that the pressure ratio for Modification-2 is at a compressor stator stagger angle of -1° while a change form that pressure ratio to the pressure ratio of Modification-5 would require changing the stagger angle to -2°. This demonstrated that the CTOOM-OPTIMIZE model in conjunction with the compressor component model CTOOMCOMP1DPERF can be used as a comprehensive tool to determine modifications in the compressor that could meet the requirement of optimal decision variable values. This also precludes the need for integrating individual components into the system.

Chapter 7 - Summary, conclusions and future work

Summary and Conclusions

- A combustion turbine operation and optimization model was successfully developed in this dissertation. It included a system level optimization model and two component level models for compressor and turbine.
- The system level optimization model that can examine power boosting and emission control technologies in concert with a degradation recovery model is the primary contribution of this work.
- The system level model can be used to determine optimal values of decision variable that should be used to minimize the operational costs and control both the emissions and the degradation within user defined limits.
- The system level model was developed for a cogeneration system as outlined in the classical CGAM problem. However, the objective function was modified to include the cost of emissions. It was seen this modification significantly increased the total operational cost rate of the system. The objective function was also modified to separate the capital and maintenance costs which allowed incorporating a degradation recovery model.
- Based on the cost coefficients used, it was demonstrated that the increased frequency of online washing had minimal impact on the operating costs of the system.
- Again, based on the cost coefficients used in the model, it was seen that there was not a significant difference in the operating costs between the use of steam injection against inlet air cooling for power boosting. However, some of the other decision variables such as the compressor pressure ratio changed substantially.
- The influence of controlling NO_x within user defined limits was studied and the results showed that, though the fuel costs remained nearly the same, other decision variables changed significantly.
- It was demonstrated that the results obtained from this thermodynamic optimization model could be used in a comprehensive component model to

determine the level of re-staggering that could meet duty conditions for optimal performance.

- The optimization model was developed in MS Excel. The optimization model used the commercially available What's Best solver that uses the generalized gradient based search algorithm.
- The component models for the compressor and the turbine used a mean-line aero-thermodynamic evaluation scheme. Loss models as available in the open literature were incorporated. The loss models used in this algorithm were obtained from low speed cascade testing and are not specific to any original equipment manufacturer (OEM) compressor or turbine. However, the use of influence coefficients in the loss models will allow calibration of the model against specific machines (compressors and turbines) in the future.
    - Fortran 90 was used as the programming language for the component models which allowed simpler techniques of passing variable information from the main program to the subroutines.
    - The program architecture was set up such that the loss models were independent of the main program. This allows the use of user defined loss models with minimal change to the solution scheme.
- The system level optimization model and the component models were validated against data available in the open literature and showed good agreement- less that 1% when compared to the CGAM solution.

Future work

- Some of the loss models in open literature such as shock losses, secondary flow drag loss coefficient characterization, and Reynolds number correction need to be implemented in the compressor model.
- The turbine loss characterization was done using the classical Ainley-Mathieson Dunham-Came correlations and lack of machine configuration in open literature did not allow exhaustive validation. The turbine model validation against tested data is left for future work.

- A combustor model with chemical kinetics and reaction chemistry is not included in this work, but can be incorporated in the future to complement the compressor and turbine models.
- The current implementation of the system level degradation model has an economic model that should be connected to the degradation parameters. This economic model is a very basic model based on assumptions and limited data available in the open literature. This can be further improved by doing a more exhaustive analysis of different combustion turbines and quantifying the economic costs of degradation.

References

Ainley, D. G. and G. C. R. Mathieson (1951). **A method of performance estimation for axial flow turbines**, R&M 2974, Aeronautical Research Council, London.

Al-Amiri, A. M., M. A. Chaker, M. M. Zamzam and C. B. Meher-Homji (2006). "*Application of inlet fogging for power augmentation of mechanical drive turbines in the oil and gas sector*," Proceedings of the 51st ASME Turbo Exposition Barcelona, Spain, American Society of Mechanical Engineers.

Ameri, M., S. H. Hejazi and K. Montaser (2005). "Performance and economic of the thermal energy storage systems to enhance the peaking capacity of the gas turbines," **Applied Thermal Engineering**, 25, 2-3, 241-251.

Anonymous (1993). **Alternative control techniques document— NO_x emissions from stationary gas turbines**, 453/R-93-007, U. S. Environmental Protection Agency, North Carolina.

Anonymous (2005). **Gas turbine engine performance**, January 2005, Emerson Process Management: Asset Optimization Division, Stafford, TX.

Anonymous (2006). **Gas turbine steam injection system for NO_x reduction**, 94023, Petrotech Inc., Louisiana.

Anonymous (2011). ***What's Best!***, 11.1.0.1, Lindo Systems, Chicago, IL.

Asplund, P. (1997). "*Gas turbine cleaning upgrade (compressor wash)*," Proceedings of the 1st ASME ASIA Congress & Exhibition Singapore, Singapore, American Society of Mechanical Engineers.

Aungier, R. H. (2003). **Axial flow compressors : A strategy for aerodynamic design and analysis**, ASME Press, New York, NY.

Aungier, R. H. (2006). **Turbine aerodynamics : Axial flow and radial inflow turbine design and analysis**, ASME Press, New York, NY.

Bathie, W. W. (1996). **Fundamentals of gas turbines**, John Wiley & Sons, Toronto, Canada.

Bejan, A., G. Tsatsaronis and M. J. Moran (1996). **Thermal design and optimization**, John Wiley, New York, NY.

Bhargava, R. K., C. B. Meher-Homji, M. A. Chaker, M. Bianchi, F. Melino, A. Peretto and S. Ingistov (2005). "*Gas turbine fogging technology: A state-of-the-art review part I: Inlet evaporative fogging- Analytical and experimental aspects*," Proceedings of the 50th ASME Turbo Exposition- Gas Turbine Technology: Focus for the Future Reno, NV, American Society of Mechanical Engineers.

Bianchi, M., L. Branchini, A. De Pascale, F. Melino, A. Peretto, R. K. Bhargava and M. A. Chaker (2010). "*Gas turbine power augmentation technologies: A systematic comparative evaluation approach*," Proceedings of the 55th ASME Turbo Exposition: Power for Land, Sea, and Air Glasgow, United Kingdom, American Society of Mechanical Engineers.

Boyce, M. P. (2012). **Gas turbine engineering handbook**, Elsevier, Waltham, MA.

Bracco, S., A. Pierfederici and A. Trucco (2007). "The wet compression technology for gas turbine power plants: Thermodynamic model," **Applied Thermal Engineering**, 27, 4, 699-704.

Brooks, F. J. (2000). **GE gas turbine performance characteristics**, GER-3567H, GE Power Systems, Schenectady, NY.

Bultzo, C. (1969). "*Steam injection, source of incremental power*," Proceedings of the ASME Meeting GT-68 Unknown, American Society of Mechanical Engineers

Coutant, J. G. (1959). "Water or steam injection in gas turbine cycle provides unique performance," **Power Engineering**, 63, 6, 93-95.

Cowell, L. (2003). "*Emissions Control in Industrial Gas Turbines*," Proceedings of the National CHP Turbine Technology & Regulatory Forum San Diego, CA, Environmental Protection Agency.

Cumpsty, N. A. (2004). **Compressor aerodynamics**, Krieger, Malabar, FL.

Diakunchak, I. S. (1991). "*Performance deterioration in industrial gas turbines*," Proceedings of the 36th International Gas Turbine and Aeroengine Congress & Exposition Orlando, FL, American Society of Mechanical Engineers.

Drud, A. S. (1994). "CONOPT—A Large-Scale GRG Code," **ORSA Journal on Computing**, 6, 2, 207-216.

Dunham, J. and P. M. Came (1970). "Improvements to the Ainley-Mathieson method of turbine performance prediction," **Journal of Engineering for Power**, 252-256.

Ediss, B. G. (1966). "Steam injection," **Chemical and Process Engineering**, 47, 12, 57-61.

Ediss, B. G. (1970). "Steam injection can improve gas turbines," **Power**, 114, 6, 82-84.

Emery, J. C., L. J. Herrig and J. R. Erwin (1958). **Systematic two-dimensional cascade tests of NACA 65 series compressor blades at low speeds**, NACA TN 3916, NASA, NACA (Unspecified Center).

Farokhi, S. (2009). **Aircraft propulsion**, John Wiley & Sons, Hoboken, NJ.

Farzaneh-Gord, M. and M. Deymi-Dashtebayaz (2011). "Effect of various inlet air cooling methods on gas turbine performance," **Energy**, 36, 2, 1196-1205.

Fitts, D. O., R. A. Symonds and E. R. Western (1990). "*Combustion system performance of a water-injected MS7001E gas turbine operating at a NO_x emission level of 25 ppmvd*," Proceedings of the 35th International Gas Turbine and Aeroengine Congress & Exposition, Brussels, Belgium, American Society of Mechanical Engineers.

Flatau, P. J., R. L. Walko and W. R. Cotton (1992). "Polynomial fits to saturation vapor pressure," **Journal of Applied Meteorology**, 31, 1507-1513.

Frangopoulos, C. A. (1992). "*Introduction to environomic analysis and optimization of energy-intensive systems*," Proceedings of the International Symposium on Efficiency, Cost, Optimization and Simulation (ECOS '92) Zaragoza, Spain, American Society of Mechanical Engineers.

Grauer, D. K. (2010). **Simulation and optimization of non-isothermal compressible flow through large bore two-stroke natural gas transmission engines,** Doctoral Dissertation, Kansas State University.

Heard, T. C. (1976). "*Reduction of gas turbine fuel consumption on gas pipelines*," Proceedings of the 21st ASME Gas Turbine Conference and Products Show Unknown, American Society of Mechanical Engineers.

Johnsen, I. A. and R. O. Bullock (1965). **Aerodynamic design of axial flow compressors**, NASA SP-36, NASA, Glenn Research Center.

Kline, S. J. and F. A. McClintock (1953). "Describing uncertainties in single sample experiments", **Mech. Engineering**, p. 3., Jan. 1953.

Knopf, F. C. (2011). **Modeling, analysis and optimization of process and energy systems**, John Wiley & Sons, Hoboken, NJ.

Kurz, R. and K. Brun (2001). "Degradation in gas turbine systems," **Journal of Engineering for Gas Turbines and Power**, 123, 1, 70-77.

Kurz, R. and K. Brun (2007). "*Gas turbine tutorial- Maintenance and operating practices: Effects on degradation and life*," Proceedings of the 36th Turbomachinery Symposium Houston, TX, Texas A&M University System's-The Turbomachinery Laboratory.

Kurz, R. and K. Brun (2009). "Degradation of gas turbine performance in natural gas service," **Journal of Natural Gas Science and Engineering**, 1, 3, 95-102.

Kurz, R., K. Brun and M. Wollie (2009). "Degradation effects on industrial gas turbines," **Journal of Engineering for Gas Turbines and Power**, 131, 6, 062401-1-7.

Lakshminarasimha, A. N. and H. I. H. Saravanamuttoo (1986). "*Prediction of fouled compressor performance using stage stacking techniques*," Proceedings of the AIAA/ASME 4th Joint Fluid Mechanics Atlanta, GA, American Society of Mechanical Engineers.

Lakshminarasimha, A. N., M. P. Boyce and C. B. Meher-Homji (1994). "Modeling and analysis of gas turbine performance deterioration," **Journal of Engineering for Gas Turbines and Power**, 116, 1, 46-52.

Lasdon, L., Z. Ugray, J. Plummer, F. Glover, J. Kelly and R. Marti (2002). "A Multistart Scatter Search Heuristic for Smooth NLP and MINLP Problems," **Society for Computational Economics Computing in Economics and Finance 2002**, 195.

Lefebvre, A. H. (1984). "*Fuel effects on gas turbine combustion- Liner temperature, pattern factor, and polutant emissions*," Proceedings of the AIAA/SAE/ASME 20th Joint Propulsion Conference Cincinnati, OH, American Institute of Aeronautics and Astronautics.

Lefebvre, A. H. and D. R. Ballal (2010). **Gas turbine combustion : alternative fuels and emissions**, Taylor & Francis, Boca Raton.

Lemmon, E. W., M. L. Huber and M. O. McLinden (2010). ***NIST Standard Reference Database 23: Reference Fluid Thermodynamic and Transport Properties-REFPROP***, 9.0, National Institute of Standards and Technology, Gaithersburg, MD.

Lewis, G. D. (1991). "*A new understanding of NO_x formation*," Proceedings of the 10th International Symposium on Air-Breathing Engines Nottingham, United Kingdom, American Institute of Aeronautics and Astronuatics.

Lieblein, S. (1959). **Incidence and deviation angle correlations for compressor cascades**, NASA-TM-X-56232, NASA, Glenn Research Center.

Lieblein, S. (1960). "Incidence and deviation angle correlations for compressor cascades," **Journal of Basic Engineering**, 82, 575-587.

Mattingly, J. D. (1996). **Elements of gas turbine propulsion**, McGraw-Hill, New York, NY.

Mee, T. R. (1999). "Inlet fogging augments power production," **Power Engineering**, 103, 2, 26-30.

Meher-Homji, C. B., M. Chaker and A. F. Bromley (2009). "*The fouling of axial flow compressors - Causes, effects, susceptibility and sensitivity*," Proceedings of the 54th ASME Turbo Exposition Orlando, FL, American Society of Mechanical Engineers.

Mehraban, K. M., S. V. M. Jezeh and S. H. M. Kazemi (2012). "*Technical and economical evaluation of media and fog systems in Fars, Qom, Yazd, Shahid Rajaee power plants*," Proceedings of the 2011 International Conference on Material Science and Information Technology (MSIT2011) Singapore, Singapore, Trans Tech Publications.

Millsaps, K. T., J. Baker and J. S. Patterson (2004). "*Detection and localization of fouling in a gas turbine compressor from aerothermodynamic measurements*," Proceedings of the 49th ASME International Gas Turbine and Aeroengine Congress & Exposition Vienna, Austria, American Society of Mechanical Engineers.

Mohanty, B. and G. Paloso Jr (1995). "Enhancing gas turbine performance by intake air cooling using an absorption chiller," **Heat Recovery Systems and CHP**, 15, 1, 41-50.

Novak, R. A. (1966). "*Streamline curvature computing procedures for fluid-flow problems*," Proceedings of the ASME Winter Annual Meeting WA/GT-3 New York, NY, American Society of Mechanical Engineers.

Novak, R. A. (1973). **Axisymmetric computing systems for axial flow turbomachinery**, Lecture 25, ASME Turbomachinery Institute Fluid Dynamics of Turbomachinery, Iowa State University, Ames, Iowa.

Novak, R. A. and R. M. Hearsey (1977). "Nearly three-dimensional intrablade computing system for turbomachinery," **Journal of Fluid Mechanics**, 99 Ser I, 1, 154-166.

Odgers, J. and D. Kretschmer (1985). "*The prediction of thermal NO_x in gas turbines*," Proceedings of the 30th ASME Gas Turbine Conference & Exhibit Houston, TX, American Society of Mechanical Engineers.

Phillips, J. N. and P. Levine (2004). "Boosting gas turbine power," **Turbomachinery International**, 45, 4, 14-17.

Popli, S., P. Rodgers, V. Eveloy, S. Al Hashimi, R. Radermacher and Y. Hwang (2011). "Boosting energy efficiency using waste-heat-powered absorption chillers," **SPE Projects, Facilities and Construction**, 6, 4, 232-238.

Rangaiah, G. P. (2009). **Multi-objective optimization : Techniques and applications in chemical engineering**, Hackensack World Scientific, Singapore.

Rao, S. S. (2010). **Engineering optimization : Theory and practice**, New Age International Publishers, New Delhi, India.

Reynolds, W. C. (1979). **Thermodynamic properties in SI: Graphs, tables, and computational equations for forty substances**, Stanford University, Palo Alto.

Rizk, N. K. and H. C. Mongia (1994). "*Emissions predictions of different gas turbine combustors*," Proceedings of the 32nd Aerospace Sciences Meeting & Exhibition Reno, NV, American Institute of Aeronautics and Astronautics.

Rokke, N. A., J. E. Hustad and S. Berg (1993). "*Pollutant emissions from gas fired turbine engines in off-shore practice-Measurements and scaling*," Proceedings of the 38th ASME International Gas Turbine and Aeroengine Congress & Exposition Cincinnati, OH, American Society of Mechanical Engineers.

Sanaye, S. and M. Tahani (2010). "Analysis of gas turbine operating parameters with inlet fogging and wet compression processes," **Applied Thermal Engineering**, 30, 2-3, 234-244.

Saravanamuttoo, H. I. H. and A. N. Lakshminarasimha (1985). "*A preliminary assessment of compressor fouling*," Proceedings of the 30th International Gas Turbine Conference & Exhibition Houston, TX, American Society of Mechanical Engineers.

Seddigh, F. and H. I. H. Saravanamuttoo (1990). "*Proposed method for assessing the susceptibility of axial compressors to fouling*," Proceedings of the 35th International Gas Turbine and Aeroengine Congress & Exposition Brussels, Belgium, American Society of Mechanical Engineers.

Sexton, M. R., H. B. Urbach and D. T. Knauss (1998). "*Evaporative compressor cooling for NO_x suppression and enhanced engine performance for naval gas turbine propulsion plants*," Proceedings of the 43rd International Gas Turbine and Aeroengine Congress & Exhibition Stockholm, Sweden, American Society of Mechanical Engineers.

Singh, D., A. Hamed and W. Tabakoff (1996). "*Simulation of performance deterioration in eroded compressors*," Proceedings of the 41st International Gas Turbine and Aeroengine Congress & Exhibition Birmingham, UK, American Society of Mechanical Engineers.

Soares, C. (2008). **Gas turbines a handbook of air, land, and sea applications**, Elsevier: Butterworth-Heinemann, Boston, MA.

Stephens, J. O. and M. J. Boho (1965). "Injection boosts gas turbine output," **Electrical World**, 163, 18, 87-90.

Tabakoff, W. and C. Balan (1983). "Study of the surface deterioration due to erosion," **Journal of Engineering for Power**, 105, 4, 834-838.

Tabakoff, W. (1987). "Study of single stage axial flow compressor performance deterioration," **Wear**, 119, 1, 51-61.

Tarabrin, A. P., A. I. Bodrov, V. A. Schurovsky and J. P. Stalder (1996). "*Analysis of axial compressors fouling and a cleaning method of their blading*," Proceedings of the 41st International Gas Turbine and Aeroengine Congress & Exhibition Birmingham, UK, American Society of Mechanical Engineers.

Tarabrin, A. P., V. A. Schurovsky, A. I. Bodrov and J. P. Stalder (1998). "*Influence of axial compressor fouling on gas turbine unit performance based on different schemes and with different initial parameters*," Proceedings of the 43rd International Gas Turbine and Aeroengine Congress & Exhibition Stockholm, Sweden, American Society of Mechanical Engineers.

Upton, A. (1974). "*Axial flow compressor and turbine blade fouling, some causes, effects and cleaning methods*," Proceedings of the 1st Symposium on Gas Turbine Operations and Maintenance Canada, National Research Council of Canada.

Valero, A., M. A. Lozano, L. Serra, G. Tsatsaronis, J. Pisa, C. Frangopoulos and M. R. von Spakovsky (1994). "CGAM problem: Definition and conventional solution," **Energy**, 19, 3, 279-286.

Vanderplaats, G. N. (2005). **Numerical optimization techniques for engineering design**, Vanderplaats Research & Development, Colorado Springs, CO.

Wu, C. H. (1952). "General theory of three-dimensional flow in subsonic and supersonic turbomachines of axial, radial, and mixed-flow types," **American Society of Mechanical Engineers - Transactions**, 74, 8, 1363-1380.

Appendix A - Uncertainty analysis

The effect of uncertainty in input data on output variables in the model was examined and is presented here. The underlying concept as in any experimental uncertainty determination was used. Kline and McClintock (1953) provide a means of determining the uncertainty in calculated variables due to uncertainty in measured variables. For the general relation,

$$j = j\left(X_1, X_2, \cdots X_i\right) \tag{A.1}$$

The uncertainty (U_j) is expressed as:

$$U_j = \sqrt{\frac{\partial j}{\partial X_1}U_{X_1} + \frac{\partial j}{\partial X_2}U_{X_2} + \cdots \frac{\partial j}{\partial X_i}U_{X_i}} \tag{A.2}$$

As an example, the pressure ratio of the compressor PR_c is given by:

$$PR_c = \frac{P_2}{P_1} \tag{A.3}$$

If the uncertainty in the inlet pressure is U_{P_1} and the uncertainty in the exit pressure is U_{P_2} then the uncertainty in the evaluated quantity PR_c is given by:

$$U_{PR_c} = \sqrt{\frac{\partial PR_c}{\partial P_1}U_{P_1} + \frac{\partial PR_c}{\partial P_2}U_{P_2}} \tag{A.4}$$

Where,

$$\frac{\partial PR_c}{\partial P_1} = -\frac{P_2}{P_1^2} \tag{A.5}$$

$$\frac{\partial PR_c}{\partial P_2} = \frac{1}{P_1} \tag{A.6}$$

The uncertainty of three input variables i.e., mass of air, pressure, and temperature were obtained from those presented in Grauer (2010). The uncertainties in the remaining variables were assumed to ensure the computations. It should be understood that the goal here was to only study the influence of uncertainty of input variables on the output variables and obtain an estimate of the propagation of the uncertainty and thus reasonable assumptions can be made for variables whose uncertainty is not readily available. Furthermore, for simplicity in estimation of uncertainty the mathematical model used for benchmarking against the CGAM problem was used. The mathematical model was called CTOOM-OPTIMIZE IDEAL and it used constant

specific heats for the development of the model. This provided closed form equations for each output variable which were more amenable to the analytical calculus procedures.

Table A-1 Uncertainty in the calculated variable due to uncertainty in the input variables

Input Variable	Uncertainty (%)	Calculated Variable	Uncertainty (%)
$\dot{m}_a$	±1.70	$\dot{m}_f$	±0.18
P_1	±0.10	$\dot{m}_s$	±1.71
PR_C	±0.14	$\dot{m}_w$	±1.71
PR_{CC}	±0.14	P_2	±0.14
$PR_{G\&PT}$	±0.14	T_2	±0.09
η_C	±0.01	P_3	±0.14
$\eta_{G\&PT}$	±0.01	P_4	±0.14
T_0	±0.08	T_5	±0.09
T_1	±0.08	T_6	±0.14
T_3	±0.08	T_7	±0.52
T_4	±0.08	T_{7P}	±0.08
T_8	±0.08	$\dot{Q}_{eva}$	±1.71
T_9	±0.08	$\dot{Q}_{eco}$	±1.71
$m_{steaminject}$	±5.00	$LMTD_{APH}$	±0.88
$f_{onlinewashing}$	±4.00	$LMTD_{ECO}$	±1.71
		$LMTD_{EVA}$	±0.98
		W_C	±1.71
		W_{GPT}	±1.69
		W_{system}	±2.40
		C_C	±2.33
		C_{CC}	±2.98

Input Variable	Uncertainty (%)	Calculated Variable	Uncertainty (%)
		C_{APH}	±1.95
		$C_{G\&PT}$	±2.17
		C_{HRSG}	±0.96
		C_t	±2.43